THE DEVELOPMENT OF AN ENANTIOSELECTIVE CATION RADICAL DIELS-ALDER REACTION AND OTHER COMPLEXITY GENERATING TRANSFORMATIONS

Peter Daniel Morse

A dissertation submitted to the faculty at the University of North Carolina at Chapel Hill in partial fulfillment of the requirements for the degree of Doctor of Philosophy in the Department of Chemistry

Chapel Hill
2015

Approved by:

David A. Nicewicz

Jeffrey S. Johnson

Erik J. Alexanian

Gerald J. Meyer

Alexander J. Miller

© 2015
Peter Daniel Morse
ALL RIGHTS RESERVED

ABSTRACT

Peter Daniel Morse: The Development of an Enantioselective Cation Radical Diels Alder
Reaction and Related Complexity Generating Transformations
(Under the direction of David A. Nicewicz)

Herein is described the development of three synthetic transformations that are united in their being initiated by the single electron oxidation of olefins to cation radical intermediates.

The development of an enantioselective cation radical Diels-Alder reaction is first described. The control of the absolute stereochemistry of cation radical reactions is a major challenge to the field. This methodology centers on the use of chiral anions as a means of inducing asymmetry, and sets important precedent that ion pairing is a viable means of enantioinduction in cation radical reactions.

An *anti*-Markovnikov intramolecular hydrofunctionalization reaction using amide and thioamide nucleophiles is also described. This transformation is a mild route to construct oxazoline and thiazoline motifs bearing substitution patterns that are challenging to synthesize by alternative methods. Additionally, evidence for disparate mechanisms for amide and thioamide substrate cyclization is presented.

Finally, progress towards the total synthesis of the natural product rubriflordilactone B is presented. The development of a route to this molecule has so far focused on the development of two key steps: a Mukuiyama vinylogous aldol reaction and subsequent polar radical crossover cycloaddition. The successful implementation of this strategy would allow the absolute

stereochemistry of the molecule to be set and five contiguous stereocenters to be formed over two steps, and would highlight the utility of photoredox catalysis in complex molecule synthesis.

ACKNOWLEDGEMENTS

There are countless people that have helped me to grow and supported me throughout my career in graduate school. This time has matured me and built me up in ways I never expected, and I would not trade the experience for anything in the world.

First and foremost I need to thank my parents. I am eternally grateful for the way you raised me and the values you've instilled in me. You've given me guidance every step of the way but never pressured me, and that has given me great peace in knowing that each path I've taken in life is one that I chose myself. I also need to thank my sister Katy and brother Chris for their support, it has been wonderful seeing how our relationships have grown as we've each started making our way out into the real world.

I would like to thank my advisor, Professor David Nicewicz, for his mentorship over the years. Thank you for allowing me to be a part of your lab and giving me the opportunity to work on fascinating and challenging projects. Thank you especially for allowing me to grow as a researcher at my own pace and showing great patience.

An especially large thanks goes to all members, past and present, of the Nicewicz lab. Our group has the best environment I could possibly ask for. If every reaction I ever ran in five years failed completely, it still would have been time well spent just to be around you all. I especially need to thank the founding class of the lab – thank you all for welcoming me into the family right from the start and fostering the atmosphere that I hope will remain with the lab perpetually. I will miss the movie nights, game nights, and lab holiday parties especially.

I am grateful for the friendship of my classmates, especially Brendan and Nate – thank you for being there through all the rough patches and always being up to grab a beer and commiserate. I am also extremely thankful for all the friendships I’ve been able to have outside the department and school. I never imagined North Carolina would feel like home, but now it’s hard to imagine being anywhere else.

Thank you also to Professors Jeff Johnson, Erik Alexanian, Alex Miller, and Gerald Meyer for serving on my committee. I would like to thank the members of the Alexanian, Meek, and Johnson labs for letting me borrow materials, use equipment, and for sharing your expertise. Thanks also the National Institutes of Health and the University of North Carolina at Chapel Hill for the funding that made this research possible.

TABLE OF CONTENTS

LIST OF TABLES x

LIST OF ABBREVIATIONS xv

CHAPTER 1: INTRODUCTION TO VISIBLE LIGHT PHOTOREDOX CATALYSIS 1

1.1 Introduction 1

1.2 Olefin cation radicals: reactivity and methods for their generation 1

1.3 Basic principles of electron transfer and photoredox catalysis 6

1.4 Photoredox catalysts 11

1.5 Early examples of olefin activation via single electron oxidation 13

1.6 Prior examples of enantioselective photoredox reactions 15

REFERENCES 21

CHAPTER 2: THE DEVELOPMENT OF AN ENANTIOSELECTIVE CATION RADICAL DIELS-ALDER REACTION 26

2.1 Overview of the traditional Diels-Alder reaction 26

2.2 A History of the cation radical Diels-Alder reaction 29

2.3 Synthesis and application of disulfonyl amide catalysts 50

2.4 Incorporation of hydrogen bonding secondary interactions into the system 55

2.5 Progress towards the development of an aromatic Claisen rearrangement 61

2.6 Application to [2+2] cycloadditions 65

2.7 Application of chiral anions to *anti*-Markovnikov hydrofunctionalizations 66

2.8 References 73

REFERENCES 70

CHAPTER 3: PHOTOREDOX CATALYZED HYDROFUNCTIONALIZATION REACTIONS FOR THE SYNTHESIS OF OXAZOLINES AND THIAZOLINES 76

3.1 Occurrence and and applications of oxazolines and thiazolines 76

3.2 Previous methods for the synthesis of oxazolines and thiazolines 77

3.3 Optimization and scope of the photoredox catalyzed hydrofunctionalization 82

3.4 Proposed mechanism of hydrofunctionalization 88

3.5 Cyclization of allylic thioamides for thiazoline synthesis 89

REFERENCES 90

CHAPTER 4: THE APPLICATION OF A POLAR-RADICAL CROSSOVER CYCLOADDITION REACTION TOWARDS THE TOTAL SYNTHESIS OF RUBRIFLORDILACTONE B 96

4.1 Introduction 96

4.2 Rubriflordilactone B 97

4.3 Total synthesis of rubriflordilactone A and related natural products 100

4.4 Retrosynthetic analysis of rubriflordilactone B 102

4.5 Background on the enantioselective Mukuiyama vinylogous aldol reaction 104

4.6 Mukuiyama vinylogous aldol optimization using siloxyfuran nucleophiles 106

4.7 Initial PRCC reaction optimization for THF ring construction 111

4.8 A move to propargyl alcohol PRCC substrates 113

REFERENCES 112

APPENDIX 1: SUPPORTING INFORMATION FOR THE DEVELOPMENT OF AN ENANTIOSELECTIVE CATION RADICAL DIELS-ALDER REACTION 118

APPENDIX 2: SUPPORTING INFORMATION FOR THE PHOTOREDOX CATALYZED HYDROFUNCTIONALIZATION REACTIONS FOR THE SYNTHESIS OF OXAZOLINES AND THIAZOLINES 149

APPENDIX 3: SUPPORTING INFORMATION FOR THE APPLICATION OF A POLAR-RADICAL CROSSOVER CYCLOADDITION REACTION TOWARDS THE TOTAL SYNTHESIS OF RUBRIFLORDILACTONE B 176

LIST OF TABLES

Figure 1.1: An overview of olefin cation radicals 2

Figure 1.2: Spin and charge density can be harnessed in orthogonal reaction vectors 3

Figure 1.3: Functional group decomposition resulting in cation radical generation 4

Figure 1.4: Electrochemical olefin oxidation allows for net oxidative difunctionalization 4

Figure 1.5: Chemical one electron oxidation of olefins to generate cation radicals 6

Figure 1.6: An FMO representation of single electron transfer between a donor and acceptor 7

Figure 1.7: An FMO representation of photoinduced electron transfer 9

Figure 1.8: Oxidation and reduction potentials of selected potentials donors and acceptors 11

Figure 1.9: Oxopyrylium and acridinium salts as organic photoredox catalysts 12

Figure 1.10: First examples of [2+2] dimerization initiated by single electron oxidation 14

Figure 1.11: Photoredox catalyzed arene bromination 15

Figure 1.12: Overview of popular modes of enantioinduction in catalysis 16

Figure 1.13: The enantioselective *alpha*-alkylation of aldehydes 17

Figure 1.14: PCET enables the development of an aza-Pinacol reaction 19

Figure 1.15: A Lewis acid and photoredox co-catalyzed enantioselective [2+2] cycloaddition .. 20

Figure 1.16: Application of a dual-functional chiral-at-iridium complex 21

Figure 2.1: Overview of the Diels-Alder reaction and relevant FMO interactions 27

Figure 2.2: Representative examples of catalytic enantioselective Diels-Alder reactions 28

Figure 2.3: Early representative examples of the scope cation radical Diels-Alder reaction 30

Figure 2.4: Stereochemical outcomes indicate that stepwise bond formation occurs 31

Figure 2.5: Examples of cation radical Diels-Alder reactions carried
out under PET conditions 33

Figure 2.6: A general mechanism for the cation radical Diels-Alder reaction 34

Figure 2.7: The first observation of enantioinduction in the cation
radical Diels-Alder reaction 35

Figure 2.8: Design of a new class of photoredox catalysts bearing chiral anions 36

Figure 2.9: The role of solvent polarity in influencing ion pairing interactions 38

Figure 2.10: Precedent for the ability of chiral anions to induce asymmetry catalytically 39

Figure 2.11: Range of acidities of various chiral Brønsted acids measured in MeCN 40

Figure 2.12: Synthesis of chiral anion bearing photoredox catalysts 41

Figure 2.13: Design of intramolecular cation radical DA reaction substrates 42

Figure 2.14: General strategy for intramolecular DA reaction substrates 43

Figure 2.15: Racemic results for cyclization of DA substrates using a TPT catalyst.................. 43

Figure 2.16: Screen of TP salts bearing chiral anions for their ability to induce asymmetry....... 44

Figure 2.17: Solvent effects on reactivity and selectivity 46

Figure 2.18: Catalyst loading and temperature effects on reactivity and selectivity 47

Figure 2.19: Investigating the effect of adding excess chiral anion to the reaction..................... 48

Figure 2.20: Substrate scope of the enantioselective cation radical DA after optimization 49

Figure 2.21: Select intermolecular DA results.. 50

Figure 2.22: Potential limitations of the *N*-trifylphosphoramidate anion moiety 51

Figure 2.23: Synthesis of chiral disulfonyl amides.. 51

Figure 2.24: Attempts to use disulfonyl amidate anions to influence enantioselectivity 52

Figure 2.25: Unsuccessful attempts to construct BINOL-derived
disulfonyl amides with sterically demanding functional groups at the 3,3'-positions 53

Figure 2.26: Further unsuccessful attempts to construct BINOL-derived
disulfonyl amides with sterically demanding functional groups at the 3,3'-positions 54

Figure 2.27: Imidodiphosphorate anions as potential chiral catalysts 55

Figure 2.28: Previous work demonstrating the ability of hydrogen bonding interactions to improve enantioselectivity in chiral ion pairing catalysis 56

Figure 2.29: Synthesis of triazole containing chiral anions 58

Figure 2.30: Attempts to design a cation radical DA reaction incorporating H-bonding opportunities 59

Figure 2.31: Attempts to use allylic amides as hydrogen bonding handles 60

Figure 2.32: Use of triazole containing TPT salt as a catalyst using the model substrate 60

Figure 2.33: Prior report of a cation radical aromatic Claisen rearrangement 62

Figure 2.34: Strategy for developing an asymmetric aromatic Claisen rearrangement 62

Figure 2.35: Attempts to use photoredox catalysts to catalyze aromatic Claisen rearrangements 63

Figure 2.36: Attempts to use chiral photoredox catalysts in the aromatic Claisen rearrangement 64

Figure 2.37: Attempt to carry out a standard Claisen rearrangement 65

Figure 2.38: Attempts to induce asymmetry in [2+2] cyclodaddition reactions 66

Figure 2.39: Select examples of *anti*-Markovnikov hydroacetoxylation reactions 67

Figure 2.40: Proposed mechanism for the catalytic hydroacetoxylation reaction 68

Figure 2.41: Hydroacetoxylation of substrates with allylic hydrogen bonding groups 69

Figure 2.42: Attempts to control the absolute stereochemistry of the hydroacetoxylation 71

Figure 3.1: Observation of oxazoline byproduct formation during the hydroacetoxylation of allylic amides 76

Figure 3.2: Naming and numbering conventions for oxazolines and thiazolines 76

Figure 3.3: Select examples of small molecules containing oxazoline and thiazoline moieties .. 77

Figure 3.4: Three-step oxazoline synthesis from a carboxylic acid 78

Figure 3.5: Examples of single step oxazoline syntheses from amino alcohols 79

Figure 3.6: General strategy for amide cyclization promoted by alkene activation 80

Figure 3.7: Metal-catalyzed cyclizations of propargyl amides 81

Figure 3.8: Acid-catalyzed cyclizations of allylic amides and thioamides 82

Figure 3.9: Results of a hydrogen atom donor co-catalyst screen 83

Figure 3.10: Scope of amide substitution patterns tolerated in the hydrofunctionalization reaction 84

Figure 3.11: PHOX-type ligand synthesis via copper-catalyzed coupling 85

Figure 3.12: Re-optimization of hydrogen atom donor for 2-bromoamide substrate 85

Figure 3.13: Scope of alkene substitution patterns 87

Figure 3.14: Plausible hydrofunctionalization mechanism 89

Figure 3.15: Initial scope of the allylic thioamide cyclization 90

Figure 3.16: Experiments to assess plausibility of thioamide oxidation as a mechanism 91

Figure 3.17: Plausible intermediate in thioamide cyclization reactions 92

Figure 4.1: A photoredox catalyzed PRCC and proposed mechanism 97

Figure 4.2: Observation of a key PRCC disconnect in the structure of rubriflordilactone B 98

Figure 4.3: The stereochemical outcome of PRCC reactions relevant to this study 99

Figure 4.4: Construction of the fused ABC ring system in the first reported total synthesis of rubriflordilactone A 101

Figure 4.5: An alternative lactone annulation strategy 102

Figure 4.6: Retrosynthetic analysis of rubriflordilactone B 103

Figure 4.7: Examples of a Lewis acid catalyzed MVAR reaction using a siloxyfuran nucleophile 104

Figure 4.8: Select examples of enantioselective MVAR reactions 105

Figure 4.9: A chiral titanium Lewis acid allows acrolein to be used as an electrophile in the enantioselective MVAR reaction 106

Figure 4.10: Initial optimization of the racemic MVAR between acrolein and a siloxyfuran ... 107

Figure 4.11: Derivatization of an aldol product allows relative stereochemistry to be established 108

Figure 4.12: Initial optimization of an MVAR using chiral ligands 109

Figure 4.13: Screen for MVAR reactivity with acrolein electrophile catalyzed by the Carreira catalyst 110

Figure 4.14: MVAR results with a β-TMS aldehyde electrophile 111

Figure 4.15: PRCC attempt between indene and a butenolide substituted allyl alcohol 112

Figure 4.16: PRCC initial result between indene and a vinyl TMS containing substrate 113

Figure 4.17: Proposed route to set the correct C20 methyl group stereochemistry 113

Figure 4.18: MVAR optimization with a propargaldehyde and desilation 114

Figure 4.19: H-atom donor screen in a screen for PRCC activity with a propargyl alcohol 115

LIST OF ABBREVIATIONS

$^*E_{\mathrm{red}}$ and $E_{\mathrm{red}}{}^*$	Excited state half wave reduction potential
$\bullet CF_3$	Trifluoromethyl radical
°C	Degrees Celsius
$+e^-$	Single electron reduction
$\pm H^+$	Protonation/deprotonation
$-e^-$	Single electron oxidation
^{13}C NMR	Carbon nuclear magnetic resonance spectroscopy
^{19}F NMR	Fluorine nuclear magnetic resonance spectroscopy
^{1}H NMR	Proton nuclear magnetic resonance spectroscopy
2-PMN	2-phenylmalononitrile
4-MeO-TPT	2,4,6-tris(4-methoxyphenyl)pyrylium tetrafluoroborate
9,10-DCA	9,10-dicyanoanthracene
A	Acceptor
Å	Angstrom
Ac	Acetyl
AcO^-	Acetate
AcOH	Acetic acid

Acr^+	Acridinium
Acrolein	Propenal
An	Anthracene
anti	on the opposite face
Ar	Aryl
atm	Atmosphere
b.p.	Boiling point
BDE	Bond dissociation energy
BET	Back electron transfer
$BF_3 \bullet OEt_2$	Boron trifluoride diethyl etherate
BF_4	Tetrafluoroborate
BINOL	1,1’-Bi-2-napthol
Bn	Benzyl
Boc	*tert*-Butoxycarbonyl
BOX	bis(oxazoline) ligand
bpy	2,2’-bipyridine
bpz	2,2’-bipyrazine
br s	broad singlet
Bz	Benzoyl
CAN	Ceric ammonium nitrate
cat.	Catalytic
Cbz	Carboxybenzoyl

$CDCl_3$	Chloroform−d_1
$CHCl_3$	Chloroform
Cinnamyl	3-Phenylprop-2-enyl
cis	on the same side
cm	centimeter
conc.	Concentrated
COSY	Correlation spectroscopy
D	Donor
d	doublet
d.r.	Diastereomeric ratio
DBU	1,8-Diazabicycloundec-7-ene
DCE	1,2-Dichloroethane
DCM	Dichloromethane
dd	doublet of doublets
ddd	doublet of doublets of doublets
DDQ	2,3-dichloro-5,6-dicyano-1,4-benzoquinone
decomp.	Decomposition
DFT	Density functional theory
DMAP	4-*N,N*-dimethylaminopyridine
DMF	*N,N*-Dimethylformamide
DMSO	Dimethyl sulfoxide
E	Energy
E	Entgegen

$E_{p/2}$	Half-peak oxidation potential
E_{red}	Half wave reduction potential
EC_{50}	Half maximal effective concentration
EDCI	1-Ethyl-3-(3-dimethylaminopropyl)carbodiimide
ee	enantiomeric excess
EI	Electron ionization
El	Electrophilic
endo	Endocyclic
$E_{\mathrm{p}/2}^{\mathrm{ox}}$	Half peak oxidation potential
Equiv.	Equivalent
ESI	Electrospray ionization
Et	Ethyl
$\mathrm{Et_2O}$	Diethyl ether
$\mathrm{Et_3N}$ / TEA	Triethylamine
EtOAc	Ethyl acetate
EtOH	Ethanol
exo	Exocyclic
F	Faraday constant
FMO	Frontier molecular orbital
GC-MS	Gas chromatography mass spectrometry
h	Hour
h	Planck constant

H_2SO_4	Sulfuric acid
HAD (and HAD−H)	Hydrogen atom donor
HAD$^-$	Hydrogen atom donor anion
HAT	Hydrogen atom transfer
HBr	Hydrobromic acid
HCOOH	Formic acid
HFIP	1,1,1,3,3,3-hexafluoroisopropanol
HIV	Human immunodeficiency virus
HMDS	Hexamethyldisilazane
HOMO	Highest occupied molecular orbital
HSQC	Heteronuclear single-quantum correlation spectroscopy
Hz	Hertz
*i*Pr	*iso*-Propyl
IC_{50}	Half maximal inhibitory concentration
IR	Infrared spectroscopy
J	scalar coupling constant
kcal	Kilocalorie
L	Ligand
L	Liter
LAH	Lithium aluminum hydride
Langlois reagent	Sodium trifluoromethanesulfinate
LED	Light emitting diode

LRMS	Low resolution mass spectroscopy
LUMO	Lowest unoccupied molecular orbital
m	*meta*
M	Molarity, mmol/mL
m	multiplet
Me	Methyl
MeCN	Acetonitrile
$MeNO_2$	Nitromethane
MeO	Methoxy
MeOH	Methanol
Mes	Mesityl
MHz	Megahertz
min	Minute
mL	milliliter
mmol	millimole
mol	Mole
MS	Molecular Sieves
Ms	Methanesulfonyl
MTS	Methyl thiosalicylate
MVAR	Mukaiyama Vinylogous Aldol Reaction
n	moles (of electrons transferred)
n	Normal chain
*n*Bu	Normal butyl

N/D	Not determined
nm	Nanometer
NMR	Nuclear magnetic resonance spectroscopy
NO_2	Nitro
NO_3-	Nitrate
nOe	Nuclear Overhauser enhancement
NOESY	Nuclear Overhauser effect spectroscopy
Nu	Nucleophile
o	*ortho*
O_2	Molecular oxygen
p	*para*
p-TsOH	*para*-Toluenesulfonic acid
pdt	Product
PET	Photoinduced electron transfer
PF_6	Hexafluorophosphate
PG	Protecting group
Ph	Phenyl
phen	phenanthrene
PhMe	Toluene
photo-NOCAS	Photochemical nucleophile/olefin combination
Phth	Phthalimide
pK_a	$-\log_{10}$ (acid dissociation constant)
PPh_3	Triphenylphosphine

ppm	parts per million
PPTS	Pyridinium *p*-toluenesulfinate
PRCC	Polar radical crossover cyclization
PTFE	Polytetrafluoroethylene
Py	Pyridine
q	quartet
quant.	Quantitative
R	Generic substituent
R	*rectus*
rt	Ambient/room temperature
s	singlet
S	*sinister*
s	Solvent
$SbCl_6^-$	Hexachloroantimonate
SCE	Saturated Calomel Electrode
SET	Single electron transfer
SHE	Standard hydrogen electrode
SI	Selectivity Index
SM	Starting material
SOMO	Singly occupied molecular orbital
Syn	on the same face
t	triplet
*t*Bu	*tert*-Butyl

TBS	*tert*-Butyldimethylsilyl
Tf	Trifluoromethanesulfonyl
TFA	Trifluoroacetic acid
THF	Tetrahydrofuran
TLC	Thin layer chromatography
TMS	Trimethylsilyl
TPT	2,4,6-triphenylpyrylium tetrafluoroborate
trans	on the opposite side
Ts	*para*-Toluenesulfonyl
TsO	Tosylate
V	Volts
X	X-type ligand
Z	Zusammen
δ	Chemical shift
ΔE_{coul}	Coulombic interaction term
ΔG	Change in Gibbs free energy
λ	Wavelength
μL	microliter
ν	Frequency

CHAPTER 1: INTRODUCTION TO VISIBLE LIGHT PHOTOREDOX CATALYSIS

1.1 Introduction

In recent years, there has been a veritable explosion of research in the field of photoredox catalysis.[1,2] This research has resulted in the discovery of a myriad of powerful new transformations for organic synthesis. These reactions are hallmarked by their ability to accomplish highly challenging bond constructions under operationally mild conditions. However, in spite of these successes, there persists a paucity of general solutions for carrying out these transformations in an enantioselective fashion. We propose that this stands as one of the largest challenges to the field at this time. The overarching goal of the research disclosed herein is the discovery and development of a novel means of inducing asymmetry in net redox-neutral reactions that are catalyzed by the single electron oxidation of olefinic starting materials. Before discussing the proposal for this research program, the history and fundamental principles of photoredox catalysis must first be reviewed, especially as they apply to the activation of olefins by their oxidation to cation radical intermediates. This step is key to the asymmetric cation radical Diels-Alder (DA), the first project to be discussed, as well as the racemic transformations presented in subsequent chapters. In this chapter, prior art in the development of enantioselective photoredox reactions will also be reviewed.

1.2 Olefin cation radicals: reactivity and methods for their generation

Cation radicals representing the formal single electron oxidation of olefins are high-energy intermediates that can participate in a variety of unique modes of reactivity (Figure 1.1:

An overview of olefin cation radicals).[3–7] While the reported reactions are varied, they display many common features. One major hallmark is their umpolung reactivity relative to their olefin precursors. For example, highly electron rich, and therefore nucleophilic, olefins are rendered electrophilic upon single electron oxidation and will go on to react with other nucleophiles (Figure 1.2).[8] Expected regiochemical outcomes are often reversed as well: intermolecular [2+2] cycloadditions give rise to more strained "head-to-head" adducts,[9,10] and nucleophiles attack at the position that gives rise to formal *anti*-Markovnikov addition products. Both of these examples will be discussed in detail.

Figure 1.1: An overview of olefin cation radicals

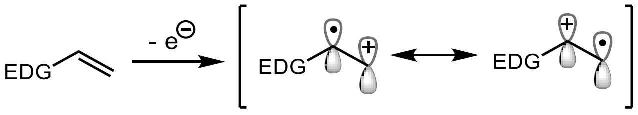

General features:
- *Umpolung reactivity: nucleophilic olefin rendered electrophilic*
- *Radical and polar reaction vectors possible*

The fact that the intermediate also possesses both spin and charge density plays a significant role in governing their reactivity patterns (Figure 1.1).[11] Many reactions have been developed that constitute formal alkene difunctionalizations, in which two reagents are subsequently added across the olefin in a net oxidative process. While two possible regioisomers can be formed, the selectivity is often predictable, as one reagent is chosen that will act as a nucleophilic trap and the other a radical trap (Figure 1.2).[8,12] The nucleophile generally adds to the position of the cation radical that results in the formation of the more stabilized of two possible radicals. The resulting radical can then combine with a variety of radical traps to give the observed products. This is typified by the photo-NOCAS reaction reported by Arnold,[8] shown below in Figure 1.2 in which methanol acts as the nucleophile and the resulting radical is trapped by an aryl radical equivalent.

Figure 1.2: Spin and charge density can be harnessed in orthogonal reaction vectors

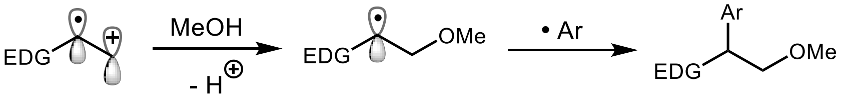
EDG
MeOH
- H⊕
EDG
OMe
• Ar
Ar
EDG
OMe

Many methods have been developed for the generation of cation radicals, one of which is the decomposition of certain functional groups. For example, Newcomb and Crich have shown that molecules bearing *O*-acyl thiohydroxamate esters vicinal to a phosphate ester will decompose upon irradiation by ultraviolet light to first generate a carbon centered radical, as shown in Figure 1.3.[13] This then promotes heterolytic bond cleavage of the adjacent phosphate ester, resulting in the generation of a cation radical, which is then trapped by allyl alcohol to ultimately produce tetrahydrofuran products. This method is well suited to carrying out basic studies on the reactivity patterns of olefin cation radical intermediates. However, the extensive pre-functionalization required of the substrates presents a significant limitation to the utility of this method in synthetic chemistry.

Figure 1.3: Functional group decomposition resulting in cation radical generation

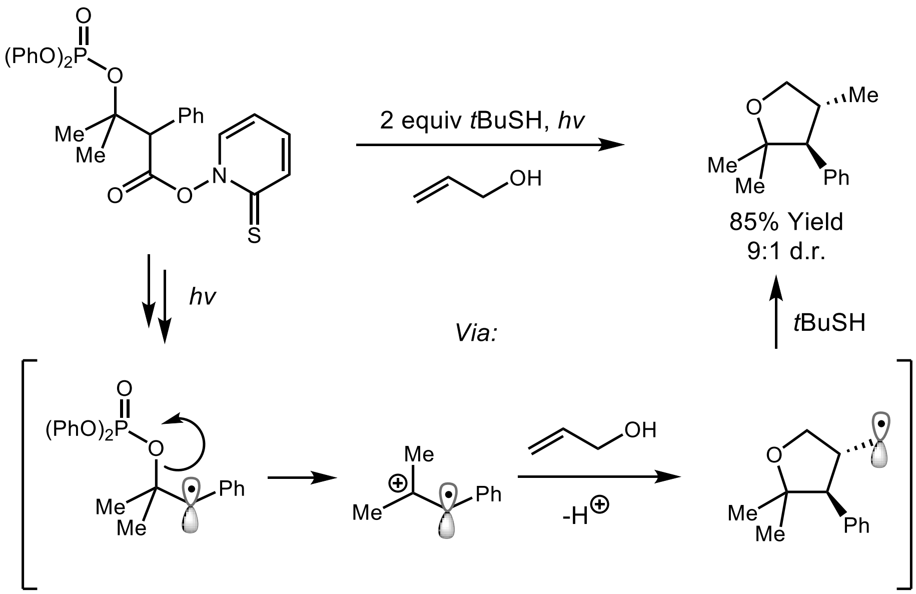
(PhO)2P
O
O
Me
Me
Ph
N
O
O
S
2 equiv *t*BuSH, *hv*
OH
O
Me
Me
Me
Ph
85% Yield
9:1 d.r.
hv
Via:
*t*BuSH
(PhO)2P
O
O
Me
Me
Ph
Me
Me
Ph
OH
-H⊕
O
Me
Me
Ph

An alternative and direct strategy is the electrochemical oxidation of an olefin using an electrolytic cell. Numerous reactions have been developed using these setups that are reviewed elsewhere.[14] Advances in the design of electrolytic cells have made these transformations accessible to the synthetic chemist, and they have been productively employed in the arena of complex molecule synthesis. However, since the continuously oxidative conditions preclude the possibility of returning electrons to the substrates, and incipient radicals are readily oxidized to carbocations, only net oxidative reactions can typically be carried out. This can be seen in the oxidative olefin difunctionalization reported by Moeller in Figure 1.4.[15] In this reaction, oxidation of an enol ether results in formation of a cation radical, which is attacked by a pendant hydroxyl group. The insipient radical is then oxidized to a carbocation, which is subsequently trapped by methanol to give the final product.

Figure 1.4: Electrochemical olefin oxidation allows for net oxidative difunctionalization

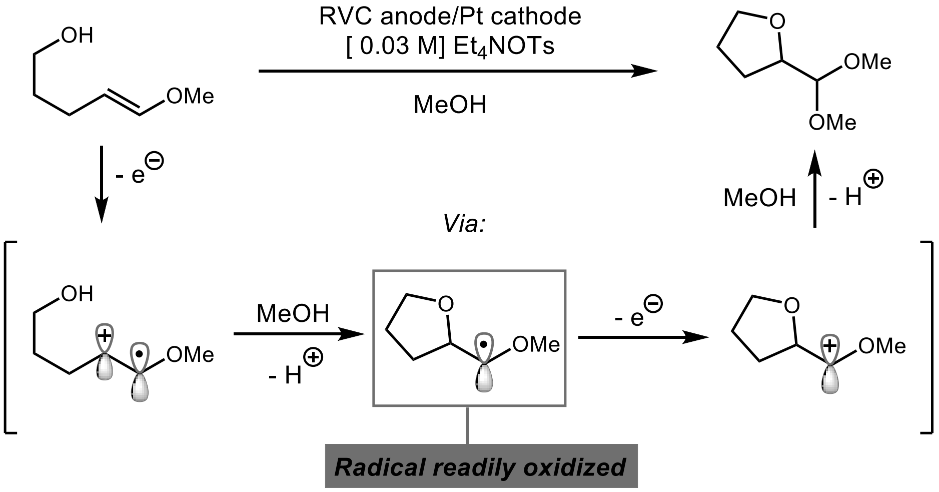

Historically, the potential use of cation radical mediated reactions in synthesis has been underexplored. A significant reason for this is likely the inherent limitations associated with the methods for their generation that have been previously discussed. Chemical oxidation is an attractive strategy that presents many benefits over both strategies presented previously.[16] This tactic involves using a second molecule, dubbed the acceptor (A), which is a sufficiently strong oxidant such that it can remove an electron from the donor substrate (D) in a single electron transfer (SET) process (Figure 1.5). Like electrochemical oxidation, cation radicals can be directly generated from precursor olefins by this method (Figure 1.5). However, because electron transfer events occur only upon collision between the substrate and oxidant, high-energy intermediates are present in lower concentrations. A major benefit of this is that it allows for oxidative and reductive processes to take place concurrently in the same reaction vessel without interfering with each other.[1] This not only allows for the oxidant to be used in catalytic quantities, but can also allow for net redox neutral reactions to be developed. As will be seen, the success of this strategy has led to the disclosure of a number of new and powerful transformations, and the scope of previously observed reactions has been significantly expanded.

Figure 1.5: Chemical one electron oxidation of olefins to generate cation radicals

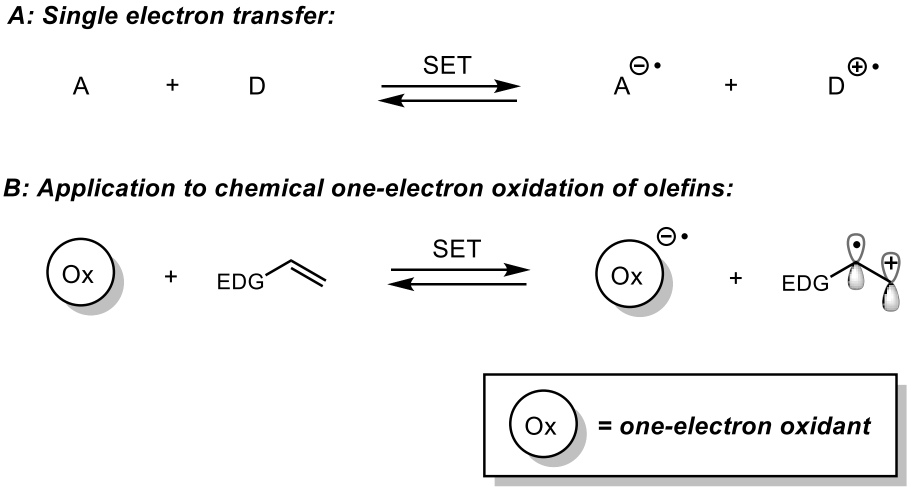
A: Single electron transfer:
A
+
D
SET
A⊖•
+
D⊕•
B: Application to chemical one-electron oxidation of olefins:
Ox
+
EDG
SET
Ox ⊖•
+
EDG
+
Ox
= one-electron oxidant

1.3 Basic principles of electron transfer and photoredox catalysis

Electron transfer between a given donor (D) and acceptor (A) is an elementary chemical process, which is mathematically well defined. In the gas phase, the free energy change for electron transfer between the donor and acceptor is given below (Equation 1):

$$\Delta G = IP_D - EA_A \ (1)$$

Here, IP_D represents the donor's ionization potential and EA_A represents the acceptor's electron affinity. In order for a particular redox event to be feasible, ΔG must be negative, meaning EA_A must be greater than IP_D. Given that these values are estimated from the respective HOMO (donor) and LUMO (acceptor) energies of the participants, this process can be visually depicted as below:

Figure 1.6: An FMO representation of single electron transfer between a donor and acceptor

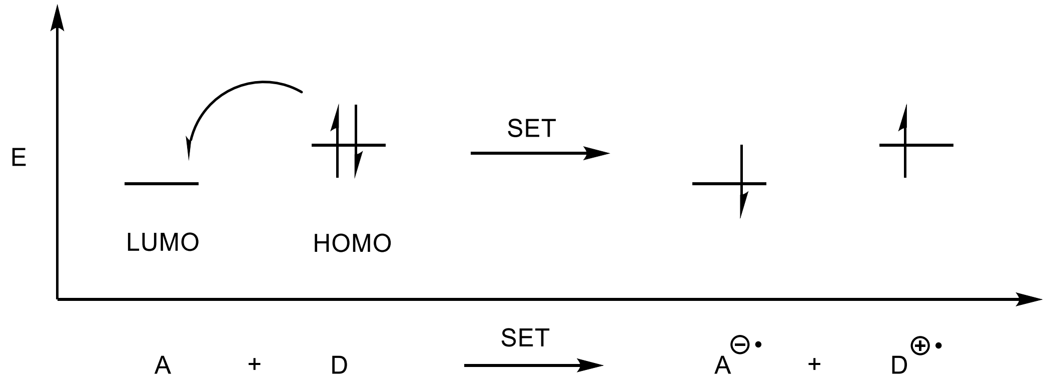

Additional factors must be taken into account when moving from the gas phase to reactions occurring in solution. In a simple situation in which an electron transfer event results in the formation of a solvent separated ion pair, the products are stabilized by both solvation (E_{solv}) and a Coulombic attraction (E_{coul}). The free energy of formation of the solvent separated ion pair (ΔG_{SSIP}) is then given by Equation 2:

$$\Delta G_{SSIP} = IP_D - EA_A - E_A^* - E_{solv} - E_{coul} \ (2)$$

The modified equation also accounts for the excitation energy of an excited acceptor species (E_A^*), if one is present in the reaction. Furthermore, EA_A and IP_D are related to the reduction potentials of the respective donor and acceptor, as shown in Equations 3 and 4:

$$IP_D = E(D^{+\cdot}/D) - \Delta G(D^{+\cdot}) + C \quad (3)$$

$$EA_A = E(A/A^{-\cdot}) - \Delta G(A^{-\cdot}) + C \quad (4)$$

In these equations, C is a constant. $\Delta G(D^{+\cdot})$ and $\Delta G(A^{-\cdot})$ represent the solvation energies of each species, and therefore can also be represented as:

$$-E_{solv} = \Delta G(D^{+\cdot}) + \Delta G(A^{-\cdot}) \quad (5)$$

From the preceding equations, the Rehm-Weller equation can be derived:

$$\Delta G_{SSIP} = 23.06[\,E(D^{+\cdot}/D) - E(A/A^{-\cdot}) - E_{Coul}\,] - E_A^* \; (6)$$

This equation can be used to determine the spontaneity of electron transfer between the ground and excited states of two different species using their respective reduction potentials and the excited state energy of the excited species. The reduction potentials found in Equations 3 through 6 can be measured using cyclic voltammetry experiments, giving values in units of volts referenced to the particular electrode used. In this text, all values given are referenced to the saturated calomel electrode (vs. SCE). Furthermore, reduction potentials are only reported for when the redox event is reversible. In these cases, such as with many of the photoredox catalysts discussed herein, values are denoted as E_{red}.

The oxidation of olefins, which are the predominant donor species in this text, is typically an irreversible process. In these cases, half-peak oxidation potentials are obtained by cyclic voltammetry experiments and are denoted as $E_{p/2}$. These potentials are obtained by calculating a simple mean between the observed onset of oxidation and the peak potential in the voltammogram. These potentials can be influenced by factors such as sweep rate, and so keeping such values constant is critical in order to establish a standard scale for comparisons. Other factors can complicate the analysis as well, such as the fact that these measurements are all obtained at the surface of an electrode as opposed to in bulk solution. Keeping these limitations in mind, reduction potentials still serve as a valuable tool for estimating if electron transfer between two species will be favorable.

As can be seen visually in Figure 1.6 and mathematically in Equation 1, the HOMO of the donor (D) must be higher in energy than the LUMO of the acceptor (A) in order for electron transfer to be exergonic ($\Delta G < 0$). This presents practical limitations to the scope of the process as it applies to synthetic chemistry, especially when one is seeking to use an olefin as the donor to be oxidized, due to their relatively high half-peak oxidation potentials ($E_{p/2}$) (Figure 1.8). Triaryl aminium salts represent some of the strongest known ground state chemical oxidants, with only the *p*-bromotriphenyl aminium salt possessing reduction potentials above +1.3 V vs. SCE.[17] Meanwhile, even highly electron rich olefins possess $E_{p/2}$ values of +1.3 V vs. SCE or greater (Figure 1.8),[6,18] meaning only a very limited number of substrates can be oxidized by these salts. In order to oxidize a variety of olefins with different substitution patterns, an alternative strategy must be devised.

Photoinduced electron transfer (PET) is a powerful mechanism for obtaining electron transfer between potential donor-acceptor pairs. Key to this process, as it relates to this research program, is the use of a fluorescent molecule as the electron acceptor. Upon excitation by a photon of visible light, an electron in the acceptor HOMO is promoted to a higher energy orbital, leaving behind a low-lying SOMO. This is mathematically observed in the excited state energy term (E_A^*) of the Rehm-Weller equation (Equation 6): a larger term serves to make the overall reaction more exergonic (Figure 1.7).

Figure 1.7: An FMO representation of photoinduced electron transfer

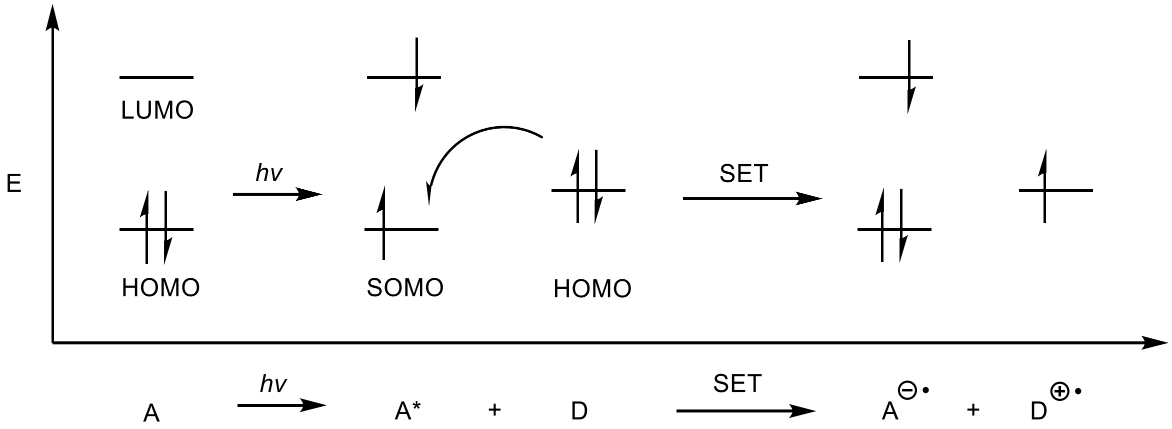

Figure 1.8 provides specific examples of potential olefinic substrates alongside one electron oxidants so that quantitative comparisons can be made. The top of the figure depicts the $E_{p/2}$ values of a variety of olefins that would be of interest to this study, with the most readily oxidizable having the lowest potentials.[5] This is overlayed with the E_{red} values of a variety of known one-electron oxidants. From this we can again see that the majority of ground state chemical oxidants are only capable of oxidizing highly electron rich olefins such as styrene derivatives. Thus, in order to establish a general strategy based around activating olefins by oxidizing them to cation radical intermediates, it is clear that photooxidants are best suited to the challenge due to their remarkably high E_{red} values. These can range from +0.81 V vs. SCE for the excited state of ruthenium trisbipyridine dichloride (*Ru(bpy)$_3$Cl$_2$)[19] to greater than +2.1 V vs. SCE for 9-mesityl-10-methyl-acridinium tetrefluoroborate (Mes-Acr).[20]

Figure 1.8: Oxidizing capabilities of selected electron donors and acceptors

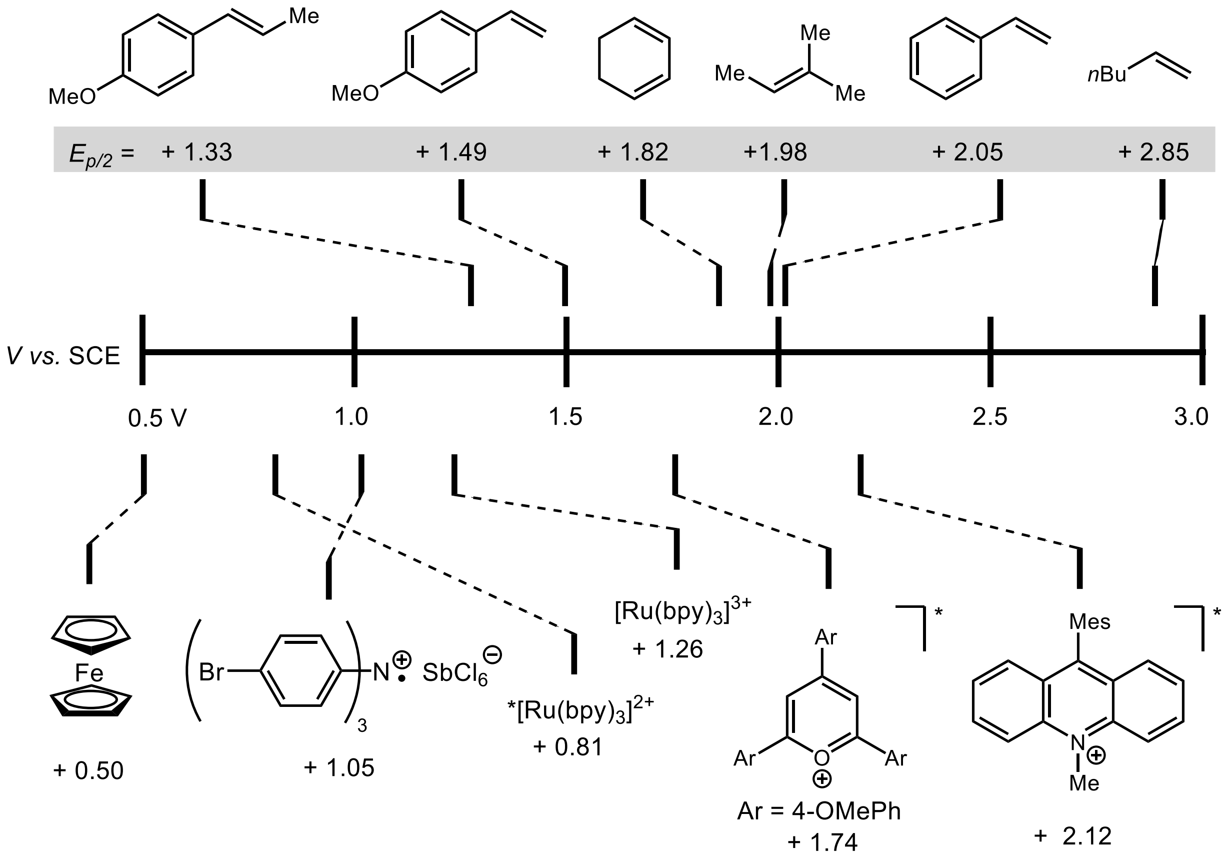
Me
MeO
MeO
Me
Me
Me
nBu
Ep/2 =
+ 1.33
+ 1.49
+ 1.82
+1.98
+ 2.05
+ 2.85
V vs. SCE
0.5 V
1.0
1.5
2.0
2.5
3.0
Fe
+ 0.50
Br
N
SbCl6
3
+ 1.05
*[Ru(bpy)3]2+
+ 0.81
[Ru(bpy)3]3+
+ 1.26
Ar
Ar
Ar
O
Ar = 4-OMePh
+ 1.74
*
Mes
N
Me
+ 2.12
*

1.4 Photoredox catalysts

Seminal work in the field of photoredox catalysis centered around the use of Ru(bpy)$_3$Cl$_2$ complexes as the catalyst.[21–23] These and other related organometallic complexes have astonishing photophysical properties that make them ideal for this application, with one of them being their long excited state lifetimes (as long as 1100 ns in MeCN).[19,24] This long lived excited state is due to a metal-to-ligand charge transfer event that occurs upon excitation, and serves to substantially delay a return to the ground state. A long excited state lifetime increases the probability that it will encounter the substrate, and so can help improve the overall rate of reaction. Modification of the ligand set can be used to develop more strongly oxidizing catalysts, with variants possessing excited state reduction potentials as high as +1.45 V vs. SCE,[25] allowing for the oxidation of electron rich styrene derivatives.

In order to oxidize a wider number of olefins, especially non-styrene derivatives, even stronger oxidants are needed, which is where we turn our attention to the use of organic photoredox catalysts. The 2,4,6-triphenyl pyrylium tetrafluoroborate (TPT) and 9-mesityl-10-methyl acridinium (Mes-Acr) classes of cationic organic compounds serve as far more strongly oxidizing electron acceptors, with some having potentials >2.00 V vs. SCE in their excited state. Another advantage of oxopyrilium salts is that their redox potential is readily tuned by altering the substituents on the three phenyl rings (Figure 1.9), and several examples have been reported. Potential drawbacks to their use include short excited state lifetimes (~9 ns) and sensitivity to degradation by nucleophiles, given the electrophilic nature of the compound (Figure 1.9).

Figure 1.9: Oxopyrylium and acridinium salts as organic photoredox catalysts

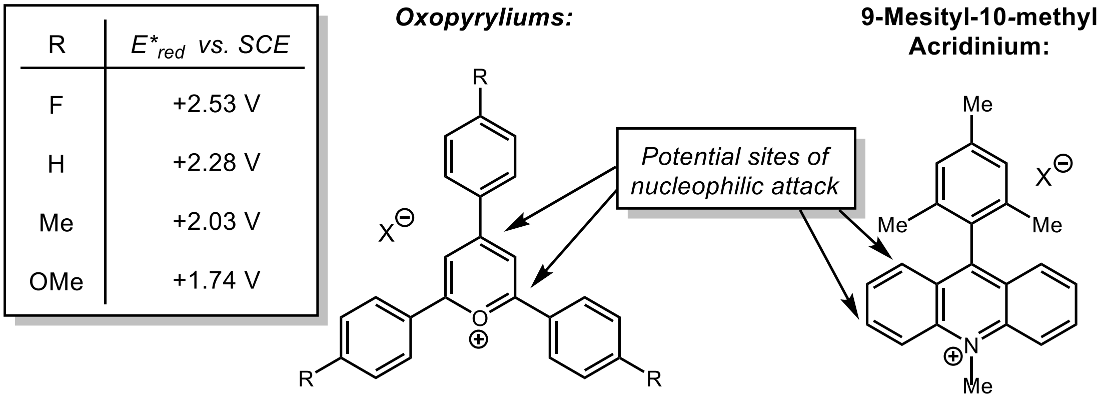

R	E^*_{red} vs. SCE
F	+2.53 V
H	+2.28 V
Me	+2.03 V
OMe	+1.74 V

Oxopyryliums:
9-Mesityl-10-methyl Acridinium:
R
X⊖
O
⊕
R
R
Potential sites of nucleophilic attack
Me
X⊖
Me
Me
⊕N
Me

The Mes-Acr salts reported by Fukuzumi have also recently garnered attention for their use as photoredox catalysts. In addition to their high excited state reduction potentials (+2.12 V vs. SCE), a triplet state has been observed with a lifetime on the order of microseconds that possesses strongly oxidizing capabilities. The exact nature of the triplet state, specifically whether it is a locally excited or intramolecular charge transfer state, is a matter of ongoing debate. The catalysts have also empirically been observed to be resistant to degradation by nucleophiles,[26] which is proposed to be a result of the mesityl group having a steric shielding effect.

1.5 Early examples of olefin activation via single electron oxidation

While olefin cation radicals have been known since much earlier as intermediates observed by mass spectrometry, one of the first examples in which they were employed as synthetic intermediates was in the dimerization of *N*-vinyl carbazole (Figure 1.10).[9] The reaction was first reported using chemical oxidants, and shortly thereafter with TPT photoredox catalysts,[7] beginning a rich field of study into the development of electron transfer catalyzed cycloaddition reactions. A notable feature of this reaction is the formation of the more sterically-strained “head-to-head” adduct with complete selectivity, which is proposed to arise from the intermediacy of a stabilized α-amino distonic radical cation. This preludes what will become another general feature of cation radical reactions: the formation of adducts with regioselectivity complementary to that arrived at by more conventional mechanisms.

Figure 1.10: First examples of [2+2] dimerization initiated by single electron oxidation

Dimerization with ground state oxidant:

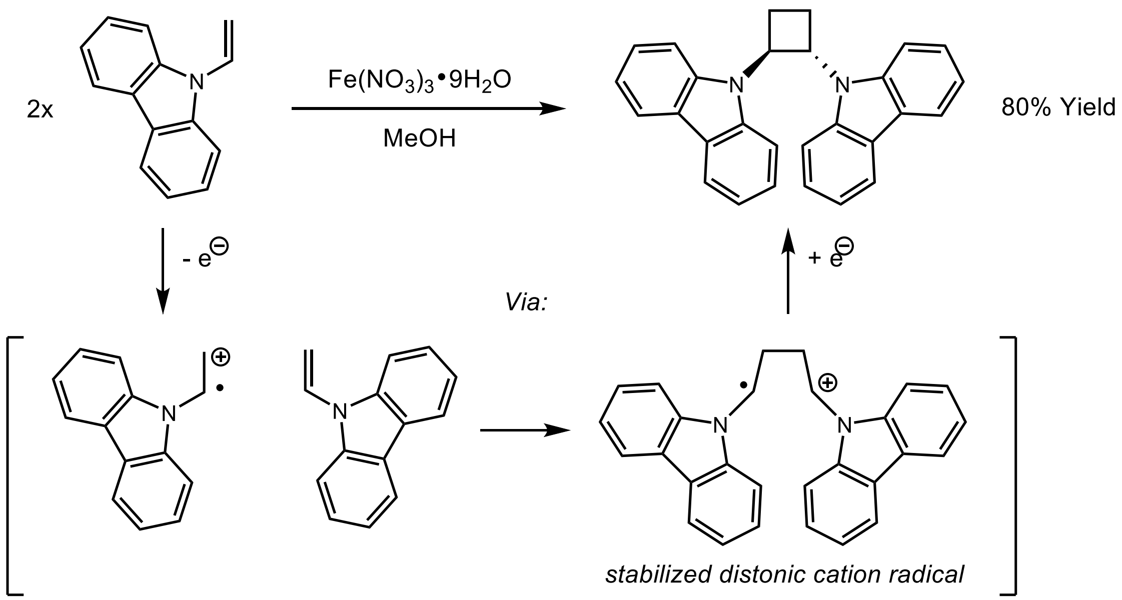

Dimerization under photoredox conditions:

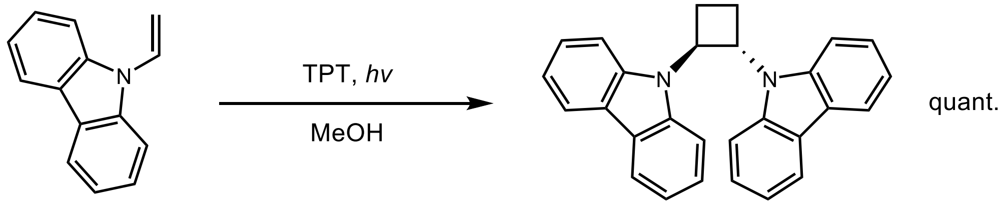

Following this initial disclosure, this strategy of catalyzing cycloadditions by single electron oxidation of the starting material has been successfully applied to a number of transformations including crossed [2+2] cycloadditions,[27,28] [2+2+2] oxygenations,[29,30] and [4+2] Diels-Alder (DA) reactions.[31] As it provides the basis for the research presented in this report, the cation radical DA will be given a thorough discussion separately in the following chapter.

The Mes-Acr photoredox catalyst discussed earlier, originally developed by Fukuzumi, has been successfully employed as a photoredox catalysts in several transformations to date.[32–34] One of these reactions is the photocatalytic bromination of electron rich arenes.[32] In this reaction, the excited state of the catalyst oxidizes an electron rich arene to a cation radical intermediate.

This is then trapped by a bromide ion, and subsequent hydrogen atom abstraction forms the brominated products. Oxygen was found to be a suitable terminal oxidant, serving to both turn over the catalyst as well as carry out the hydrogen atom abstraction to produce hydrogen peroxide. It is also proposed that hydrogen peroxide can re-enter the catalyst cycle as an oxidant to ultimately generate water as the stoichiometric waste product.

Figure 1.11: Photoredox catalyzed arene bromination

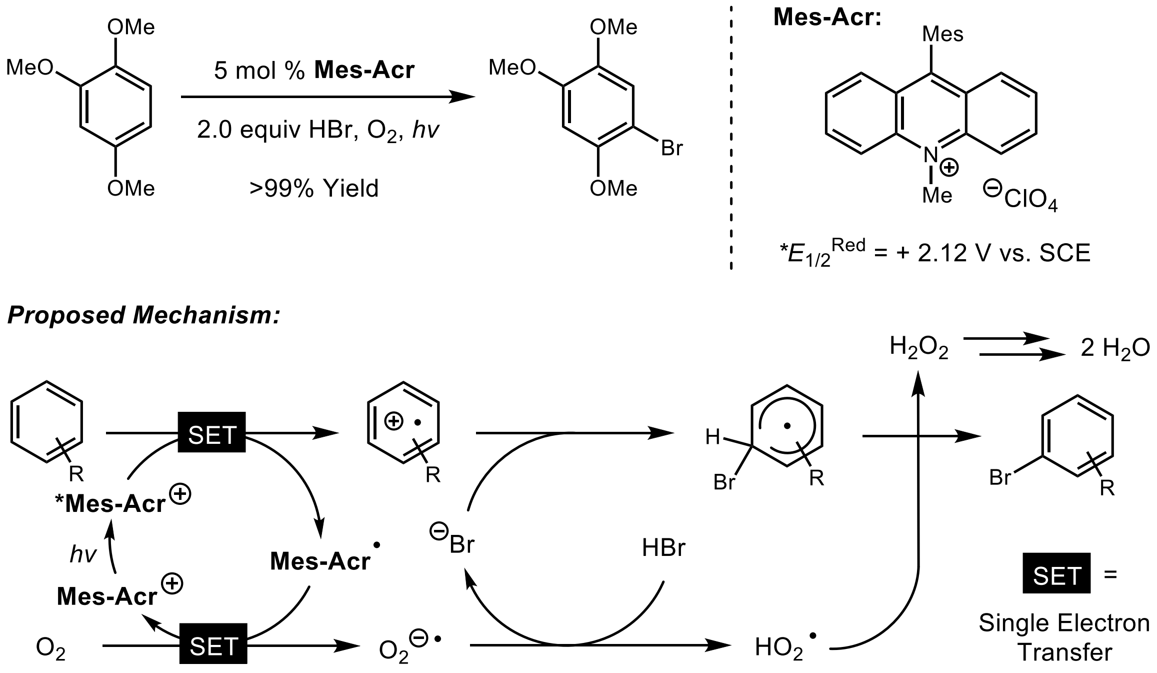
OMe
MeO
OMe
5 mol % Mes-Acr
2.0 equiv HBr, O2, hv
>99% Yield
OMe
MeO
Br
OMe
Mes-Acr:
Mes
N⊕
Me
⊖ClO4
*E1/2Red = + 2.12 V vs. SCE
Proposed Mechanism:
R
SET
*Mes-Acr⊕
hv
Mes-Acr⊕
O2
SET
Mes-Acr•
⊕•
R
⊖Br
O2⊖•
H
Br
R
HBr
HO2•
H2O2
2 H2O
Br
R
SET =
Single Electron Transfer

1.6 Prior examples of enantioselective photoredox reactions

The development of enantioselective transformations stands as one of the most formidable challenges to the field of photoredox catalysis at this point in time. Numerous hurdles exist to the development of such reactions. One potential issue is the configurational instability of radicals and radical ions, which can pose a challenge to controlling their stereochemistry in any sense.

Figure 1.12: Overview of popular modes of enantioinduction in catalysis

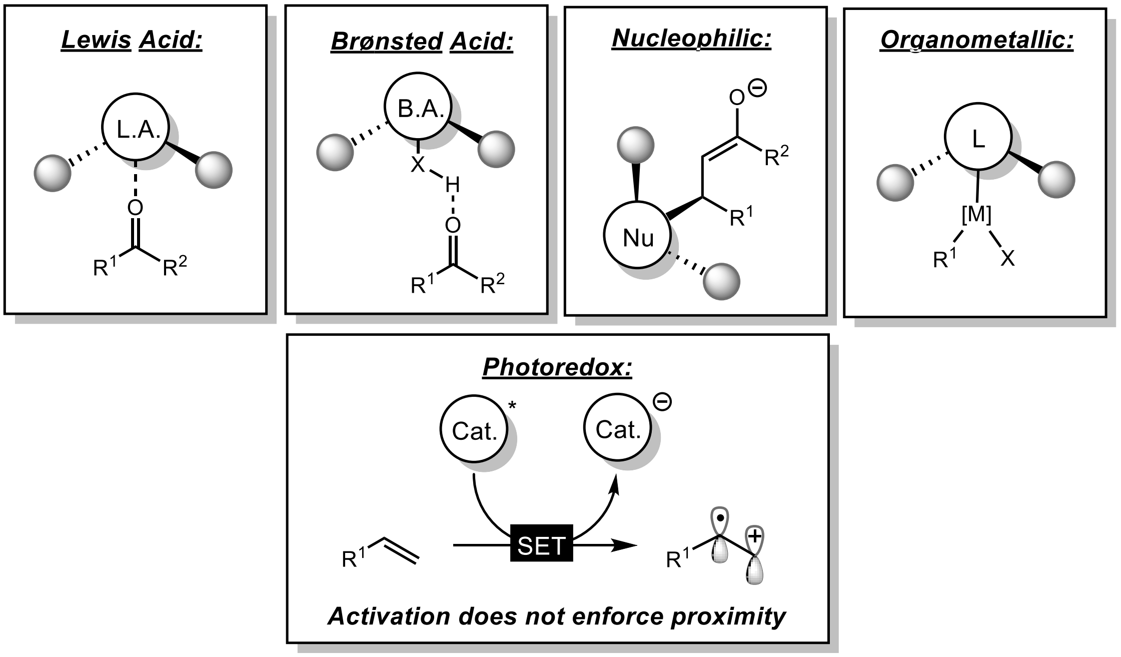

Activation does not enforce proximity

More importantly, the most popular and successful strategy for rendering a catalytic reaction enantioselective is to employ a catalyst that incorporates an element of chirality into its periphery.[35] Now, upon activation of the substrate by the catalyst, a chiral complex is formed such that the stereochemistry of subsequent steps is influenced by the catalyst's chirality, inducing asymmetry. Photoredox catalysis is not readily amenable to such strategies, though they have been attempted.[36,37] The reason for this is that after the activating electron transfer event, the catalyst and substrate are no longer necessarily associated with each other (Figure 1.12). In fact, designing a system in which their proximity is enforced post-electron transfer would potentially be detrimental to reactivity, as this would facilitate back electron transfer to regenerate starting material.

The challenge then becomes to design a system in which an additional element of chirality becomes associated with the prochiral intermediates during the enantio-determining step of the reaction. The successful implementation of such a method would hinge on eliminating the possibility of any racemic background pathways. In discussing prior art in this field, we draw a distinction between enantioselective photoredox catalysis, which centers around the excitation of the catalyst by a photon, and enantioselective photochemistry in which the substrate is directly excited by light. We limit our discussion here to the former. While there has also been groundbreaking research in enantioselective photochemistry in recent years, it is not directly related to this project and so is beyond the scope of discussion.

Figure 1.13: The enantioselective α-alkylation of aldehydes

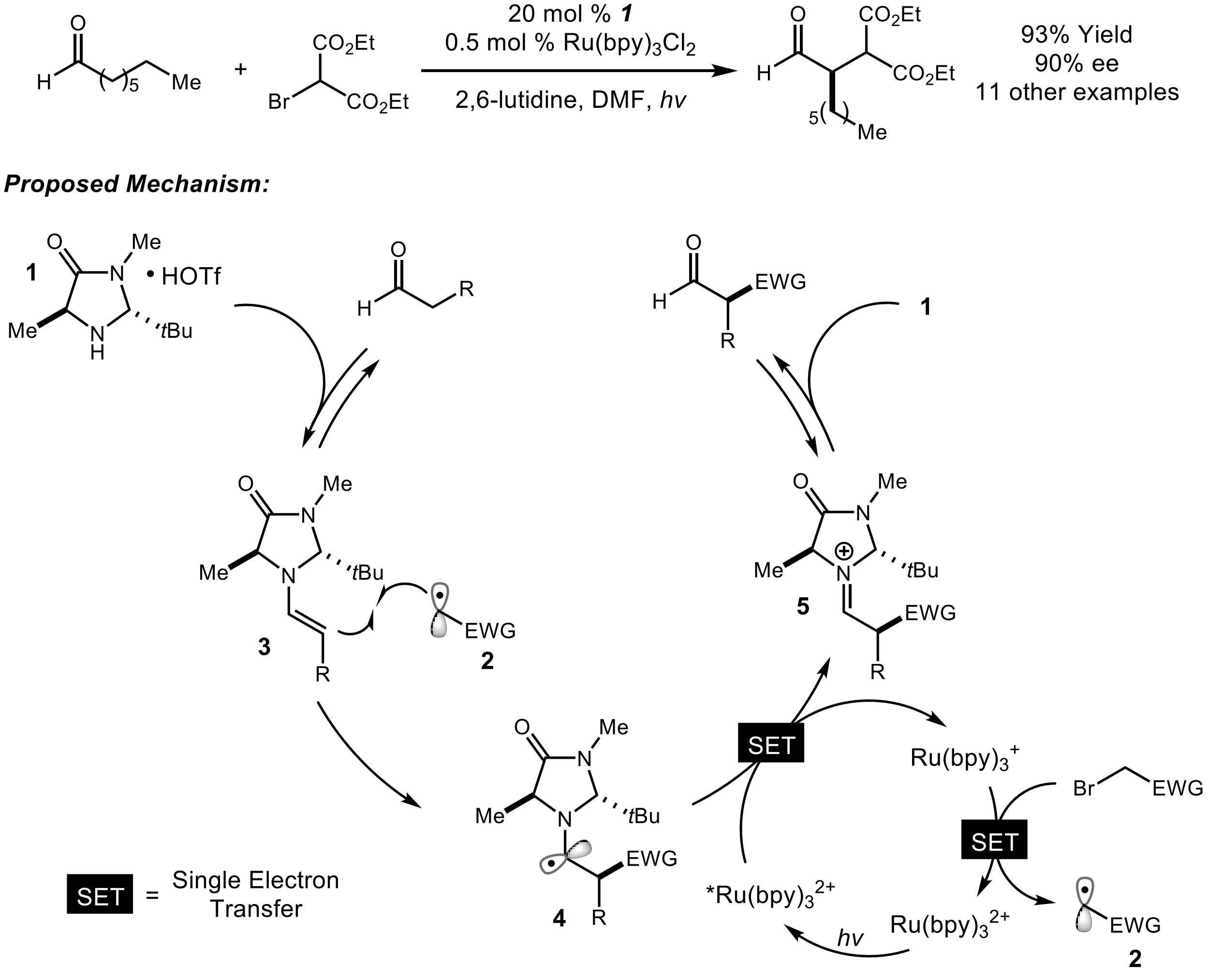

20 mol % 1
0.5 mol % Ru(bpy)3Cl2
2,6-lutidine, DMF, hv
93% Yield
90% ee
11 other examples
Proposed Mechanism:
1
• HOTf
3
2
4
5
SET
Ru(bpy)3+
*Ru(bpy)32+
Ru(bpy)32+
hv
SET = Single Electron Transfer

Pioneering work in this field was carried out by the MacMillan lab, who were able to use photoredox catalysis in conjunction with chiral enamine catalysis to accomplish the enantioselective α-alkylation of aldehydes (Figure 1.13).[22] In this seminal report, a chiral imidazolidinone catalyst condenses onto the aldehyde of the starting material, generating an enamine intermediate (**3**). Meanwhile in the simultaneous photoredox cycle, a reducing equivalent of Ru(bpy)$_2^+$ is generated that donates an electron to an alkyl bromide, generating an electron deficient radical after expulsion of bromide (**2**). This radical then encounters the chiral enamine compound and combines to form an enantioenriched α-amino radical species (**4**). This radical then serves to reduce *Ru(bpy)$_3^{2+}$ back to Ru(bpy)$_3^+$. Hydrolysis of the resultant iminium ion furnishes the alpha-alkylated product and regenerates the imidazolidinone catalyst.

Figure 1.14: PCET enables the development of an aza-Pinacol reaction

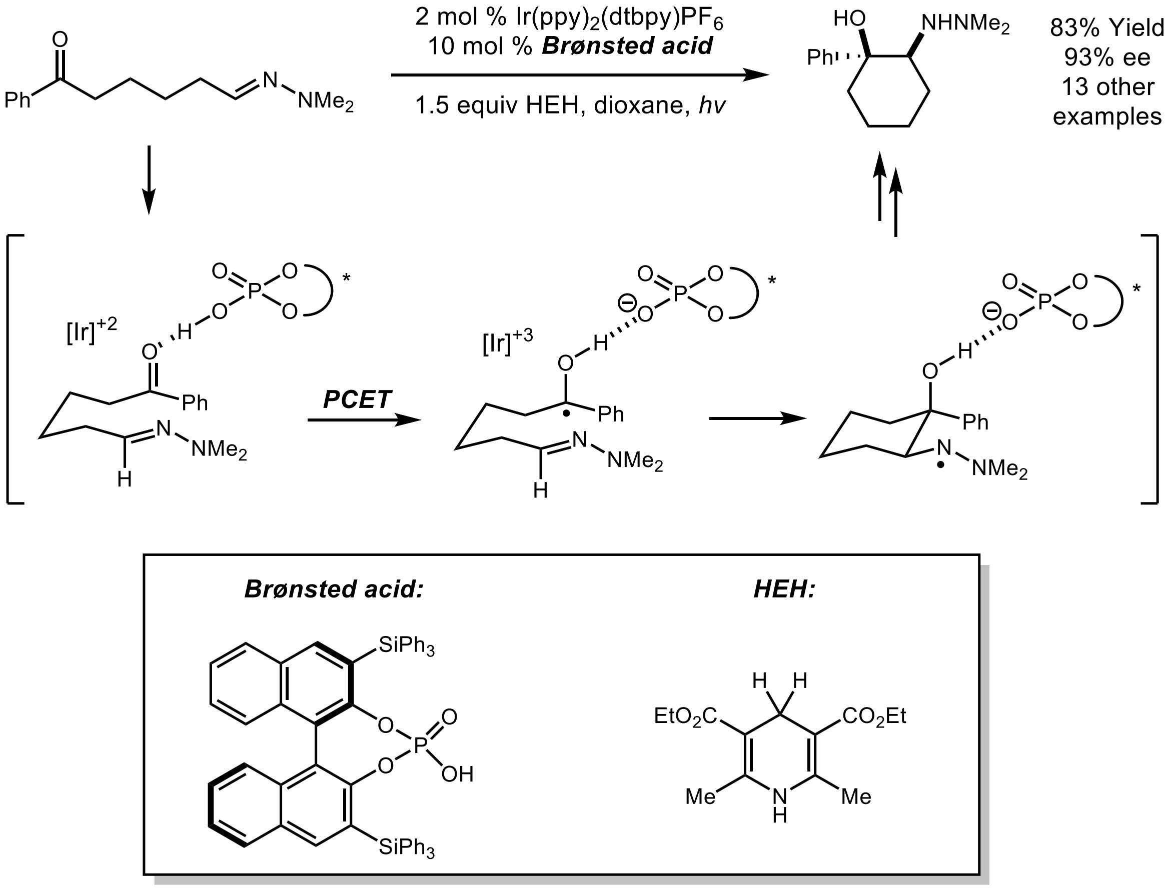

O
Ph
N
NMe2
2 mol % Ir(ppy)2(dtbpy)PF6
10 mol % Brønsted acid
1.5 equiv HEH, dioxane, hv
HO
NHNMe2
Ph
83% Yield
93% ee
13 other examples
[Ir]+2
PCET
[Ir]+3
*
Brønsted acid:
SiPh3
OH
HEH:
EtO2C
CO2Et
Me
N
H

The Knowles group has subsequently developed an asymmetric aza-Pinacol cyclization that centers around the use of proton coupled electron transfer (PCET) in order to form a chiral activated complex (Figure 1.14).[38] The strategy also employs a dual catalyst system comprised of the $Ru(bpy)_3^{2+}$ complex and a chiral phosphoric acid. In the proposed mechanism, the chiral phosphoric acid forms a hydrogen bonding complex with a carbonyl functional group in the starting material. This LUMO-lowering hydrogen bonding interaction effectively lowers the reduction potential of the carbonyl. Upon encountering $*Ru(bpy)_3^{2+}$, the substrate is simultaneously protonated and reduced, forming a neutral ketyl radical. The ketyl radical retains its hydrogen bonding interaction with the chiral phosphate, which is sufficient to control the absolute stereochemistry of the subsequent enantiodetermining C—C bond forming step. A number of substrates were shown to cyclize in good yields with high levels of enantioselectivity, though notably the methodology appears to be limited to α-aryl ketones.

Figure 1.15: A Lewis acid and photoredox co-catalyzed enantioselective [2+2] cycloaddition

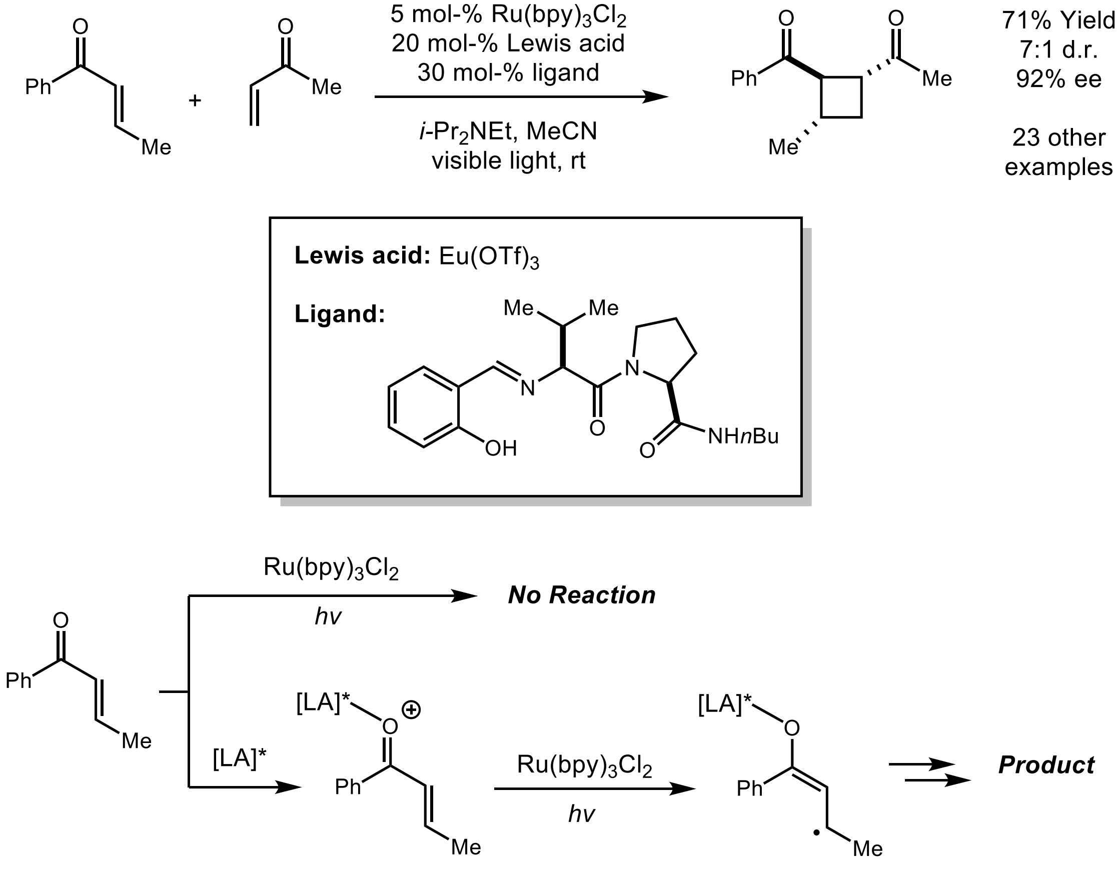
O
Ph
Me
+
O
Me
5 mol-% $Ru(bpy)_3Cl_2$
20 mol-% Lewis acid
30 mol-% ligand
i-Pr_2NEt, MeCN
visible light, rt
O
Ph
O
Me
Me
71% Yield
7:1 d.r.
92% ee
23 other examples
Lewis acid: $Eu(OTf)_3$
Ligand:
Me
Me
N
O
N
OH
O
NH*n*Bu
$Ru(bpy)_3Cl_2$
hv
No Reaction
[LA]*
[LA]*
O
Ph
Me
$Ru(bpy)_3Cl_2$
hv
[LA]*
O
Ph
Me
Product

Recently, the Yoon group has employed a similar strategy that enables them to carry out enantioselective crossed [2+2] cycloadditions between enones.[39] In this case, a chiral Lewis acid is used as the co-catalyst, which also has a LUMO-lowering effect on the enone substrate. This ensures that only substrates complexed with the Lewis acid will be reduced by the photoredox catalyst, in this case again $Ru(bpy)_3^{2+}$. In a control experiment, they demonstrate that no productive reactivity is observed in the absence of the Lewis acid, indicating that the substrate cannot be directly reduced by the photoredox catalyst, which would result in a background racemic reaction. After reduction of the complexed enone, an equivalent of acrolein is encountered, and a [2+2] cycloaddition occurs to generate the desired products.

Figure 1.16: Application of a dual-functional chiral-at-iridium complex

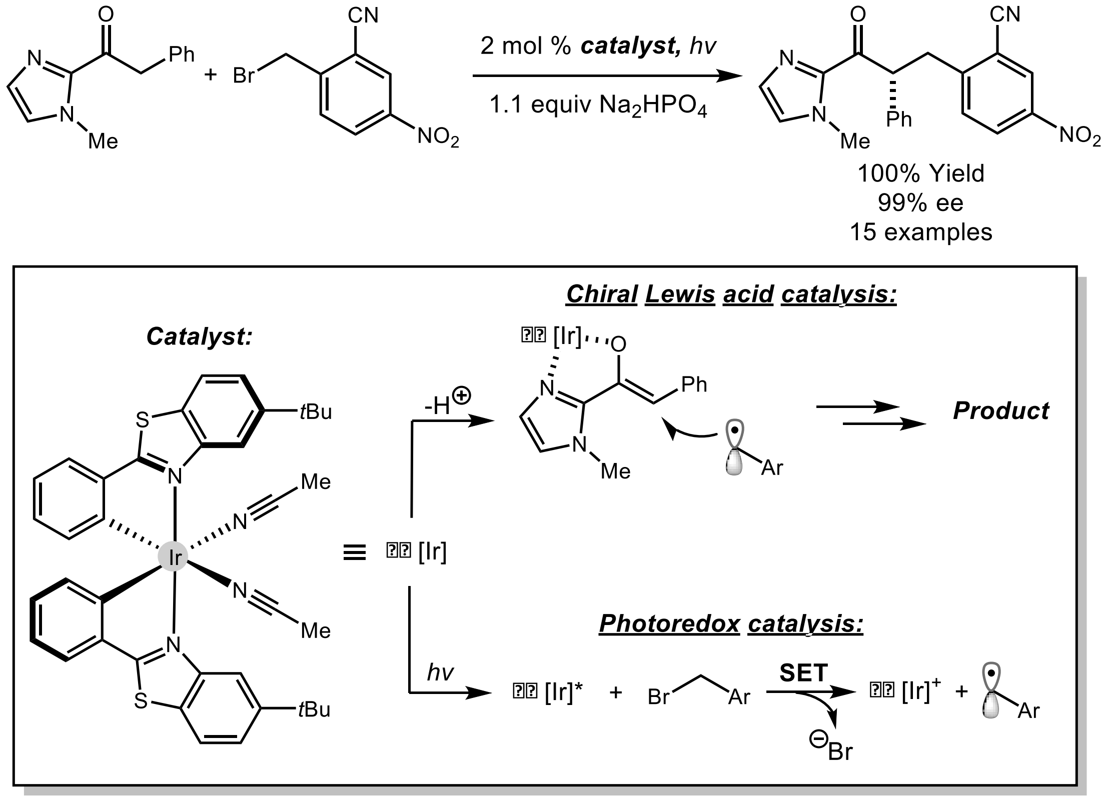
2 mol % catalyst, hv
1.1 equiv Na_2HPO_4
100% Yield
99% ee
15 examples
Catalyst:
Chiral Lewis acid catalysis:
Photoredox catalysis:
-H⊕
hv
SET
Product
≡ [Ir]
[Ir]*
[Ir]+
⊖Br
tBu
Me
Ph
Ar
NO2
CN
Br

A chiral-at-iridium complex has recently been reported by the Meggers group that, in a related reaction manifold, separately acts as both a chiral Lewis acid and photoredox catalyst.[40]

This catalyst is used to carry out the asymmetric α-alkylation of acyl imidazoles (Figure 1.16). In a mechanism analogous to the MacMillan transformation discussed earlier (Figure 1.13), the excited state of the iridium photoredox catalyst first reduces an electron deficient alkyl bromide, producing an electron deficient radical species. At the same time, a second equivalent of the iridium complex associates with the acyl imidazole substrate, resulting in enolate formation upon deprotonation by the included equivalent of weak base. The activated substrate then encounters the previously generated alkyl radical in the enantio-determining radical addition step. This radical anion intermediate reduces the equivalent of the catalyst used in the photoredox cycle to regenerate the active species, completing the cycle. The transformation gives very high levels of enantioinduction with a variety of substrates.

These first reports in the field of enantioselective photoredox have allowed for the development of powerful new transformations and provide insight into factors governing selectivity that will guide future studies. There are many features that unite these reactions, one of the most obvious being the central importance of carbonyls as handles for both reactivity and association with the chiral co-catalyst. Additionally, the photoredox catalysts employed activate the substrates by single electron reduction in each case. No general methods have been developed to control the absolute stereochemistry of reactions proceeding via single electron oxidation of the substrate, which is a limitation that we seek to address herein.

REFERENCES

(1) Prier, C. K.; Rankic, D. A.; MacMillan, D. W. C. *Chem. Rev.* **2013**, *113* (7), 5322–5363.

(2) Nicewicz, D. A.; Nguyen, T. M. *ACS Catal.* **2014**, *4* (1), 355–360.

(3) Schmittel, M.; Burghart, A. *Angew. Chem. Int. Ed. Engl.* **1997**, *36* (23), 2550–2589.

(4) Campbell, J. M.; Xu, H.-C.; Moeller, K. D. *J. Am. Chem. Soc.* **2012**, *134* (44), 18338–18344.

(5) Johnston, L. J.; Schepp, N. P. *J. Am. Chem. Soc.* **1993**, *115* (15), 6564–6571.

(6) Lew, C. S. Q.; Brisson, J. R.; Johnston, L. J. *J. Org. Chem.* **1997**, *62* (12), 4047–4056.

(7) Ledwith, A. *Acc. Chem. Res.* **1972**, *5* (4), 133–139.

(8) Mangion, D.; Arnold, D. R. *Acc. Chem. Res.* **2002**, *35* (5), 297–304.

(9) Crellin, R. A.; Lambert, M. C.; Ledwith, A. *J. Chem. Soc. Chem. Commun.* **1970**, No. 11, 682–683.

(10) Bell, F. A.; Crellin, R. A.; Fujii, H.; Ledwith, A. *J. Chem. Soc. Chem. Commun.* **1969**, No. 6, 251–252.

(11) Tanko, J. M.; Phillips, J. P. *J. Am. Chem. Soc.* **1999**, *121* (25), 6078–6079.

(12) Cao, M.-Y.; Ren, X.; Lu, Z. *Tetrahedron Lett.* **2015**, *56* (24), 3732–3742.

(13) Crich, D.; Huang, X.; Newcomb, M. *J. Org. Chem.* **2000**, *65* (2), 523–529.

(14) Moeller, K. D. *Tetrahedron* **2000**, *56* (49), 9527–9554.

(15) Sutterer, A.; Moeller, K. D. *J. Am. Chem. Soc.* **2000**, *122* (23), 5636–5637.

(16) Kavarnos, G. J.; Turro, N. J. *Chem. Rev.* **1986**, *86* (2), 401–449.

(17) Giese, G.; Heesing, A. *Chem. Ber.* **1991**, *124* (11), 2623–2628.

(18) Schepp, N. P.; Johnston, L. J. *J. Am. Chem. Soc.* **1996**, *118* (12), 2872–2881.

(19) Juris, A.; Balzani, V.; Belser, P.; von Zelewsky, A. *Helv. Chim. Acta* **1981**, *64* (7), 2175–2182.

(20) Fukuzumi, S.; Kotani, H.; Ohkubo, K.; Ogo, S.; Tkachenko, N. V.; Lemmetyinen, H. *J. Am. Chem. Soc.* **2004**, *126* (6), 1600–1601.

(21) Teplý, F. *Collect. Czechoslov. Chem. Commun.* **2011**, *76* (7), 859–917.

(22) Nicewicz, D. A.; MacMillan, D. W. C. *Science* **2008**, *322* (5898), 77–80.

(23) Ischay, M. A.; Anzovino, M. E.; Du, J.; Yoon, T. P. *J. Am. Chem. Soc.* **2008**, *130* (39), 12886–12887.

(24) Juris, A.; Balzani, V.; Barigelletti, F.; Campagna, S.; Belser, P.; von Zelewsky, A. *Coord. Chem. Rev.* **1988**, *84*, 85–277.

(25) Crutchley, R. J.; Lever, A. B. P. *J. Am. Chem. Soc.* **1980**, *102* (23), 7128–7129.

(26) Wilger, D. J.; Grandjean, J.-M. M.; Lammert, T. R.; Nicewicz, D. A. *Nat. Chem.* **2014**, *6* (8), 720–726.

(27) Riener, M.; Nicewicz, D. A. *Chem. Sci.* **2013**, *4* (6), 2625–2629.

(28) Ischay, M. A.; Lu, Z.; Yoon, T. P. *J. Am. Chem. Soc.* **2010**, *132* (25), 8572–8574.

(29) Parrish, J. D.; Ischay, M. A.; Lu, Z.; Guo, S.; Peters, N. R.; Yoon, T. P. *Org. Lett.* **2012**, *14* (6), 1640–1643.

(30) Gesmundo, N. J.; Nicewicz, D. A. *Beilstein J. Org. Chem.* **2014**, *10*, 1272–1281.

(31) Bauld, N. L.; Bellville, D. J.; Harirchian, B.; Lorenz, K. T.; Pabon Jr, R. A.; Reynolds, D. W.; Wirth, D. D.; Chiou, H. S.; Marsh, B. K. *Acc. Chem. Res.* **1987**, *20* (10), 371–378.

(32) Ohkubo, K.; Mizushima, K.; Iwata, R.; Fukuzumi, S. *Chem. Sci.* **2011**, *2* (4), 715.

(33) Ohkubo, K.; Fujimoto, A.; Fukuzumi, S. *Chem. Commun.* **2011**, *47* (30), 8515–8517.

(34) Ohkubo, K.; Suga, K.; Fukuzumi, S. *Chem. Commun.* **2006**, No. 19, 2018–2020.

(35) Walsh, P.; Kowzlowski, M. *Fundamentals Of Asymmetric Catalysis*; University Science Books: Sausalito, Calif, 2008.

(36) Hamada, T.; Ishida, H.; Usui, S.; Watanabe, Y.; Tsumura, K.; Ohkubo, K. *J. Chem. Soc. Chem. Commun.* **1993**, No. 11, 909–911.

(37) Hamada, T.; Ishida, H.; Usui, S.; Tsumura, K.; Ohkubo, K. *J. Mol. Catal.* **1994**, *88* (1), L1–L5.

(38) Rono, L. J.; Yayla, H. G.; Wang, D. Y.; Armstrong, M. F.; Knowles, R. R. *J. Am. Chem. Soc.* **2013**, *135* (47), 17735–17738.

(39) Du, J.; Skubi, K. L.; Schultz, D. M.; Yoon, T. P. *Science* **2014**, *344* (6182), 392–396.

(40) Huo, H.; Shen, X.; Wang, C.; Zhang, L.; Röse, P.; Chen, L.-A.; Harms, K.; Marsch, M.; Hilt, G.; Meggers, E. *Nature* **2014**, *515* (7525), 100–103.

CHAPTER 2: THE DEVELOPMENT OF AN ENANTIOSELECTIVE CATION RADICAL DIELS-ALDER REACTION

In this chapter we disclose our strategy and progress towards the development of an enantioselective cation radical Diels-Alder reaction. Before the disclosure of this methodology, it would be beneficial to take a thorough look at the history and features of this transformation.

2.1 Overview of the traditional Diels-Alder reaction

The Diels-Alder (DA) reaction remains one of the most powerful transformations available in the practicing synthetic chemist's arsenal.[1,2] This [4+2] cycloaddition occurs between an appropriate diene and dienophile, and is hallmarked by broad substrate scope and predicable stereochemical outcomes, allowing for two carbon-carbon bonds and up to four contiguous stereocenters to be constructed in a single operation with complete atom economy.

The favorability of a particular DA reaction is dictated by the HOMO (highest occupied molecular orbital)-LUMO (lowest unoccupied molecular orbital) gap between the diene and dienophile components (Figure 2.1). In a normal demand DA reaction, dienophiles are employed that bear electron withdrawing substituents that provide a LUMO (lowest unoccupied molecular orbital) lowering effect. Reactivity is most favorable when these are used in conjunction with highly electron rich dienes, as they would possess high lying HOMOs (highest occupied molecular orbital). Numerous examples of inverse demand DA reactions have been reported as well,[3] in which the situation is reversed and an electron deficient diene undergoes cyclization with an electron rich dienophile.

A variety of catalysts have been shown to further enhance the rate of both normal and inverse demand Diels-Alder reactions,[4] with Lewis and Brønsted acids being among the most commonly employed. In these cases, the observed rate enhancement is the result of the catalyst associating with the dienophile, which has a further LUMO lowering effect.

Figure 2.1: Overview of the Diels-Alder reaction and relevant FMO interactions

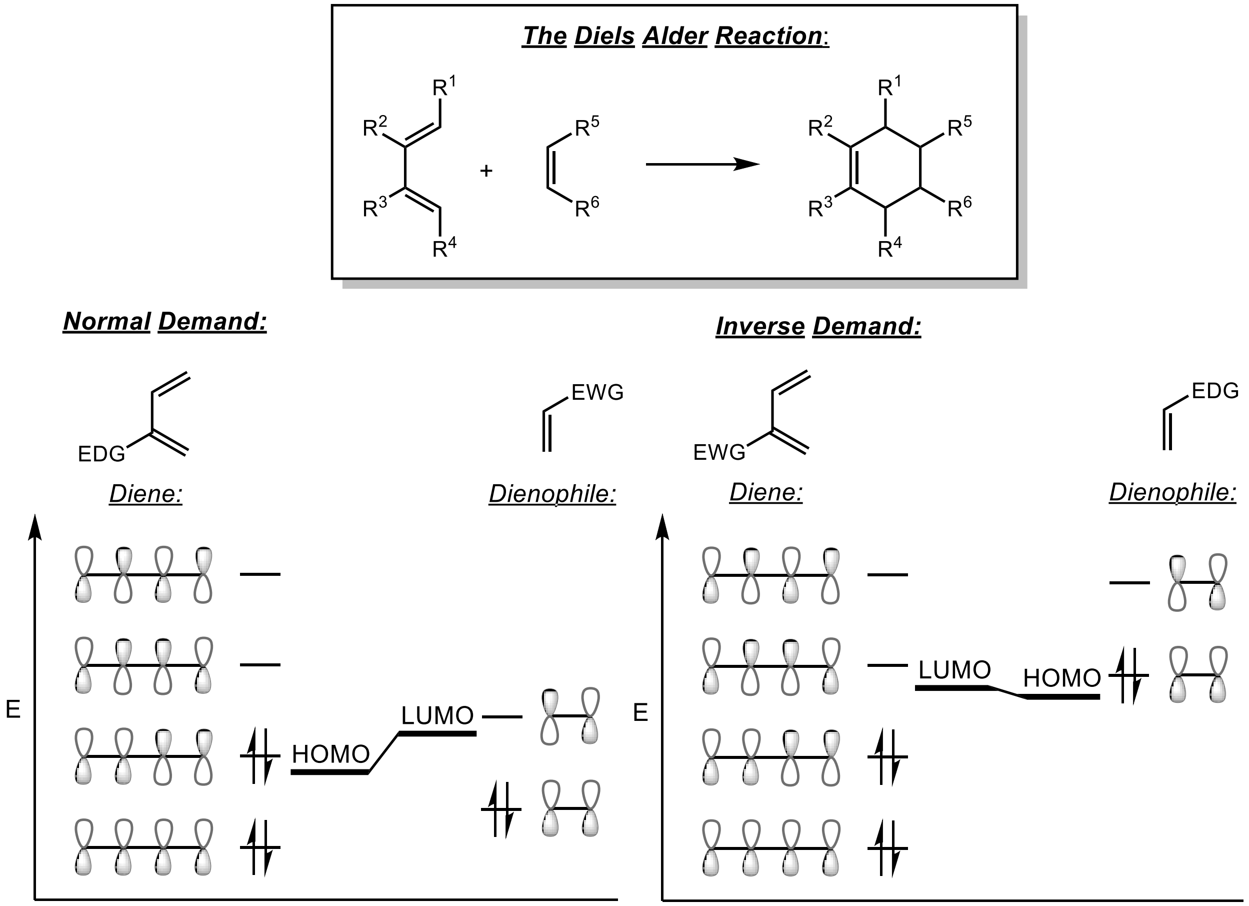
The Diels Alder Reaction:
R1
R2
R3
R4
R5
R6
+
Normal Demand:
EDG
EWG
Diene:
Dienophile:
E
HOMO
LUMO
Inverse Demand:
EWG
EDG
Diene:
Dienophile:
E
LUMO
HOMO

Chiral Lewis and Brønsted acids have also been reported to catalyze asymmetric versions of the DA reaction. The mechanism of enantioinduction is fairly analogous in both cases: the LUMO lowering effect of the catalyst ensures that only associated substrate molecules participate in the cycloaddition. The catalyst bears an element of chirality and is itself enantiopure. This chirality is frequently used to project out a sterically demanding group that serves to block one of the prochiral faces of the associated substrate.[5] This ensures that the other substrate will only react at the available face, resulting in the formation of enantioenriched products.

Figure 2.2: Representative examples of catalytic enantioselective Diels-Alder reactions

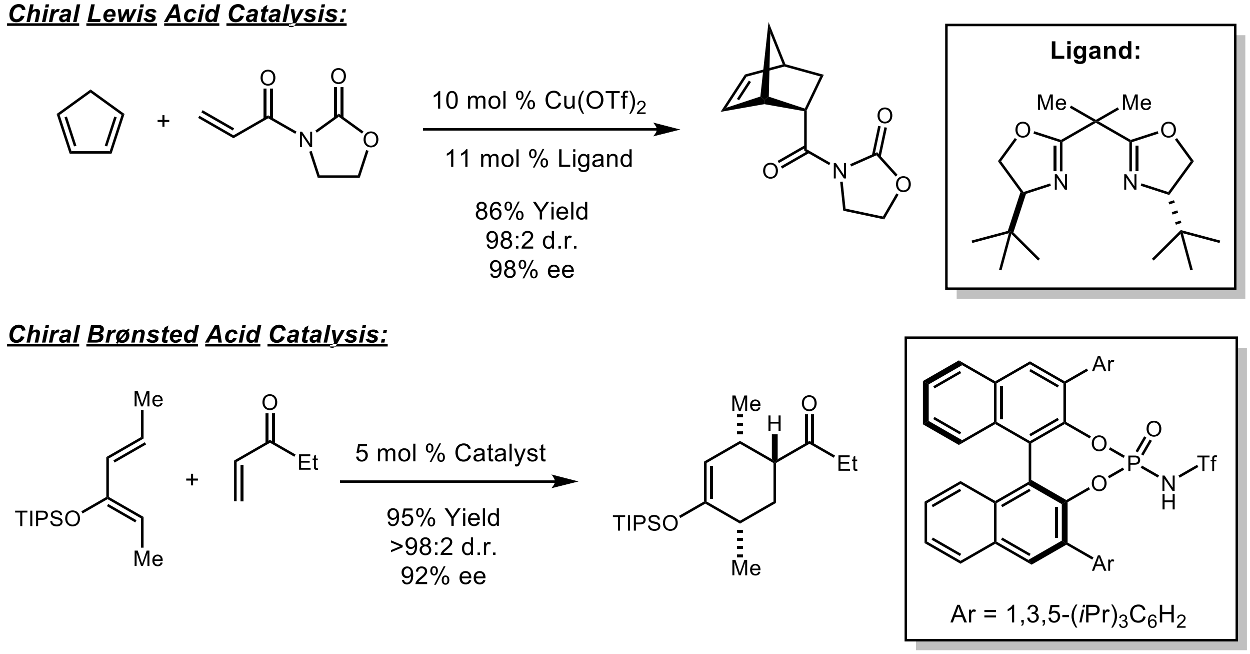
Chiral Lewis Acid Catalysis:
10 mol % Cu(OTf)2
11 mol % Ligand
86% Yield
98:2 d.r.
98% ee
Ligand:
Chiral Brønsted Acid Catalysis:
5 mol % Catalyst
95% Yield
>98:2 d.r.
92% ee
TIPSO
Ar = 1,3,5-(iPr)3C6H2

Lewis acids bearing bisoxazoline (BOX) or pyridine bisoxazoline (pyBOX) ligands are among the most popular chiral catalysts for this reaction. They tend to work best when the substrate provides a site for bidentate chelation with the catalyst to provide structural rigidity, as is the case with the oxazolidinone substrate shown in Figure 2.2.[6] The chiral *N*-triflylphosphoramides developed by Yamamoto can give high levels of enantioinduction in some cases even when a single coordinating handle is present in the substrate.[7]

While the scope of the DA reaction is vast, even catalyzed reactions have so far been limited by the necessity of “matching” the electronic properties of substrates. Obtaining reactivity between pairs of electronically neutral or electron rich dienes and dienophiles is incredibly challenging under thermal conditions, though in some cases racemic intramolecular reactions can be carried out with very high levels of heating (>200 °C)[8] or metal catalysts.[9]

2.2 A History of the cation radical Diels-Alder reaction

The cation radical Diels-Alder reaction is a remarkable transformation due to its ability to overcome the previously described limitation of traditional Diels-Alder chemistry and allow for reactivity to be obtained between pairs of electron rich substrates.

It was a full twelve years after the initial disclosure of the [2+2] dimerization of carbazole by triarylaminium salts that the Bauld group first demonstrated that the strategy could be used to affect [4+2] dimerizations of cyclohexadiene and other conjugated dienes (Figure 2.3).[10] While many early examples were limited to dimerization reactions, the group also found that cross-addition products could be obtained when the dienophile component was significantly lower in oxidation potential than the diene.[11,12]

Figure 2.3: Early representative examples of the scope cation radical Diels-Alder reaction

Cyclohexadiene Dimerization:

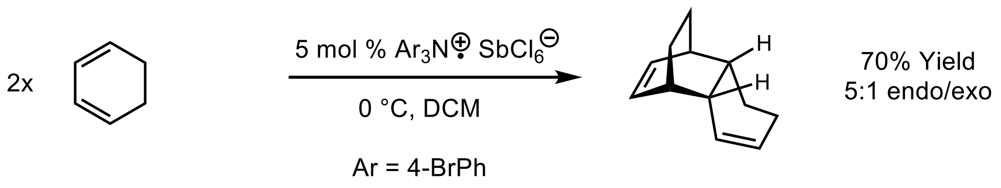
2x
5 mol % $Ar_3N^{\oplus\bullet}$ $SbCl_6^{\ominus}$
0 °C, DCM
Ar = 4-BrPh
H
H
70% Yield
5:1 endo/exo

Crossed Diene-Diene Cycloadditions:

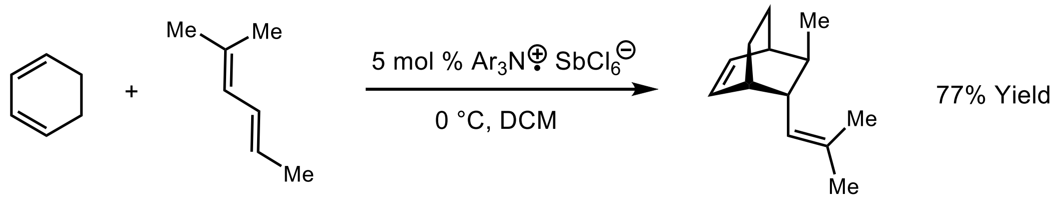
+
Me
Me
Me
5 mol % $Ar_3N^{\oplus\bullet}$ $SbCl_6^{\ominus}$
0 °C, DCM
Me
Me
Me
77% Yield

Diene-Electron Rich Alkene Cycloadditions:

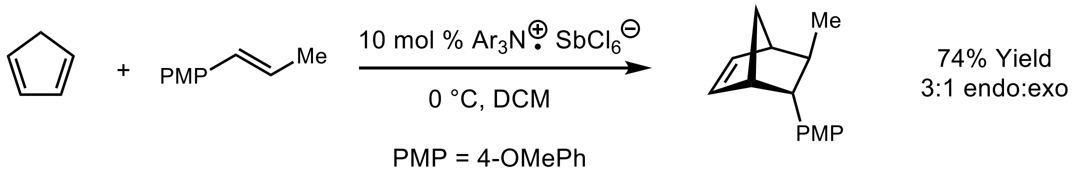
+
PMP
Me
10 mol % $Ar_3N^{\oplus\bullet}$ $SbCl_6^{\ominus}$
0 °C, DCM
PMP = 4-OMePh
Me
PMP
74% Yield
3:1 endo:exo

They subsequently found that photoinduced electron transfer (PET) conditions proved a mild and attractive alternative protocol for carrying out the requisite single electron oxidation of the dienophilic component, in this case by using dicyanoanthracene as the photoredox catalyst. Furthermore, this method allowed for the reaction to be extended from a diene/diene format to an electron rich olefin/diene format. In many cases, acyclic dienes can be employed, however some substitution pattern is often required that will hold the diene in the more reactive *s*-cis conformation.

Figure 2.4: Stereochemical outcomes indicate that stepwise bond formation occurs

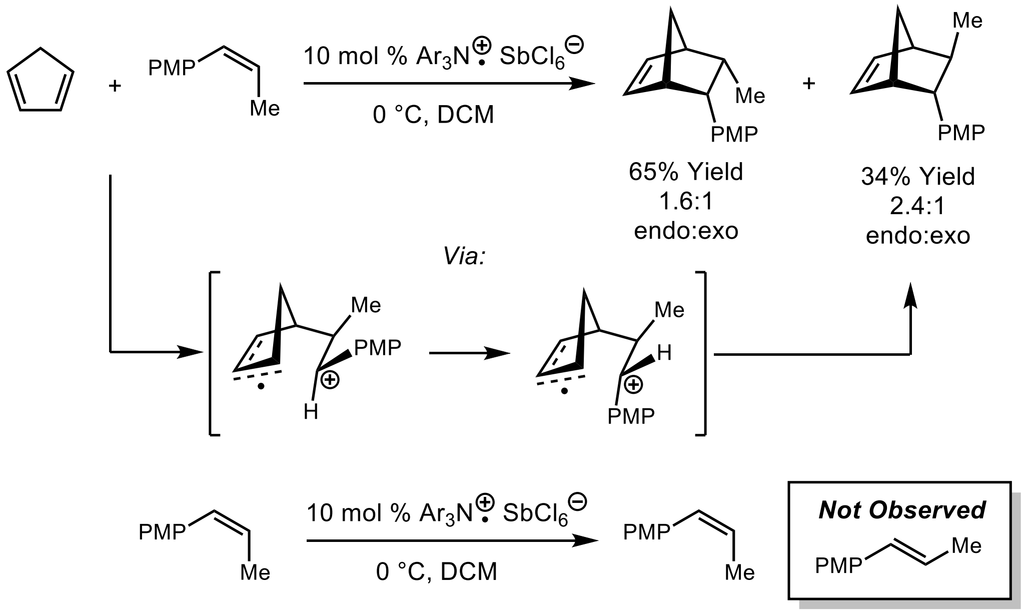

PMP
Me
10 mol % Ar$_3$N$^{\oplus}$• SbCl$_6^{\ominus}$
0 °C, DCM
Me
PMP
Me
PMP
65% Yield
1.6:1
endo:exo
34% Yield
2.4:1
endo:exo
Via:
Me
PMP
H
Me
H
PMP
PMP
Me
10 mol % Ar$_3$N$^{\oplus}$• SbCl$_6^{\ominus}$
0 °C, DCM
PMP
Me
Not Observed
PMP
Me

Studies on the mechanism of the reaction have been carried out that indicate that the reaction occurs via stepwise bond formation.[13–16] For example, in the cycloaddition between cyclopentadiene and *cis*-anethole, products with both *cis* and *trans* stereochemistry are observed (Figure 2.4). However, treatment of *cis*-anethole with the triarylaminium salt in isolation does not result in isomerization to *trans*-anethole. Therefore, the authors propose that isomerization to the *trans*-product is the result of a bond rotation that occurs on a distonic radical cation intermediate after the first bond formation has occurred. This hypothesis has been affirmed by computational results that indicate that multiple stepwise mechanisms are energetically similar, and are all ca. 17 kcal/mol lower in energy than a concerted pathway.[17]

In 1991, the Steckhan group introduced the use of cationic oxopyrylium salts as catalysts for this transformation,[18] and were able to obtain [4+2] cyclization between indole and cyclohexadiene in 70% yield, as well as similar yields with related substrates. In this case, the low oxidation potential of the secondary arylamine in the product proved problematic, resulting in a competing reverse reaction pathway. To overcome this issue, the group found that including stoichiometric acetyl chloride in the reaction would selectively acylate the product, which was found to raise its oxidation potential outside the range of the catalyst, preventing reversibility.

More recently, the Yoon group has shown that ruthenium tris-bipyrazine ($Ru(bpz)_3^{2+}$) complexes can act as remarkably efficient catalysts for the cation radical DA (Figure 2.5).[19] The modified ligand set is employed in this case because it raises the excited state potential of the complex to +1.45 V vs. SCE, as compared to +0.81 V vs. SCE for the tris-bipyridine complex. This makes the oxidation of electron rich olefins such as anethole possible, and allows for them to be employed as the dienophile component. The rate of reaction is greatly diminished when run without the presence of oxygen (N_2 atmosphere). Oxygen is proposed to aid in the reoxidation of the catalyst from Ru^+ to the active Ru^{2+} form. Using this system, the desired [4+2] cycloadducts are obtained in very highl yields with high levels of diastereoselectivity, often as quickly as in one hour, using 0.5 mol % loadings of the catalyst. Furthermore, acyclic dienes with a minimal bias for the s-*cis* conformation, including isoprene, readily cyclized under these conditions.

Figure 2.5: Examples of cation radical Diels-Alder reactions carried out under PET conditions

Cyanoarenes as PET Sensitizers:

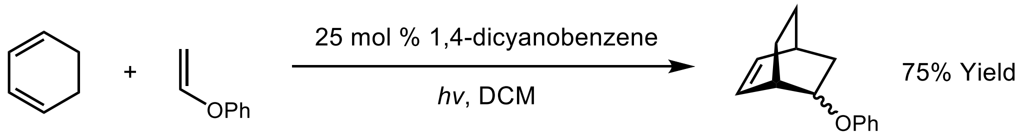

+
OPh
25 mol % 1,4-dicyanobenzene
hv, DCM
OPh
75% Yield

Oxopyrylium Photoredox Catalysts:

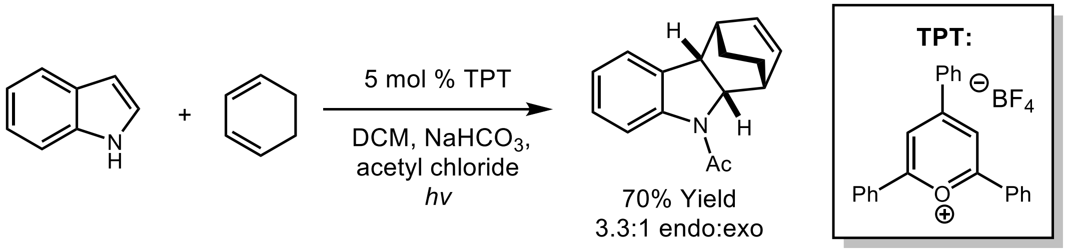

N
H
+
5 mol % TPT
DCM, NaHCO3,
acetyl chloride
hv
H
N
H
Ac
70% Yield
3.3:1 endo:exo
TPT:
Ph
BF4
Ph
O
Ph

Ruthenium Polypyridyl Photoredox Catalysts:

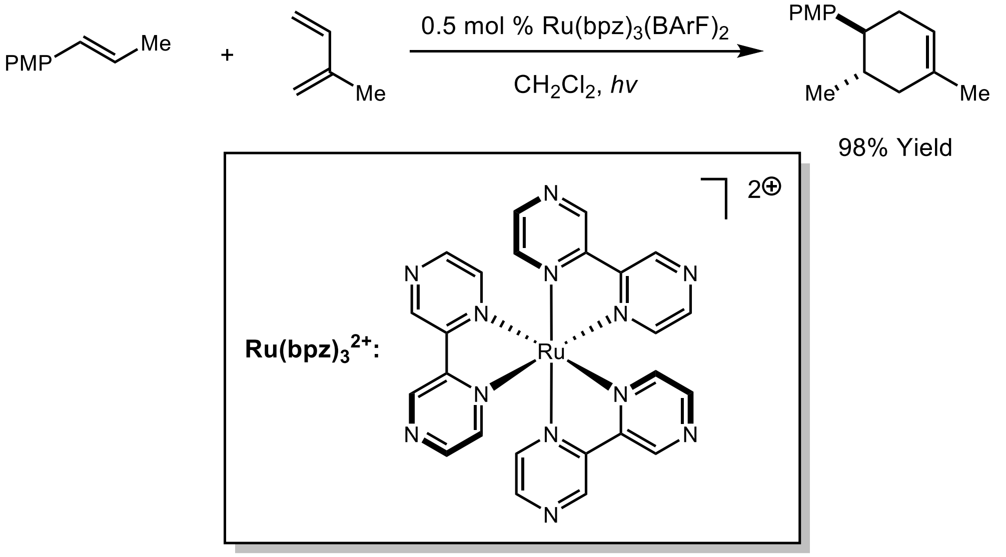

PMP
Me
+
Me
0.5 mol % Ru(bpz)3(BArF)2
CH2Cl2, hv
PMP
Me
Me
98% Yield
Ru(bpz)3 2+:
2⊕
N
Ru

In each case described so far, the mechanism of the transformation is fairly analogous. The appropriately chosen photoredox catalyst becomes excited by a photon of visible light and an electron is promoted to an excited state. Upon encountering an equivalent of the suitably oxidizable dienophile, an electron transfer event can take place to generate the olefinic cation radical intermediate. The now highly electrophilic species will readily cyclize with the diene. As was previously mentioned, the bond formations occur in a stepwise fashion. Because several pathways are similar in energy, the exact mechanism likely depends on the substrate.[17] After formation of the initial cycloadduct, a reduction event furnishes the final cyclohexene product. There are two possibilities for how this can occur: either the reduced photoredox catalyst acts as the reductant, completing a true catalytic cycle, or a second substrate equivalent acts as the reductant, beginning a chain propagation mechanism.

Figure 2.6: A general mechanism for the cation radical Diels-Alder reaction

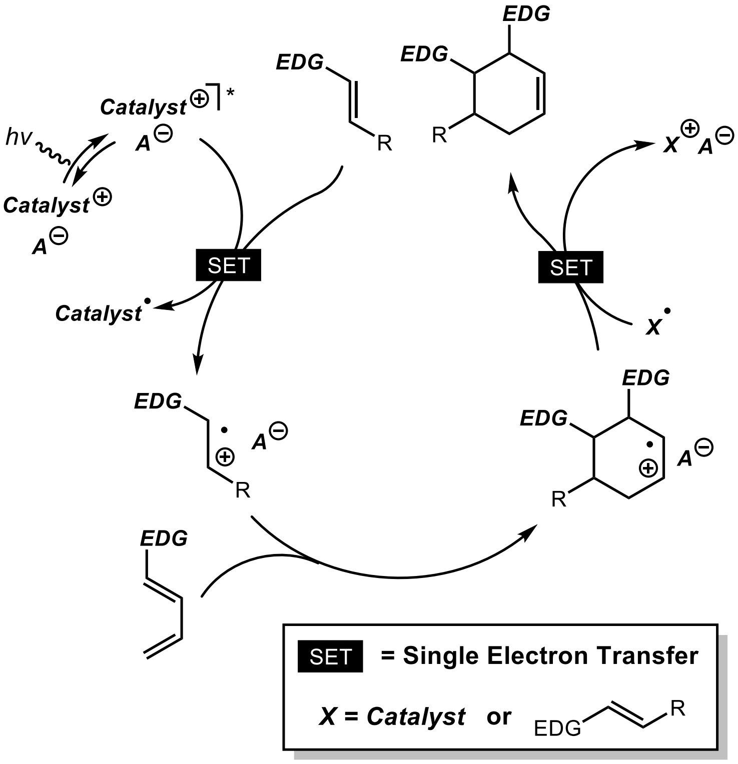
EDG
EDG
EDG
R
R
Catalyst
A
hv
Catalyst
A
SET
SET
Catalyst
X
A
X
EDG
EDG
A
R
EDG
A
R
EDG
SET = Single Electron Transfer
X = Catalyst or
EDG
R

In spite of the fact that all the methods developed so far have shown a great deal of maturation for the cation radical DA reaction, there currently exists no general strategy for carrying out this reaction in a catalytic asymmetric fashion. A major obstacle to the development of such a reaction is that the substrates discussed so far do not contain any of the chelating functional handles that are required for both the asymmetric normal demand Diels-Alder reactions discussed previously, as well as in the enantioselective photoredox reactions detailed in the previous chapter.

Figure 2.7: The first observation of enantioinduction in the cation radical Diels-Alder reaction

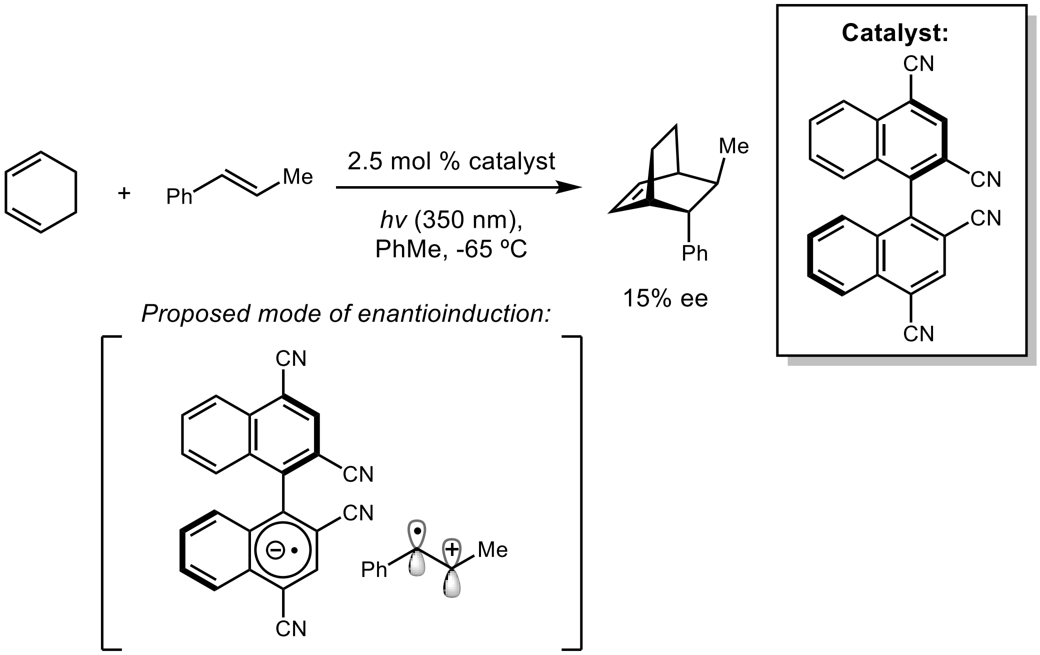

To the best of our knowledge, an example by the Schuster group (Figure 2.7) stands as the only observation of any level of enantioinduction in the cation radical Diels-Alder reaction.[20] Their strategy centers on the design and use of an axially chiral neutral cyanoarene as the photoredox catalyst. When the reaction is run at cryogenic temperatures in toluene as the solvent, a modest 15% ee is observed. Their model for enantioinduction is that, following the key electron transfer event between anethole and the cyanoarene, the coulombic attraction between the resulting radical cation and anion keeps the two in close proximity for some period of time. This allows the chiral catalyst to control the facial approach of the incoming diene, resulting in the observed level of enantioselectivity. This provides a strong precedent for using ion pairing as a means of inducing asymmetry in cation radical reactions. At the same time, this strategy has inherent limitations that would be challenging to overcome. Particularly, holding the photoredox catalyst and substrate in close proximity after electron transfer facilitates back electron transfer. This would serve to regenerate starting material in a non-productive pathway, greatly diminishing the overall rate of reaction. Unfortunately no yield for the transformation was reported, and so the magnitude of this effect cannot be assessed.

Figure 2.8: Design of a new class of photoredox catalysts bearing chiral anions

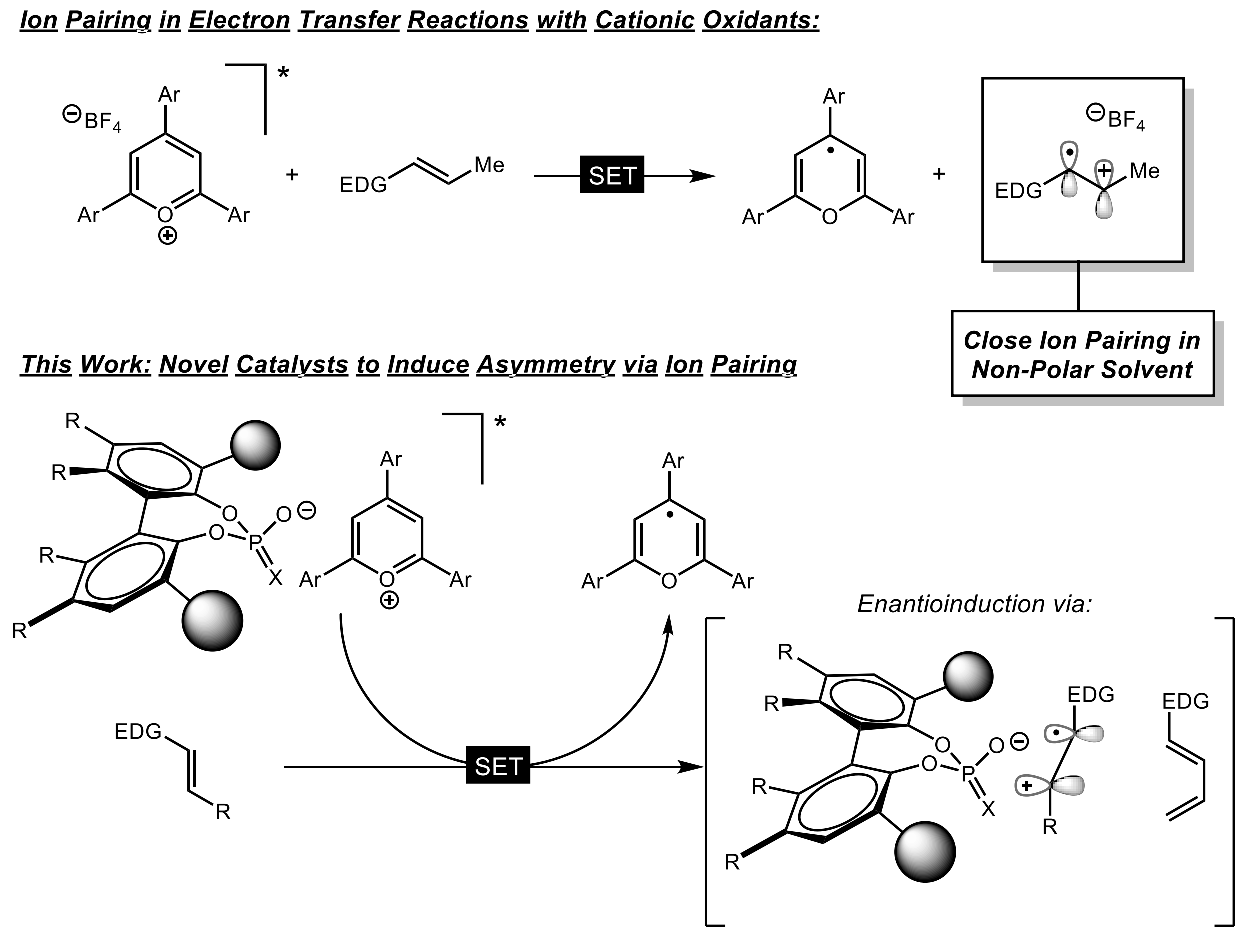
Ion Pairing in Electron Transfer Reactions with Cationic Oxidants:
⊖BF4
Ar
Ar
Ar
O
⊕
*
+
EDG
Me
SET
Ar
Ar
O
Ar
+
⊖BF4
EDG
Me
Close Ion Pairing in Non-Polar Solvent
This Work: Novel Catalysts to Induce Asymmetry via Ion Pairing
R
R
R
R
O
O
P
O⊖
X
Ar
Ar
Ar
O
⊕
*
Ar
Ar
Ar
O
EDG
R
SET
Enantioinduction via:
R
R
R
R
O
O
P
O⊖
X
EDG
R
EDG

In our search for a general method for rendering this transformation asymmetric, we uncovered an interesting possibility by examining the mechanism of a reaction in which an organic photoredox catalyst, such as a triphenylpyrylium tetrafluoroborate (TPT) salt, was employed. Due to their positively charged nature, these molecules necessarily bear some sort of non-coordinating counterion, typically a tetrafluoroborate anion. If a cation radical DA reaction were to be run in a non-polar solvent using a TPT catalyst, then after the initial electron transfer event this anion should now be paired with the charged cation radical intermediate (Figure 2.8). In fact, the coulombic attraction would hypothetically keep it in association with all the cationically charged intermediates of the catalyst cycle.

Given the precedent from the Schuster group, we were intrigued by the possibility of here again using ion pairing to induce asymmetry, but in a very different manifold. If the tetrafluoroborate anion could be replaced with a chiral anion of some variety, then it too ought to remain closely paired with the cation radical intermediates of the reaction. This could then be used to control the facial approach of the diene and render the reaction enantioselective. And so, our goal at the outset of this project became first and foremost to assess the validity of this hypothesis and ascertain whether this would be able to induce asymmetry in the cation radical Diels-Alder reaction.

One feature we believed would have central importance in the success of this project was enforcing tight ion paring interactions between substrate and anion through choice of solvent. More polar solvents are able to stabilize and therefore solubilize charged species in the solution. This has the effect of separating ion pairs, and so at the outset we hypothesized that using non-polar solvents would be essential to ensure that the cation radical intermediates of the DA reaction are held within close proximity of the anion, so that its chiral information could be relayed.

Figure 2.9: The role of solvent polarity in influencing ion pairing interactions

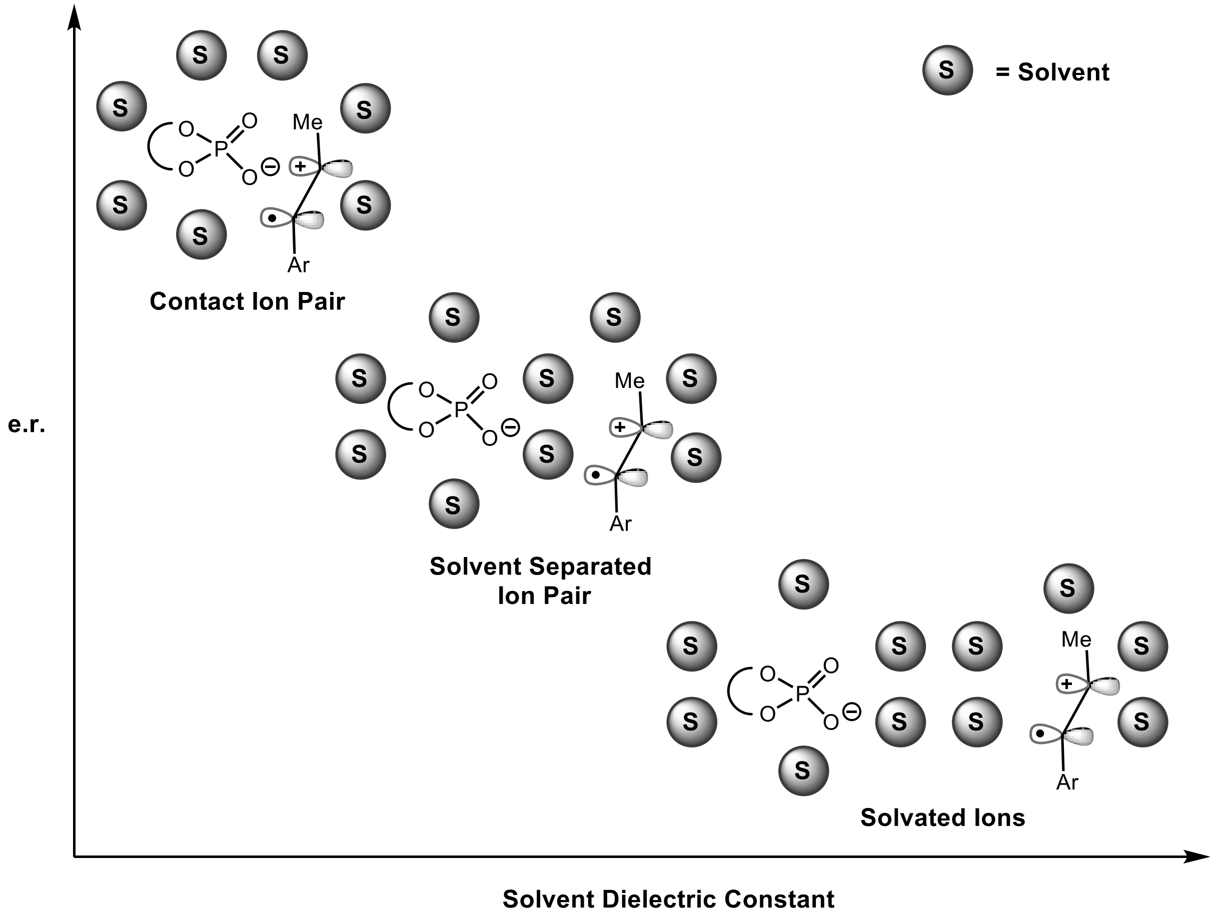

Chiral anions have also become an area of intense interest in chemical research, and have been successfully used to control the absolute stereochemistry of several reactions.[21,22] The most important precedent for this study comes from the Toste group.[23] In an initial report, they designed a system to simply ascertain whether such electrostatic interactions alone can be used to relay chiral information from catalyst to substrate. The designed reaction uses a silver salt bearing a chiral phosphate anion as the catalyst and was used to catalyze the opening of *meso*-aziridinium ions. The aziridium ion is first generated when a chloride ion is abstracted from a racemic substrate by the silver salt (Figure 2.10). After the metathesis reaction occurs, precipitating silver chloride, the phosphate anion and aziridinium are now necessarily paired. This ion pairing interaction proves sufficient to direct the approach of the incoming nucleophile and provide the ring-opened products with high levels of enantioinduction. Since this first report, the field has advanced significantly and numerous other examples of chiral anions have been reported by this and other labs.

Figure 2.10: Precedent for the ability of chiral anions to induce asymmetry catalytically

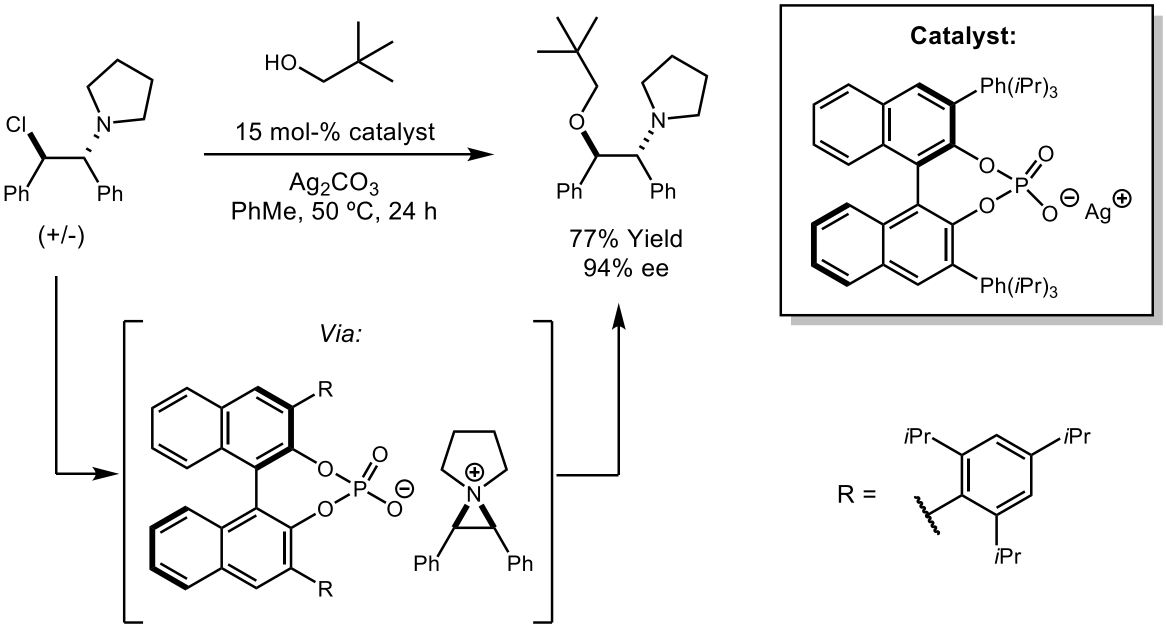

Cl
N
Ph
Ph
(+/-)
HO
15 mol-% catalyst
Ag2CO3
PhMe, 50 °C, 24 h
O
N
Ph
Ph
77% Yield
94% ee
Catalyst:
Ph(iPr)3
O
O
P
O
O
Ag
Ph(iPr)3
Via:
R
O
P
O
O
O
R
N
Ph
Ph
R =
iPr
iPr
iPr

For the design of our chiral complexes, we chose to also focus our attention on chiral anions derived from the corresponding Brønsted acid. The reason for this is that a variety of chiral Brønsted acids have been reported in the literature, and their properties are highly tunable.[24–26] We hypothesized that the nucleophilicity of the anion would be of central importance in the design of our catalyst system. The anion acting as a nucleophile at any point in the transformation and forming a covalent adduct with the TPT catalyst or intermediates of the reaction would presumably impede reactivity. To a first approximation, the nucleophilicity of an anion is inversely correlated with the pKa of the conjugate acid, thus we proposed that this effect could be mitigated through the use of strong acids as our anion precursors.

Figure 2.11: Range of acidities of various chiral Brønsted acids measured in MeCN

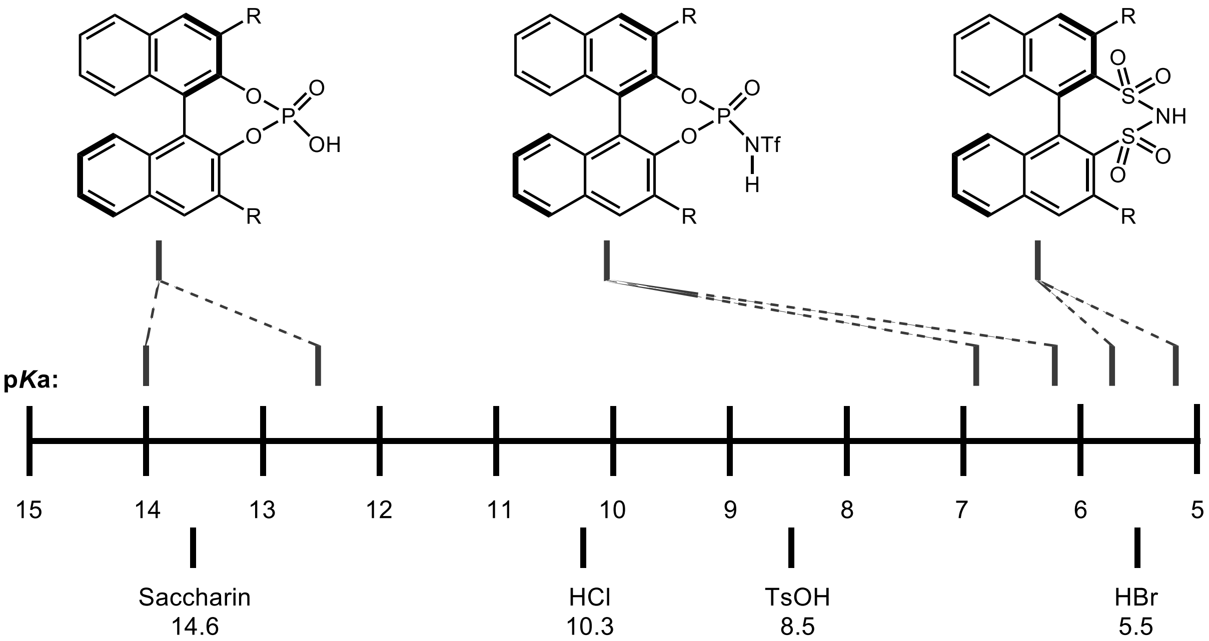

Rueping has recently reported the acidities of a variety of commonly used Brønsted acids in acetonitrile, providing a standard scale for comparing their reactivity.[27] Phosphoric acids proved to be relatively weak, with pKas ranging from ca. 14 to 12.5, while *N*-triflylphosphoramides proved to be significantly more acidic due to the electron withdrawing nature of the triflyl group. Disulfonyl amides were found to be more acidic still, yet are as of now sparsely used, likely due to the challenges associated with their synthesis which will be discussed in Section 1.3. The steric and electronic properties of these acids can be further tuned by modifying the substituents at the 3,3'-positions of the biaryl moiety.

We chose to develop our first generation of catalysts from *N*-triflylphosphoramides due to their relative ease of preparation and low nucleophilicity. The first task was to develop a route to access the desired oxopyrylium salts bearing these chiral anions. It was found that treating an oxopyrylium salt with sodium ethoxide resulted in ring opening to furnish a linear ene-dione in good yields. We subsequently found that treatment of the ene-dione with an equimolar quantity of the chosen Brønsted acid promoted cyclization to regenerate the oxopyrylium salt, now paired with a chiral anion. The reactions were complete in minutes with heating to approximately 50-60 °C, and our first generation purification consisted of simple recrystallization from ethanol, which furnished the salts as bright orange solids.

Figure 2.12: Synthesis of chiral anion bearing photoredox catalysts

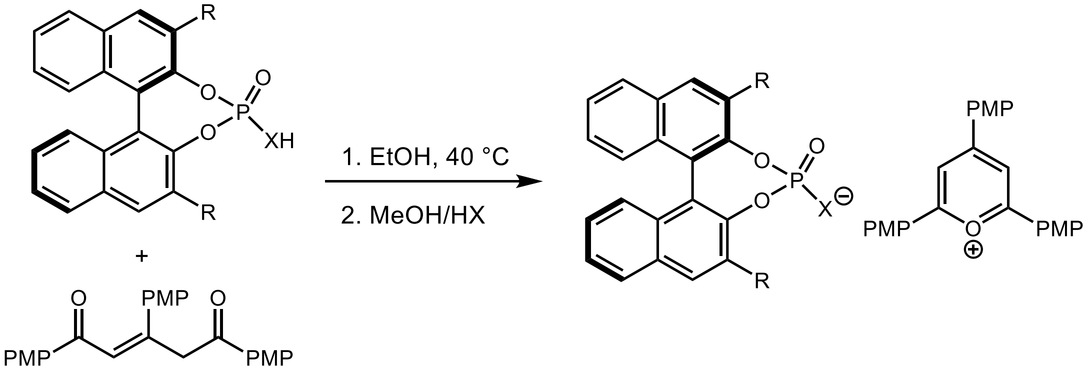

As the research program progressed, it was found that this strategy led to batches of catalyst that gave variable levels of enantioselectivity. After screening a number of potential purification protocols, we found that carrying out the cyclization in excess EtOH at 40 °C followed by a simple liquid/liquid extraction between MeOH and hexanes furnished highly pure samples of the complexes that gave consistent results.

With a route to potential catalysts in hand, the next step was to develop a model substrate for the reaction on which to screen for reactivity. Dr. Tien Nguyen, a fellow graduate student, worked on the development of an intermolecular reaction, and confronted issues of low reactivity in numerous situations. In order to improve on this problem of reactivity, we set out to develop an intramolecular version of the reaction, and so a number of substrates were synthesized that contained tethered diene and dienophile moieties.

The oxidation potentials of both the diene and dienophile must be taken into consideration in the design of a substrate for this reaction. It has been observed that the best results are obtained when the dienophile is the more readily oxidized component in the reaction. Oxidation of the diene can often result in either undesired product formation such as [2+2] cycloadducts, or a lack of reactivity. Since substituted dienes such as cyclohexadiene bear oxidation potentials of ca +1.8 V vs. SCE, we chose to use 4-methoxy styrene derivatives as dienophiles, which are oxidized at ca +1.3 V vs. SCE (*vide infra*). We chose to employ 2,4,6-tri(4-methoxyphenyl)pyrylium tetrafluoroborate (4-OMe-TPT) as the catalytic photooxidant for this study, as its excited state reduction potential lies at ca. +1.74 V vs. SCE.

Figure 2.13: Design of intramolecular cation radical DA reaction substrates

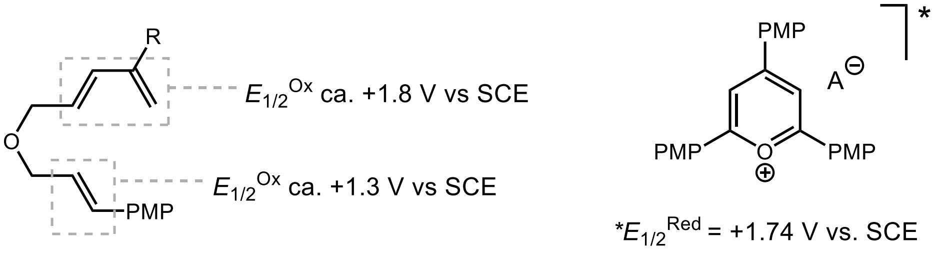
R
$E_{1/2}^{Ox}$ ca. +1.8 V vs SCE
O
$E_{1/2}^{Ox}$ ca. +1.3 V vs SCE
PMP
PMP
A⊖
PMP
O
PMP
⊕
*
*$E_{1/2}^{Red}$ = +1.74 V vs. SCE

The synthesis of the diene component was carried out by methodology initially disclosed by the Wender group.[28] The first step of the synthesis was a pyrrolidine-catalyzed aldol reaction between a chosen aldehyde and formaldehyde. This was followed by an HWE reaction to construct the diene component with the desired substitution pattern. Next, the ester was reduced using DIBAL to provide a hydroxyl group. The original report described a two-pot procedure in which the alcohol could be brominated and immediately alkylated with a malonic ester. We attempted to translate this method to use an alkoxide as the nucleophile for synthesis of our desired ethereal linkage, but observed no product formation using the reported conditions. We found that the reaction could be quenched after the bromination step and subjected to an aqueous workup to give nearly pure brominated material. Furthermore, the crude product could be re-dissolved in THF, stirred over molecular sieves, and treated with the alkoxide to give the desired products in moderate yield.

Figure 2.14: General strategy for intramolecular DA reaction substrates

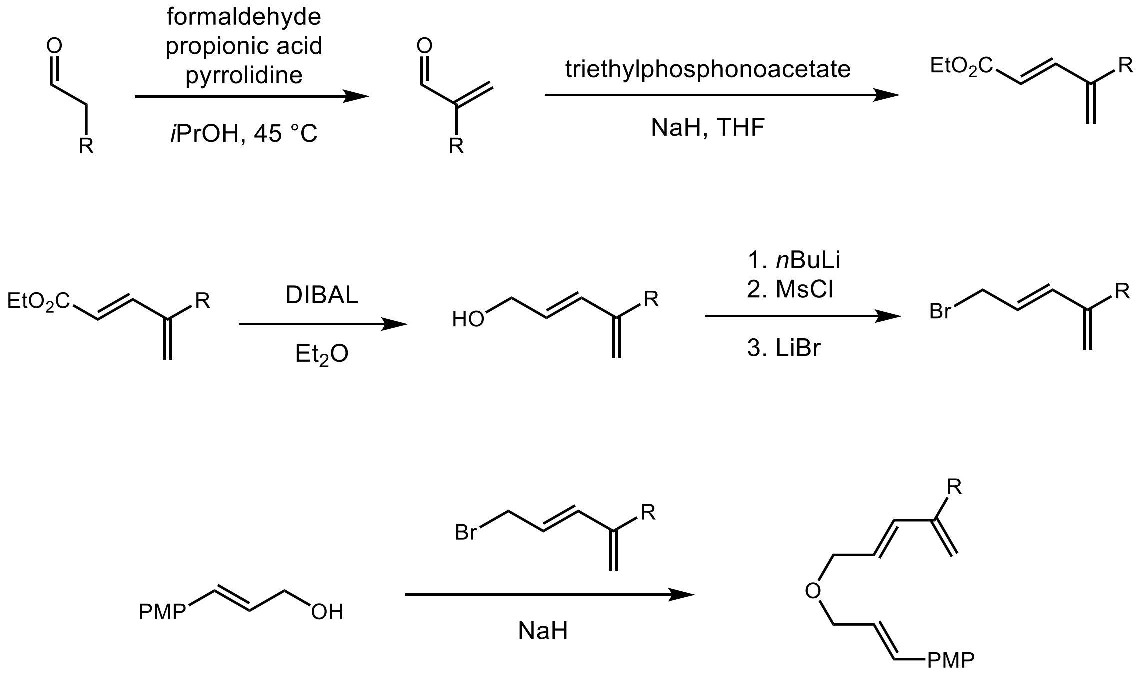

formaldehyde
propionic acid
pyrrolidine
iPrOH, 45 °C
triethylphosphonoacetate
NaH, THF
EtO2C
R
DIBAL
Et2O
HO
1. nBuLi
2. MsCl
3. LiBr
Br
PMP
OH
NaH
O

We carried out our preliminary studies using a substrate containing an isopropyl group at an internal position of the diene. This substrate was subjected to racemic reaction conditions using 4-OMe-TPT as the catalytic photooxidant in DCM as the solvent. The substrate rapidly underwent the desired [4+2] reaction with high diastereoselectivity even when very low catalyst loadings were used.

Figure 2.15: Non-enantioselective results for cyclization of DA substrates using a TPT catalyst

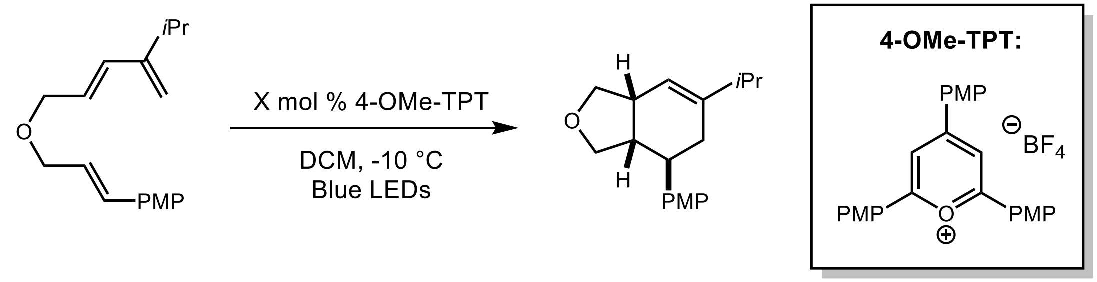

iPr
O
PMP
X mol % 4-OMe-TPT
DCM, -10 °C
Blue LEDs
H
H
4-OMe-TPT:
BF4

mol %	Yield	d.r.
3	>98%	5:1
0.5	79%	14:1

Encouraged by the observed high level of reactivity, we set out to screen for reactivity with several triphenylpyrylium (TP) complexes bearing chiral anions. Phosphate anions resulted in no observed reactivity. Moving to a less nucleophilic *N*-triflylphosphoramide with phenyl rings at the 3,3'-positions also resulted in no reactivity. However, moving to the more sterically-demanding triphenyl silyl ($SiPh_3$) group, a modest yield was obtained along with good levels of enantioinduction. Since this increase in steric demand proved beneficial, we continued the trend by employing *para*-*tert*-butyl triphenylsilyl groups. Unfortunately this had a deleterious effect on conversion, and the effect on selectivity could not be ascertained.

Figure 2.16: Screen of TP salts bearing chiral anions for their ability to induce asymmetry

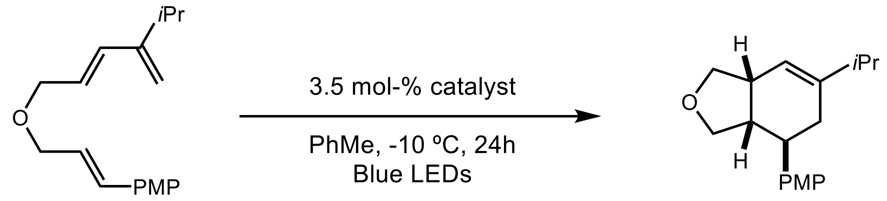

Catalyst:

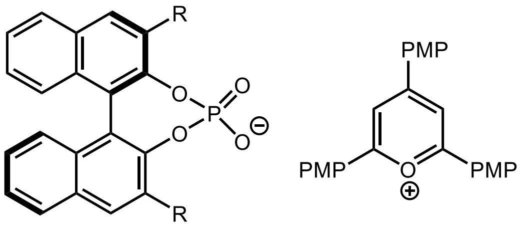

Entry	R	Yield	d.r.	e.r.
1a	Ph	<5%	N.D.	N.D.
1b	$SiPh_3$	<5%	N.D	N.D.

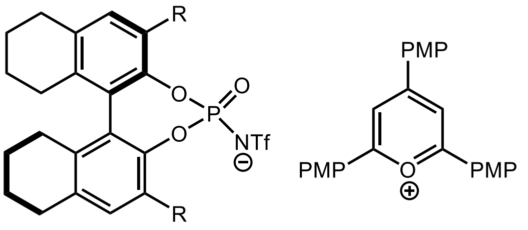

Entry	R	Yield	d.r.	e.r.
1c	Ph	<5%	N.D.	N.D.
1d	$SiPh_3$	25%	3:1	66:33
1e	Si(4-*t*BuPh)$_3$	8%	N.D.	N.D.

We propose the reason for the success of the $SiPh_3$ group is that it has sufficient steric bulk to frustrate the nucleophilicity of the phosphoramidate anion, allowing it to act as a less coordinating anion. This claim is supported by the observation that these complexes are visibly fluorescent in solution, while the 3,3’-phenyl analogues are only marginally so. It is challenging to speculate on why then the addition of the *para*-*tert*-butyl groups does not have a further beneficial effect. It is possible that the further steric hindrance significantly decreases the probability of the excited state of the catalyst coming in contact with a substrate molecule.

With the $SiPh_3$-*N*-triflylphosphoramidate catalyst (**1d**) proving most effective, we then screened this catalyst and substrate combination in a number of solvents. We were particularly interested in the effect of solvent polarity on selectivity, as this would strongly influence the nature of the ion pairing interactions between catalyst and substrate. Surprisingly, it was observed that aromatic solvents are necessary for any level of enantioinduction to be observed. For example, modest enantiomeric excess was obtained when using trifluorotoluene as the solvent, which has a dielectric constant of 11.5. Dichloromethane (DCM), while it has a comparable dielectric constant of 9.08, resulted in no enantioselectivity. This effect could be explained by favorable π-stacking interactions involving the solvent and/or the substrate and chiral anion, though no additional evidence was obtained to investigate this hypothesis.

Figure 2.17: Solvent effects on reactivity and selectivity

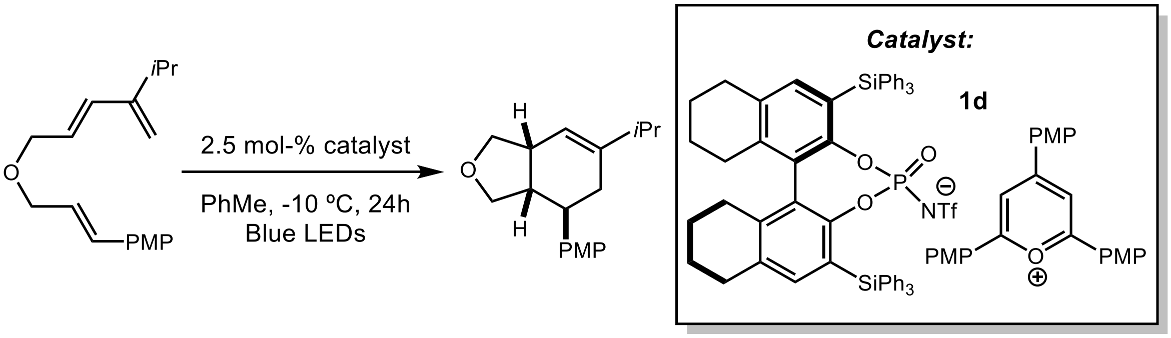

Entry	Solvent	Dielectric Constant	Yield	d.r.	e.r.
1	$PhCF_3$	11.5	23%	10:1	61:39
2	DCM	9.08	44%	10:1	50:50
3	THF	7.6	<5%	N.D.	N.D.
4	Et_2O	7.5	<5%	N.D.	N.D.
5	PhBr	5.55	27%	3:1	66:34
6	$CHCl_3$	4.81	15%	N.D.	50:50
7	Toluene	2.38	36%	3:1	75:25
8	Xylenes	2.37	<10%	N.D.	72:28
9*	Benzene	2.28	26%	5:1	61:39

*Performed at room temperature

Within the series of aromatic solvents investigated, an additional pattern emerges. Enantiomeric excess shows a negative correlation with solvent dielectric constant: lower polarity aromatic solvents give higher levels of enantioselectivity. This finding serves to corroborate our hypothesis that tight ion pairing is necessary for the successful relay of chiral information from catalyst to product.

Changes to the catalyst loading gave consistent levels of selectivity up until ca. 5%, with loadings much higher having a deleterious effect on both enantioselectivity and yield. Results proved fairly consistent within a range of temperatures, with reactivity beginning to suffer below -30 °C.

Figure 2.18: Catalyst loading and temperature effects on reactivity and selectivity

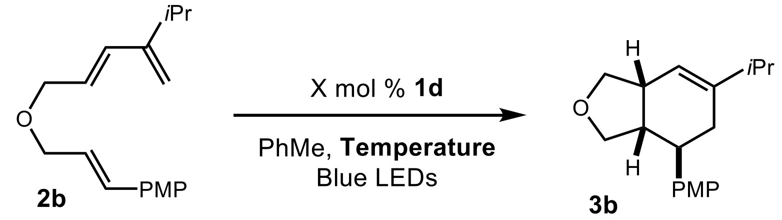

mol %	Temperature (°C)	Yield	d.r.	e.r.	Remaining SM
3.5	-10	36%	3:1	74:26	N.D.
3.5	-60	31%	4:1	75:25	N.D.
2.5	-30	26%	5:1	75:25	60%
5	-30	59%	5:1	74:26	39%
10	-30	26%	4:1	68:32	52%

Additives were also screened in this transformation in order to find if they might have a beneficial effect on the selectivity of the reaction. One such area of investigation was the addition of excess chiral anion to the reaction in the form of a tetrabutylammonium salt. We found that various quantities of this additive had a uniformly negative impact on both the yield and enantioselectivity of the reaction. Other additives, such as the chiral Brønsted acid itself, had a deleterious effect as well (data not shown).

Figure 2.19: Investigating the effect of adding excess chiral anion to the reaction

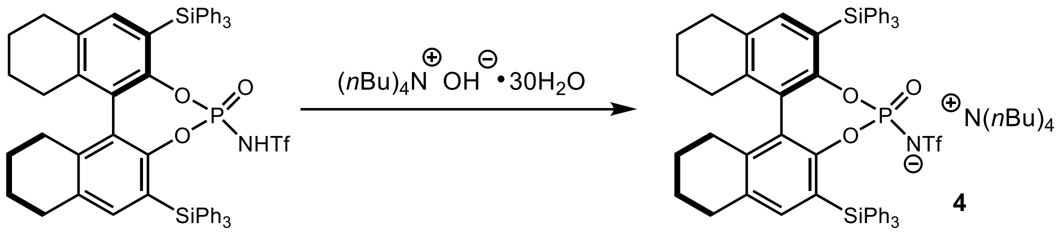

4

$$\mathbf{2b}\ \xrightarrow[\text{PhMe, -10 °C; Blue LEDs}]{\text{6 mol \% } \mathbf{1d}\text{; } \mathbf{X} \text{ mol \% } \mathbf{4}}\ \mathbf{3b}$$

mol % **4**	Yield	e.r.
0	50%	65:35
3	20%	60:40
6	12%	53:47
12	7%	N.D.

With optimized conditions in hand we then set out to explore the scope of the transformation by varying both the diene and dienophile components of the substrate. Substrates bearing large groups at the internal position of the diene, such as benzyl and cyclohexyl, reacted with similar levels of conversion and enantioenrichment as the isopropyl model substrate. Moving to either a smaller methyl group at this position, or removing it entirely, resulted in diminished yields and no enantioselectivity. This indicates that the large substituents are beneficial both for their ability to enforce the more reactive s-*cis* conformation, but also have a significant interaction with the chiral anion.

Figure 2.20: Substrate scope of the enantioselective cation radical DA after optimization

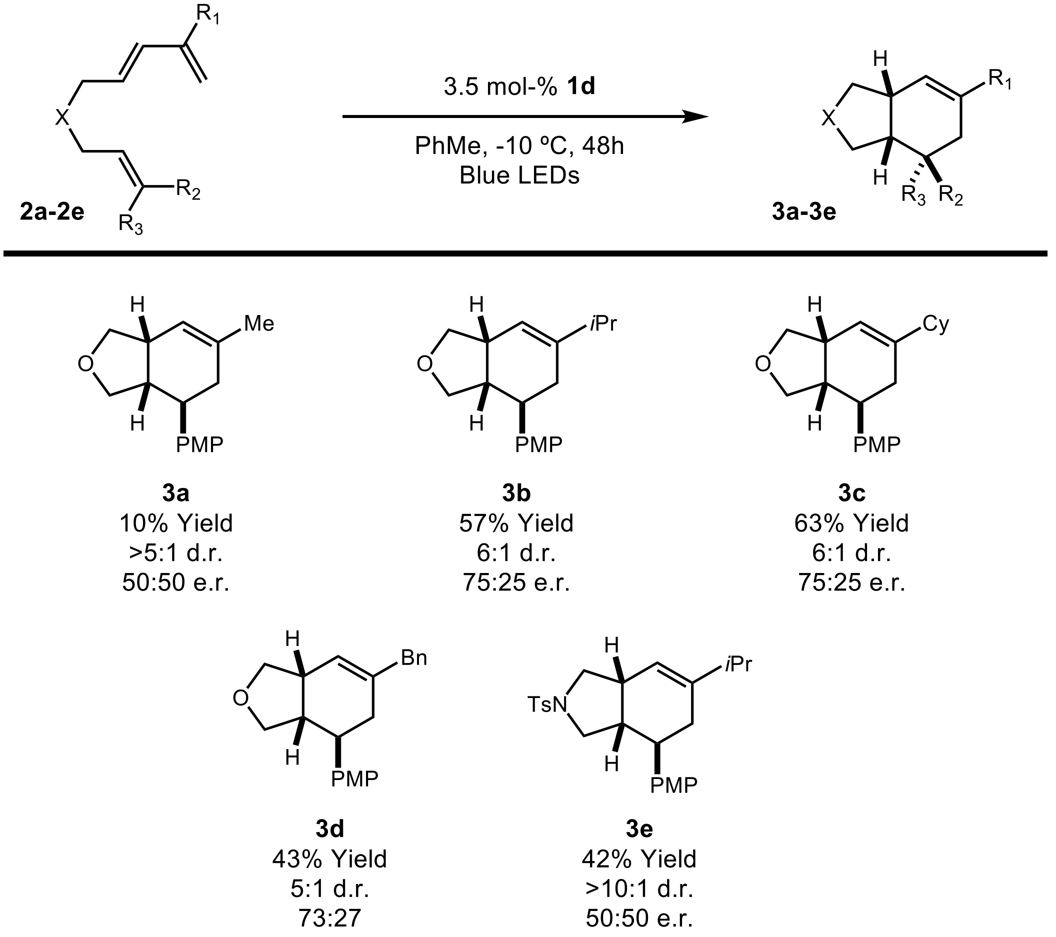
R1
X
R2
R3
2a-2e
3.5 mol-% **1d**
PhMe, -10 °C, 48h
Blue LEDs
H
R1
X
H
R3 R2
3a-3e
H
Me
O
H
PMP
H
*i*Pr
O
H
PMP
H
Cy
O
H
PMP
H
Bn
O
H
PMP
H
*i*Pr
TsN
H
PMP

3a
10% Yield
>5:1 d.r.
50:50 e.r.

3b
57% Yield
6:1 d.r.
75:25 e.r.

3c
63% Yield
6:1 d.r.
75:25 e.r.

3d
43% Yield
5:1 d.r.
73:27

3e
42% Yield
>10:1 d.r.
50:50 e.r.

In the intermolecular variant of this transformation, Dr. Nguyen was able to obtain similar levels of enantioselectivity with a select set of substrates. The highest yields were obtained when using cyclopentadiene as the diene, due to its highly activated nature. While good selectivity was also observed with 2,3-dimethylbutadiene, the yield suffered drastically in this and many other cases.

The results presented so far represent the highest levels of enantioselectivity yet observed in the cation radical DA reaction, and serve as a valuable proof-of-concept as to the viability of this mode of enantioinduction. The rest of this chapter presents a discussion of several attempts to further improve the transformation, as well as applications of this catalyst system to new synthetic transformations.

Figure 2.21: Select intermolecular DA results

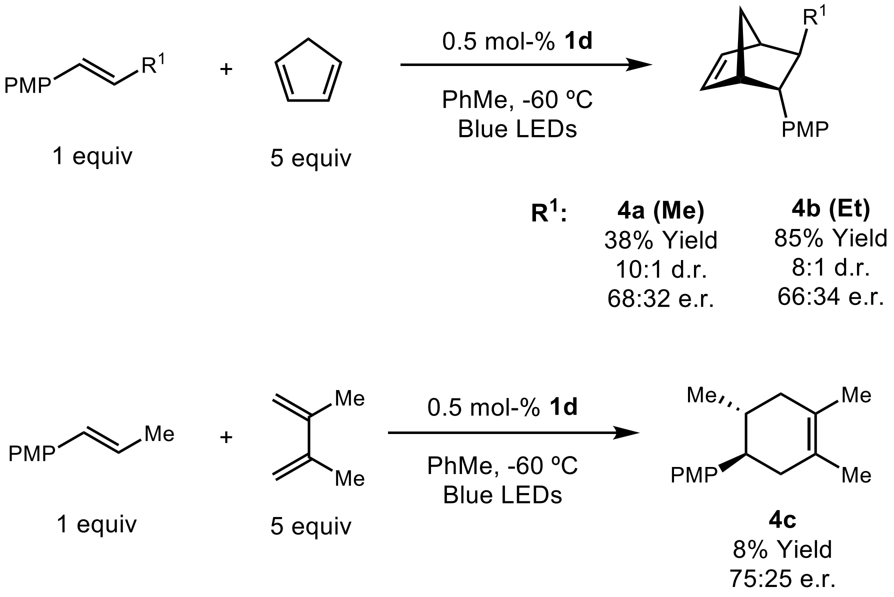
PMP
R1
+
1 equiv
5 equiv
0.5 mol-% 1d
PhMe, -60 °C
Blue LEDs
R1
PMP
R1:
4a (Me)
38% Yield
10:1 d.r.
68:32 e.r.
4b (Et)
85% Yield
8:1 d.r.
66:34 e.r.
PMP
Me
+
Me
Me
1 equiv
5 equiv
0.5 mol-% 1d
PhMe, -60 °C
Blue LEDs
Me
Me
Me
PMP
4c
8% Yield
75:25 e.r.

2.3 Synthesis and application of disulfonyl amide catalysts

Having exhausted all avenues for reaction optimization, it was clear that further improvements to this transformation would have to be the result of designing new catalyst systems. The *N*-triflylphosphoramidate anion possesses several features that we thought might be detrimental to achieving very high levels of enantioselectivity. For example, the triflylamide group is projected far from the chiral pocket, which could limit the successful relay of chiral information. Additionally, the inclusion triflylamide group alters the symmetry of the molecule and results in its two open quadrants being non-equivalent. This means that substrate association with the catalyst is non-equivalent depending on the quadrant from which it approaches.

Figure 2.22: Potential limitations of the *N*-trifylphosphoramidate anion moiety

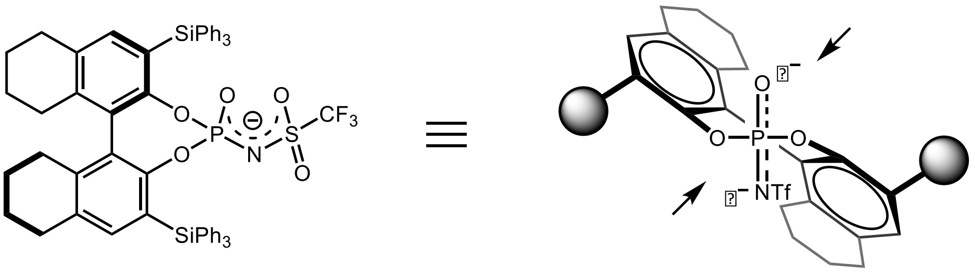
SiPh3
O
O
CF3
O
P
N
S
O
O
SiPh3
≡
O
O–P–O
NTf

- Anion projected far from chiral pocket
- Several Lewis basic sites

- Non-equivalent open quadrants

Chiral disulfonyl amides came to our attention as an alternative scaffold that could address many of these issues. In addition to being truly C_2 symmetric and having a more withdrawn anionic moiety, they have been found to be considerably more acidic than *N*-trifylphosphoramide, which serves to further decrease the nucleophilicity of the conjugate sulfonyl amidate.[29,30]

Figure 2.23: Synthesis of chiral disulfonyl amides

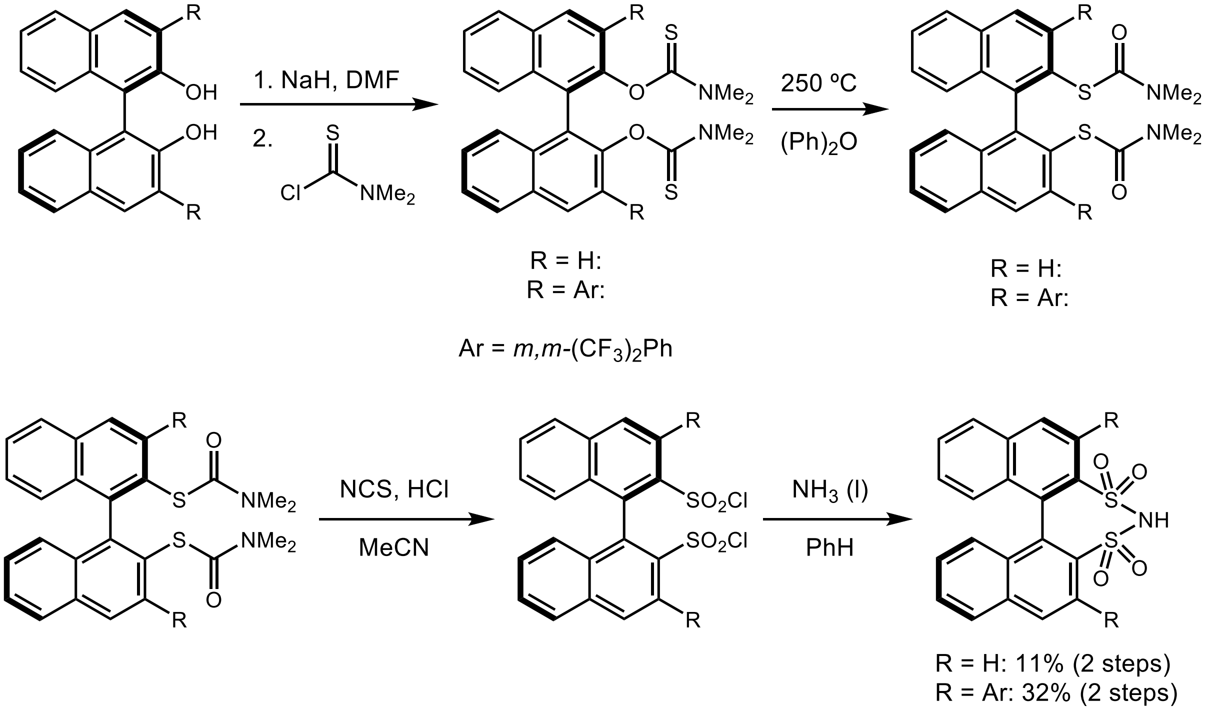
R
OH
OH
R
1. NaH, DMF
2. S
Cl NMe2
R
S
O NMe2
O NMe2
S
R
250 ºC
(Ph)2O
R
O
S NMe2
S NMe2
O
R
R
O
S NMe2
S NMe2
O
R
NCS, HCl
MeCN
R
SO2Cl
SO2Cl
R
NH3 (l)
PhH
R
O
S O
NH
S O
O
R

R = H:
R = Ar:

R = H:
R = Ar:

Ar = *m,m*-$(CF_3)_2$Ph

R = H: 11% (2 steps)
R = Ar: 32% (2 steps)

The synthesis of disulfonyl amides requires the installation of sulfur in place of oxygen in the BINOL scaffold. This is most commonly done by acylating the phenols with *N,N*-

dimethylthiocarbamoyl chloride followed by Newman-Kwart rearrangement and hydrolysis. We were able to use this strategy to first synthesize an unsubstituted complex, as well as a variant bearing *m,m*-trifluoromethylphenyl groups at the 3,3'-positions of the BINOL scaffold. Upon converting these to the corresponding TP salt, they were found not to function as catalysts for the DA reaction under standard conditions (Figure 2.24). We attribute this to the lack of sufficient steric bulk to frustrate the nucleophilicity of the anion, as in the case of the *N*-trifylphosphoramidates bearing phenyl substitution discussed previously.

Figure 2.24: Attempts to use disulfonyl amidate anions to influence enantioselectivity

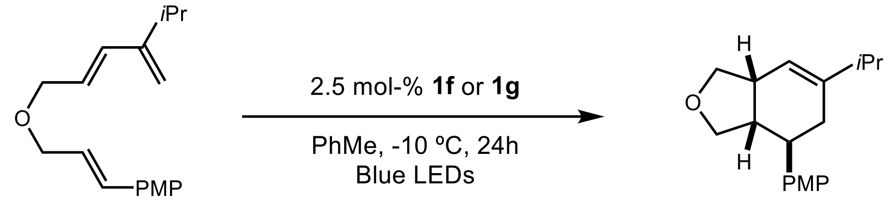

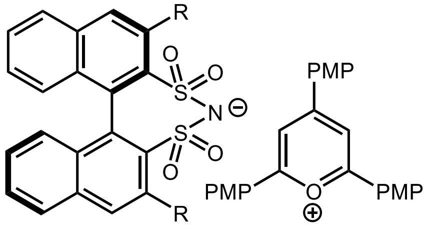

Entry	R	Result
1f	H	No Reaction
1g	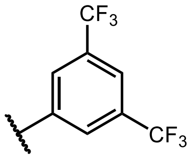	No Reaction

Attempts to install bulkier groups such as the $SiPh_3$ moiety were not successful. With the groups pre-installed on BINOL, only *mono*-acylation of the *bis*-phenol was observed (Figure 2.25), and so the route had to be modified. The alternative strategy was to install the requisite sulfur atoms first, and subsequently functionalize at the 3,3'-positions with the desired groups. A method for late stage directed *ortho*-lithiation has been reported that allows for halogenation of the unsubstituted disulfonyl amide at the 3,3'-positions. A modest 54% yield was reported, however in our hands, no more than traces of potential product could be observed by crude NMR.[31] Several modifications to the procedure were attempted, including the use of *tert*-butyl lithium and a variety of electrophiles. Even quenching the reaction with D_2O failed to show any appreciable level of deuterium incorporation. We are unable to reconcile this discrepancy.

Figure 2.25: Unsuccessful attempts to construct BINOL-derived disulfonyl amides with sterically demanding functional groups at the 3,3'-positions

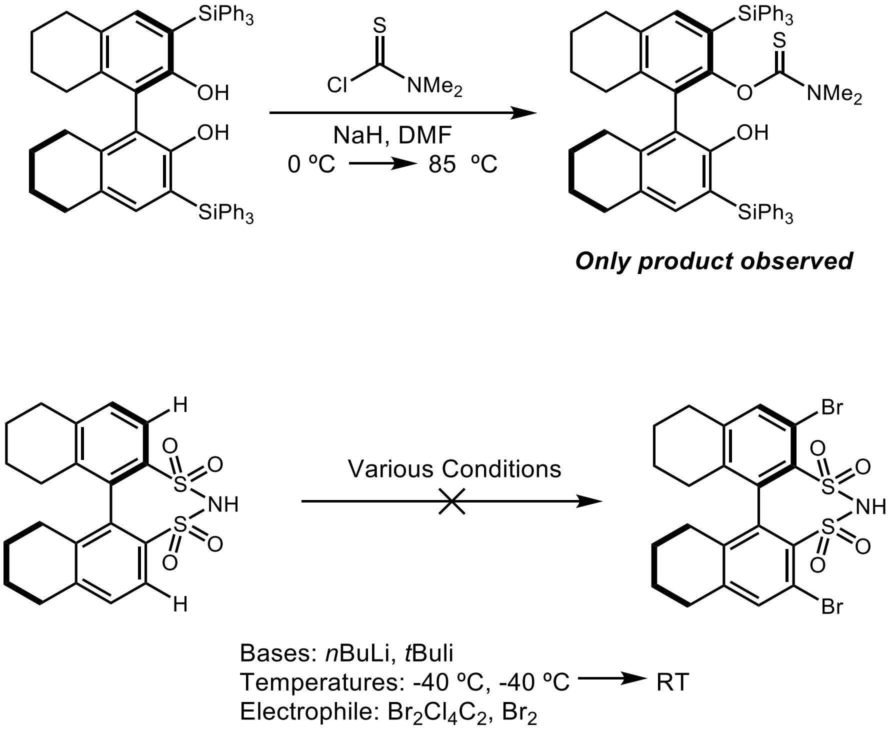
SiPh3
OH
OH
SiPh3
S
Cl
NMe2
NaH, DMF
0 °C → 85 °C
SiPh3
S
O
NMe2
OH
SiPh3
Only product observed
H
O
S
O
NH
S
O
O
H
Various Conditions
Br
O
S
O
NH
S
O
O
Br
Bases: nBuLi, tBuli
Temperatures: -40 °C, -40 °C → RT
Electrophile: Br2Cl4C2, Br2

An alternative reported strategy has been the directed lithiation of sulfonate esters, also reported to give modest yields in the literature.[32] Unfortunately under a variety of conditions we were here again never able to observe any halogenation of our substrates (Figure 2.26), and so were never able to construct the desired TP salts with sterically demanding groups.

Figure 2.26: Further unsuccessful attempts to construct BINOL-derived disulfonyl amides with sterically demanding functional groups at the 3,3'-positions

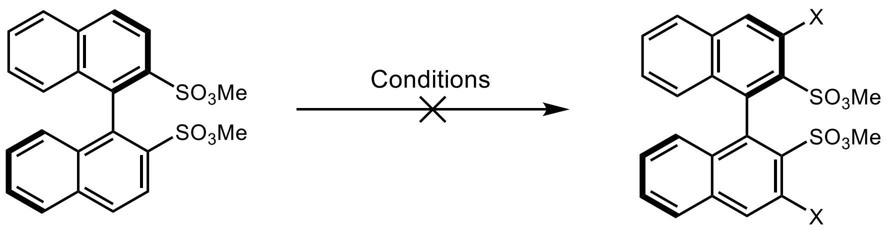

Base	Electrophile	Temperature
*n*BuLi	Br_2	-78 °C
*t*BuLi	Br_2	-60 °C
*t*BuLi	Br_2	0 °C
*t*BuLi	$Br_2Cl_4C_2$	0 °C
*t*BuLi	NBS	0 °C
*n*BuLi	D_2O	0 °C
*t*BuLi	D_2O	0 °C
*t*BuLi	D_2O	-78 °C

Around this time, a new class of dimeric chiral Brønsted acids were reported by List[33,34] that are capable of imparting high levels of enantioselectivity in multiple transformations. This scaffold was appealing because of its highly demanding chiral environment, and so we set out to synthesize a small library of variants with different groups at the 3,3'-positions. Unfortunately under our optimal reaction conditions, no reactivity was ever observed using this system, even when running the reaction at ambient temperature (Figure 2.27). Switching to DCM, however, resulted in complete conversion and in one case a slight level of enantioinduction was observed. This is remarkable because no other system yet investigated has shown any level of enantioselectivity in solvents of moderate polarity. This result could not be improved upon, as any strategy to improve selectivity caused a precipitous loss of reactivity.

Figure 2.27: Imidodiphosphorate anions as potential chiral catalysts

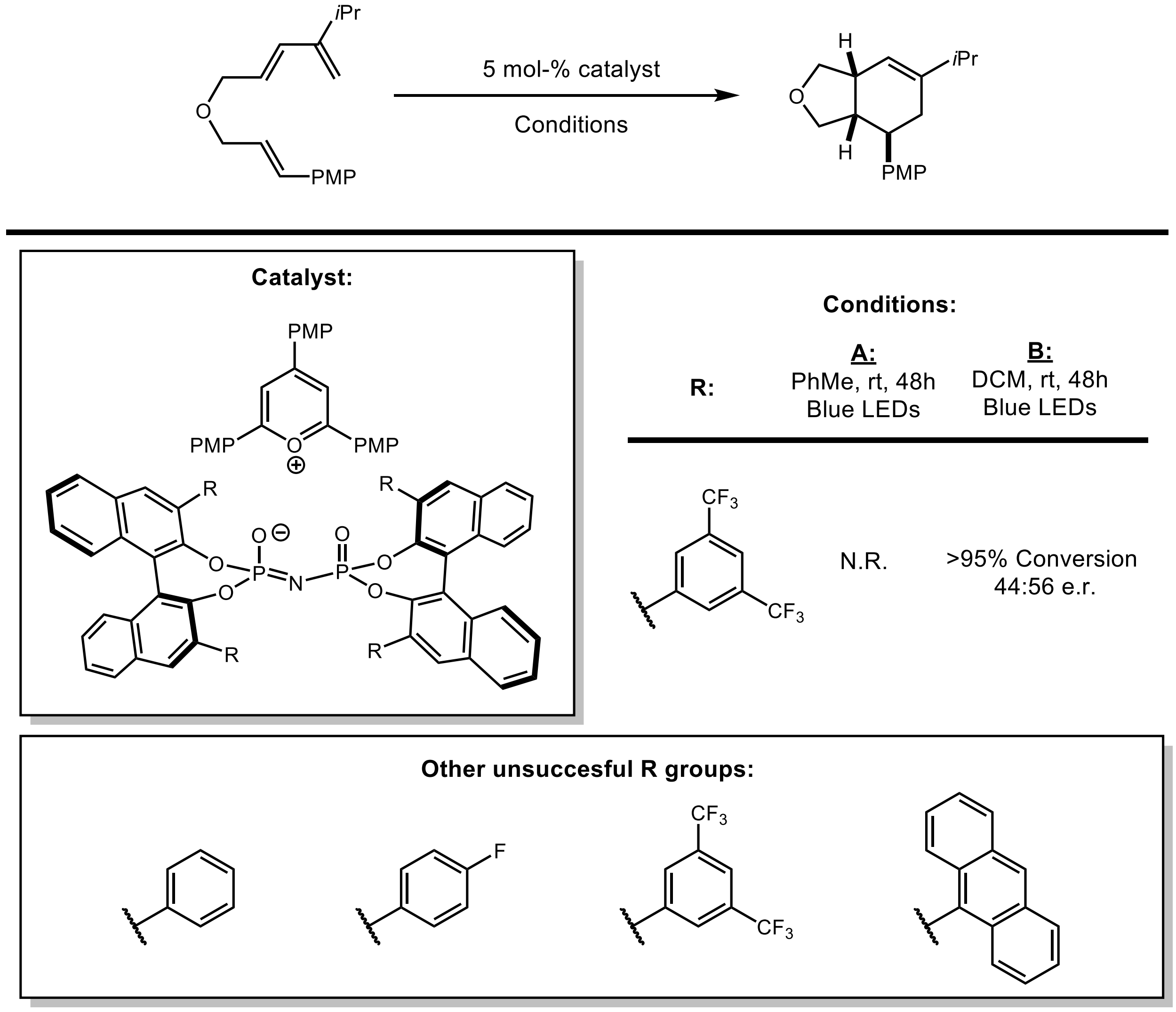
iPr
O
PMP
5 mol-% catalyst
Conditions
H
H
O
iPr
PMP
Catalyst:
PMP
PMP
PMP
O
⊕
R
R
R
R
O⊖
O
O
O
O
O
P
N
P
Conditions:
R:
A:
PhMe, rt, 48h
Blue LEDs
B:
DCM, rt, 48h
Blue LEDs
CF3
CF3
N.R.
>95% Conversion
44:56 e.r.
Other unsuccesful R groups:
F
CF3
CF3

2.4 Incorporation of hydrogen bonding secondary interactions into the system

All approaches to controlling enantioselectivity in this transformation have so far centered around the use of steric blocking groups to destabilize one of two possible enantiomeric transition states. This strategy is common in enantioselective catalysis, but is best applied in systems where a strong and directional bond exists between substrate and catalyst, as in transition metal catalysis and nucleophilic catalysis. On the other hand, in areas of catalysis which rely entirely on non-covalent interactions between substrate and catalyst, it is often beneficial for multiple points of contact to exist between the two. In these cases, enantioinduction is achieved by a selective rate acceleration of one of the two enantiomeric transition states. Multiple stabilizing interactions can serve to further organize the desired transition states and in doing so improve selectivity.[35]

We hypothesized that such a strategy would be amenable to our system and provide a twofold benefit. By adding an additional point of hydrogen bonding between the intermediate and chiral anion, the rigidifying effect could help to enhance enantioselectivity. Furthermore, stabilizing the desired transition state could also help to increase the rate of reaction and improve yields.[35]

Figure 2.28: Previous work demonstrating the ability of hydrogen bonding interactions to improve enantioselectivity in chiral ion pairing catalysis

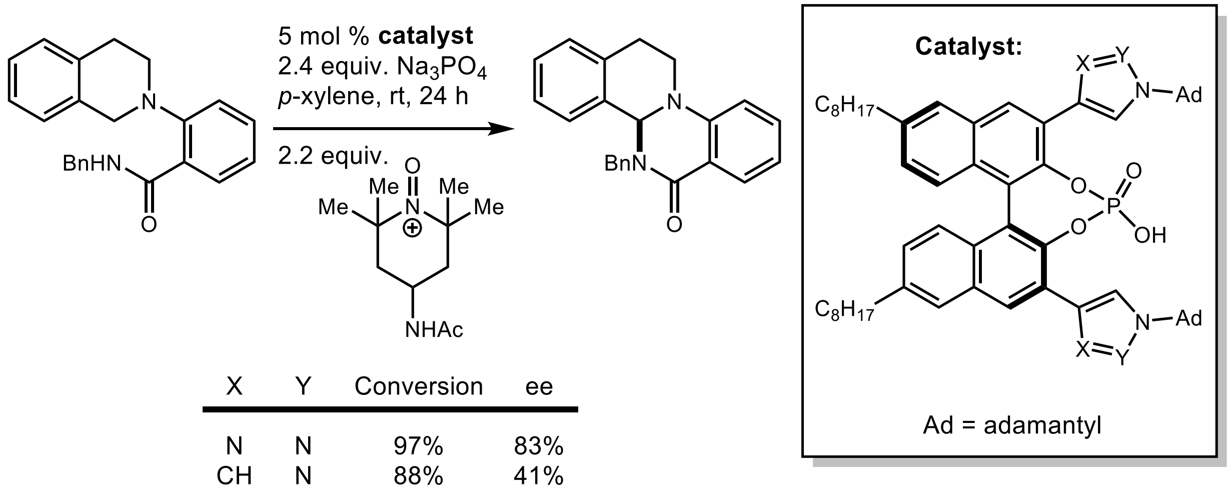

X	Y	Conversion	ee
N	N	97%	83%
CH	N	88%	41%
N	CH	93%	45%

As a first attempt to employ this strategy, we focused on the synthesis of BINOL-derived anions that incorporate triazole functional groups at the 3,3'-positions. Triazoles are reported to be amide bioisosteres and are capable of acting as both hydrogen bond donors and acceptors. They have recently been successfully employed by the Toste group as chiral phase transfer catalysts to carry out enantioselective dehydrogenative cross coupling reactions (Figure

2.28).[36,37] They propose that the hydrogen bonding capabilities of the triazoles are of central importance to their success in this system: by forming an attractive stabilizing interaction with the substrate, the desired transition state is selectively accelerated over the undesired. This claim is supported by the construction of analogues of the catalyst in which each of the nitrogen atoms is sequentially replaced by a methine unit. Both of these variants should have very similar steric properties to the original catalyst, yet both give enantioselectivities half that of the triazole-containing catalyst.

For our system we set out to construct similar analogues to those in the previous report, but without the alkyl substitution in the backbone and again replacing the phosphoric acid with an *N*-triflylphosphoramide. Following the reported protocols, we were able to synthesize the desired Brønsted acid in a straightforward manner.

Figure 2.29: Synthesis of triazole containing chiral anions

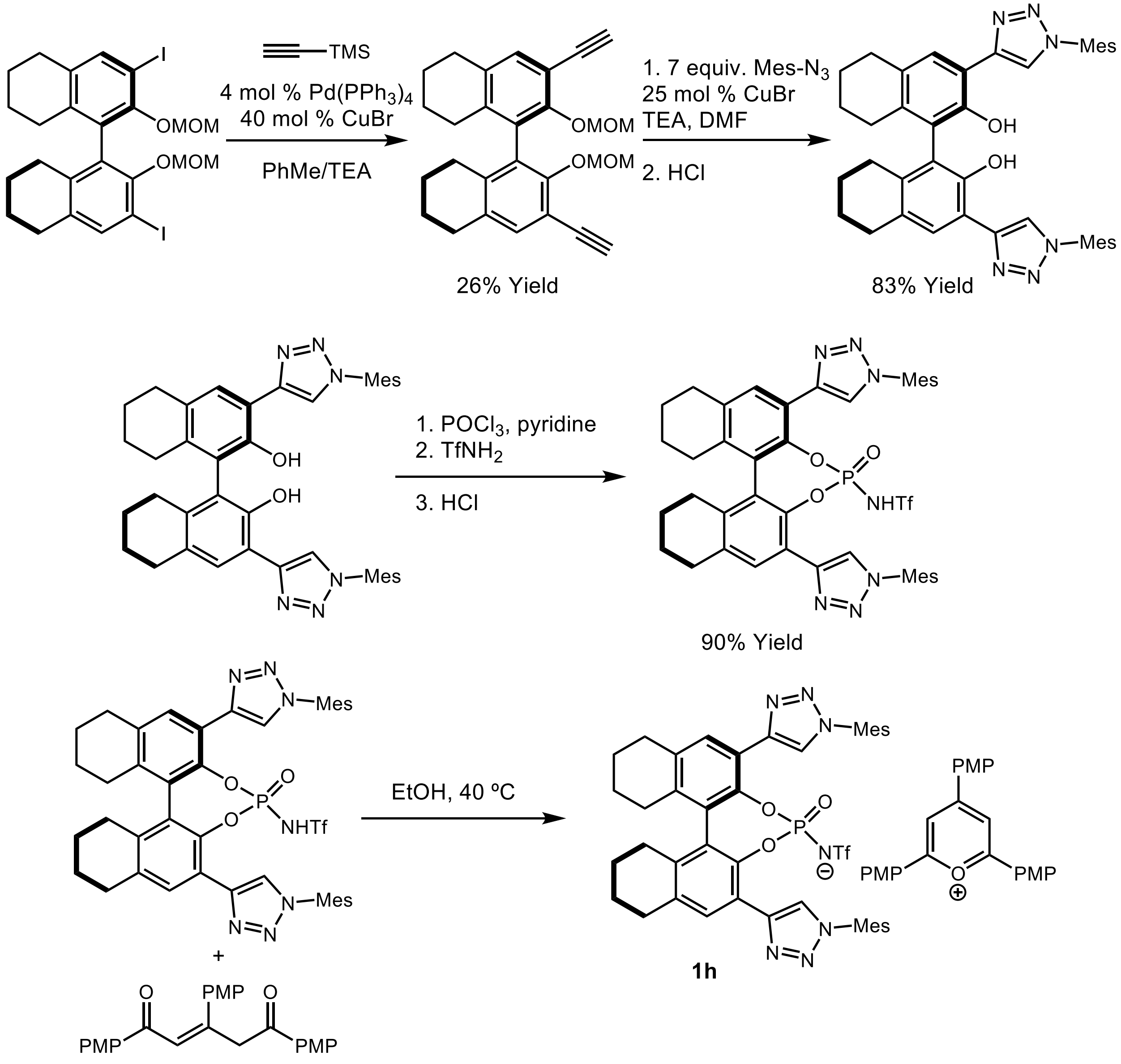
TMS
4 mol % Pd(PPh3)4
40 mol % CuBr
PhMe/TEA
OMOM
OMOM
I
I
26% Yield
1. 7 equiv. Mes-N3
25 mol % CuBr
TEA, DMF
2. HCl
N=N
N—Mes
OH
OH
83% Yield
1. POCl3, pyridine
2. TfNH2
3. HCl
O
P
NHTf
90% Yield
EtOH, 40 ºC
+
PMP
NTf
1h

To create a model system for our studies, we first attempted an intermolecular DA reaction, as the substrates could be rapidly prepared. We designed systems where either the diene or dienophile contained enamide functional groups. They have been shown empirically in the past to act as nucleophilic (and therefore electron rich) olefins, and incorporate an amide as a hydrogen bonding functional site in close proximity to the reaction center.

Figure 2.30: Attempts to design a cation radical DA reaction incorporating H-bonding opportunities

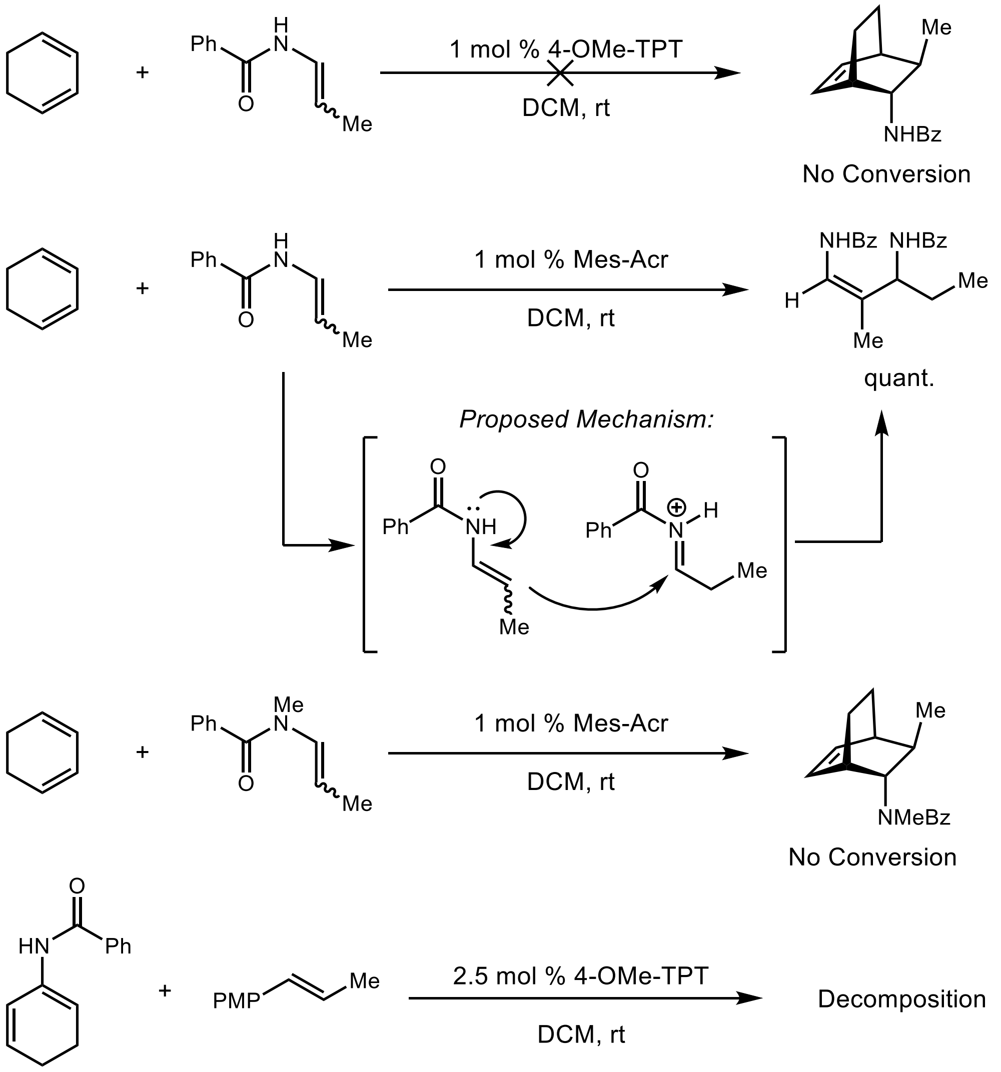

1 mol % 4-OMe-TPT
DCM, rt
No Conversion
1 mol % Mes-Acr
DCM, rt
quant.
Proposed Mechanism:
1 mol % Mes-Acr
DCM, rt
No Conversion
2.5 mol % 4-OMe-TPT
DCM, rt
Decomposition

N-prop-1-enyl benzamide was first prepared as a model substrate and subjected to racemic reaction conditions in order to assess its fitness as a dienophile. Unfortunately it was found only to undergo a dimerization reaction. These types of addition products are known to occur via Brønsted acid catalyzed pathways. The single electron oxidation of the enamide likely renders the amide proton highly acidic. This could then protonate another equivalent of starting material to generate an iminium ion, which is then attacked by a third equivalent of starting material to give the observed product. We methylated the amide as an attempt to protect against this pathway, and while this was successful in preventing dimerization the substrate also failed to undergo any other observable reaction. An enamide-containing diene was also prepared from cyclohexenone, but also resulted in decomposition when subjected to the standard reaction conditions.

Figure 2.31: Attempts to use allylic amides as hydrogen bonding handles

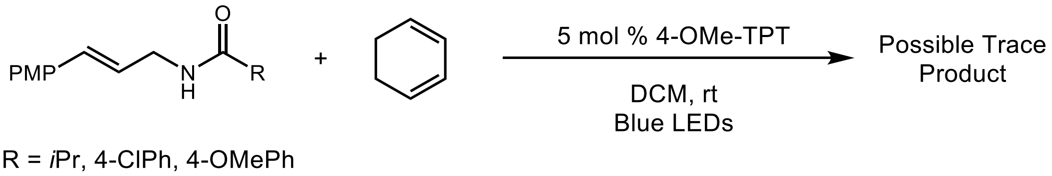

Lastly, we attempted to use an electron rich allylic amide as a dienophile in a DA reaction employing cyclohexadiene as the diene. Three variants of the substrate were used, modifying the substitution on the amide moiety. Minimal conversion was observed with both the aryl amide substrates. With the isopropyl substrate, 41% conversion of the substrate was observed at 4 hours and potential product peaks were seen by crude NMR (Figure 2.31). However, the relatively sluggish and non-selective nature of the reaction indicated that this would not likely transfer well to the enantioselective reaction conditions and so was abandoned.

Figure 2.32: Use of triazole containing TPT salt as a catalyst using the model substrate

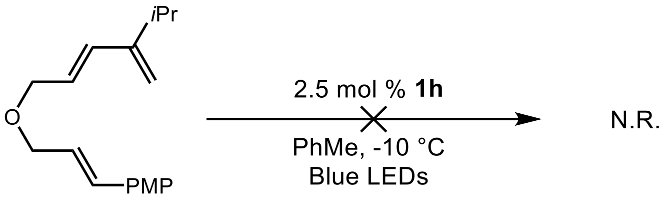

While we have thus far been unsuccessful in designing a hydrogen bonding substrate, we attempted to use our triazole containing complex **1h** as a catalyst for the cation radical DA reaction using our model substrate **2b**. Under several conditions, no conversion to product was observed (Figure 2.32).

The lack of organization between substrate and chiral anion in the transition state is still our best hypothesis as to why obtaining very high levels of enantioselectivity remains a challenge in the cation radical Diels-Alder reaction. Our highest hopes for improving the enantioselectivity with our catalysts still lie in developing a system that can incorporate opportunities for stabilizing secondary interactions. Whether these take the form of hydrogen bonds or some other type of interaction is an open choice at this point.

2.5 Progress towards the development of an aromatic Claisen rearrangement

Having developed a new catalyst system and demonstrated that it was capable of inducing asymmetry in cation radical DA reactions, we next became interested in seeing if these salts could successfully be used to control the absolute stereochemistry of other reactions that are initiated by single electron oxidation of a substrate to a cation radical.

One of the first reactions that attracted our attention was a report of an aromatic Claisen rearrangement that is promoted by triaryl aminium salts.[38] The reaction was shown to give moderate yields using a number of electron rich aromatic substrates. The only allylic fragment used was allenyl, and the reason for this limitation is not commented on. As a set of control reactions, the substrates were treated with trifluoroacetic acid (TFA) as the solvent, as well as HCl and hexachloroantimonic acid. The formation of the desired products was not observed. This allowed them to rule out the possibility of Brønsted acid catalysis.

Figure 2.33: Prior report of a cation radical aromatic Claisen rearrangement

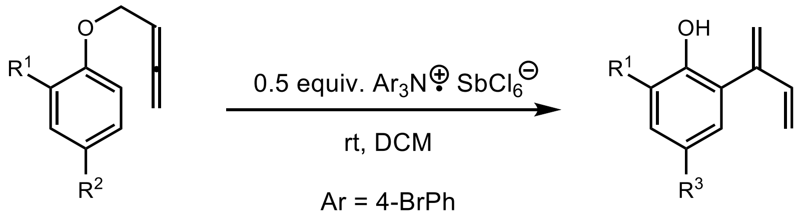

R^1	R^2	Yield
H	OMe	55%
OMe	H	60%
OMe	Me	65%
H	OEt	60%

As the reaction is proposed to proceed through single electron oxidation of the substrate, we thought that it might be amenable to our catalyst system and allow us to develop an enantioselective aromatic Claisen rearrangement, of which few examples have so far been reported. We also thought that the reaction would proceed through a 6-membered transition state, the organization of which would be beneficial in obtaining high levels of selectivity. Furthermore, we hypothesized that the driving force for re-aromatization of the product could aid the overall rate of reaction.

Figure 2.34: Strategy for developing an asymmetric aromatic Claisen rearrangement

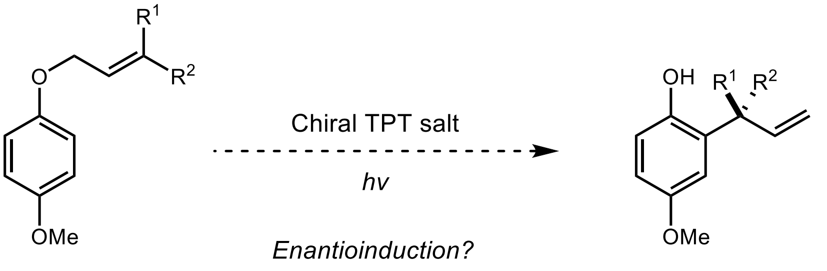

The first matter was to construct a number of potential substrates for the reaction that would result in the formation of a stereocenter after rearrangement. Towards this goal we carried out the *O*-alkylation of 4-methoxyphenol with crotyl, cinnamyl, and prenyl groups to provide a representative sampling of substitution patterns. While the rearrangement of the prenyl group would not set a stereocenter, it would provide an important indication as to whether the method would allow for the construction of quaternary stereocenters.

Figure 2.35: Attempts to use photoredox catalysts to catalyze aromatic Claisen rearrangements

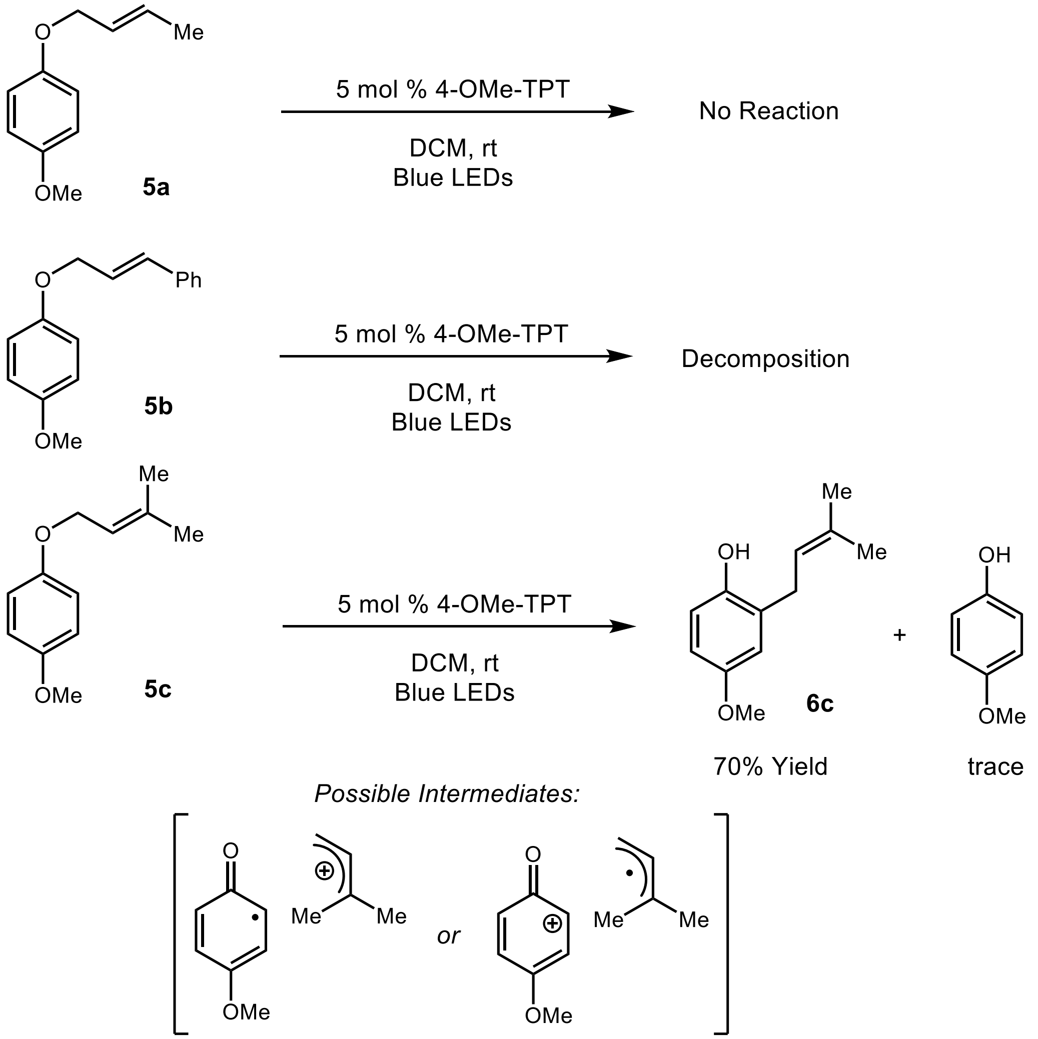

O
Me
OMe
5a
5 mol % 4-OMe-TPT
DCM, rt
Blue LEDs
No Reaction
O
Ph
OMe
5b
5 mol % 4-OMe-TPT
DCM, rt
Blue LEDs
Decomposition
Me
O
Me
OMe
5c
5 mol % 4-OMe-TPT
DCM, rt
Blue LEDs
OH
Me
Me
OMe
6c
70% Yield
+
OH
OMe
trace
Possible Intermediates:
O
⊕
Me
Me
OMe
or
O
⊕
Me
Me
OMe

When irradiated in DCM at room temperature with catalytic quantities of 4-OMe-TPT, the crotyl substrate underwent no reaction, while the cinnamyl substrate decomposed completely. Perhaps the most interesting result was obtained with the crotyl substrate, which cleanly rearranged in a 70% yield to a product arising from 1,3-alkyl migration to the *ortho*-position of the aromatic ring. This result indicates to us that after single electron oxidation, a bond scission occurs to fragment the intermediate. These two fragments would then be free to recombine at the less sterically hindered position of the allyl fragment, giving rise to the observed product. This could also explain the difference in reactivity between the first two substrates: as the crotyl fragment is less able to stabilize spin or charge density than the other two substrates, bond scission may not be favorable.

In spite of these results, each substrate was also subjected to enantioselective reaction conditions, on the hypothesis that the change to an aromatic solvent and mediation by the presence of a more nucleophilic anion could significantly change the reactivity patterns observed so far. However, using either complexes **1d** or **1i** as potential catalysts, no reactivity was in this case observed with any of the substrates.

Figure 2.36: Attempts to use chiral photoredox catalysts in the aromatic Claisen rearrangement

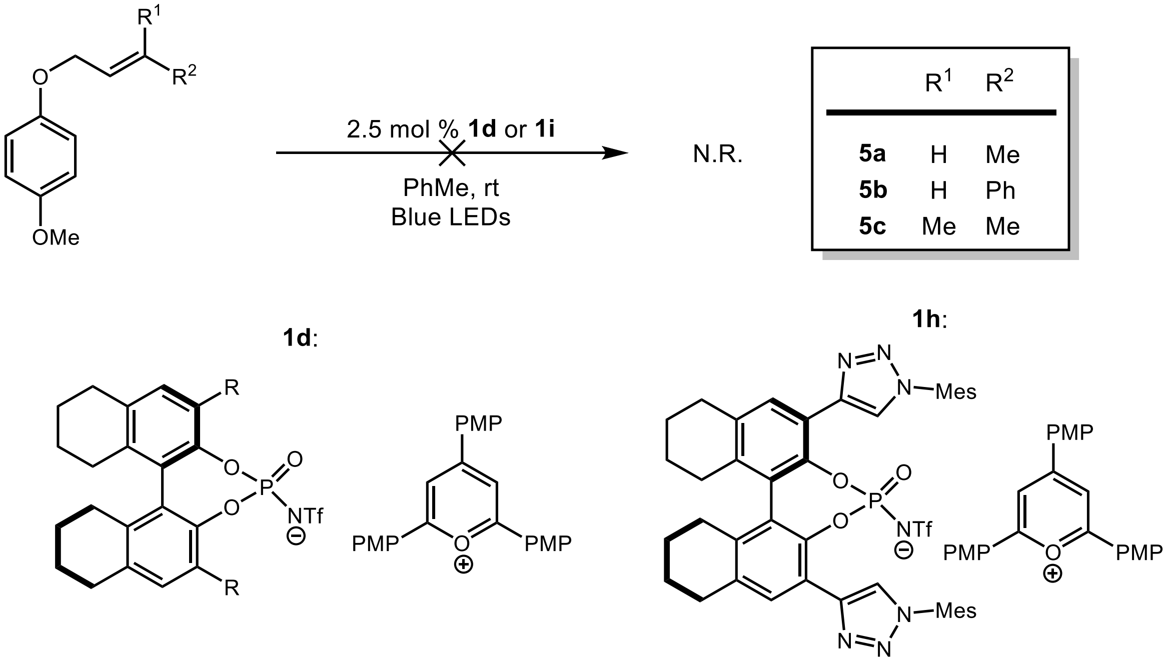

	R^1	R^2
5a	H	Me
5b	H	Ph
5c	Me	Me

One attempt was also made to carry out an asymmetric Claisen rearrangement using a non-aromatic substrate. Here again however, only a product arising from bond cleavage was observed. At this time we chose to abandon this strategy, but much remains to be studied in this reaction. One possible avenue for future inquiry might be further altering the substitution of the aromatic ring, especially at the *meta*-position.

Figure 2.37: Attempt to carry out a standard Claisen rearrangement

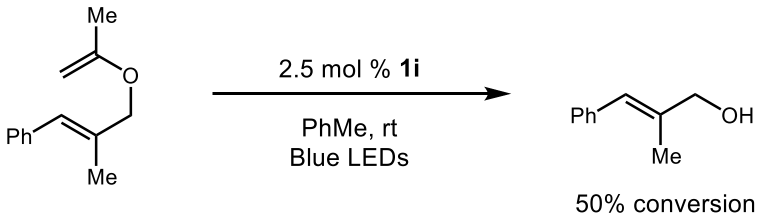

2.6 Application to [2+2] cycloadditions

Finally, a few attempts were made at carrying out enantioselective [2+2] cycloadditions. The dimerization of *N*-vinylcarbazole gave no enantioselectivity. We additionally attempted to carry out a resolution of a racemic [2+2] adduct synthesized by Dr. Michelle Riener in our lab. This was based on the hypothesis that the cyclobutane products are themselves oxidizable, and should undergo benzylic bond fragmentation subsequently. Only racemic starting material was recovered. This result should not have been too surprising, as the kinetic profile of the reaction does not match that normally needed for a resolution to occur – while the reaction does proceed through an achiral intermediate, a final irreversible step is required which is not the case here.

Figure 2.38: Attempts to induce asymmetry in [2+2] cyclodaddition reactions

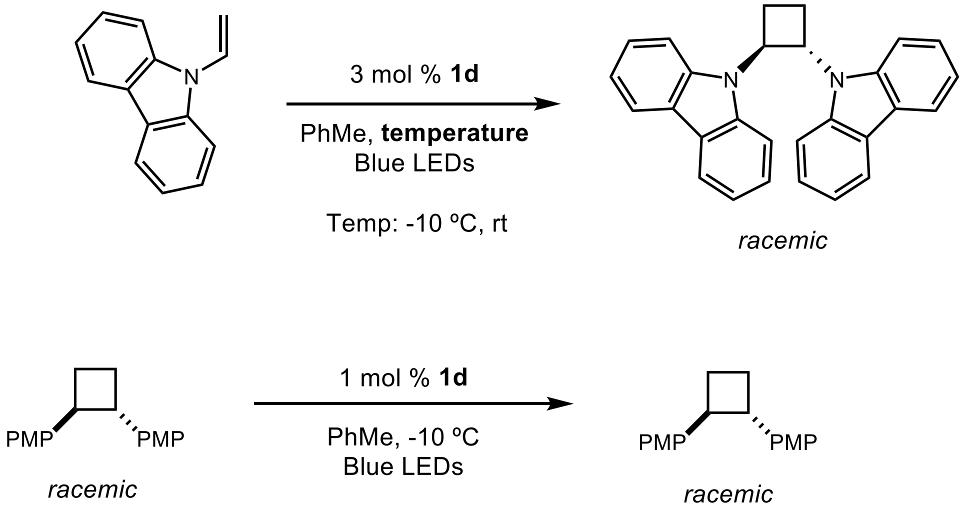
N
3 mol % **1d**
PhMe, **temperature**
Blue LEDs
Temp: -10 ºC, rt
N
N
racemic
PMP
PMP
racemic
1 mol % **1d**
PhMe, -10 ºC
Blue LEDs
PMP
PMP
racemic

2.7 Application of chiral anions to *anti*-Markovnikov hydrofunctionalizations

As a final path of inquiry, we set out to explore whether these catalysts could be used to control the absolute stereochemistry of one of the *anti*-Markovnikov hydrofunctionalization reactions developed in our lab.[39–42] We chose to focus our efforts on the intermolecular hydroacetoxylation reaction first reported by Dr. Andrew Perkowski in our group.[43] This transformation allows for acetic acid to be added across styrenyl olefins and tertiary olefins with complete selectivity for the *anti*-Markovnikov regioisomeric products.

Figure 2.39: Select examples of *anti*-Markovnikov hydroacetoxylation reactions

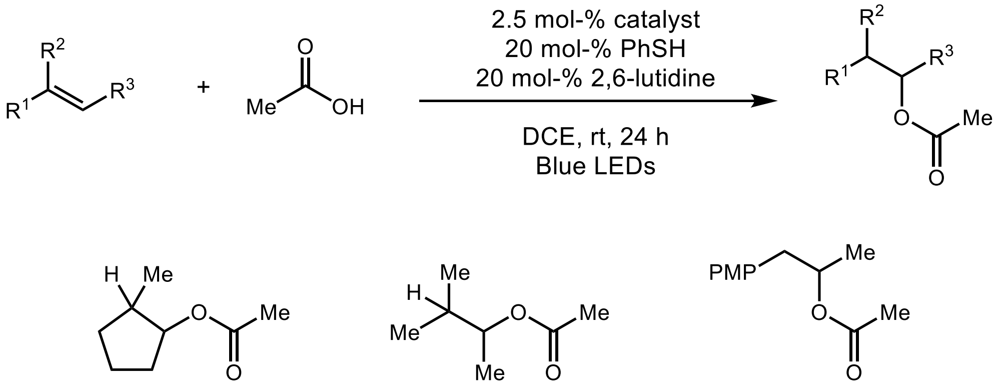
R2
R1
R3
+
O
Me
OH
2.5 mol-% catalyst
20 mol-% PhSH
20 mol-% 2,6-lutidine
DCE, rt, 24 h
Blue LEDs
R2
R1
R3
O
Me
O
H
Me
O
Me
O
Me
H
Me
O
Me
Me
O
PMP
Me
O
Me
O

61% Yield
1.9:1 d.r.

74% Yield

71% Yield

The proposed mechanism for the reaction begins in a fashion somewhat analogous to the cation radical DA mechanism. In this case, the 9-mesityl-10-methyl acridinium tetrafluoroborate (Mes-Acr) photoredox catalyst is employed and in its excited state, encounters an electron rich olefin and removes an electron from it to generate a cation radical intermediate. However, now the cation radical intermediate is intercepted by an equivalent of acetic acid. The observed regioselectivity in the reaction is proposed to be driven by the formation of the more stable of two possible resulting radical intermediates.

Figure 2.40: Proposed mechanism for the catalytic hydroacetoxylation reaction

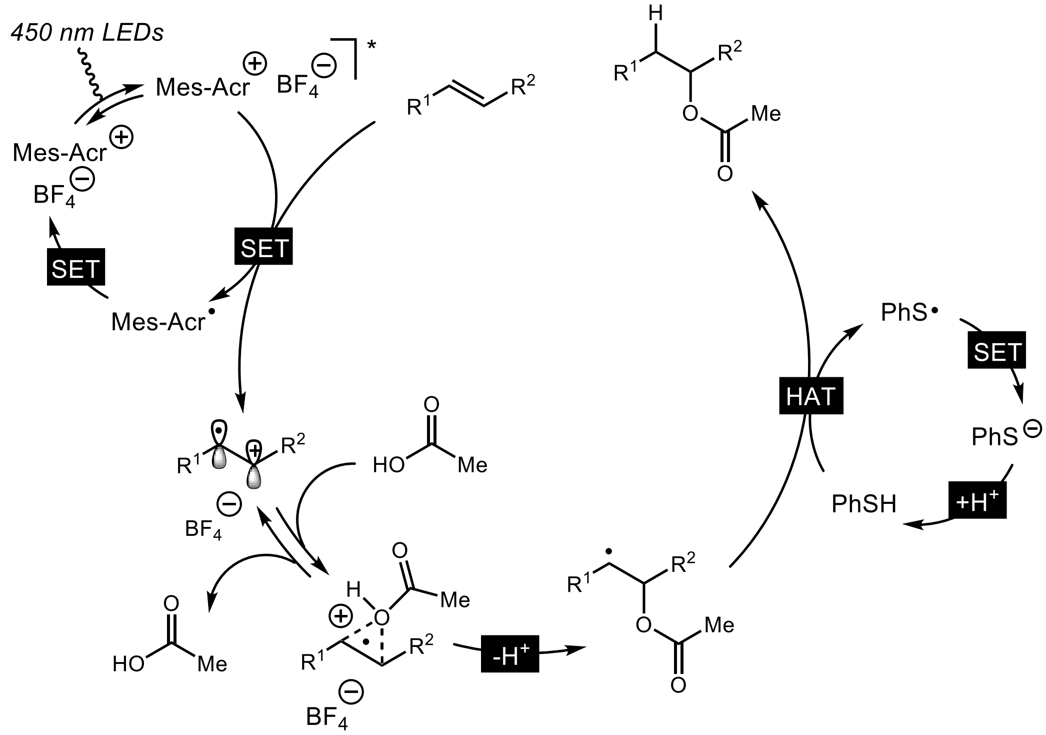

Key to the success of the reaction is the inclusion of catalytic quantities of a redox active H-atom donor. This co-catalyst acts by first taking part in H-atom donation with the free radical intermediate of the reaction to furnish the final product. This process results in the formation of a thiyl radical, which is also critical in the reaction, as it serves to turn over the reduced form of Mes-Acr to regenerate the active photoredox catalyst. Finally, the resulting thiolate anion is protonated to regenerate thiophenol and complete the catalytic cycle.

We had several reasons to believe that this would be a fruitful reaction to investigate with our chiral catalyst system. As in the DA reaction, if the reaction were to be run in toluene, then presumably there should again be a desirable ion pairing interaction between the cation radical intermediate and our chiral anion, which would allow for the relay of chiral information. Since the acetate anion would be a stronger nucleophile than an olefin, we were also hopeful that this would help increase the overall rate of reaction. Working on an intermolecular reaction employing simple substrates was also appealing from a practical standpoint, as it would allow us to rapidly screen reaction conditions and reagents.

We were interested again in using hydrogen bond donating or accepting substrates in this transformation as a possible way of improving enantioselectivity. Since no such substrates had been reported in the initial disclosure of the hydroacetoxylation, the first matter was to test a number of potential new substrates for reactivity under racemic reaction conditions.

Figure 2.41: Hydroacetoxylation of substrates with allylic hydrogen bonding groups

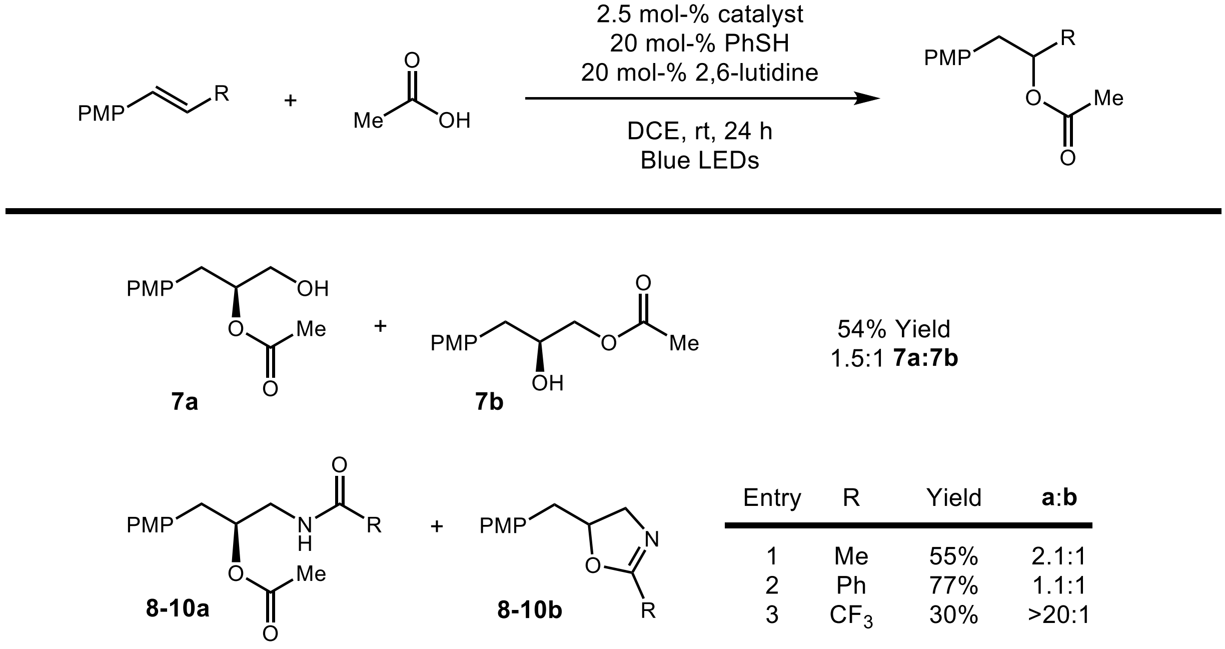

7a + **7b**

54% Yield
1.5:1 **7a**:**7b**

8-10a + **8-10b**

Entry	R	Yield	**a**:**b**
1	Me	55%	2.1:1
2	Ph	77%	1.1:1
3	CF_3	30%	>20:1

4-methoxy-cinnamyl alcohol was found to undergo *anti*-Markovnikov hydroacetoxylation under the optimized reaction conditions in good yield. A mixture of two products were observed, with **7b** likely arising from spontaneous trans-esterification to the less sterically hindered primary alcohol.

While appreciable yields of the hydroacetoxylation product were seen when using allylic amides as substrate, an interesting side product was observed in this case as well. NMR and mass spectrometry confirmed it to be an oxazoline, which is likely to arise from intramolecular cyclization of the pendant amide functional group onto the olefin. No oxazoline formation was observed for a substrate containing a trifluoromethyl group bound to the amide. This is possibly due to the electron withdrawing nature of the group decreasing the amide's nudelophilicity. At this point we were unsure whether this product arose from direct attack by the amide onto the cation radical, or whether a two-step process was occurring in which hydroacetoxylation first takes place, followed by a substitution reaction in which the acetate is displaced by the amide. We were delighted by this result, as we thought that it had the potential to be developed into a direct and mild method for synthesizing oxazolines. The further development of this reaction will be the topic of the following chapter.

We then proceeded to investigate the use of our chiral anions to control the absolute stereochemistry of this reaction. When attempting to run the reaction in toluene, it was observed that the amide substrates would not fully dissolve in such nonpolar solvent. However, using a 9:1 ratio of toluene to acetic acid allowed complete solubility to be achieved. The acetic acid used also contained 5% acetic anhydride as a desiccant. In this case, chiral complexes were used that consisted of the Mes-Acr photoredox catalyst with previously discussed chiral anions. Oxopyrylium salts have not proven to be productive catalysts in the racemic version of this transformation, likely due to their high susceptibility to degradation by nucleophiles. In each experiment detailed in Figure 2.42, no enantioselectivity was observed with any substrate and catalyst pair tested. As these experiments were only an initial screen for selectivity, isolated yields of the products were not obtained. We observed that when 2,6-lutidine was removed from the reaction mixture, complete selectivity for the oxazoline product was obtained, but this product was also racemic. It is interesting that absolutely no enantioinduction is observed. While there are many possible reasons for this, one is that in this case the catalyst is simply not

Figure 2.42: Attempts to control the absolute stereochemistry of the hydroacetoxylation

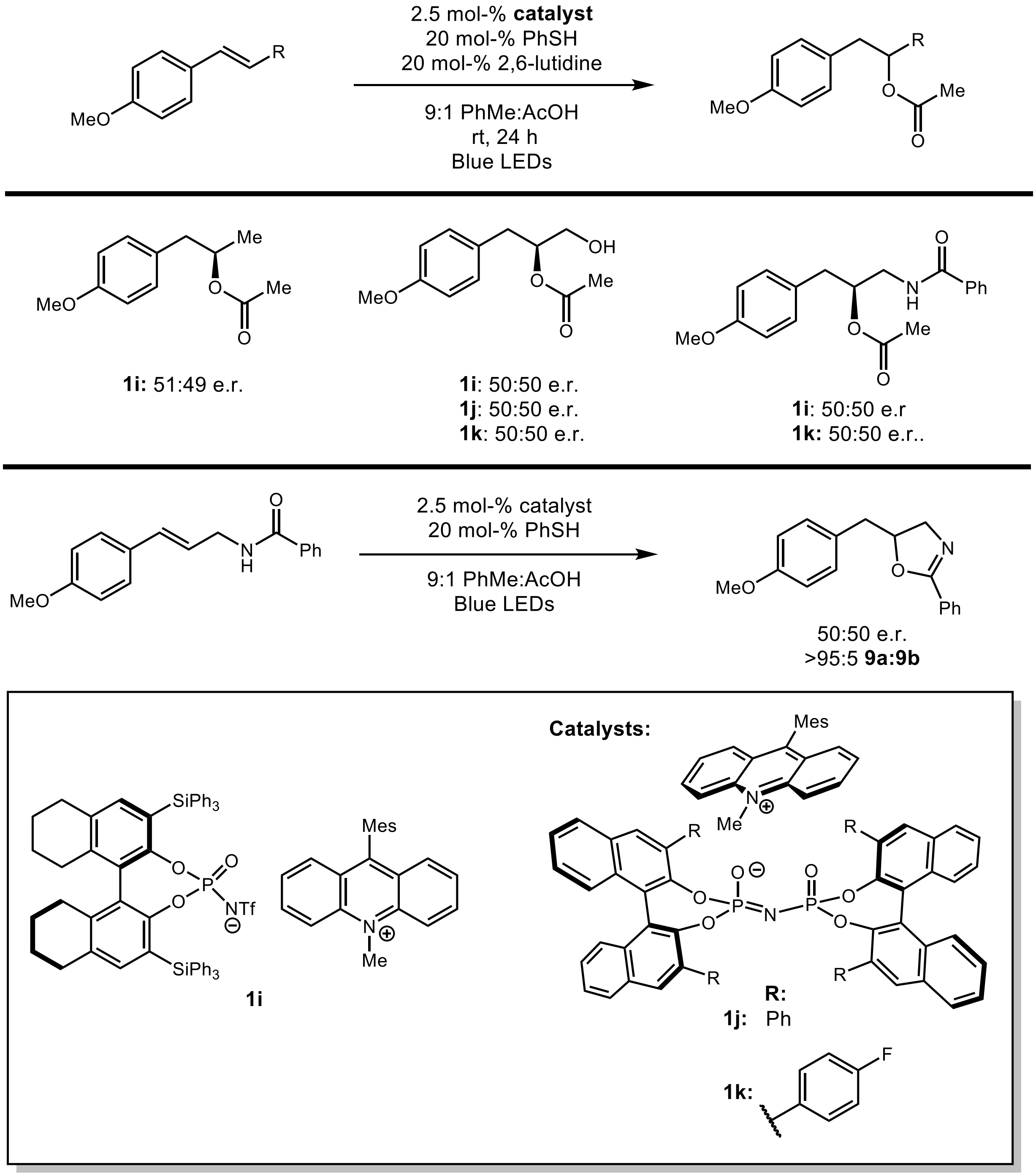
2.5 mol-% **catalyst**
20 mol-% PhSH
20 mol-% 2,6-lutidine
9:1 PhMe:AcOH
rt, 24 h
Blue LEDs
MeO
R
O
Me
1i: 51:49 e.r.
1i: 50:50 e.r.
1j: 50:50 e.r.
1k: 50:50 e.r.
1i: 50:50 e.r
1k: 50:50 e.r..
OH
N
H
Ph
2.5 mol-% catalyst
20 mol-% PhSH
9:1 PhMe:AcOH
Blue LEDs
50:50 e.r.
>95:5 **9a:9b**
Catalysts:
Mes
SiPh3
NTf
Me
1i
R:
1j: Ph
1k:
F

associated with the intermediates during the enantiodetermining step of the reaction. This would be possible if said step actually occurs on a neutral intermediate which has no coulombic attraction to the chiral anion. While this strategy has not been met with success, other tactics for controlling the absolute stereochemistry of *anti*-Markovnikov hydrofunctionalizations are currently underway.

The results of this chapter have taught a great deal about important factors in the design of catalysts that can carry out asymmetric cation radical DA reactions. While the systems are so far are not developed to the level of being synthetically useful, we have made significant progress towards this goal and intend to further improve the design of our catalysts.

REFERENCES

(1) Nicolaou, K. C.; Snyder, S. A.; Montagnon, T.; Vassilikogiannakis, G. *Angew. Chem. Int. Ed.* **2002**, *41* (10), 1668–1698.

(2) Takao, K.; Munakata, R.; Tadano, K. *Chem. Rev.* **2005**, *105* (12), 4779–4807.

(3) Jiang, X.; Wang, R. *Chem. Rev.* **2013**, *113* (7), 5515–5546.

(4) Kagan, H. B.; Riant, O. *Chem. Rev.* **1992**, *92* (5), 1007–1019.

(5) Walsh, P.; Kowzlowski, M. *Fundamentals Of Asymmetric Catalysis*; University Science Books: Sausalito, Calif, 2008.

(6) Evans, D. A.; Miller, S. J.; Lectka, T. *J. Am. Chem. Soc.* **1993**, *115* (14), 6460–6461.

(7) Nakashima, D.; Yamamoto, H. *J. Am. Chem. Soc.* **2006**, *128* (30), 9626–9627.

(8) Lin, S.; Padilla, C. E.; Ischay, M. A.; Yoon, T. P. *Tetrahedron Lett.* **2012**, *53* (24), 3073–3076.

(9) Liao, W.; Yu, Z.-X. *J. Org. Chem.* **2014**, *79* (24), 11949–11960.

(10) Bellville, D. J.; Wirth, D. W.; Bauld, N. L. *J. Am. Chem. Soc.* **1981**, *103* (3), 718–720.

(11) Pabon, R. A.; Bellville, D. J.; Bauld, N. L. *J. Am. Chem. Soc.* **1983**, *105* (15), 5158–5159.

(12) Bauld, N. L.; Bellville, D. J.; Harirchian, B.; Lorenz, K. T.; Pabon, R. A.; Reynolds, D. W.; Wirth, D. D.; Chiou, H. S.; Marsh, B. K. *Acc. Chem. Res.* **1987**, *20* (10), 371–378.

(13) Bauld, N. L.; Gao, D. *J. Chem. Soc. Perkin Trans. 2* **2000**, No. 5, 931–934.

(14) Lorenz, K. T.; Bauld, N. L. *J. Am. Chem. Soc.* **1987**, *109* (4), 1157–1160.

(15) Reynolds, D. W.; Lorenz, K. T.; Chiou, H. S.; Bellville, D. J.; Pabon, R. A.; Bauld, N. L. *J. Am. Chem. Soc.* **1987**, *109* (16), 4960–4968.

(16) Yueh, W.; Bauld, N. L. *J. Am. Chem. Soc.* **1995**, *117* (21), 5671–5676.

(17) Haberl, U.; Wiest, O.; Steckhan, E. *J. Am. Chem. Soc.* **1999**, *121* (28), 6730–6736.

(18) Gieseler, A.; Steckhan, E.; Wiest, O.; Knoch, F. *J. Org. Chem.* **1991**, *56* (4), 1405–1411.

(19) Lin, S.; Ischay, M. A.; Fry, C. G.; Yoon, T. P. *J. Am. Chem. Soc.* **2011**, *133* (48), 19350–19353.

(20) Kim, J. I.; Schuster, G. B. *J. Am. Chem. Soc.* **1990**, *112* (26), 9635–9637.

(21) Phipps, R. J.; Hamilton, G. L.; Toste, F. D. *Nat. Chem.* **2012**, *4* (8), 603–614.

(22) Mahlau, M.; List, B. *Angew. Chem. Int. Ed.* **2013**, *52* (2), 518–533.

(23) Hamilton, G. L.; Kanai, T.; Toste, F. D. *J. Am. Chem. Soc.* **2008**, *130* (45), 14984–14986.

(24) Schreiner, P. R. *Chem. Soc. Rev.* **2003**, *32* (5), 289–296.

(25) Taylor, M. S.; Jacobsen, E. N. *Angew. Chem. Int. Ed.* **2006**, *45* (10), 1520–1543.

(26) Cheon, C. H.; Yamamoto, H. *Chem. Commun.* **2011**, *47* (11), 3043–3056.

(27) Kaupmees, K.; Tolstoluzhsky, N.; Raja, S.; Rueping, M.; Leito, I. *Angew. Chem. Int. Ed.* **2013**, *52* (44), 11569–11572.

(28) Wender, P. A.; Croatt, M. P.; Deschamps, N. M. *Angew. Chem. Int. Ed.* **2006**, *45* (15), 2459–2462.

(29) Treskow, M.; Neudörfl, J.; Giernoth, R. *Eur. J. Org. Chem.* **2009**, *2009* (22), 3693–3697.

(30) Guin, J.; Rabalakos, C.; List, B. *Angew. Chem.* **2012**, *124* (35), 8989–8993.

(31) He, H.; Chen, L.-Y.; Wong, W.-Y.; Chan, W.-H.; Lee, A. W. M. *Eur. J. Org. Chem.* **2010**, *2010* (22), 4181–4184.

(32) Hatano, M.; Sugiura, Y.; Ishihara, K. *Tetrahedron Asymmetry* **2010**, *21* (9–10), 1311–1314.

(33) Čorić, I.; List, B. *Nature* **2012**, *483* (7389), 315–319.

(34) Liao, S.; Čorić, I.; Wang, Q.; List, B. *J. Am. Chem. Soc.* **2012**, *134* (26), 10765–10768.

(35) Knowles, R. R.; Jacobsen, E. N. *Proc. Natl. Acad. Sci.* **2010**, *107* (48), 20678–20685.

(36) Neel, A. J.; Hehn, J. P.; Tripet, P. F.; Toste, F. D. *J. Am. Chem. Soc.* **2013**, *135* (38), 14044–14047.

(37) Milo, A.; Neel, A. J.; Toste, F. D.; Sigman, M. S. *Science* **2015**, *347* (6223), 737–743.

(38) Dhanalekshmi, S.; Venkatachalam, C. S.; Balasubramanian, K. K. *J. Chem. Soc. Chem. Commun.* **1994**, No. 4, 511–512.

(39) Hamilton, D. S.; Nicewicz, D. A. *J. Am. Chem. Soc.* **2012**, *134* (45), 18577–18580.

(40) Wilger, D. J.; Grandjean, J.-M. M.; Lammert, T. R.; Nicewicz, D. A. *Nat. Chem.* **2014**, *6* (8), 720–726.

(41) Nguyen, T. M.; Manohar, N.; Nicewicz, D. A. *Angew. Chem. Int. Ed.* **2014**, *53* (24), 6198–6201.

(42) Nguyen, T. M.; Nicewicz, D. A. *J. Am. Chem. Soc.* **2013**, *135* (26), 9588–9591.

(43) Perkowski, A. J.; Nicewicz, D. A. *J. Am. Chem. Soc.* **2013**, *135* (28), 10334–10337.

(44) Rueping, M.; Nachtsheim, B. J.; Koenigs, R. M.; Ieawsuwan, W. *Chem. – Eur. J.* **2010**, *16* (44), 13116–13126.

(45) Sewgobind, N. V.; Wanner, M. J.; Ingemann, S.; de Gelder, R.; van Maarseveen, J. H.; Hiemstra, H. *J. Org. Chem.* **2008**, *73* (16), 6405–6408.

CHAPTER 3: PHOTOREDOX CATALYZED HYDROFUNCTIONALIZATION REACTIONS FOR THE SYNTHESIS OF OXAZOLINES AND THIAZOLINES

At the conclusion of the prior chapter, we disclosed that during our attempts to use allylic amides as substrates for an *anti*-Markovnikov hydrofunctionalization reaction we observed the formation of oxazolines as byproducts. These products are the result of the amide group acting as a nucleophile leading to an intramolecular cyclization reaction. As oxazolines are found in a variety of small molecules, we chose to pursue this result to develop a mild and general strategy for synthesizing oxazolines and thiazolines.

Figure 3.1: Observation of oxazoline byproduct formation during the hydroacetoxylation of allylic amides

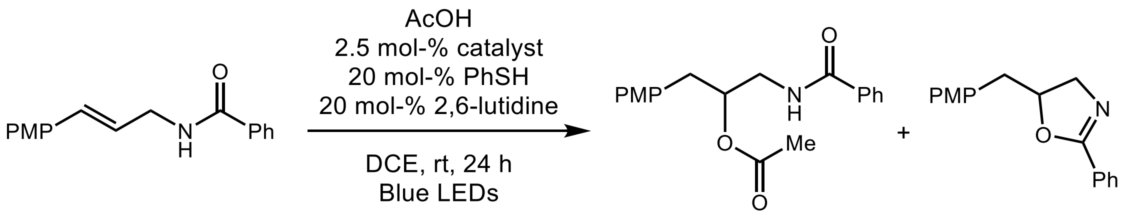

3.1 Occurrence and applications of oxazolines and thiazolines

Figure 3.2: Naming and numbering conventions for oxazolines and thiazolines

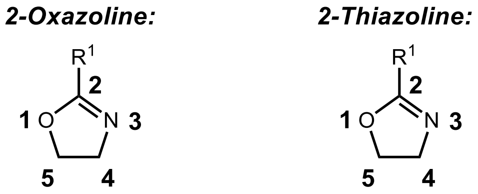

Oxazolines and thiazolines are prevalent motifs found in a variety of naturally and unnaturally occurring small molecules. Many natural products bearing these moieties have been found to possess potent levels of bioactivity, including antibiotic,[1,2] anti-tumor,[3] antiinflammatory,[4] and anti-fungal activity.[5] Additionally, these structures appear frequently in the architecture of ligands for asymmetric catalysis, with two of the most prevalent examples being the bisoxazoline (BOX) and phosphinooxazoline (PHOX) classes.[6,7]

Figure 3.3: Select examples of small molecules containing oxazoline and thiazoline moieties

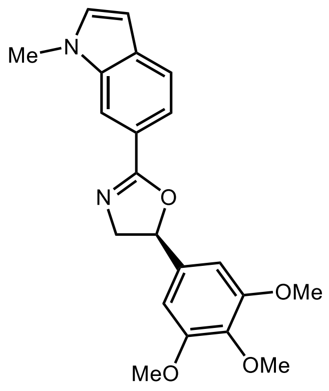

A-289090
Tubulin Polymerization
Inhibitor

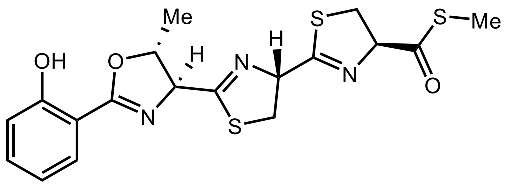

Coelibactin
Siderophore

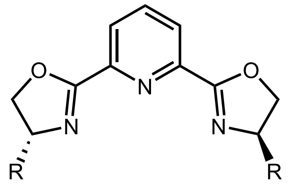

PyBOX Ligand

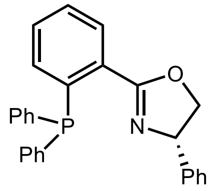

PHOX Ligand

3.2 Previous methods for the synthesis of oxazolines and thiazolines

Many methods have been previously developed for the synthesis of oxazolines and thiazolines, given their previously described prevalence and significance as motifs in small molecules. One popular strategy, especially in the synthesis of ligands for asymmetric catalysis, centers on intermolecular cyclizations of amino alcohols. The appeal of this tactic is that many 1,2-amino alcohols can be readily prepared from the corresponding amino acid, which allows rapid access to enantiopure material. However, at the same time the scope of the reaction is limited to cheap and abundant naturally occurring chiral amino acids. Accessing amino alcohols with other substitution patterns is less trivial.

Figure 3.4: Three-step oxazoline synthesis from a carboxylic acid

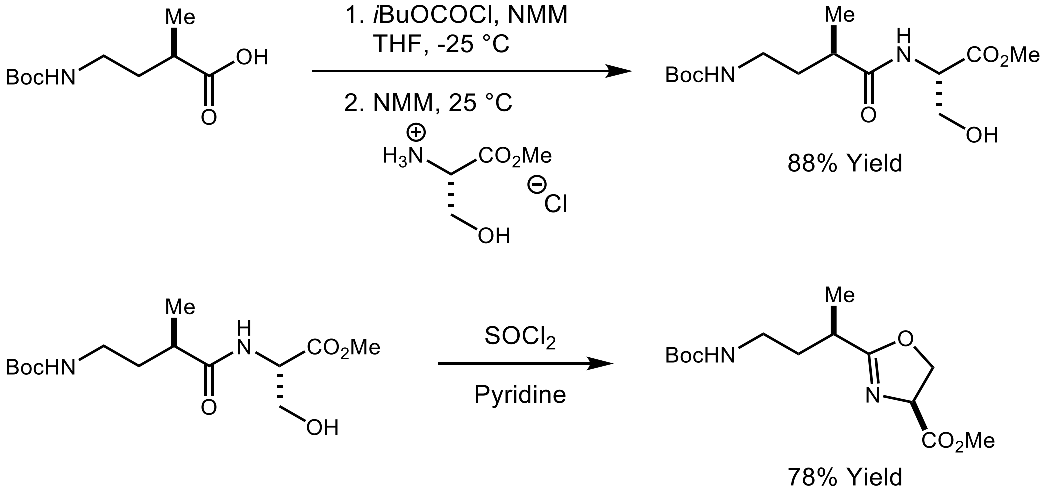
Me
BocHN
OH
O
1. iBuOCOCl, NMM
THF, -25 °C
2. NMM, 25 °C
H3N
CO2Me
Cl
OH
Me
H
N
CO2Me
BocHN
O
OH
88% Yield
Me
H
N
CO2Me
BocHN
O
OH
SOCl2
Pyridine
Me
BocHN
O
N
CO2Me
78% Yield

In a multi-step sequence, amino alcohols have been shown to react with an acyl chloride to first form an amide.[8] This can then be treated with thionyl chloride followed by base to induce ring closure. This sequence is generally high yielding with a wide number of substrates. Similarly, nitriles will cyclize with amino alcohols in a one-step reaction promoted by zinc chloride.[9] A one-pot oxidative cyclization sequence has also been reported between amino alcohols and aldehydes.[10] Following condensation by the substrate onto the aldehyde, *N*-bromosuccinimide selectively oxidizes the resulting aminal to the oxazoline in very good yields.

Figure 3.5: Examples of single step oxazoline syntheses from amino alcohols

One step zinc catalyzed cyclization:

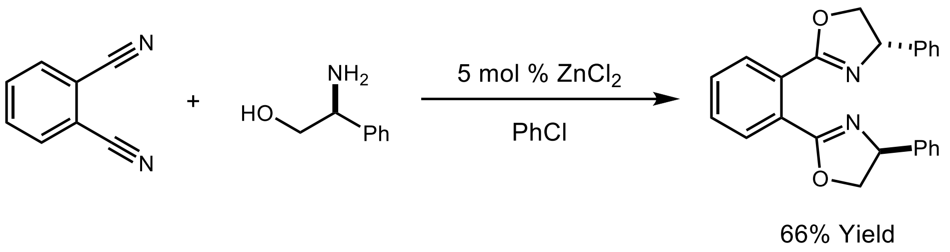

NBS promoted oxidative cyclization:

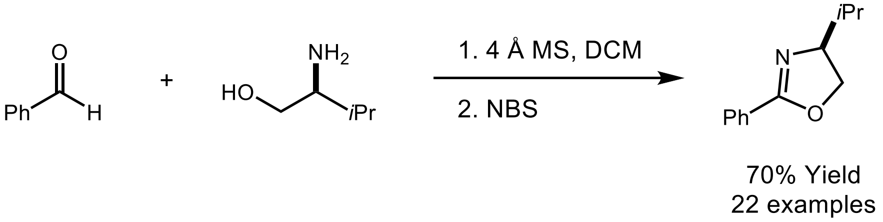

Oxazolines can also be constructed directly be the cyclization of a pendant amide onto a degree of unsaturation. This method is especially well suited to situations where substitution at the 5-position of the product is desired. One strategy for carrying out these cyclizations that is widely employed involves the activation of the alkene by a stoichiometric electrophile.[11–13] Subsequent attack by the amide furnishes oxidative cyclization products. Many electrophilic species have been reported to work well in this manifold, and numerous enantioselective reactions have been developed as well.[14,15] While the products of these reactions are very useful because of the incorporation of a second functional handle, an additional reduction would be required to arrive at the formal hydrofunctionalization products.

Figure 3.6: General strategy for amide cyclization promoted by alkene activation

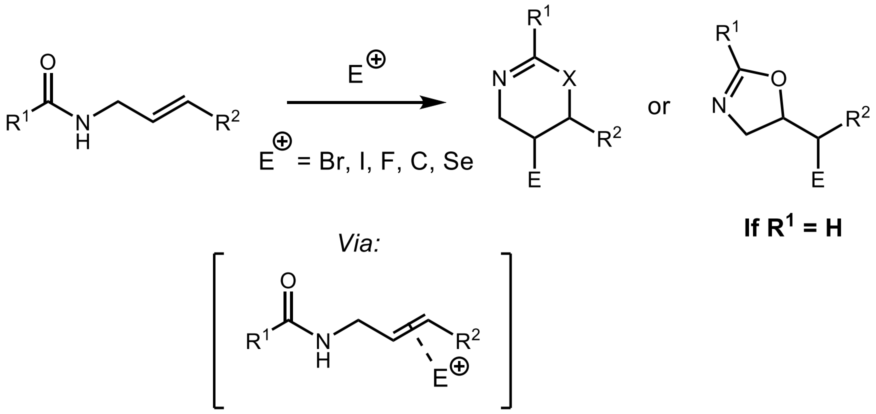

The direct hydrofunctionalization of an alkene by amide or thioamide nucleophiles are significantly more challenging and represent a limitation of existing methodology. There have been several reports of redox-neutral cyclizations of propargyl amides to furnish oxazolines bearing an *exo*-olefins. In certain cases, these alkenes will spontaneously rearrange to the internal position to form oxazoles. These reactions have been shown to be catalyzed by several metals including gold(I)/(III), silver(I), and copper(I) salts.[16–20] The gold-catalyzed cyclizations are reported to proceed via activation of the alkyne by the metal followed by nucleophilic attack. The resulting vinyl gold species is subsequently proto-demetalated to reach the final product.

Figure 3.7: Metal-catalyzed cyclizations of propargyl amides

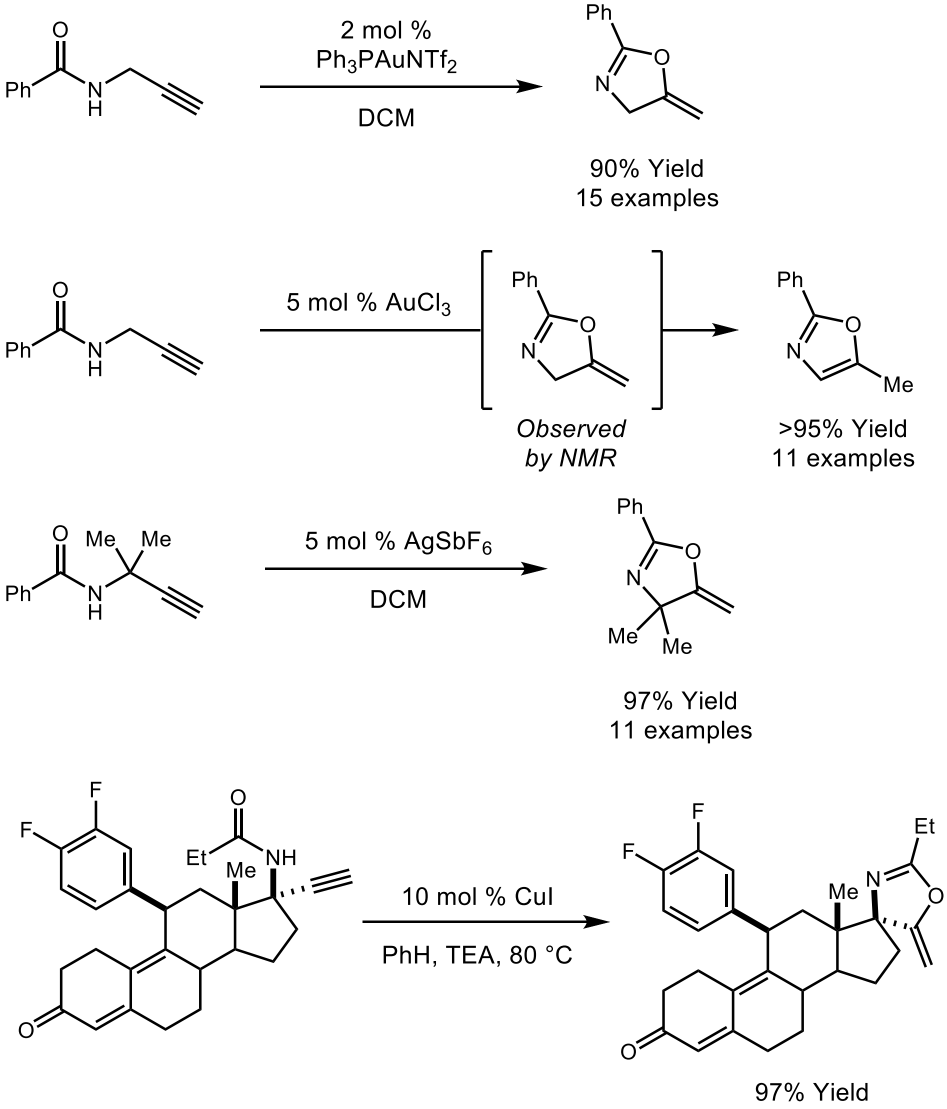
O
Ph
N
H
2 mol %
Ph3PAuNTf2
DCM
Ph
O
N
90% Yield
15 examples
O
Ph
N
H
5 mol % AuCl3
Ph
O
N
Observed
by NMR
Ph
O
N
Me
>95% Yield
11 examples
O
Me
Me
Ph
N
H
5 mol % AgSbF6
DCM
Ph
O
N
Me
Me
97% Yield
11 examples
F
F
O
Et
NH
Me
O
10 mol % CuI
PhH, TEA, 80 °C
F
F
Et
N
O
Me
O
97% Yield

To the best of our knowledge, olefin hydrofunctionalization of allylic amides has only been reported to be catalyzed by treating the substrates with concentrated sulfuric acid. The cyclization of the corresponding thioamides can be achieved with catalytic *p*-toluenesulphonic acid.[11] While yields were good in these reports, the use of strong acids serves to significantly limit the potential substrate scope of the reaction. Furthermore, these methods result in the exclusive formation of products arising from Markovnikov regioselectivity.

Figure 3.8: Acid-catalyzed cyclizations of allylic amides and thioamides

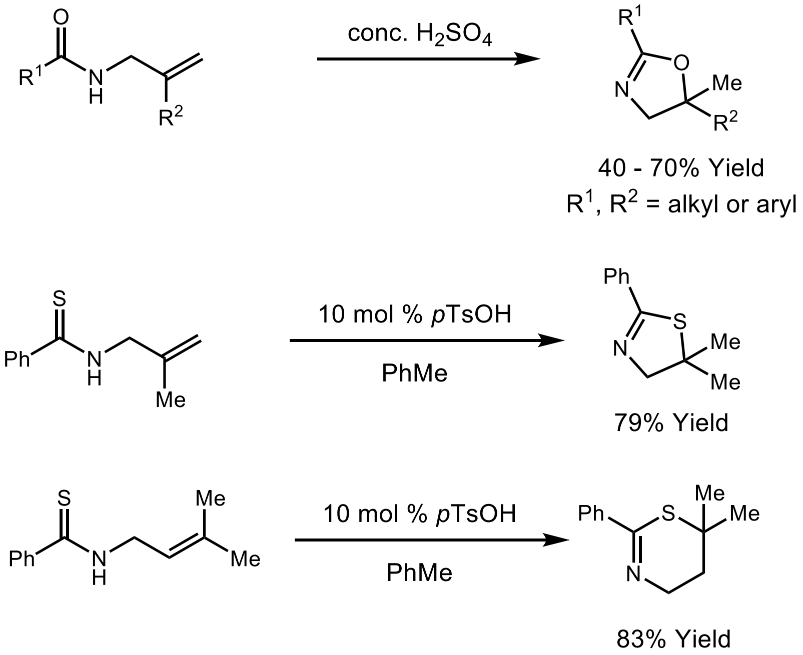

Given the limitations of the existing methods discussed previously, we saw an opportunity to develop a mild and catalytic method for synthesizing oxazolines from allylic amides that would be highly useful and practical. Additionally, this method would complement prior work by producing products resulting from *anti*-Markovnikov selectivity.

3.3 Optimization and scope of the photoredox catalyzed hydrofunctionalization

After removing the extraneous components from the reaction scheme shown in Figure 3.1, our first task was to screen a number of potential hydrogen atom donor co-catalysts to assess their effect on the yield of the reaction. Thiophenol gave greater than 95% yield by NMR and 82% after isolation. Comparable results were also obtained with phenyl disulfide, and so we chose to continue the study with this co-catalyst for practical reasons: phenyl disulfide is a bench stable solid that can be weighed, as opposed to thiophenol which has a pungent aroma and must be transferred via syringe.

Figure 3.9: Results of a hydrogen atom donor co-catalyst screen

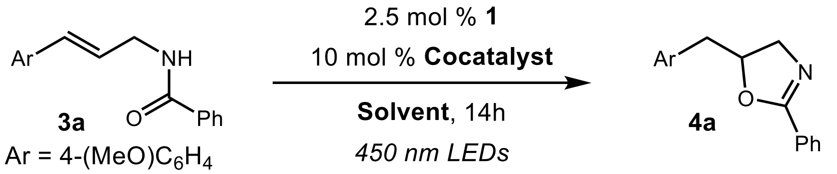

Entry	Cocatalyst	Solvent	Yield[a]
1	Sodium Benzene Sulfinate	DCE	<5%
2	Methylthiosalicylate	DCE	6%
3	Thiophenol	DCE	>95%
4	Phenyl Disulfide	DCE	>95%
5	Phenyl Disulfide	DCM	86%

[a] Yield determined by ^{1}H NMR vs. hexamethyldisiloxane as an internal standard

With optimal conditions in hand, we then explored the scope of substitution patterns that would be well tolerated at the amide position of the substrate. When the reactions were run for 14 hours, a variety of aromatic and aliphatic substrates were found to cyclize to the desired oxazolines in good yields. However, strongly electron withdrawing groups such as trifluoromethyl and 2-pyridinyl amides gave no detectable product formation, presumably due to their decreased nucleophilicity. In substrate **4h**, the amide proton was shifted strongly downfield (8.18 ppm), which we hypothesized was the result of intramolecular hydrogen bonding with the pyridine ring and could be at least partially responsible for the lack of reactivity. To test this possibility, the substrate was protonated using *p*-toluenesulphonic acid to form the pyridinium salt. This substrate unfortunately also failed to undergo cyclization under our optimized reaction conditions.

Figure 3.10: Scope of amide substitution patterns tolerated in the hydrofunctionalization reaction

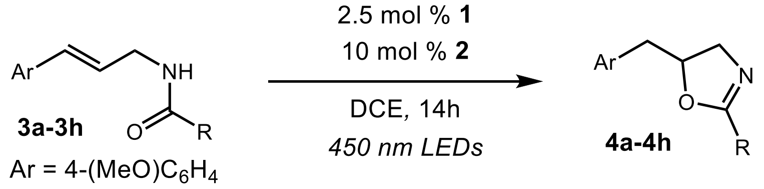
Ar
NH
3a-3h
O
R
Ar = 4-(MeO)C6H4
2.5 mol % 1
10 mol % 2
DCE, 14h
450 nm LEDs
Ar
N
O
4a-4h
R

Entry	R	Yield
1	**4a** 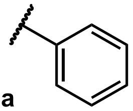	82%
2	**4b** 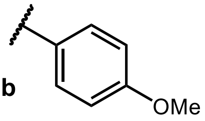	77%
3	**4c** 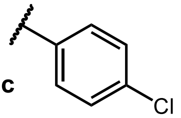	78%
4	**4d** 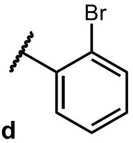	54%
5	**4e** *i*Pr	79%
6	**4f** Me	77%
7	**4g** CF_3	<5%
8	**4h** 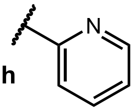	<5%
9	**4i** 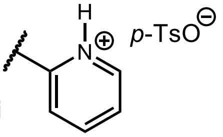	<5%

[a]With 20 mol-% 4-(OMe)PhSH

We were particularly interested in the cyclization of the substrate bearing a bromide at the 2-position of the phenyl ring (**3d**), as the product could then be transformed into a PHOX-type ligand by installing an aryl phosphine group using established copper catalyzed coupling conditions.[21] Because these and other ligands are most often derived from amino acids (*vide infra*), they almost exclusively bear substitution at the 4-position of the oxazoline. To the best of our knowledge, ligands with substitution exclusively at the 5-position have not been well studied and may prove to have interesting effects. As our method would provide rapid access to such analogues, it may be of use to researchers interested in this area. As such, we explored the use of bromo-benzamide as a substrate in this reaction.

Figure 3.11: PHOX-type ligand synthesis via copper-catalyzed coupling

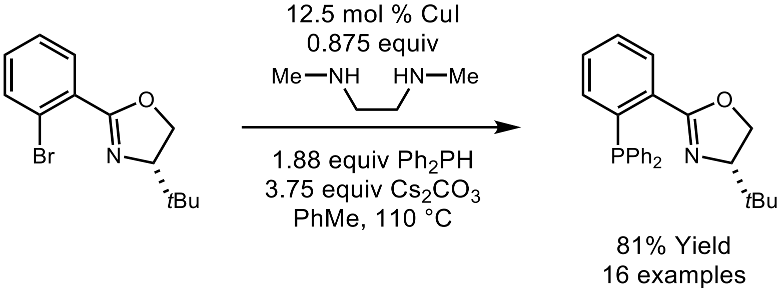
12.5 mol % CuI
0.875 equiv
Me—NH HN—Me
1.88 equiv Ph2PH
3.75 equiv Cs2CO3
PhMe, 110 °C
Br
N
O
tBu
PPh2
81% Yield
16 examples

Figure 3.12: Re-optimization of hydrogen atom donor for 2-bromoamide substrate

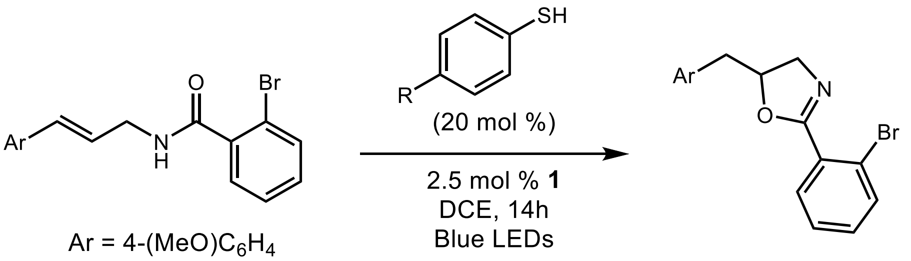
SH
R
(20 mol %)
2.5 mol % 1
DCE, 14h
Blue LEDs
Ar
N
H
O
Br
Ar = 4-(MeO)C6H4

Entry	R^1	Yield
1	NO_2	55%
2	H	54%
3	OMe	82%
4	OMe	88%[a]

[a]With 1 equiv. 4-(OMe)PhSH

Under normal reaction conditions, modest yields of the desired product could be obtained, albeit accompanied by significant levels of non-selective degradation of the substrate. In an attempt to improve the yield of this transformation, we modified the electronic properties of the hydrogen atom bond donor catalyst and found the more electron rich 4-methoxythiophenol resulted in significantly improved yields. This could further be improved to an 88% isolated yield by using a full equivalent of the thiol. Since tuning the electronic properties of the thiol could influence several steps of the catalyst cycle, such as turning the catalyst over, donating a hydrogen atom, and becoming protonated, it is difficult at this point to speculate on the origin of this beneficial effect.

Figure 3.13: Scope of alkene substitution patterns

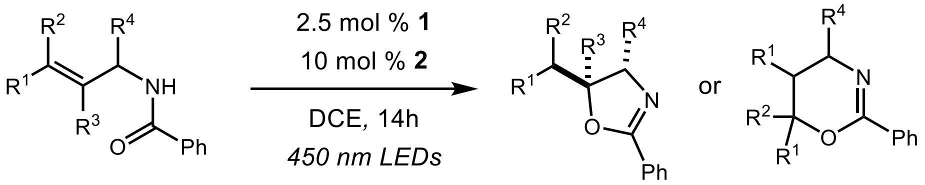

3j-3n **4j-4n**

Entry	Substrate	Product	Time	Yield
1	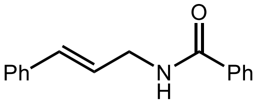 **3j**	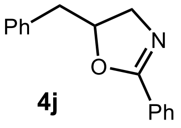 **4j**	14h	76%
2	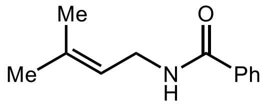 **3k**	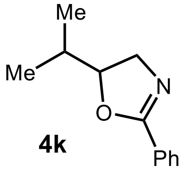 **4k**	48h	59%
3	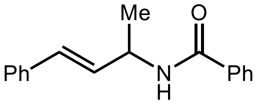 **3l**	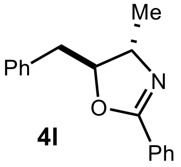 **4l**	36h	64% 2:1 d.r.
4	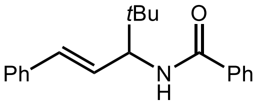 **3m**	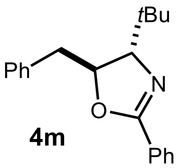 **4m**	36h	81% 2:1 d.r.
5	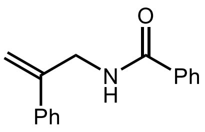 **3n**	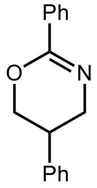 **4n**	48h	53%[a]

[a]With 1.0 equiv 4-(OMe)PhSH

Tolerance of the alkene component was then explored in this transformation. A variety of substitution patterns on the alkene portion of the substrate were also well-tolerated under the reaction conditions, and we observed that trisubstituted aliphatic alkenes could be employed in addition to styrenyl olefins. Substrates bearing a pre-existing stereocenter cyclized with modest levels of diastereoselectivity. Additionally, we were able to show, using substrate **3n**, that 6-membered rings can also be constructed. Here again a full equivalent of thiol was used in order to help accelerate the rate of reaction. This substrate also demonstrates that complete *anti*-Markonvikov selectivity is achieved even when it is the result of a kinetically slower 6-*endo* cyclization pathway. We propose that, as in previously reported *anti*-Markovnikov hydrofunctionalizations from our lab, the selectivity observed is governed by the thermodynamics of forming the more stable of two possible radical intermediates after nucleophilic attack by the amide onto the cation radical.

3.4 Proposed mechanism of hydrofunctionalization

The mechanism of the transformation is proposed to operate in a catalytic cycle similar to the hydroacetoxylation reaction discussed in the previous chapter. After excitation by a photon of visible light, the Mes-Acr photoredox catalyst encounters an equivalent of substrate and oxidizes the olefin to a cation radical intermediate. This charged intermediate is then attacked by the amide nucleophile, and deprotonation forms a neutral radical intermediate. The radical can then abstract a hydrogen atom from thiophenol to generate a thiyl radical. This radical can undergo electron transfer with the reduced form of Mes-Acr to regenerate its active form. Protonation of the resulting thiolate anion then regenerates thiophenol to complete the catalyst cycle.

Figure 3.14: Plausible hydrofunctionalization mechanism

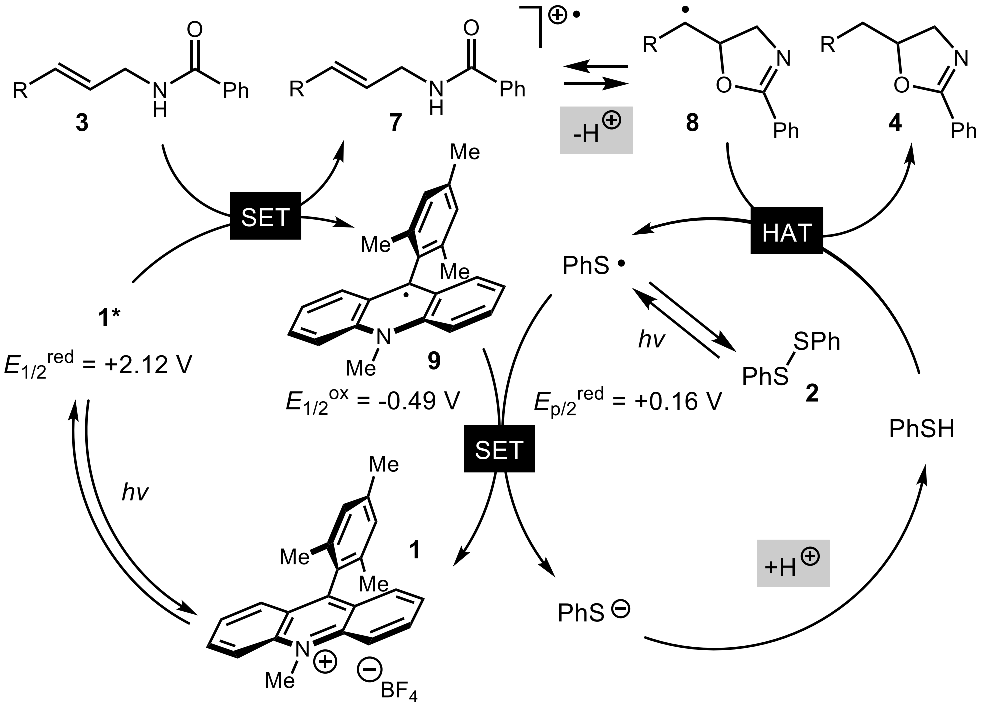

3
7
8
4
-H⊕
SET
HAT
1*
$E_{1/2}^{red}$ = +2.12 V
9
$E_{1/2}^{ox}$ = -0.49 V
PhS •
hv
2
$E_{p/2}^{red}$ = +0.16 V
PhSH
SET
hv
1
+H⊕
PhS⊖

3.5 Cyclization of allylic thioamides for thiazoline synthesis

We then turned our attention to the cyclization of thioamides to the corresponding thiazolines. Here again, we found that our optimal conditions provided the desired products in good yields. At this point we became curious if a different mechanism could be occurring with these substrates. Specifically, we wondered if it was possible to oxidize the thioamide itself instead of the olefin, and if doing so could still result in productive reactivity.

Figure 3.15: Initial scope of the allylic thioamide cyclization

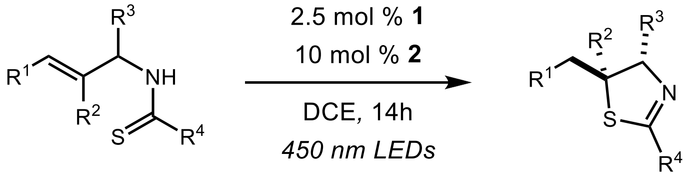

Entry	Substrate	Product	Yield
	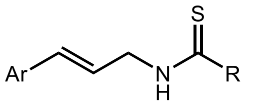	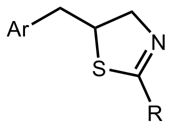	
1	**3o** Ar = 4-(MeO)C_6H_4, R = 4-(MeO)C_6H_4		80%
2	**3p**Ar = 4-(MeO)C_6H_4, R = 4-(Cl)C_6H_4		60%
3	**3q** Ar = 4-(MeO)C_6H_4, R = *i*Pr		62%
4	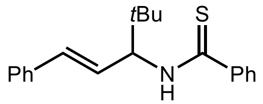 **3r**	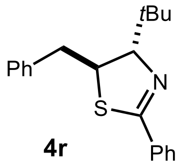 **4r**	72% 4:1 d.r.

If this were a viable mechanism, then it would have the potential to significantly expand the scope of the reaction, as it would not be limited by the oxidation potential of the olefin. We would then be able to use mono and di-substituted aliphatic olefins as substrates. We ran a series of experiments to test this hypothesis, and began by collecting cyclic voltammetry data on *N*-allylbenzamide as well as its thioamide analogue. *N*-allylbenzamide was found to possess an oxidation potential outside the measurable window of our setup (> +2.5 V vs. SCE), indicating that it would not be oxidized by the Mes-Acr catalyst. Accordingly, no product formation was observed when this substrate was subjected to standard reaction conditions. The thioamide, on the other hand, was found to have a half-wave oxidation potential of +1.53 V vs. SCE, well within range of the catalyst. We were therefore very pleased to find that the substrate readily cyclizes to a thiazoline under normal reaction conditions. In this case, exclusive formation of the product arising from Markovnikov selectivity was observed. Substrate **3s** was prepared to investigate substituent effects on the selectivity in cases where the olefin is not oxidizable, and in this case a 1.1:1 mixture of regiosomeric products. The selectivity observed in these cases indicates that a different mechanism than that proposed in Scheme 2 is in operation, as the product formation is not governed by the relative stabilities of radical intermediates. These product distributions are consistent with those previously reported for free radical cyclization reactions.[22]

Figure 3.16: Experiments to assess plausibility of thioamide oxidation as a mechanism

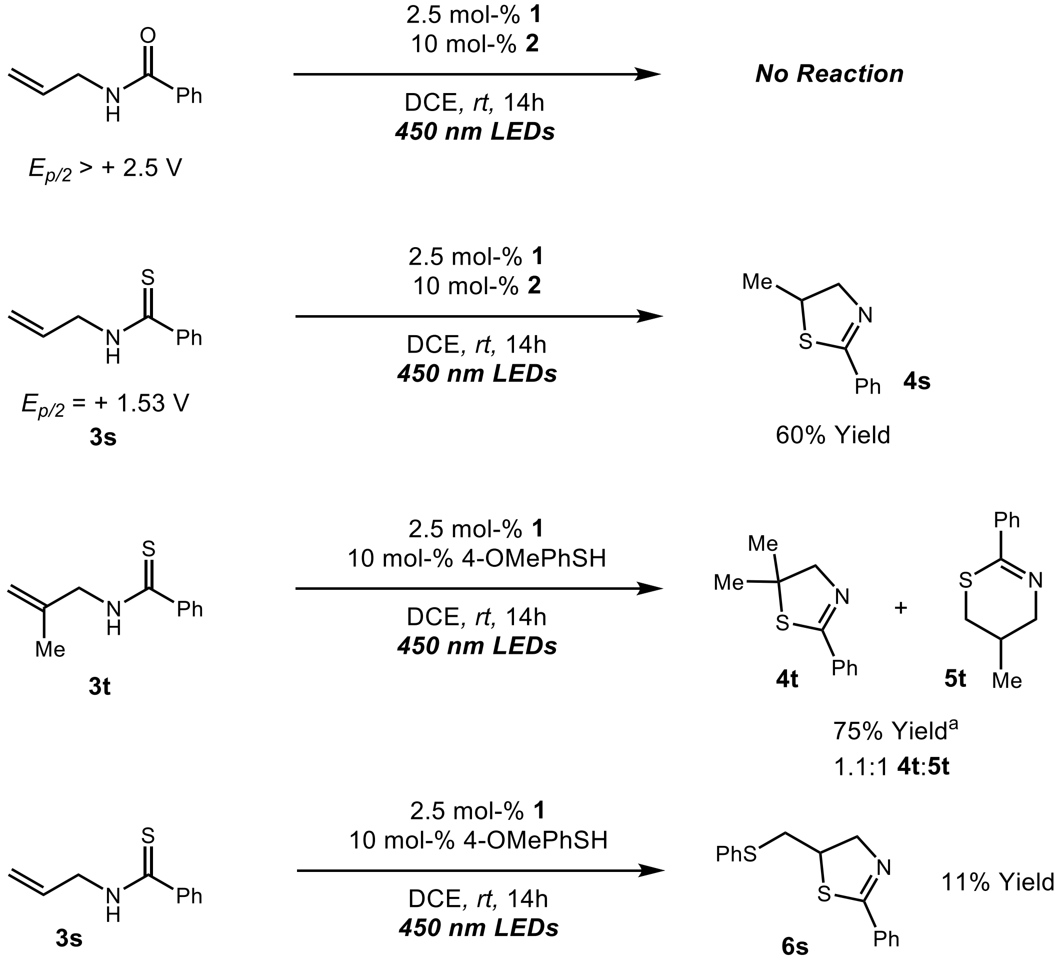
O
N
H
Ph
$E_{p/2}$ > + 2.5 V
2.5 mol-% **1**
10 mol-% **2**
DCE, *rt*, 14h
450 nm LEDs
No Reaction
S
N
H
Ph
$E_{p/2}$ = + 1.53 V
3s
2.5 mol-% **1**
10 mol-% **2**
DCE, *rt*, 14h
450 nm LEDs
Me
N
S
Ph
4s
60% Yield
S
N
H
Ph
Me
3t
2.5 mol-% **1**
10 mol-% 4-OMePhSH
DCE, *rt*, 14h
450 nm LEDs
Me
Me
N
S
Ph
4t
+
Ph
S
N
5t
Me
75% Yield[a]
1.1:1 **4t**:**5t**
S
N
H
Ph
3s
2.5 mol-% **1**
10 mol-% 4-OMePhSH
DCE, *rt*, 14h
450 nm LEDs
PhS
N
S
Ph
6s
11% Yield

We also sought to rule out the possibility that the observed reaction was the result of direct excitation of the substrates by a photon of visible light, or by phenyl disulfide acting as the lone catalyst. In a control reaction the Mes-Acr photooxidant was omitted, and while small quantities of an alkene difunctionalization product were isolated, no hydrofunctionalization products were found.

Figure 3.17: Plausible intermediate in thioamide cyclization reactions

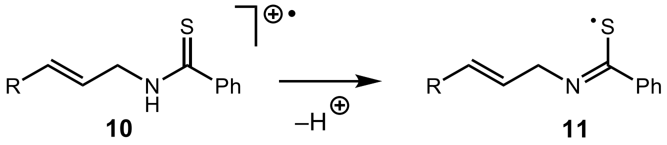

These observations lead us to believe that with substrates **3r** and **3s**, single electron oxidation of the thioamide is followed by loss of a proton to furnish a free radical intermediate such as **11**. This radical then cyclizes with the pendant olefin and subsequently abstracts a hydrogen atom to furnish the final product. The rest of the catalyst cycle is likely similar to what has been discussed previously: the resulting thiyl radical is able to turn over the photoredox catalyst to generate a thiolate anion. This anion is then protonated by the proton lost earlier in the mechanism to regenerate thiophenol and complete the cycle. In substrates **3n** – **3q**, where more activated olefins are present, we cannot rule out the possibility that oxidation of the olefin is an operative mechanism.

In conclusion, we have developed a mild and efficient method for the synthesis of novel oxazolines and thiazolines that requires no stoichiometric reagents apart from the substrates and operates under very mild conditions. A variety of substitution patterns are well tolerated, and anti-Markovnikov selectivity is exclusively observed when amides are employed as the nucleophile. This selectivity is proposed to result from the formation of more thermodynamically stable radical intermediates over the course of the reaction. The reactivity of the unsaturated thioamides in this case provides the corresponding thiazolines with a preference for the formation of the 5-exo over 6-endo adducts, presumably lending support for the oxidation of the thioamide group as being the operative mechanism.

REFERENCES

(1) Pirrung, M. C.; Tumey, L. N.; McClerren, A. L.; Raetz, C. R. H. *J. Am. Chem. Soc.* **2003**, *125* (6), 1575–1586.

(2) Kline, T.; Andersen, N. H.; Harwood, E. A.; Bowman, J.; Malanda, A.; Endsley, S.; Erwin, A. L.; Doyle, M.; Fong, S.; Harris, A. L.; Mendelsohn, B.; Mdluli, K.; Raetz, C. R. H.; Stover, C. K.; Witte, P. R.; Yabannavar, A.; Zhu, S. *J. Med. Chem.* **2002**, *45* (14), 3112–3129.

(3) Carmeli, S.; Moore, R. E.; Patterson, G. M. L.; Corbett, T. H.; Valeriote, F. A. *J. Am. Chem. Soc.* **1990**, *112* (22), 8195–8197.

(4) Nicolaou, K. C.; Lizos, D. E.; Kim, D. W.; Schlawe, D.; de Noronha, R. G.; Longbottom, D. A.; Rodriquez, M.; Bucci, M.; Cirino, G. *J. Am. Chem. Soc.* **2006**, *128* (13), 4460–4470.

(5) Bode, H. B.; Irschik, H.; Wenzel, S. C.; Reichenbach, H.; Müller, R.; Höfle, G. *J. Nat. Prod.* **2003**, *66* (9), 1203–1206.

(6) Ghosh, A. K.; Mathivanan, P.; Cappiello, J. *Tetrahedron Asymmetry* **1998**, *9* (1), 1–45.

(7) Helmchen, G.; Pfaltz, A. *Acc. Chem. Res.* **2000**, *33* (6), 336–345.

(8) Evans, D. A.; Gage, J. R.; Leighton, J. L.; Kim, A. S. *J. Org. Chem.* **1992**, *57* (7), 1961–1963.

(9) Bolm, C.; Weickhardt, K.; Zehnder, M.; Ranff, T. *Chem. Ber.* **1991**, *124* (5), 1173–1180.

(10) Schwekendiek, K.; Glorius, F. *Synthesis* **2006**, *2006* (18), 2996–3002.

(11) Engman, L. *J. Org. Chem.* **1991**, *56* (10), 3425–3430.

(12) Cahard, E.; Bremeyer, N.; Gaunt, M. J. *Angew. Chem. Int. Ed.* **2013**, *52* (35), 9284–9288.

(13) Lemercier, B. C.; Pierce, J. G. *Org. Lett.* **2014**, *16* (7), 2074–2076.

(14) Wang, Y.-M.; Wu, J.; Hoong, C.; Rauniyar, V.; Toste, F. D. *J. Am. Chem. Soc.* **2012**, *134* (31), 12928–12931.

(15) Rauniyar, V.; Lackner, A. D.; Hamilton, G. L.; Toste, F. D. *Science* **2011**, *334* (6063), 1681–1684.

(16) Jin, C.; Burgess, J. P.; Kepler, J. A.; Cook, C. E. *Org. Lett.* **2007**, *9* (10), 1887–1890.

(17) Hashmi, A. S. K.; Blanco Jaimes, M. C.; Schuster, A. M.; Rominger, F. *J. Org. Chem.* **2012**, *77* (15), 6394–6408.

(18) Hashmi, A. S. K.; Weyrauch, J. P.; Frey, W.; Bats, J. W. *Org. Lett.* **2004**, *6* (23), 4391–4394.

(19) Harmata, M.; Huang, C. *Synlett* **2008**, *2008* (9), 1399–1401.

(20) Meng, X.; Kim, S. *Org. Biomol. Chem.* **2011**, *9* (12), 4429–4431.

(21) Tani, K.; Behenna, D. C.; McFadden, R. M.; Stoltz, B. M. *Org. Lett.* **2007**, *9* (13), 2529–2531.

(22) Hartung, J.; Kneuer, R.; Rummey, C.; Bringmann, G. *J. Am. Chem. Soc.* **2004**, *126* (38), 12121–12129.

(23) Kotani, H.; Ohkubo, K.; Fukuzumi, S. *J. Am. Chem. Soc.* **2004**, *126* (49), 15999–16006.

(24) Prediger, P.; Barbosa, L. F.; Génisson, Y.; Correia, C. R. D. *J. Org. Chem.* **2011**, *76* (19), 7737–7749.

(25) Zhang, L.; Dong, C.; Ding, C.; Chen, J.; Tang, W.; Li, H.; Xu, L.; Xiao, J. *Adv. Synth. Catal.* **2013**, *355* (8), 1570–1578.

(26) Fürstner, A.; Ernst, A. *Tetrahedron* **1995**, *51* (3), 773–786.

(27) Sorimachi, K.; Terada, M. *J. Am. Chem. Soc.* **2008**, *130* (44), 14452–14453.

(28) Casey, M.; Moody, C. J.; Rees, C. W. *J. Chem. Soc. [Perkin 1]* **1987**, No. 0, 1389–1393.

(29) Klauber, E. G.; Mittal, N.; Shah, T. K.; Seidel, D. *Org. Lett.* **2011**, *13* (9), 2464–2467.

(30) Jaganathan, A.; Garzan, A.; Whitehead, D. C.; Staples, R. J.; Borhan, B. *Angew. Chem. Int. Ed.* **2011**, *50* (11), 2593–2596.

(31) Engman, L. *J. Org. Chem.* **1991**, *56* (10), 3425–3430.

(32) Mayer, R.; Scheithauer, S. *Chem. Ber.* **1965**, *98* (3), 829–837.

CHAPTER 4: THE APPLICATION OF A POLAR-RADICAL CROSSOVER CYCLOADDITION REACTION TOWARDS THE TOTAL SYNTHESIS OF RUBRIFLORDILACTONE B

4.1 Introduction

In the preceding chapter, we disclosed the development of an *anti*-Markovnikov hydrofunctionalization reaction that involves the nucleophilic attack of an amide nucleophile onto an alkene cation radical. The mechanism of this transformation is believed to be closely related to that of similar hydrofunctionalization reactions also developed within our lab. Another extension of this core methodology is an example of a polar-radical crossover cycloaddition (PRCC) that can construct complex tetrahydrofuran (THF) rings from oxidizable olefins and allylic alcohols (Figure 4.1).[1] In this case, the initial nucleophilic attack is followed by radical cyclization onto the pendant alkene. The resulting radical is then trapped by hydrogen atom abstraction from an included hydrogen atom donor to arrive at the final tetrahydrofuran products.

This transformation has many qualities that make it ideal for application to the arena of complex molecule synthesis. For one, it is an intermolecular reaction in which very simple, unactivated substrates can be used to construct complex heterocycles with up to four contiguous stereocenters. Furthermore, the relatively mild conditions employed imply that the reaction could be amenable to application late in a synthesis (provided no other oxidizable groups are present in the molecule). We were therefore eager to demonstrate the utility of this PRCC by employing it in the total synthesis of a natural product.

Figure 4.1: A photoredox catalyzed PRCC and proposed mechanism

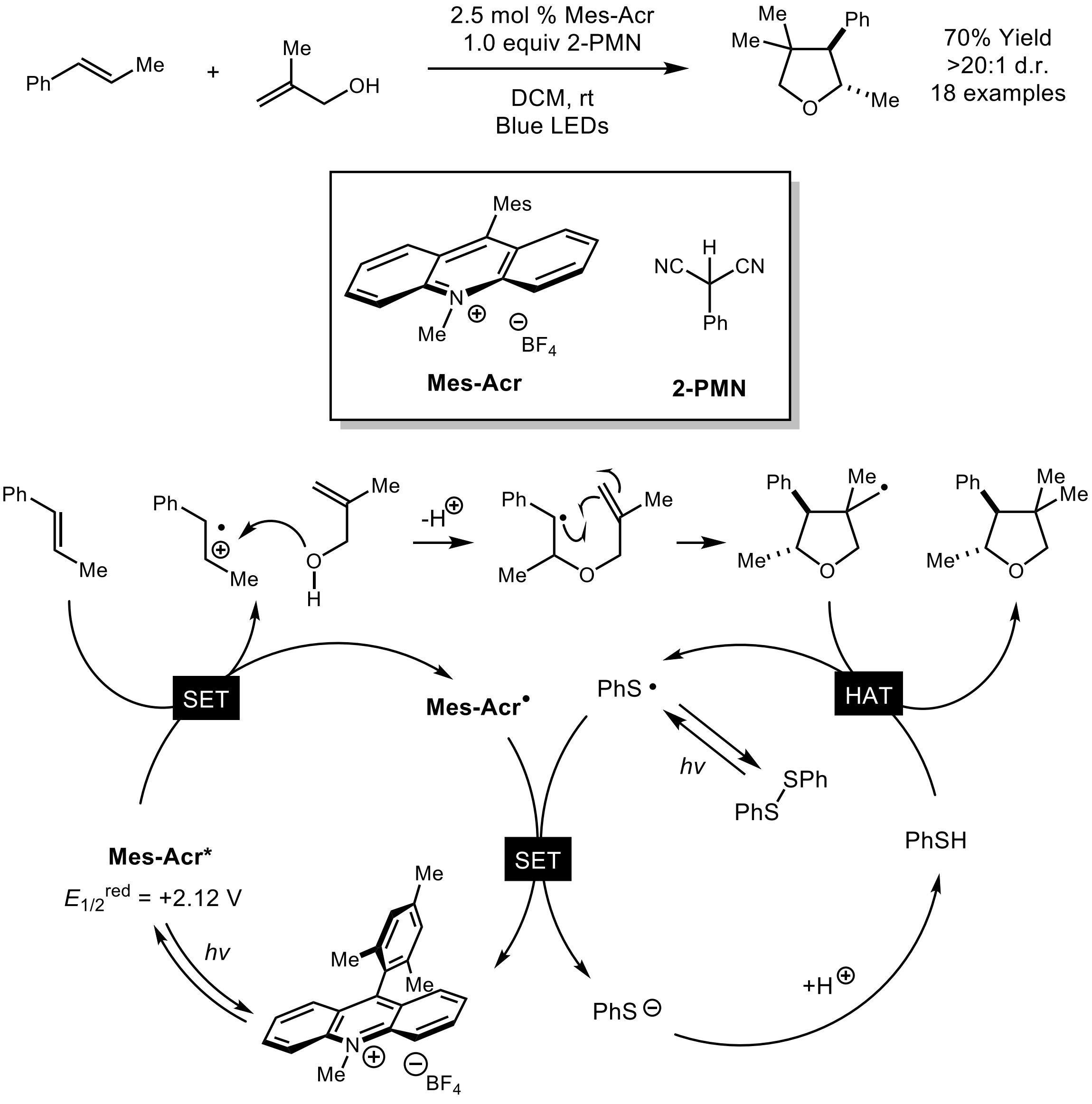
Ph
Me
+
Me
OH
2.5 mol % Mes-Acr
1.0 equiv 2-PMN
DCM, rt
Blue LEDs
Me
Me
Ph
O
Me
70% Yield
>20:1 d.r.
18 examples
Mes
N
Me
BF4
Mes-Acr
H
NC
CN
Ph
2-PMN
Ph
Me
Ph
Me
Me
O
H
-H⊕
Ph
Me
O
Me
Ph
Me
Me
O
Ph
Me
Me
Me
O
SET
Mes-Acr•
PhS •
hv
SPh
PhS
HAT
PhSH
Mes-Acr*
E1/2red = +2.12 V
hv
SET
Me
Me
Me
N
Me
BF4
PhS ⊖
+H⊕

4.2 Rubriflordilactone B

Rubriflordilactone B is a bisnortriterpenoid natural product that was isolated, along with rubriflordilactone A, from the leaves of *Schisandra rubriflora* in 2006.[2] While rubriflordilactone A did not prove to possess significant anti-cancer or anti-HIV-1 activity, rubriflordilactone B was shown to have an EC_{50} of 9.75 μg/mL in initial screens for HIV-1 inhibition activity. The structures of the two compounds have many similarities, including nearly identical fused ABCD ring western halves, as well butenolide G ring fragments. The key difference between the two structures lies in the central DEF ring system. Rubriflordilactone A possesses oxygenation at C12 of the central aromatic D ring, and as such the F ring is a fused dihydropyran moiety. Rubriflordilactone B is instead oxygenated at C16 of the E ring, giving a fused THF F ring.

Figure 4.2: Observation of a key PRCC disconnect in the structure of rubriflordilactone B

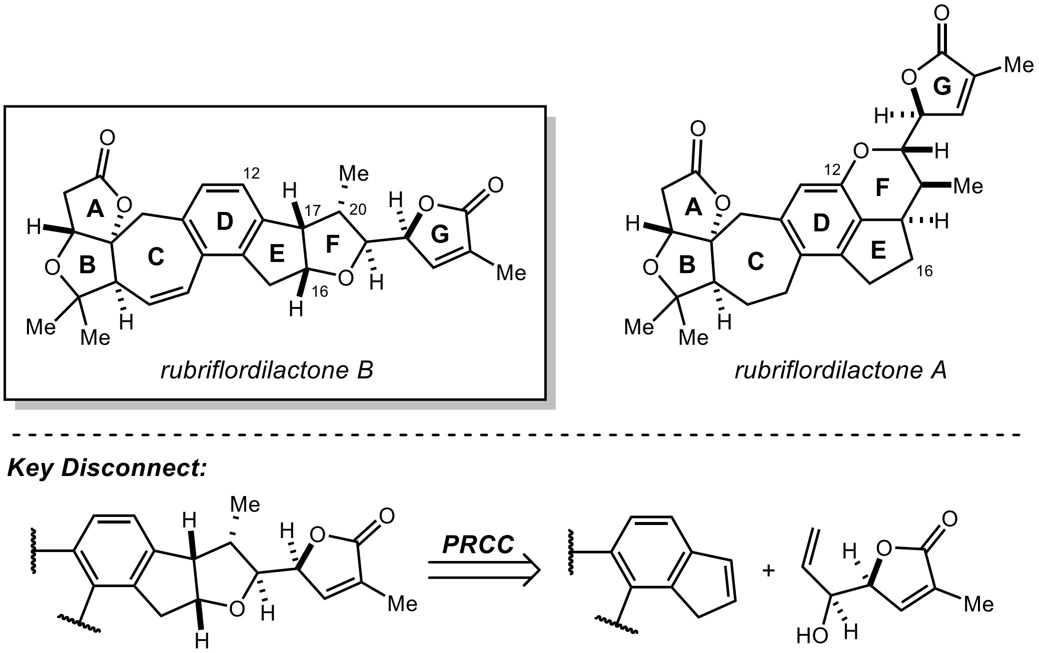

The substitution pattern of the THF ring is what brought our attention to this natural product as a target for application of the PRCC. Disconnecting at the C16 C-O bond and C17-C20 bond, along the bonds that could be formed by the PRCC, reveals an advanced indene fragment and an allylic alcohol connected to the butenolide G ring as potential late-stage synthons that would allow for convergent access to the final target (Figure 4.2). This observation was highly encouraging as to the feasibility of this approach, as indene as well as substituted allylic alcohols have both been shown to be viable partners for PRCC reactions in previously published work (Figure 4.3). We were further intrigued by the possibility of using this method to construct the THF ring relatively late in the synthesis, building a degree of convergence into the desired route.

Figure 4.3: The stereochemical outcome of PRCC reactions relevant to this study

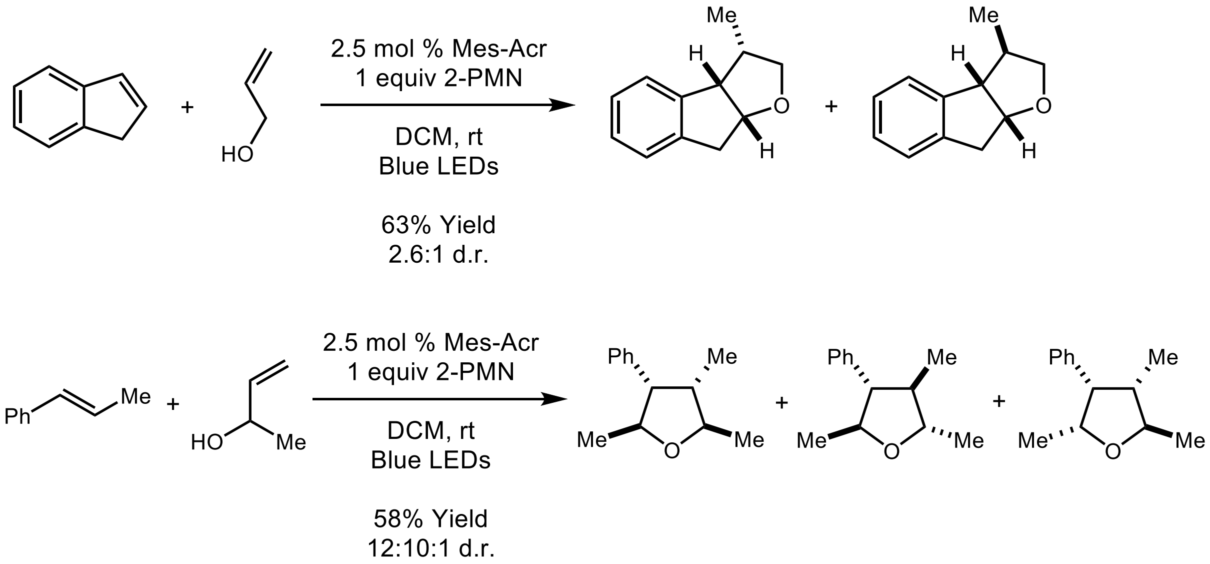
2.5 mol % Mes-Acr
1 equiv 2-PMN
DCM, rt
Blue LEDs
63% Yield
2.6:1 d.r.
HO
Me
H
O
H
2.5 mol % Mes-Acr
1 equiv 2-PMN
DCM, rt
Blue LEDs
58% Yield
12:10:1 d.r.
Ph
Me
HO
Me
Ph
Me
Me
O
Me

Key to the successful implementation of the PRCC reaction would be correctly setting the stereochemistry of the THF ring at C16, C17, and C20. Two transformations from the initial report of the PRCC gave us good precedent that the reaction would proceed with the desired diastereoselectivity (Figure 4.3). In one example, indene was employed in conjunction with allyl alcohol, leading to PRCC products possessing both the desired *cis* ring fusion, and modest selectivity for the desired methyl group stereochemistry at C20. In a second example, 3-hydroxy-1-butene was shown to cyclize with anethole, giving products possessing *trans* relative stereochemistry between the vicinal methyl groups. This would be analogous to the desired *trans* relationship between the butenolide fragment and vicinal methyl group at C20 and C22 respectively in the THF F ring of rubriflordilactone B.

4.3 Total synthesis of rubriflordilactone A and related natural products

To date no total syntheses of rubriflordilactone B have been reported in the literature, however rubriflordilactone A has recently been synthesized for the first time.[3] Valuable insight can be gained from this report to aid our own synthetic efforts, especially since the two molecules share identical western portions.

The total synthesis of rubriflordilactone A begins with an enantioselective copper catalyzed DA reaction to set the absolute stereochemistry of what will become the 7-membered C ring (Figure 4.4). Several steps are then taken to append a fused lactone with a TES-protected alcohol at the ring junction *alpha* to the carbonyl. Cyclopropanation with bromoform followed by bromide abstraction then gives the ring expanded 7-membered ring **4**. The group then exchanges the TES protecting group for an acetyl group, and under basic conditions, the resulting enolate adds into the carbonyl to achieve annulation the lactone A-ring. The resulting hydroxyl group is removed via a reductive process to give the desired tricycle **7** with correct absolute and relative stereochemistry. As the remainder of the synthesis targets structures not also present in rubriflordilactone B, it is not reviewed in detail.

Figure 4.4: Construction of the fused ABC ring system in the first reported total synthesis of rubriflordilactone A

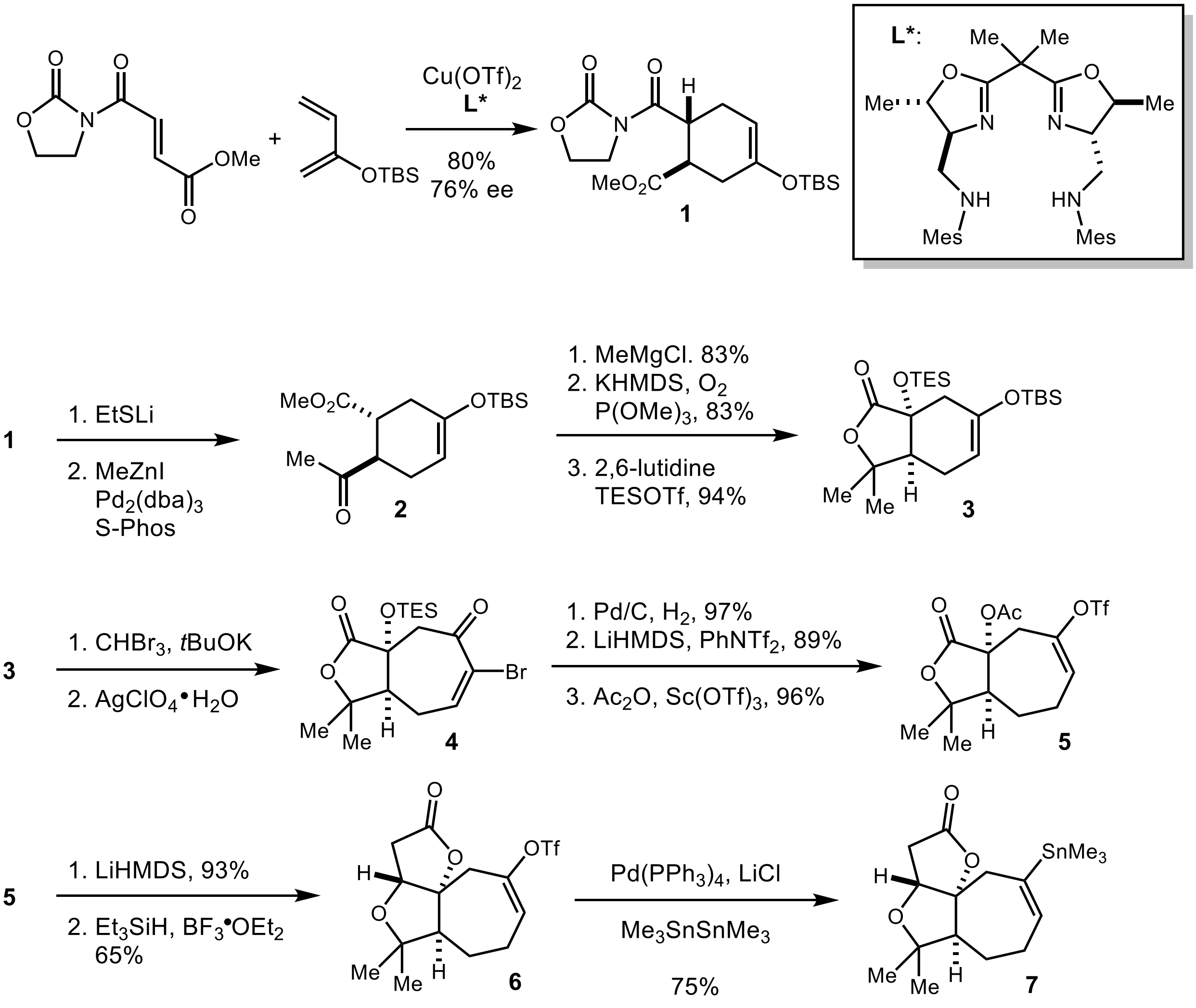
Cu(OTf)2
L*
80%
76% ee
1
L*:
Me
Me
Mes
Mes
1
1. EtSLi
2. MeZnI
Pd2(dba)3
S-Phos
2
1. MeMgCl. 83%
2. KHMDS, O2
P(OMe)3, 83%
3. 2,6-lutidine
TESOTf, 94%
3
3
1. CHBr3, tBuOK
2. AgClO4•H2O
4
1. Pd/C, H2, 97%
2. LiHMDS, PhNTf2, 89%
3. Ac2O, Sc(OTf)3, 96%
5
5
1. LiHMDS, 93%
2. Et3SiH, BF3•OEt2
65%
6
Pd(PPh3)4, LiCl
Me3SnSnMe3
75%
7

Microndilactone A is a related natural product possessing a similar ABC ring system which has also been successfully synthesized.[4] In the reported route, a vastly different strategy is used for the annulation of the lactone A ring onto the precursor B ring. In this case, *α*-oxygenation of lactone **10** is followed by reduction to hemiacetal **11**. Triethylphosphonoacetate is then deprotonated and treated with the substrate, initiating an interesting HWE, conjugate addition, and trans-esterification cascade sequence that forms the A ring with desired stereochemistry in a single step.

Figure 4.5: An alternative lactone annulation strategy

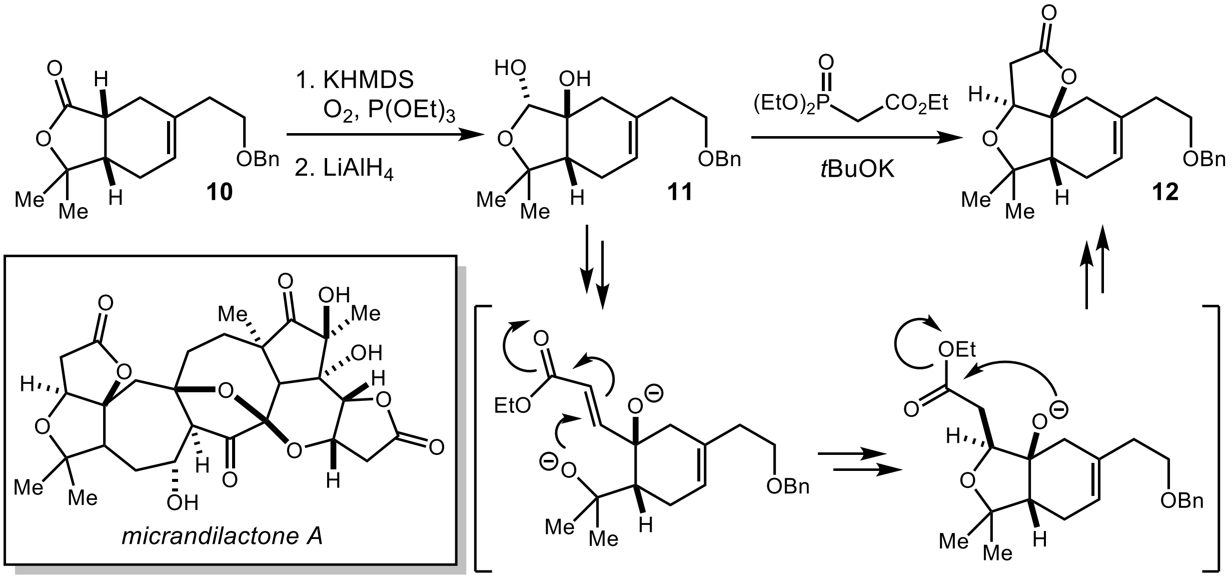

4.4 Retrosynthetic analysis of rubriflordilactone B

Armed with a model for our key disconnect and potential tactics for constructing the fused AB ring system, we devised a more complete retrosynthetic analysis of rubriflordilactone B. An important consideration is when in the course of the synthesis to attempt the key PRCC reaction. Given the tolerance of the reaction to a variety of functional groups, the exception being those that are competitively oxidized by the catalyst, it can likely be carried out late in the synthesis, allowing for two complex fragments to be joined. We proposed that the reaction should, however, be carried out prior to installation of the 7-membered C ring. The *cis*-olefin it possesses is also styrenyl, raising the possibility of competitive reactivity at this site.

Figure 4.6: Retrosynthetic analysis of rubriflordilactone B

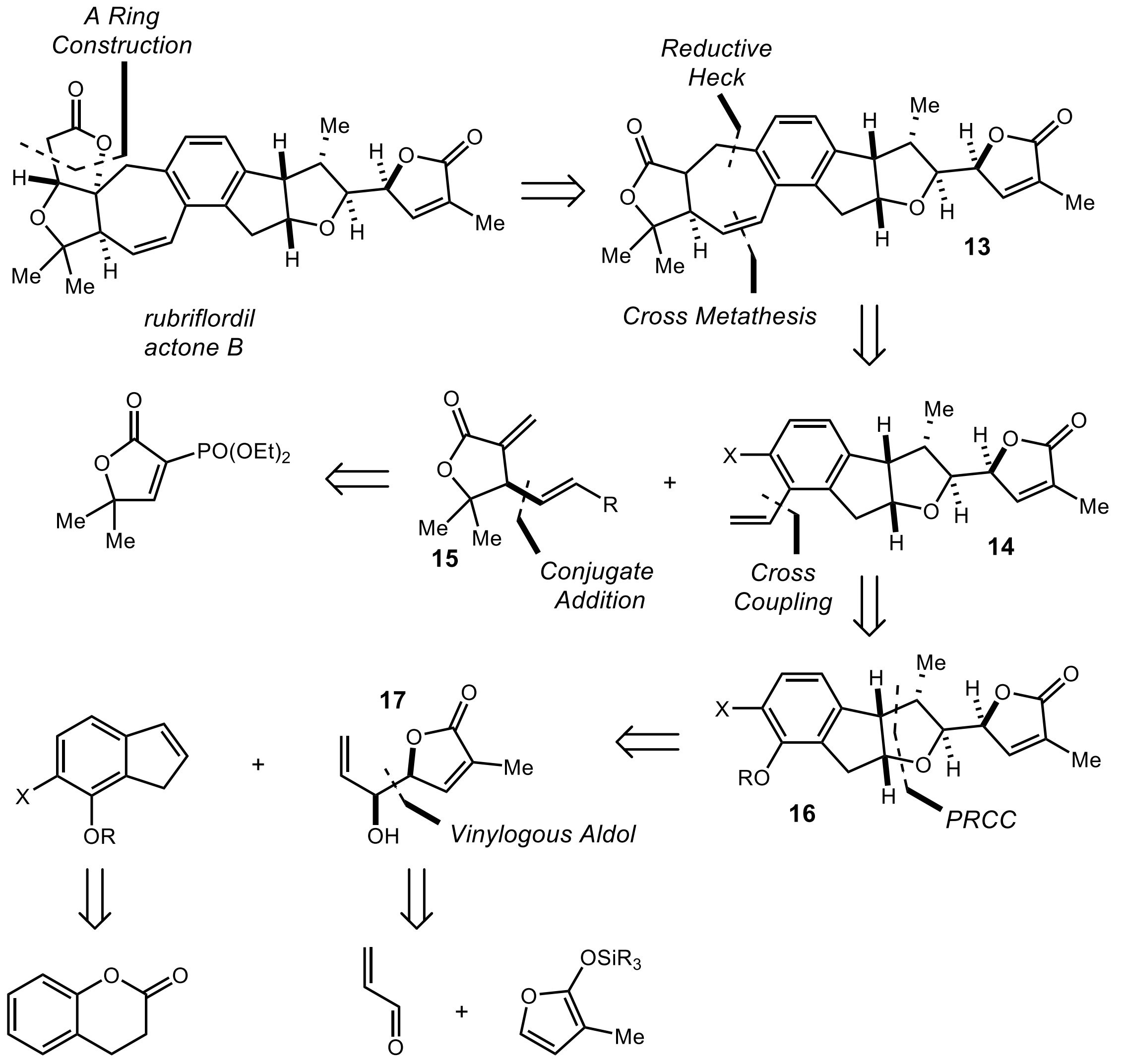
A Ring Construction
rubriflordil actone B
Reductive Heck
Cross Metathesis
13
15
Conjugate Addition
14
Cross Coupling
17
Vinylogous Aldol
16
PRCC

We therefore proposed to first disconnect at the A ring lactone to give **13,** given the tactics previously employed for its construction. The C ring can be appended by a reductive Heck reaction followed by ring-closing metathesis to give **14** and γ-butyrolactone **15**. The requisite olefin of **14** can be installed via cross coupling, bringing us to **16**, which we propose to be a good candidate substrate for the key PRCC reaction. This leads to **17** as the ideal butenolide fragment for the PRCC step. This butenolide could be itself synthesized in an enantiopure fashion via a Mukuiyama vinylogous aldol reaction (MVAR) between acrolein and a siloxyfuran. The substituted indene fragment we propose can be constructed in several steps from dihydrocoumarin.[5]

With a route to our target now planned, the first step in the synthesis was to develop a method for obtaining the butenolide fragment **17** in an enantioselective manner.

4.5 Background on the enantioselective Mukuiyama vinylogous aldol reaction

The Mukuyama vinylogous aldol reaction is a powerful transformation that has been shown to give high levels of enantioselectivity with numerous substrates, allowing for the construction of numerous chiral building blocks.[6,7] Particularly relevant to this research are examples in which siloxyfurans are used as the nucleophilic component.[8–14]

Figure 4.7: Examples of a Lewis acid catalyzed MVAR reaction using a siloxyfuran nucleophile

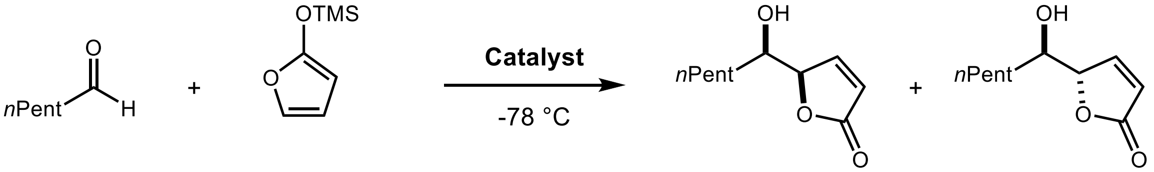

Catalyst	syn:anti	Yield
0.4 equiv $SnCl_4$	76:24	88%
0.6 equiv $BF_3{\cdot}OEt_2$	81:19	95%
0.2 equiv TMSOTf	82:18	95%
0.06 equiv TBAF	33:67	74%

Jefford has shown that a variety of catalysts can be used to induce the MVAR between 2-trimethylsiloxyfuran and capronaldehyde.[14] Using a variety of Lewis acid catalysts such as tin tetrachloride, boron trifluoride etherate, and trimethylsilyl triflate, high yields and good selectivity for the *syn* diastereomeric product was observed. They proposed that this is consistent with an open transition state for the reaction. Upon switching to fluoride sources such as tetrabutylammonium fluoride (TBAF), however, selectivity was reversed to give predominantly *anti* products. This is thought to be the result of the suppression of secondary orbital interactions in the anionic transition state that lead to a kinetic selectivity.

Of particular interest to us are enantioselective versions of the MVAR,[10,11,15,16] which could be used to set the absolute stereochemistry of our intermediates in the proposed total synthesis route. One example of such methodology was disclosed by the Evans group, who reported that several chiral Lewis acids incorporating bis-oxazoline (BOX) ligands and pyridine bis-oxazoline (pyBOX) can catalyze MVAR reactions between siloxyfurans and numerous aldehydes. In each case, however, *trans* products are formed with high selectivity.[10,11]

Figure 4.8: Select examples of enantioselective MVAR reactions

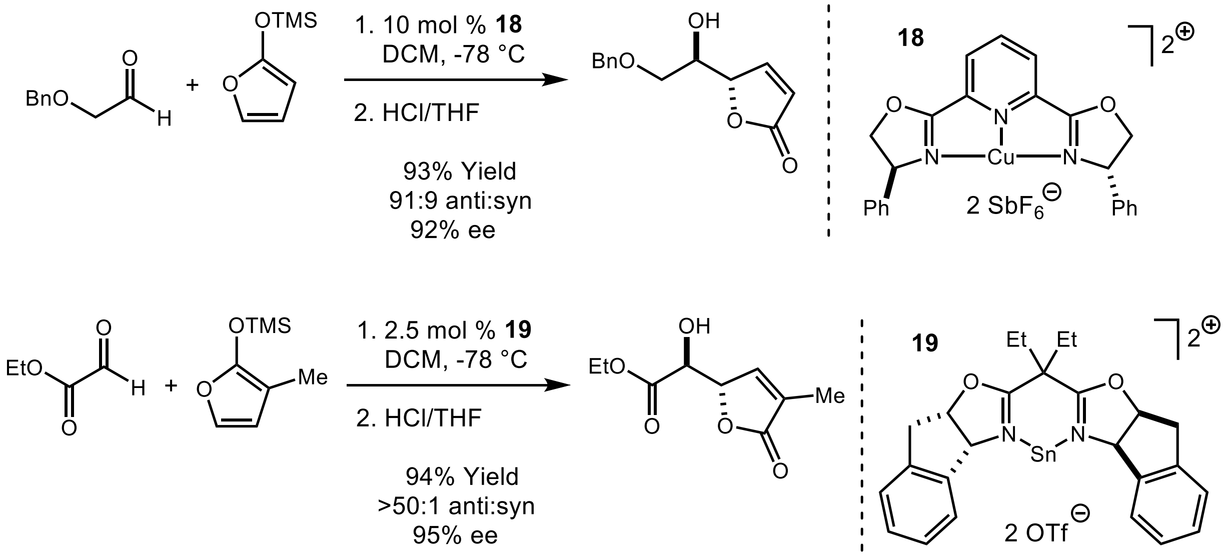
OTMS
BnO
H
O
1. 10 mol % 18
DCM, -78 °C
2. HCl/THF
93% Yield
91:9 anti:syn
92% ee
OH
18
2⊕
N
Cu
Ph
2 SbF6⊖
Ph
EtO
Me
1. 2.5 mol % 19
DCM, -78 °C
2. HCl/THF
94% Yield
>50:1 anti:syn
95% ee
19
Et
Et
Sn
2 OTf⊖

In addition to the Evans system, the Carreira group has developed a highly active titanium Lewis acid catalyst bearing a tridentate Schiff base ligand that can be used at very low loadings and gives very high levels of enantioselectivity in several transformations (Figure 4.9).[15,16] Additionally, the catalyst has been shown to work well when acrolein is used as the electrophile, which is a significant precedent for this work.[17]

Figure 4.9: A chiral titanium Lewis acid allows acrolein to be used as an electrophile in the enantioselective MVAR reaction

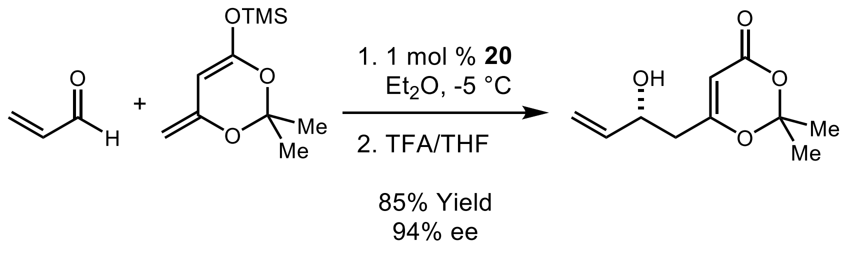
O
H
+
OTMS
O
O
Me
Me
1. 1 mol % **20**
Et$_2$O, -5 °C
2. TFA/THF
85% Yield
94% ee
OH
O
O
O
Me
Me

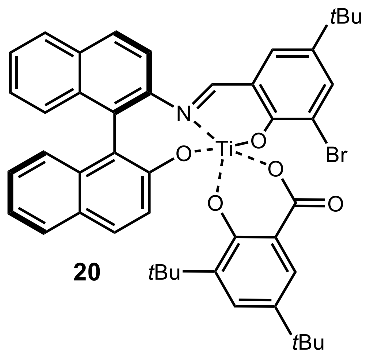
tBu
N
O
Ti
O
O
Br
O
O
O
tBu
tBu

20

4.6 Mukuiyama vinylogous aldol optimization using siloxyfuran nucleophiles

Several obstacles needed to be overcome in order to construct our desired allylic alcohol fragment using an enantioselective MVAR. Since unsaturation is required in the desired product, an aldehyde bearing unsaturation would be required as the electrophilic partner. This, in turn, allows for the possibility of conjugate addition competing with the desired aldol pathway. Additionally, a chiral catalyst system would have to be identified that is not only high yielding and highly enantioselective, but is also selective for the desired *syn* diastereomer.

Figure 4.10: Initial optimization of the racemic MVAR between acrolein and a siloxyfuran

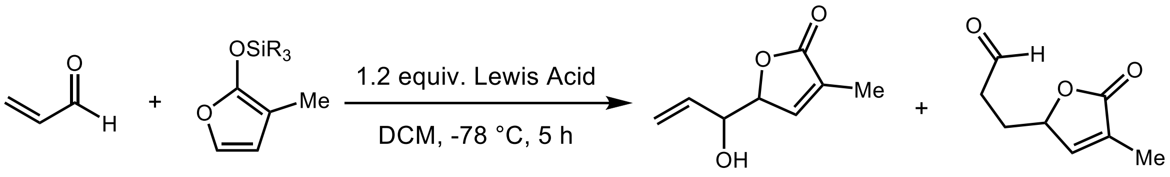

1.2 equiv. **21** **22** **23**

R	Lewis Acid	Result	Aldol:Michael **22:23**
TMS	none	**23**, quantitative	--
TMS	BF_3•OEt_2	decomposition	--
TMS	$ZnBr_2$	<5% **22**	--
TMS	$TiCl_4$	**23**	1:3
TMS	$TiCl_3(O\textit{i}Pr)$	10% **22**	1:1
TMS	$TiCl_2(O\textit{i}Pr)_2$	30% **22** (5.7:1 d.r.)	6:1
TMS	$TiCl(O\textit{i}Pr)_3$	10% **22**	1:1
TMS	$Ti(O\textit{i}Pr)_4$	**23**, quant.	>1:20
TBS	$TiCl_2(O\textit{i}Pr)_2$	*43% **22** (6.5:1 d.r.)*	*7.2:1*

Work on developing this route was initiated by Dr. Nathan Gesmundo in our lab, who began by investigating the ideal transformation between acrolein and a siloxyfuran nucleophile (Figure 4.10). In a control reaction omitting a catalyst, it was found that the inherent reactivity between the partners is a complete selectivity for the product of conjugate addition **23**. The use of several Lewis acids, including BF_3•OEt_2 and $ZnBr_2$, resulted in only the decomposition of the starting materials. Titanium Lewis acids lead to varied results depending on the ligands employed. Curiously, both $TiCl_4$ and $Ti(O\textit{i}Pr)_4$ were both found to be selective for the conjugate addition product, but mixtures of the ligands improved selectivity for the aldol product. The best result was obtained with $TiCl_2(OiPr)_2$, which gave 6:1 selectivity in favor of the aldol product . This was further improved by switching to a TBS ether on the siloxyfuran, giving product in a 43% yield with 6.5:1 d.r and 7.2:1 chemoselectivity. However, X-ray quality crystals of a 4-chlorobenzoyl ester derivative of this product allowed us to unambiguously assign the relative stereochemistry of the product as the undesired *trans*-isomer.

Figure 4.11: Derivatization of an aldol product allows relative stereochemistry to be established

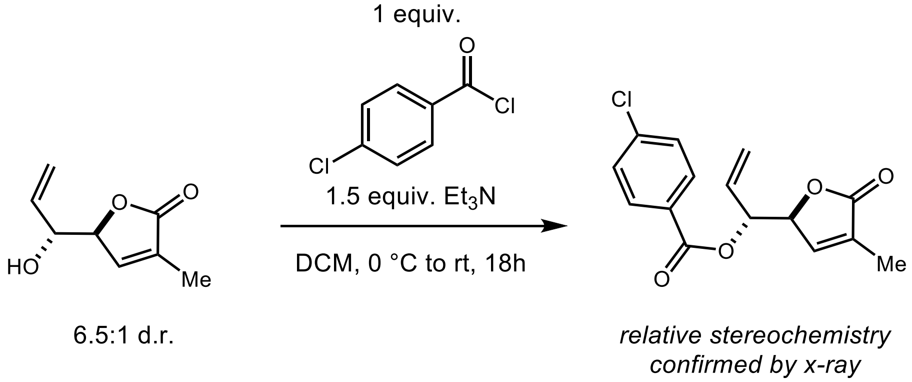
1 equiv.
O
Cl
Cl
1.5 equiv. Et3N
DCM, 0 °C to rt, 18h
HO
O
O
Me
6.5:1 d.r.
Cl
O
O
O
O
Me
relative stereochemistry
confirmed by x-ray

From here we turned our attention to the use of chiral Lewis acid catalysts in the hopes that one of these scaffolds would give selectivity for the desired *syn* product. First, a number of Lewis acids bearing both BOX and pyBOX ligands were screened for catalytic activity in DCM as the solvent. The reactions were halted at 4 hours and at this point, yields of the desired product were low in each case, with modest selectivity observed for the *anti*-diastereomer.

Figure 4.12: Initial optimization of an MVAR using chiral ligands

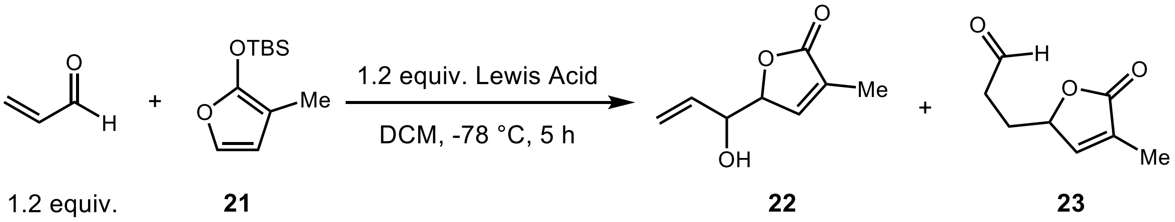
OTBS
Me
H
1.2 equiv. Lewis Acid
DCM, -78 °C, 5 h
OH
Me
H
Me
1.2 equiv.
21
22
23

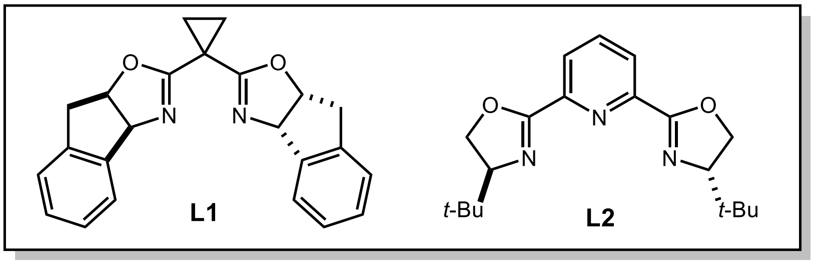
L1
t-Bu
L2
t-Bu

Entry	Lewis Acid	**22** *anti*:*syn* **L1** (GC-MS)	**L1** NMR analysis	**22** *anti*:*syn* **L2** (GC-MS)
1	Bi(OTf)$_3$	2.3:1	**--**	2.1:1
2	Cu(OTf)$_2$	2.3:1	21% **22** (2:1 d.r.) 10% **23**	2.1:1
3	In(OTf)$_3$	2.1:1	--	2.1:1
4	La(OTf)$_3$	2.1:1	20% **22** (1.9:1 d.r.) 13% **23**	2.5:1
5	Mg(OTf)$_2$	N/A	0% **22**, 33% **23**	N/A
6	Sm(OTf)$_3$	2.2:1	--	2.2:1
7	ScOTf)$_3$	2.2:1	16% **22** (2.2:1 d.r.) 10% **23**	2.1:1
8	Sn(OTf)$_2$	2.2:1	9% **22** (2:1 d.r.) 14% **23**	2:1
9	Yb(OTf)$_3$	2.2:1	--	2:1
10	Zn(OTf)$_2$	3.1:1	18% **22** (2.6:1 d.r.) 10% **23**	3.1:1
11	ZrCl$_4$	2.2:1	--	3.1:1
12	TBSOTf	1.7:1	15% **22** (2:1 d.r.) <5% **23**	--

We then turned our attention to the use of the Carreira catalyst described previously, given the precedent for its high-efficiency using acrolein as an electrophile. In the reported conditions for this transformation, 2,6-lutidine is used as an additive for reasons that are not specified. When using our desired siloxyfuran as the nucleophilic nucleophile partner, however, conjugate addition is the only product observed using both the first and second generation variants of the catalyst, as well as when 2,6-lutidine was included in the reaction. We then constructed a variant of our electrophile with a β-TMS group in the hopes that it would serve as a steric blocking group to drive selectivity towards the aldol product. This strategy was successful, and using the second generation catalyst we were able to obtain 2:1 selectivity for the aldol product and for the first time observed moderate selectivity for the desired *syn*-diastereomer.

Figure 4.13: Screen for MVAR reactivity with acrolein electrophile catalyzed by the Carreira catalyst

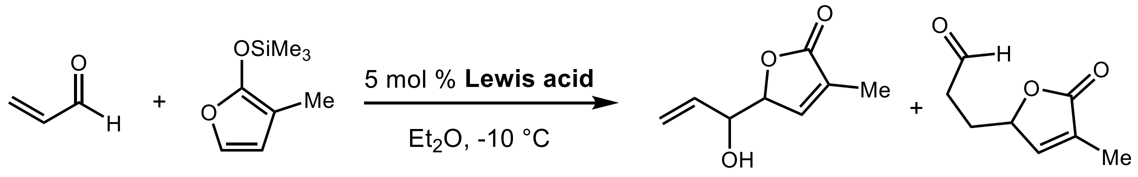

1.2 equiv. **21** **22** **23**

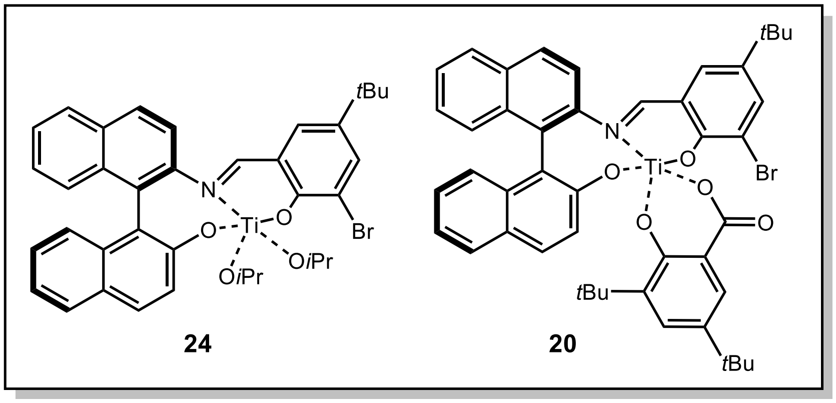

24 **20**

Entry	Lewis Acid	Additive	Product
1	**24**	None	**23**
2	**24**	2,6-lutidine	**23**
3	**20**	None	**23**
4	**20**	2,6-lutidine	**23**

Figure 4.14: MVAR results with a β-TMS aldehyde electrophile

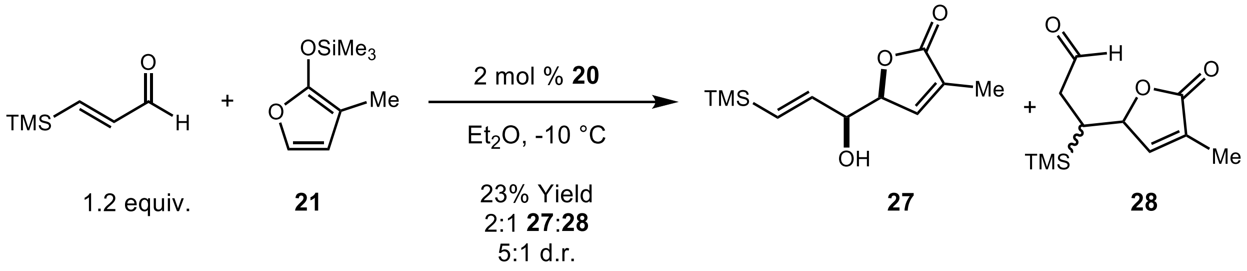

4.7 Initial PRCC reaction optimization for THF ring construction

Encouraged by this preliminary success, we sought to test our butenolides as substrates in the PRCC reaction with indene. Sufficient quantities of the minor *syn*-diastereomer of the aldol reaction with acrolein were isolated to test this substrate, despite it being the minor product in all reactions examined. Under optimal conditions from the initial publication, two products were isolated (Figure 4.15). The first, obtained in 10% yield, appeared to be the result of hydroetherification due to hydrogen atom transfer occurring prior to the desired radical cyclization. The second product, obtained in 15% yield, appeared to be the desired PRCC product, as it closely matched the reported NMR spectra of this portion of rubriflordilactone B. NOESY experiments were used to investigate the stereochemistry of the product. Cross peaks were observed between the protons at C16, C17, C22, as well as the C20 methyl group, indicating that all four protons are present on the same face of the THF ring. This implies that multiple undesired processes have occurred in the transformation, leading to an undesired diastereomer. First, initial nucleophilic attack by the hydroxyl group has occurred to the unsought face of the indene ring, which is responsible for the incorrect C16 stereochemistry. Secondly, radical cyclization occurred on the wrong face of the terminal alkene, giving undesired C20 stereochemistry.

Figure 4.15: PRCC attempt between indene and a butenolide substituted allyl alcohol

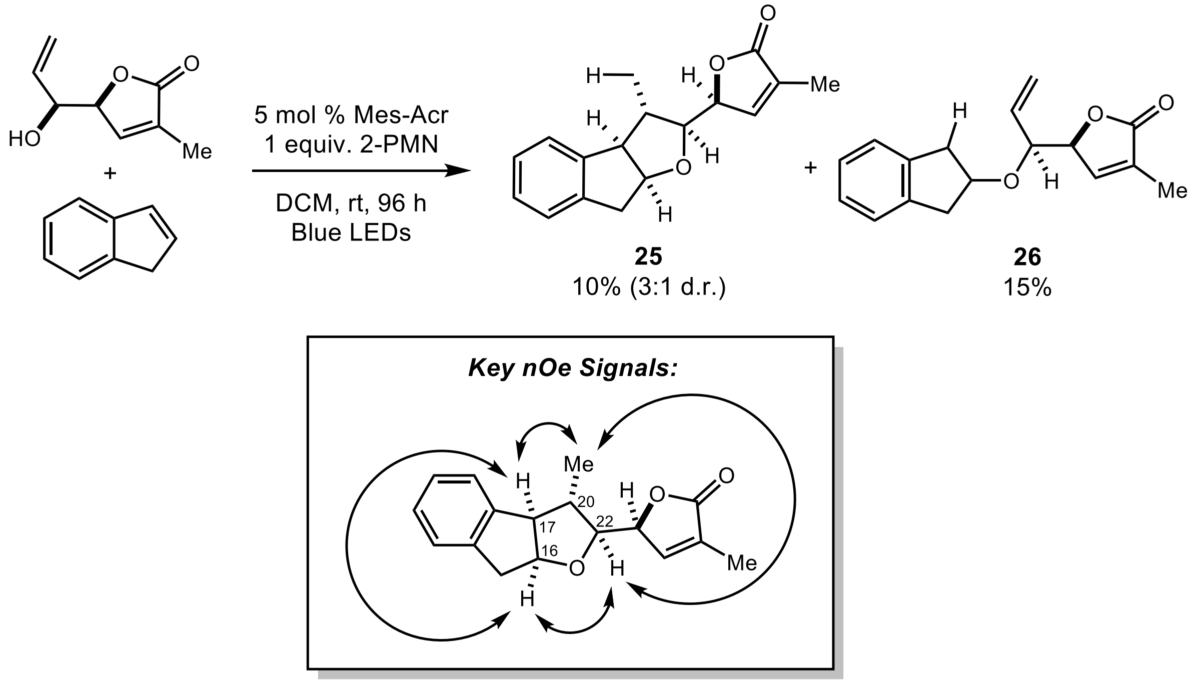

25
10% (3:1 d.r.)

26
15%

When the substrate bearing a vinyl TMS group was subjected to the same conditions, small quantities of a similar cycloadduct were obtained (Figure 4.16). The facial selectivity of nucleophilic attack was reversed in this instance, as the correct stereochemistry at C16, C17, and C22 was obtained, however the incorrect stereochemistry was still obtained at C20. Because **25** and **29** were the only cycloadducts isolated, they are presumed to be the major diastereomers of the reaction at this time. In the proposed mechanism for this reaction, the bond forming steps do not necessarily occur while the intermediates are associated with the photoredox catalyst or H-atom donor. This leaves very few options for manipulating reaction parameters (such as solvent) in the hopes of altering the diastereoselectivity of the PRCC towards the desired product. Because of this, substrate control will likely have to be used in order to obtain the desired stereochemical outcome.

Figure 4.16: PRCC initial result between indene and a vinyl TMS containing substrate

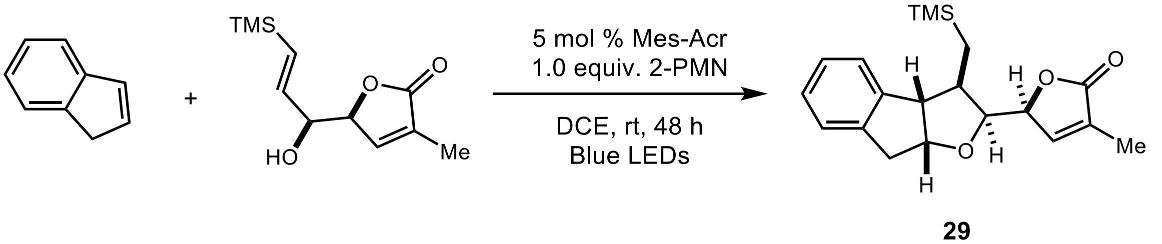

29
10%

The ability of the vinyl silane to reverse the facial selectivity of nucleophilic attack was encouraging in this regard, and led to a modified strategy. If a propargyl alcohol were used as the substrate and lead to nucleophilic attack on the same desired face of indene, the product of the PRCC would contain an *exo*-alkene. Based on the concavity of the ring system due to the *cis*-ring junction between C16 and C17, hydrogenation of this alkene could be used to then set the desired C20 methyl group stereochemistry.

Figure 4.17: Proposed route to set the correct C20 methyl group stereochemistry

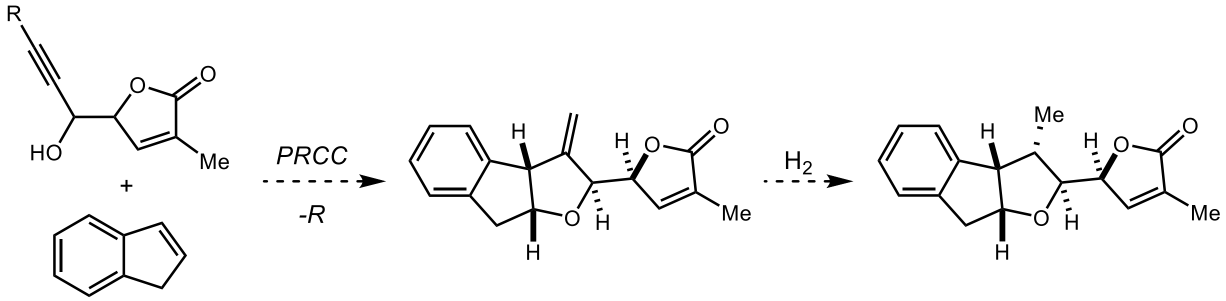

4.8 A move to propargyl alcohol PRCC substrates

Towards this goal, we carried out the MVAR with our siloxyfuran and a TIPS protected propargaldehyde and found that the desired *syn*-diastereomer of the aldol product was formed in quantitative conversion with 10:1 d.r.. Treatment of this product with TBAF buffered with acetic acid gave the desilated product in a 65% unoptimized yield, however an erosion of diastereoselectivity to 4:1 was observed as well (Figure 4.18). The Boger lab has done extensive optimization of TBAF deprotections in the presence of sensitive and epimerizable functional groups,[18] and we are hopeful that further optimization of the TBAF/acetic acid ratios will lead to improvements in d.r.

Figure 4.18: MVAR optimization with a propargaldehyde and desilation

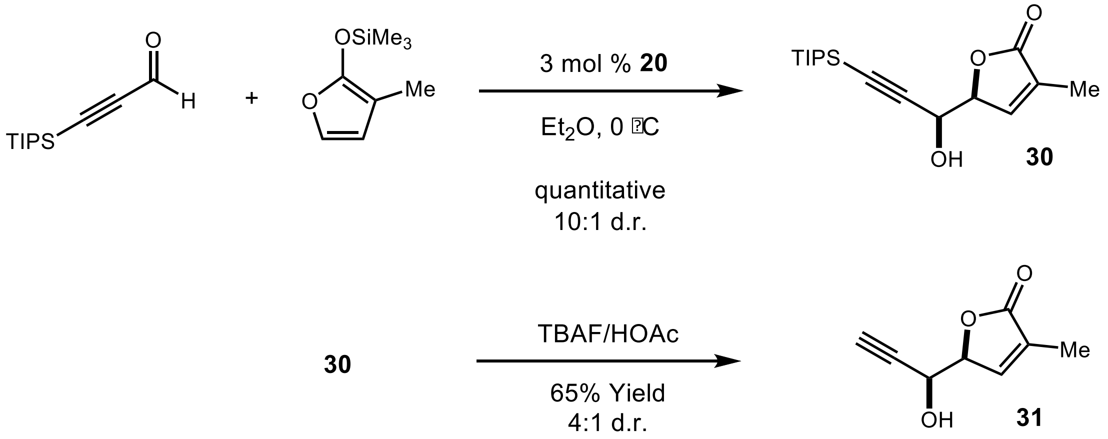

Both the TIPS-protected and terminal alkyne containing propargyl alcohols were tested for their potential fitness as coupling partners in the PRCC reaction with indene. In both cases, a screen of potential H-atom co-catalysts was first carried out. With the TIPS-protected alkyne, at a 48 hour timepoint, full consumption of the starting material was observed but no product could be identified. Large quantities of starting material remained in all cases when thiols were used as co-catalysts. In the case of the terminal alkyne, starting material was consumed in each case but again no desired product could be isolated. One possible problem could be the propensity of thiols to undergo conjugate addition with enones, such as the one present in the butenolide portions of both starting materials. We will therefore focus future efforts on the use of other carbon based H-atom donors, as well as sterically hindered thiols.

Figure 4.19: H-atom donor screen in a screen for PRCC activity with a propargyl alcohol

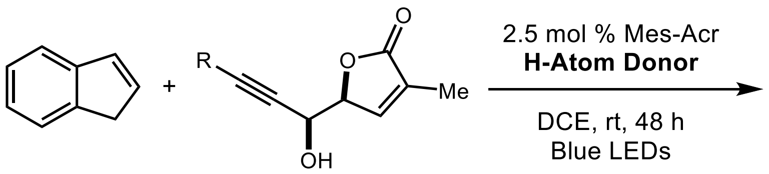

Entry	R	H-Atom Donor	Result
1	TIPS	1 equiv. **2-PMN**	decomposition
2	TIPS	20 mol % **A**	NR
3	TIPS	20 mol % **B**	NR
4	TIPS	20 mol % **C**	NR
5	H	1 equiv. **2-PMN**	decomposition
6	H	1 equiv. **A**	decomposition
7	H	20 mol % **A**	decomposition
8	H	20 mol % **B**	decomposition

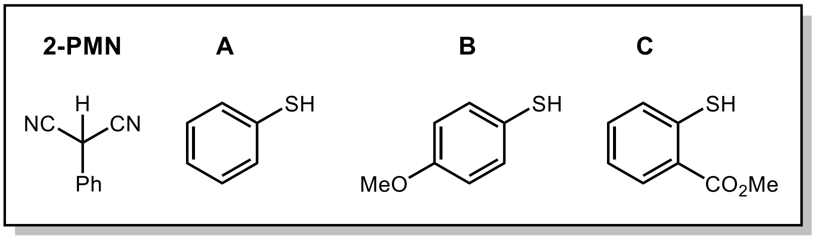

Our initial successes in obtaining small quantities of the desired cycloadducts are encouraging in the sense that we will be able to improve this reaction to the point of making it a viable key step in the total synthesis of rubriflordilactone B. A second key to the success of this strategy is ensuring that it will work well when an indene derivative bearing appropriate handles for further manipulation is used as the substrate, and such studies are being undertaken by other members of the Nicewicz lab. We are very hopeful that the unification of these works will result in a highly elegant and concise enantioselective total synthesis that highlights the utility of photoredox catalysis as a tool for complex molecule synthesis.

REFERENCES

(1) Grandjean, J.-M. M.; Nicewicz, D. A. *Angew. Chem. Int. Ed.* **2013**, *52* (14), 3967–3971.

(2) Xiao, W.-L.; Yang, L.-M.; Gong, N.-B.; Wu, L.; Wang, R.-R.; Pu, J.-X.; Li, X.-L.; Huang, S.-X.; Zheng, Y.-T.; Li, R.-T.; Lu, Y.; Zheng, Q.-T.; Sun, H.-D. *Org. Lett.* **2006**, *8* (5), 991–994.M

(3) Li, J.; Yang, P.; Yao, M.; Deng, J.; Li, A. *J. Am. Chem. Soc.* **2014**, *136* (47), 16477–16480.

(4) Zhang, Y.-D.; Tang, Y.-F.; Luo, T.-P.; Shen, J.; Chen, J.-H.; Yang, Z. *Org. Lett.* **2006**, *8* (1), 107–110.

(5) Onyango, E. O.; Jacobi, P. A. *J. Org. Chem.* **2012**, *77* (17), 7411–7427.

(6) Casiraghi, G.; Battistini, L.; Curti, C.; Rassu, G.; Zanardi, F. *Chem. Rev.* **2011**, *111* (5), 3076–3154.

(7) Rassu, G.; Zanardi, F.; Battistini, L.; Casiraghi, G. *Synlett* **1999**, *1999* (9), 1333–1350.

(8) Von der Ohe, F.; Brückner, R. *Tetrahedron Lett.* **1998**, *39* (14), 1909–1910.

(9) Ohe, F. von der; Brückner, R. *New J. Chem.* **2000**, *24* (9), 659–669.

(10) Evans, D. A.; Kozlowski, M. C.; Murry, J. A.; Burgey, C. S.; Campos, K. R.; Connell, B. T.; Staples, R. J. *J. Am. Chem. Soc.* **1999**, *121* (4), 669–685.

(11) Evans, D. A.; Kværnø, L.; Dunn, T. B.; Beauchemin, A.; Raymer, B.; Mulder, J. A.; Olhava, E. J.; Juhl, M.; Kagechika, K.; Favor, D. A. *J. Am. Chem. Soc.* **2008**, *130* (48), 16295–16309.

(12) Ferrié, L.; Figadère, B. *Org. Lett.* **2010**, *12* (21), 4976–4979.

(13) Szlosek, M.; Franck, X.; Figadère, B.; Cavé, A. *J. Org. Chem.* **1998**, *63* (15), 5169–5172.

(14) Jefford, C. W.; Rossier, J.-C.; Boukouvalas, J.; Sledeski, A. W.; Huang, P.-Z. *J. Nat. Prod.* **2004**, *67* (8), 1383–1386.

(15) Singer, R. A.; Carreira, E. M. *J. Am. Chem. Soc.* **1995**, *117* (49), 12360–12361.

(16) Carreira, E. M.; Singer, R. A.; Lee, W. *J. Am. Chem. Soc.* **1994**, *116* (19), 8837–8838.

(17) Lu, P.; Bach, T. *Angew. Chem. Int. Ed.* **2012**, *51* (5), 1261–1264.

(18) Boger, D. L.; Miyazaki, S.; Kim, S. H.; Wu, J. H.; Loiseleur, O.; Castle, S. L. *J. Am. Chem. Soc.* **1999**, *121* (13), 3226–3227.

APPENDIX 1: SUPPORTING INFORMATION FOR THE DEVELOPMENT OF AN ENANTIOSELECTIVE CATION RADICAL DIELS-ALDER REACTION

General Methods. Infrared (IR) spectra were obtained using a Jasco 260 Plus Fourier transform infrared spectrometer. Proton, carbon, and fluorine magnetic resonance spectra (^{1}H NMR and ^{13}C NMR) were recorded on a Bruker model DRX 400 or 600 (^{1}H NMR at 400 MHz or 600 MHz and ^{13}C NMR at 100 MHz or 150 MHz spectrometer. Chemical shifts for protons are reported in parts per million downfield from tetramethylsilane and are referenced to residual protium in solvent (^{1}H NMR: $CHCl_3$ at 7.26 ppm). Chemical shifts for carbons are reported in parts per million downfield from tetramethylsilane and are referenced to the carbon resonances of the residual solvent peak (^{13}C NMR: $CDCl_3$ at 77.0 ppm). NMR data are represented as follows: chemical shift, multiplicity (s = singlet, d = doublet, dd = doublet of doublet, ddd = doublet of doublet of doublet, dddd = doublet of doublet of doublet of doublet, dtd = doublet of triplet of doublet, t = triplet, q = quartet, qd = quartet of doublet, sept = septuplet, m = multiplet), coupling constants (Hz), and integration. Mass spectra were obtained using either a Micromass Quattro II (triple quad) instrument with nanoelectrospray ionization or an Agilent 6850 series gas chromatograph instrument equipped with a split-mode capillary injection system and Agilent 5973 network mass spec detector (MSD). Thin layer chromatography (TLC) was performed on SiliaPlate 250 µm thick silica gel plates purchased from Silicycle. Visualization was accomplished using fluorescence quenching, $KMnO_4$ stain, or ceric ammonium molybdate (CAM) stain followed by heating. Organic solutions were concentrated under reduced pressure using a Büchi rotary evaporator. Purification of the reaction products was carried out by chromatography using Siliaflash-P60 (40-63 µm) or Siliaflash-T60 (5-20 µm) silica gel purchased from Silicycle. All reactions were carried out under an inert atmosphere of nitrogen in

flame-dried glassware with magnetic stirring unless otherwise noted. Irradiation of photochemical reactions was carried out using a Par38 Royal Blue Aquarium LED lamp (Model # 6851) fabricated with high-power Cree LEDs as purchased from Ecoxotic (www.ecoxotic.com), with standard borosilicate glass vials purchased from Fisher Scientific. Yield refers to isolated yield of analytically pure material unless otherwise noted. NMR yields were determined using hexamethyldisiloxane as an internal standard. Cyclic voltammograms were obtained with a glassy carbon working electrode, Ag/AgCl reference electrode, platinum wire counter electrode, and Pine Instruments Wavenow potentiostat. All measurements were taken in N_2-sparged MeCN with 0.1 M tetrabutylammonium hexafluorophosphate ($TBAPF_6$) as a supporting electrolyte where the analyte concentration was 5-10 mM. The potential was scanned from 1.0 V to a vertex potential of 2.5 V in the forward direction at a sweep rate of 100 mV/s, and the reverse sweep showed no indication of a reversible electrochemical event. The half-wave potential for irreversible oxidation is estimated at $E_{p/2}$ the potential where the current is equal to one-half the peak current of the oxidation event. The values for $E_{p/2}$ are referenced to SCE (Saturated Calomel Electrode) by adding +30 mV to the potential measured against Ag/AgCl (3 M NaCl) .

Materials. Commercially available reagents were purchased from Sigma Aldrich, Acros, Alfa Aesar, or TCI, and used as received unless otherwise noted. Diethyl ether (Et_2O), dichloroethane (DCE), dichloromethane (DCM), tetrahydrofuran (THF), toluene, and dimethylformamide (DMF) were dried by passing through activated alumina columns under nitrogen prior to use. Triethylamine (Et_3N) was distilled from calcium hydride. Other common solvents and chemical reagents were purified by standard published methods if noted.

I. Enantioselective Cation Radical Diels-Alder General Procedure

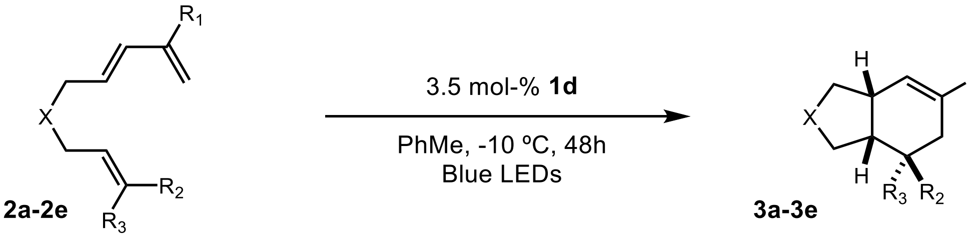

General Procedure A: Substrate (0.2 mmol) and **1c** (3.5 mol-%) were added to a flame dried vial with stir bar added, covered in aluminum foil to block light, and transferred to a glove box. The material was dissolved in PhMe (1.0 mL) and the vial was sealed. The vial was then removed from the glove box and placed in a cryobath set to the appropriate tempterature after removing the foil cover. The cryobath contained an irradiation setup consisting of blue LED strips wrapped around a small section of a test tube rack (pictured below). After stirring and cooling for 10 minutes in darkness, the sample was irradiated by the LEDs for 72h. The reaction mixture was passed through a plug of silica and eluted with DCM to remove the catalyst at the end of the reaction. The crude mixture was then concentrated and purified by column chromatography to provide the pure products.

(3a*S*,4*R*,7a*R*)-6-isopropyl-4-(4-methoxyphenyl)-1,3,3a,4,5,7a-hexahydroisobenzofuran (3b)

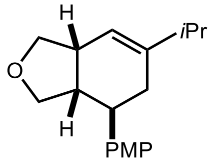

Compound **3b** was prepared according to the general procedure and obtained in a 57% yield as a colorless solid after purification by column chromatography with silica gel and DCM.

^{1}H NMR: **(400 MHz, CDCl$_3$)** δ 7.18 (d, *J* = 8.7 Hz, 2H), 6.88 (d, *J* = 8.6 Hz, 2H), 5.61 (s, 1H), 4.12 (t, *J* = 7.2 Hz, 1H), 3.82 (s, 4H), 3.44 (dd, *J* = 11.6, 7.0 Hz, 1H), 3.34 (dd, *J* = 11.2, 7.7 Hz, 1H), 2.86 (td, *J* = 11.2, 6.2 Hz, 1H), 2.67 – 2.54 (m, 1H), 2.54 – 2.42 (m, 1H), 2.34 – 2.08 (m, 3H), 1.05 (dd, *J* = 6.8, 1.7 Hz, 6H).

^{13}C NMR: **(151 MHz, CDCl$_3$)** δ 158.07, 146.43, 137.16, 127.64, 115.85, 113.93, 71.48, 71.44, 70.66, 55.25, 55.21, 48.53, 45.30, 42.70, 38.15, 34.44, 21.65, 21.51, 21.49.

MS (GC-MS) Calculated *m/z* = 272.39, Found *m/z* = 272.20

IR (thin film): 3902, 3870, 3819, 3801, 3749, 3710, 3031, 2959, 2929, 2869, 2003, 1792, 1732, 1584, 1463

6-benzyl-4-(4-methoxyphenyl)-1,3,3a,4,5,7a-hexahydroisobenzofuran (3d)

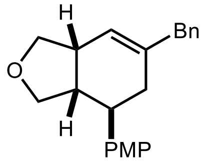

Compound **3d** was prepared according to the general procedure and obtained in a 43% yield as a colorless solid after purification by column chromatography with silica gel and DCM.

^{1}H NMR: **(600 MHz, CDCl$_3$)** δ 7.28 (dd, *J* = 15.8, 8.4 Hz, 2H), 7.21 (t, *J* = 7.4 Hz, 1H), 7.17 (d, *J* = 7.5 Hz, 2H), 7.09 (d, *J* = 8.6 Hz, 2H), 6.82 (d, *J* = 8.2 Hz, 2H), 5.64 (s, 1H), 4.10 (t, *J* = 7.3 Hz, 1H), 3.78 (s, 3H), 3.76 (t, *J* = 7.4 Hz, 1H), 3.44 (dd, *J* = 11.6, 7.1 Hz, 1H), 3.40 – 3.20 (m, 3H), 2.82 (td, *J* = 11.2, 6.3 Hz, 1H), 2.61 (q, *J* = 10.4 Hz, 1H), 2.40 (dd, *J* = 18.2, 6.4 Hz, 1H), 2.22 (qd, *J* = 11.2, 6.9 Hz, 1H), 2.12 (ddt, *J* = 14.5, 10.7, 5.5 Hz, 1H).

^{13}C NMR: **(151 MHz, CDCl$_3$)** δ 158.14, 140.14, 139.46, 136.78, 128.88, 128.31, 127.62, 126.13, 120.34, 113.95, 77.21, 76.79, 71.28, 70.62, 55.21, 48.60, 45.45, 43.63, 42.61, 39.98.

MS (GC-MS) Calculated *m/z* = 320.43, Found *m/z* = 320.20

IR (thin film): 3082, 3060, 3027, 3000, 2932, 2908, 2836, 1652, 1607, 1577, 1511, 1495, 1453, 1441, 1420

6-cyclohexyl-4-(4-methoxyphenyl)-1,3,3a,4,5,7a-hexahydroisobenzofuran (3c)

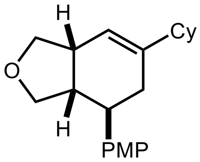

Compound **3c** was prepared according to the general procedure and obtained in a 63% yield as a colorless solid after purification by column chromatography with silica gel and DCM.

^{1}H NMR: (400 MHz, Chloroform-*d*) δ 7.14 (d, *J* = 8.6 Hz, 2H), 6.85 (d, *J* = 8.7 Hz, 2H), 5.56 (s, 1H), 4.08 (t, *J* = 7.2 Hz, 1H), 3.79 (s, 3H), 3.76 (t, *J* = 7.3 Hz, 1H), 3.40 (dd, *J* = 11.6, 7.0 Hz, 1H), 3.30 (dd, *J* = 11.2, 7.7 Hz, 1H), 2.83 (td, *J* = 11.2, 6.2 Hz, 1H), 2.63 – 2.51 (m, 1H), 2.51 – 2.40 (m, 1H), 2.25 – 2.06 (m, 2H), 1.89 – 1.61 (m, 6H), 1.33 – 1.06 (m, 5H).

^{13}C NMR: **(101 MHz, CDCl$_3$)** δ 158.14, 145.99, 137.26, 127.63, 116.28, 114.00, 71.50, 70.68, 55.25, 48.65, 45.39, 45.02, 42.83, 38.90, 32.25, 32.14, 26.75, 26.36.

MS (GC-MS) Calculated *m/z* for [M+H] = 312.45, Found *m/z* for [M+H] = 312.22

IR (thin film): 2924, 2851, 1611, 512, 1448, 1302, 1249, 1178, 1110, 1035

(1*R*,4*S*,5*S*,6*R*)-5-(4-methoxyphenyl)-6-methylbicyclo[2.2.1]hept-2-ene (4a)

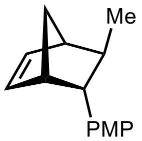

Compound **4a** was prepared according to the general procedure and purified by column chromatography with silica gel with 1% EtOAc/Hexanes as the eluent. Spectral data were in agreement with reported literature values.

(1*S*,4*R*,5*R*,6*R*)-5-ethyl-6-(4-methoxyphenyl)bicyclo[2.2.1]hept-2-ene (4b)

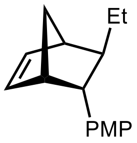

Compound **4b** was prepared according to the general procedure and purified by column chromatography with silica gel with 1% EtOAc/Hexanes as the eluent.

^{1}H NMR: (400 MHz, Chloroform-*d*) δ = 7.08 (d, J = 8.7 Hz, 2 H), 6.76 (d, J = 8.7 Hz, 2 H), 6.30 (dd, J = 3.0, 5.3 Hz, 1 H), 5.85 (dd, J = 2.8, 5.5 Hz, 1 H), 3.76 (s, 3 H), 2.90 (br. s., 1 H), 2.73 (t, J = 3.6 Hz, 1 H), 2.64 (br. s., 1 H), 1.67 - 1.54 (m, 2 H), 1.51 - 1.42 (m, 4 H), 0.93 - 0.87

(m, 3 H)

MS (GC-MS) Calculated *m/z* = 228.15, Found *m/z* = 228.2

(1*S*,2*S*)-4'-methoxy-2,4,5-trimethyl-1,2,3,6-tetrahydro-1,1'-biphenyl (4c)

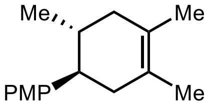

Compound **4c** was prepared according to the general procedure and purified by column chromatography with silica gel with 1% EtOAc/Hexanes as the eluent. Spectral data were in agreement with reported literature values.[19]

Preparation of Chiral Brønsted Acids

1,1,1-trifluoro-*N*-((11b*R*)-4-oxido-2,6-diphenyl-8,9,10,11,12,13,14,15-octahydrodinaphtho[2,1-*d*:1',2'-*f*][1,3,2]dioxaphosphepin-4-yl)methanesulfonamide (s1)

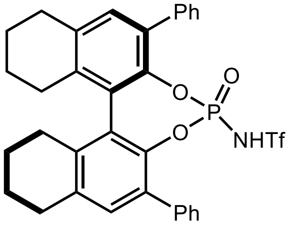

s1

Compound **s1** was prepared according to published procedure and the spectra matched reported values.[44]

(11b*R*)-4-hydroxy-2,6-bis(triphenylsilyl)-8,9,10,11,12,13,14,15-octahydrodinaphtho[2,1-*d*:1',2'-*f*][1,3,2]dioxaphosphepine 4-oxide (s2)

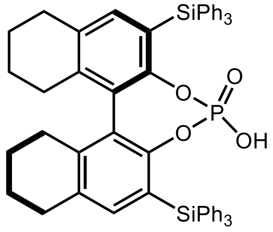

s2

Compound **s2** was prepared according to published procedure and the spectra matched reported values.[45]

1,1,1-trifluoro-*N*-((11b*R*)-4-oxido-2,6-bis(triphenylsilyl)-8,9,10,11,12,13,14,15-octahydrodinaphtho[2,1-*d*:1',2'-*f*][1,3,2]dioxaphosphepin-4-yl)methanesulfonamide (s3)

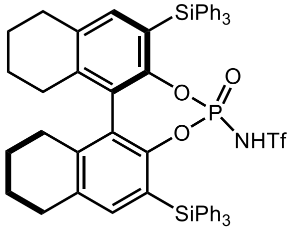

s3

Compound **s3** was prepared according to published procedure and the spectra matched reported values.[44]

(*R*)-3,3'-bis(1-mesityl-1*H*-1,2,3-triazol-4-yl)-5,5',6,6',7,7',8,8'-octahydro-[1,1'-binaphthalene]-2,2'-diol) (s5)

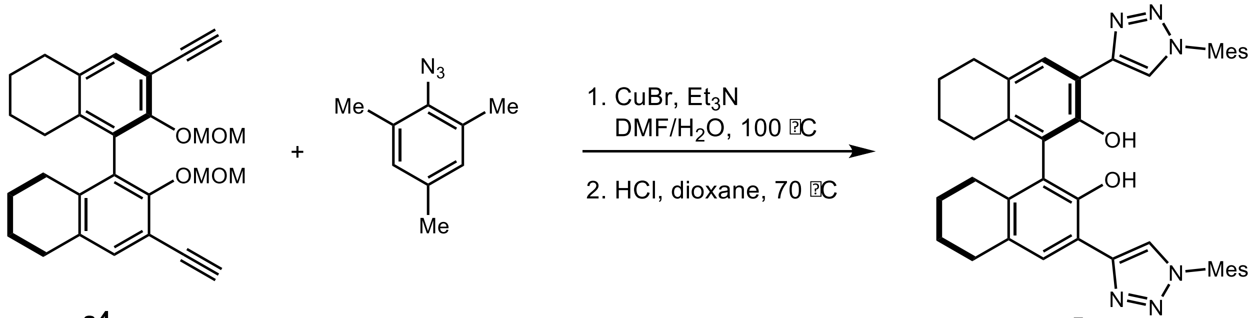
N3
Me
Me
Me
OMOM
OMOM
+
1. CuBr, Et3N
DMF/H2O, 100 ?C
2. HCl, dioxane, 70 ?C
OH
OH
N=N
N—Mes
N—Mes
N=N

s4

s5

Compound **s5** was synthesized according to the procedure reported by Toste et. al.[36]

^{1}H NMR: **(600 MHz, Chloroform-*d*)** δ 10.09 (s, 2H), 7.92 (s, 2H), 7.40 (s, 2H), 7.01 (s, 4H), 2.91 – 2.77 (m, 4H), 2.59 (dt, *J* = 17.2, 5.8 Hz, 2H), 2.37 (s, 6H), 2.29 (dt, *J* = 18.3, 6.4 Hz, 2H), 2.00 (s, 12H), 1.87 – 1.68 (m, 8H).

^{13}C NMR: **(151 MHz, $CDCl_3$)** ^{13}C NMR (151 MHz, $CDCl_3$) δ 150.39, 147.60, 140.18, 137.85, 135.06, 133.29, 129.10, 128.57, 125.98, 124.52, 121.01, 111.88, , 29.43, 27.20, 23.20, 23.15, 21.15, 17.24.

MS (LTQ FT-ICR) Calculated *m/z* for [M+H] = 664.85, Found *m/z* for [M+H] = 665.35965

N-((11b*R*)-2,6-bis(1-mesityl-1*H*-1,2,3-triazol-4-yl)-4-oxido-8,9,10,11,12,13,14,15-octahydrodinaphtho[2,1-*d*:1',2'-*f*][1,3,2]dioxaphosphepin-4-yl)-1,1,1-trifluoromethanesulfonamide (s6)

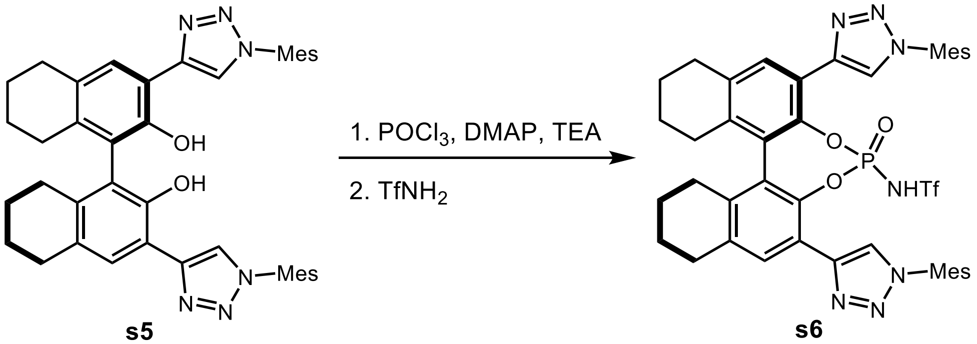
N=N
N—Mes
OH
OH
N—Mes
N=N
1. POCl3, DMAP, TEA
2. TfNH2
O
P
O
O
NHTf

s5

s6

^{1}H NMR: **(600 MHz, CDCl$_3$)** δ 13.52 (s, 1H), 8.30 (s, 2H), 7.69 (s, 2H), 7.03 (s, 4H), 3.11 – 2.80 (m, 4H), 2.79 – 2.65 (m, 2H), 2.38 (s, 8H), 2.04 (s, 12H), 1.81 (q, *J* = 8.8, 7.2 Hz, 6H), 1.57 (dd, *J* = 8.5, 4.7 Hz, 2H).

^{13}C NMR: **(151 MHz, CDCl$_3$)** δ 144.25, 144.19, 141.61, 141.09, 140.56, 135.93, 134.86, 132.52, 129.74, 129.39, 127.76, 125.96, 117.26, 77.21, 76.79, 28.98, 28.10, 22.30, 22.18, 21.18, 17.25.

MS (LTQ FT-ICR) Calculated *m/z* for [M+H] = 727.31, Found *m/z* for [M+H] = 727.31472

4-(((11b*R*)-2,6-bis(3,5-bis(trifluoromethyl)phenyl)-4-hydroxy-4λ^5-dinaphtho[2,1-*d*:1',2'-*f*][1,3,2]dioxaphosphepin-4-ylidene)amino)-2,6-bis(3,5-bis(trifluoromethyl)phenyl)dinaphtho[2,1-*d*:1',2'-*f*][1,3,2]dioxaphosphepine 4-oxide (s7)

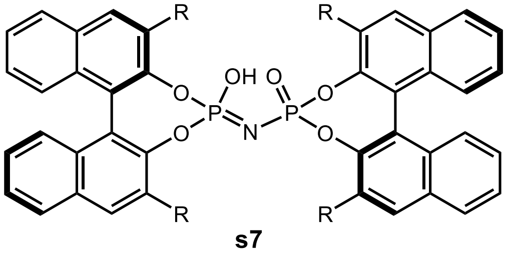

s7

R = *m,m*-(CF$_3$)$_2$Ph

Compound **s7** was prepared according to published procedure and the spectra matched reported values.

II. Preparation of Oxopyrilium Salts Bearing Chiral Anions

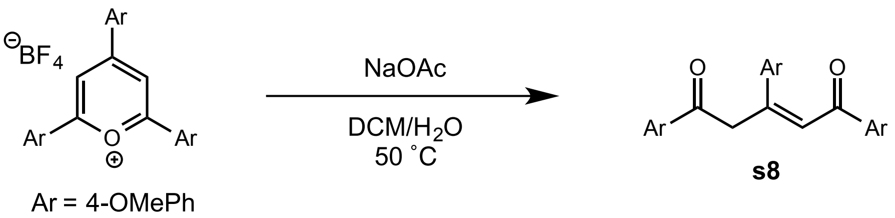

Ar
BF4
Ar
Ar
O
Ar = 4-OMePh
NaOAc
DCM/H2O
50 ˚C
O
Ar
O
Ar
Ar
s8

Compound **s8** was prepared by the following procedure: To a clean dry RBF was added triaryloxopyrylium tetrafluoroborate and sodium acetate. Then the solids were dissolved in a 1:1 mixture of DCM/H2O. Equipped with reflux condenser and heated to 50 °C overnight. Cooled to room temperature then the organic and aqueous layers separated, then the aqueous layer was extracted with DCM 3x, organic layers combined and washed with brine, dried over Na_2SO_4 and concentrated *in vacuo*. Chromatographed in 25% EtOAc/Hexanes to give the desired product.

^{1}H NMR: (400 MHz, Chloroform-*d*) δ = 8.08 (d, J = 8.8 Hz, 2 H), 8.01 (d, J = 8.8 Hz, 6 H), 7.53 (d, J = 8.8 Hz, 2 H), 7.42 (s, 1 H), 7.01 - 6.90 (m, 6 H), 4.86 (s, 2 H), 3.90 (s, 3 H), 3.89 (s, 3 H), 3.85 (s, 3 H)

^{13}C NMR: **(101 MHz, $CDCl_3$)** δ = 195.1, 189.4, 163.5, 163.2, 160.6, 151.7, 134.3, 132.3, 130.6, 128.3, 121.8, 114.1, 113.7, 55.5, 42.3

MS (GC-MS) Calculated *m/z* for [M+H] = 417.17, Found *m/z* for [M+H] =

IR (thin film):

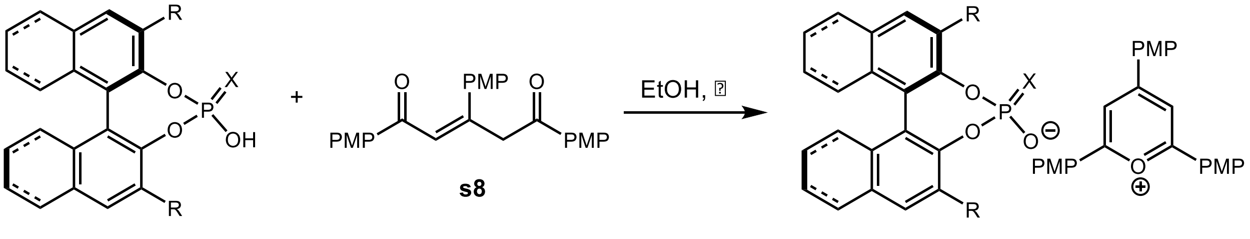

R
O
X
P
O
OH
R
+
O
PMP
O
PMP
PMP
s8
EtOH,
R
O
X
P
O
O
R
PMP
PMP
O
PMP

General Procedure B: The Brønsted acid (1 equiv.) and **s7** (1 equiv.) were added to a vial and suspended in EtOH. Upon heating to approx. 60 °C using a heat gun for 5 minutes, all material dissolved and the solution took on a bright orange color. The crude reaction mixture was allowed to cool and concentrated upon complete consumption of the starting material. The crude product was dissolved in MeOH and shaken with hexanes. After separation, concentration of the MeOH layer and drying under high vacuum overnight afforded pure oxopyrilium salts. These compounds are benchtop stable for several weeks but should be stored at low temperatures for extended periods.

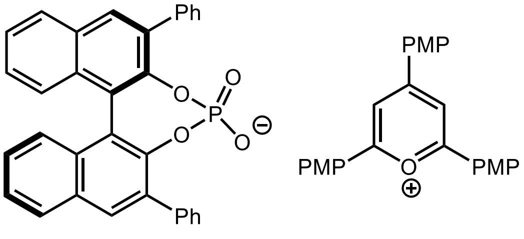

1a

Compound **1a** was prepared according to general procedure B using xx mg **s1** (xx mmol) and xx mg **s8** (xx mmol) in 8 mL EtOH. **1a** was obtained in a XX% yield as an orange solid after extraction.

^{1}H NMR: **(600 MHz, Chloroform-*d*)** δ 8.03 – 7.72 (m, 14H), 7.49 – 7.38 (m, 2H), 7.32 (dd, *J* = 28.8, 8.5 Hz, 2H), 7.24 (t, *J* = 7.7 Hz, 4H), 7.09 (d, *J* = 3.7 Hz, 4H), 6.77 (d, *J* = 8.5 Hz, 4H), 6.33 (d, *J* = 8.4 Hz, 2H).

^{13}C NMR: (151 MHz, $CDCl_3$) δ 166.89, 165.40, 164.67, 161.42, 138.01, 137.08, 134.74, 134.17, 132.45, 132.24, 131.20, 131.16, 131.03, 130.40, 130.33, 130.09, 130.05, 128.35, 128.26, 127.75, 127.13, 127.09, 127.01, 126.92, 126.02, 125.99, 125.25, 125.21, 123.40, 120.35, 115.43, 115.24, 109.88, 55.67, 55.28.

MS (LTQ FT-ICR) Positive mode: Calculated *m/z* for [M+H] =399.16, Found *m/z* for [M+H] = 399.15862

Negative mode: Calculated *m/z* for [M+H] =727.31, Found *m/z* for [M+H] = 727.31472

IR (thin film): 3432, 2077, 1631, 1606, 1589, 1512, 1484, 1438, 1306, 1261, 1243, 1178, 1096

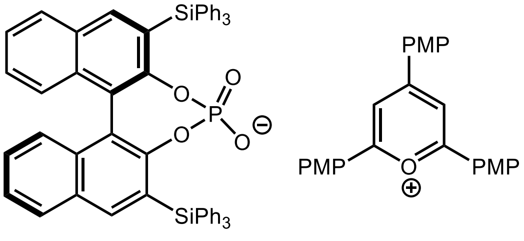

1b

1b

Compound **1b** was prepared according to general procedure B using 100 mg **s2** (.116 mmol) and 48.1 mg **s8** (.116 mmol) in 8 mL EtOH. **1b** was obtained in a 83% yield as an orange solid after extraction.

^{1}H NMR: **(600 MHz, Chloroform-*d*)** δ 8.27 (d, *J* = 9.0 Hz, 4H), 8.16 (s, 2H), 8.13 (d, *J* = 8.6 Hz, 2H), 7.97 (s, 2H), 7.69 (d, *J* = 8.3 Hz, 2H), 7.64 – 7.52 (m, 12H), 7.33 (d, *J* = 8.5 Hz, 2H), 7.29 (t, *J* = 7.5 Hz, 2H), 7.22 (t, *J* = 7.7 Hz, 2H), 7.01 (d, *J* = 7.8 Hz, 18H), 6.91 (d, *J* = 8.7 Hz, 4H), 6.48 (d, *J* = 8.4 Hz, 2H), 3.67 (s, 6H), 3.33 (s, 3H).

^{13}C NMR: **(151 MHz, $CDCl_3$)** δ 167.02, 165.35, 164.58, 161.97, 141.05, 136.99, 135.46, 134.49, 133.62, 130.77, 129.82, 128.59, 128.45, 127.13, 126.96, 126.37, 124.13, 123.94, 122.44, 121.54, 115.38, 115.31, 111.46, 77.21, 77.00, 76.79, 55.73, 55.58.

MS (LTQ FT-ICR) Positive mode: Calculated *m/z* for [M+] =399.16, Found *m/z* for [M+] = 399.15862

Negative mode: Calculated *m/z* for [M-] =863.22, Found *m/z* for [M-] =863.21778

IR (thin film): 3428, 3069, 3049, 2937, 2041, 1628, 1604, 1512, 1486, 1438, 1408, 1262, 1244, 1178, 1104

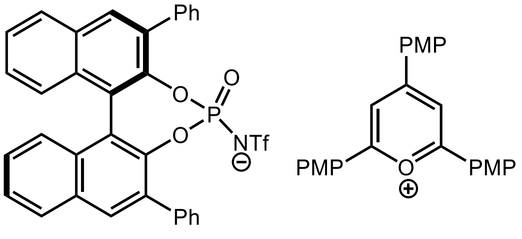

1c

Compound **1c** was prepared according to general procedure B using 28.9 mg **s3** (.046 mmol) and 19.1 mg **s8** (.046 mmol) in 2 mL EtOH. **1c** was obtained in a 74% yield as an orange solid after extraction.

^{1}H NMR: **(600 MHz, Chloroform-*d*)** δ 8.27 (s, 2H), 8.25 – 8.14 (m, 6H), 7.64 – 7.45 (m, 14H), 7.13 – 6.96(m, *J* = 8.7 Hz, 24H), 6.94 (d, *J* = 8.4 Hz, 2H), 3.91 (s, 6H), 3.82 (s, 3H), 2.79 – 2.54 (m, 6H), 2.40 (d, *J* = 16.7 Hz, 1H), 2.30 (d, *J* = 17.9 Hz, 1H), 1.90 – 1.55 (m, 8H).

^{13}C NMR: **(151 MHz, CDCl$_3$)** δ 167.61, 166.26, 165.02, 162.29, 136.99, 136.92, 135.56, 134.93, 133.27, 130.59, 128.49, 128.44, 127.09, 126.99, 124.03, 121.33, 116.03, 115.70, 111.02, 56.22, 55.99, 29.22, 29.08, 27.96, 27.86, 22.92, 22.82, 22.75.

MS (LTQ FT-ICR) Positive mode: Calculated *m/z* for [M+] =399.16, Found *m/z* for [M+] = 399.15862

Negative mode: Calculated *m/z* for [M-] =863.22, Found *m/z* for [M-] =863.21778

IR (thin film): 3734. 3648. 3586, 1716, 1588, 1508, 1487, 1243, 1177, 1105

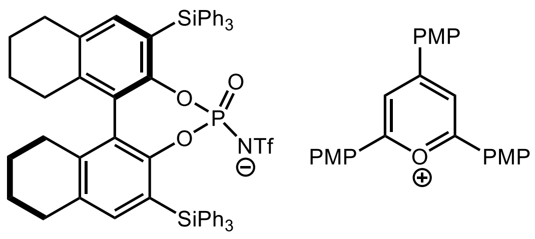

1d

Compound **1d** was prepared according to general procedure B using 120.1 mg **s6** (0.1196 mmol) and 49.3 mg **s8** (0.1184 mmol) in 8 mL EtOH. **1d** was obtained in a 77% yield as an orange solid after extraction.

^{1}H NMR: (600 MHz, $CDCl_3$) δ 8.57 (s, 2H), 8.29 (s, 3H), 8.17 (d, *J* = 8.4 Hz, 6H), 7.92 (s, 2H), 7.03 (d, *J* = 8.2 Hz, 4H), 6.89 (s, 2H), 6.82 (s, 4H), 3.86 (s, 6H), 3.74 (s, 3H), 2.88 (dd, *J* = 15.0, 7.7 Hz, 2H), 2.85 – 2.67 (m, 2H), 2.69 – 2.54 (m, 2H), 2.26 (s, 6H), 2.21 (d, *J* = 16.5 Hz, 2H), 1.88 (s, 12H), 1.82 – 1.64 (m, 6H), 1.52 (dt, *J* = 10.3, 4.8 Hz, 2H).

^{13}C NMR: **(151 MHz, $CDCl_3$)** δ 167.91, 165.96, 165.13, 162.39, 142.77, 139.42, 134.99, 133.47, 132.13, 130.22, 128.86, 128.21, 127.93, 125.96, 124.12, 120.99, 115.79, 115.66, 110.45, 77.21, 77.00, 76.79, 55.88, 29.17, 27.84, 22.71, 22.55, 21.06, 17.40.

MS (LTQ FT-ICR) Positive mode: Calculated *m/z* for [M+] =399.16, Found *m/z* for [M+] = 399.15857

Negative mode: Calculated *m/z* for [M-] =1004.22, Found *m/z* for [M-] =1002.26177

IR (thin film): 2938, 2844, 2044, 1630, 1604, 1512, 1485, 1463, 1439, 1307, 1261, 1243, 1178

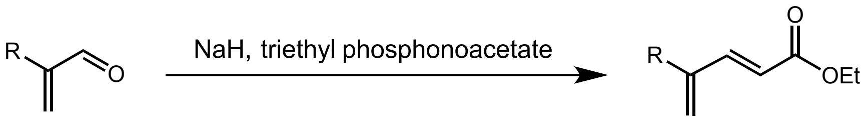

III. Preparation of Substrates

General Procedure C: The preparation of substrates **s9-s11** was carried out according to the procedure reported by Wender et al.[28]

ethyl (*E*)-5-methyl-4-methylenehex-2-enoate (s9)

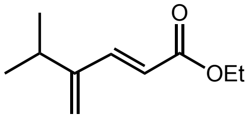

Compound **s9** was synthesized according to the published procedure and obtained in aa 60% yield after column chromatography on silica gel using EtOAc:HX (1:3), and matched reported spectra.[28]

ethyl (*E*)-4-benzylpenta-2,4-dienoate (s10)

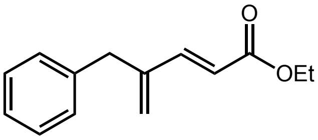

Compound **s10** was synthesized according to the published procedure and obtained in an 54% yield after column chromatography on silica gel using DCM/HX (1:1).

^{1}H NMR: **(600 MHz, $CDCl_3$)** δ 7.38 (d, *J* = 15.9 Hz, 1H), 7.30 (t, *J* = 7.5 Hz, 2H), 7.22 (t, *J* = 7.4 Hz, 1H), 7.19 (d, *J* = 7.5 Hz, 2H), 5.92 (d, *J* = 15.9 Hz, 1H), 5.54 (s, 1H), 5.25 (s, 1H), 4.19 (q, *J* = 7.1 Hz, 2H), 3.58 (s, 2H), 1.29 (t, *J* = 7.2 Hz, 3H).

^{13}C NMR: **(151 MHz, $CDCl_3$)** δ 167.01, 145.92, 143.47, 138.28, 128.75, 128.47, 126.36, 125.53, 119.07, 77.21, 77.00, 76.79, 60.40, 38.15, 14.25.

MS (GC-MS) Calculated *m/z* = 216.12, Found *m/z* = 216.20

IR (thin film): 3432, 3086, 3063, 3027, 2981, 2905, 1712, 1633, 1603, 1496, 1454, 1365, 1272, 1174

ethyl (*E*)-4-cyclohexylpenta-2,4-dienoate (s11)

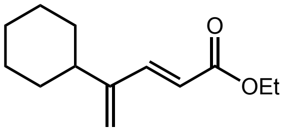

Compound **s11** was synthesized according to the published procedure and obtained in a 58% yield after column chromatography on silica gel using DCM:HX (1:1).

^{1}H NMR: (600 MHz, CDCl$_3$) δ 7.31 (d, *J* = 16.0 Hz, 1H), 5.98 (d, *J* = 16.0 Hz, 1H), 5.37 (s, 1H), 5.32 (s, 1H), 4.25 (q, *J* = 7.1 Hz, 2H), 2.39 – 2.15 (m, 1H), 1.93 – 1.60 (m, 5H), 1.48 – 1.14 (m, 8H).

^{13}C NMR: **(151 MHz, CDCl$_3$)** δ 194.74, 173.16, 155.54, 132.72, 77.21, 77.00, 76.79, 60.04, 42.23, 35.77, 33.00, 26.44, 26.02, 14.28.

MS (GC-MS) Calculated *m/z* for [M+H] = 208.30, Found *m/z* for [M+H] = 208.22

IR (thin film): 3854, 3434, 2980, 2926, 2853, 1734, 1716, 1630, 1603, 1388, 1366, 1284, 1262, 1165

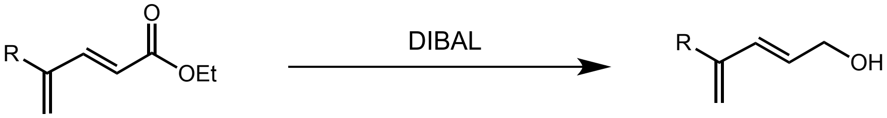

General Procedure D: Compounds **s12-s14** were prepared according to the procedure reported by Wender et al.[28]

(*E*)-5-methyl-4-methylenehex-2-en-1-ol (s12)

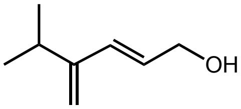

Compound **s12** was prepared according to the reported procedure and matched published spectra.[28]

(*E*)-4-benzylpenta-2,4-dien-1-ol (s13)

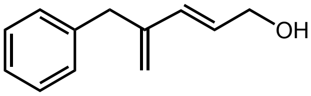

Compound **s13** was prepared according to the reported procedure in a 60% yield using 2.48 g (11.47 mmol) of starting material **s10.**

^{1}H NMR: **(600 MHz, CDCl$_3$)** δ 7.29 (dd, *J* = 8.2, 7.0 Hz, 3H), 7.21 (d, *J* = 7.3 Hz, 4H), 6.34 (d, *J* = 15.8 Hz, 1H), 5.87 (dt, *J* = 15.8, 5.8 Hz, 1H), 5.18 (d, *J* = 1.7 Hz, 1H), 4.92 (d, *J* = 1.9 Hz, 1H), 4.16 (d, *J* = 5.4 Hz, 2H), 3.57 (s, 2H), 1.43 (s, 1H).

^{13}C NMR: δ 144.20, 139.25, 132.77, 128.82, 128.77, 128.29, 126.06, 118.27, 63.55, 38.73

MS (GC-MS) Calculated *m/z* for [M+H] = 174.24, Found *m/z* for [M+H] = 174.20

IR (thin film): 3433, 3027, 2934, 2081, 1644, 1494, 1453, 1204, 1074

(*E*)-4-cyclohexylpenta-2,4-dien-1-ol (s14)

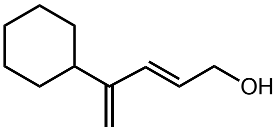

Compound **s14** was prepared according to the reported procedure in an 76% yield using 7.05 g (33.85 mmol) of starting material **s11.**

^{1}H NMR: **(600 MHz, Chloroform-*d*)** δ 6.21 (d, *J* = 15.8 Hz, 1H), 5.91 (dt, *J* = 15.7, 5.9 Hz, 1H), 4.99 (s, 1H), 4.94 (s, 1H), 4.21 (t, *J* = 5.8 Hz, 2H), 2.19 (t, *J* = 12.1 Hz, 1H), 1.80 (t, *J* = 15.6 Hz, 4H), 1.32 (q, *J* = 12.9 Hz, 2H), 1.19 (p, *J* = 11.7, 11.1 Hz, 3H).

^{13}C NMR: **(151 MHz, $CDCl_3$)** δ 151.14, 133.49, 126.83, 113.00, 63.90, 60.86, 40.37, 39.86, 34.19, 33.35, 32.90, 26.87, 26.54, 26.45, 26.27.

MS (GC-MS) Calculated *m/z* for [M+H] = 166.29, Found *m/z* for [M+H] = 166.20

IR (thin film): 3418, 2924, 2851, 1644, 1448, 1093

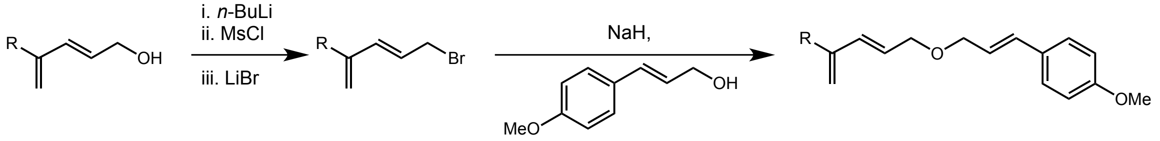

General Procedure D: Diene was dissolved in THF (0.4 M) in a flame-dried round bottom flask and kept under positive pressure of N_2. The solution was cooled to -78 °C in a dry ice/acetone batch. *n*-BuLi (2.5 M in hexane, 1.1 equiv.) added dropwise via syringe. After stirring for ~5 minutes, MsCl (1.1 equiv.) was added dropwise via syringe, and solution then stirred for an additional 30 minutes. At the same time, a separate round bottom flask was charged with LiBr (5.0 equiv.), 4 Å molecular sieves, and THF. The solution was stirred for 15 minutes and transferred slowly via cannula into the reaction mixture. Reaction continued stirring at -78 °C for 30 minutes, then the dry ice/acetone bath was removed and the reaction continued to stir at room temperature for 1.5 hours. The mixture was quenched by the addition of saturated aqueous ammonium chloride (100 mL), extracted 3x with Et_2O, dried over Na_2SO_4, and concentrated under reduced pressure. The crude product was dissolved in dry THF (0.4 M) and stirred for 1 hour over 4 Å molecular sieves. Meanwhile, 4-methoxycinnamyl alcohol (2.0 equiv) was added in small portions to a stirred solution of NaH (2.1 equiv, 60% dispersion in mineral oil) in dry

THF (0.4 M) at 0 °C. The mixture was stirred for 15 minutes, then the solution containing the alkyl bromide was transferred via cannula over several minutes. The reaction was allowed to warm to room temperature and stirred for 4 hours. The reaction was quenched by the slow addition of saturated aqueous ammonium chloride and extracted 3x with Et_2O. Combined organic layers were dried over Na_2SO_4 and concentrated. Products were purified by column chromatography using EtOAc/HX.

1-methoxy-4-((*E*)-3-(((*E*)-5-methyl-4-methylenehex-2-en-1-yl)oxy)prop-1-en-1-yl)benzene (2a)

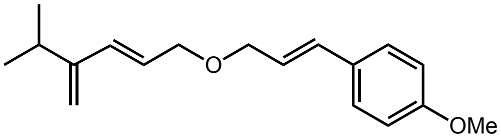

Compound **2a** was synthesized according to general procedure D using 5.0 g (39.6 mmol) **s12** and 4.65 mg 4-methoxycinnamyl alcohol. The product was obtained as a tan oil in 64% yield after purification by column chromatography on silica using DCM:HX (1:3).

^{1}H NMR: **(400 MHz, $CDCl_3$)** δ 7.33 (d, *J* = 8.7 Hz, 2H), 6.86 (d, *J* = 8.7 Hz, 2H), 6.56 (d, *J* = 15.9 Hz, 1H), 6.33 – 6.09 (m, 3H), 5.87 (dt, *J* = 15.9, 6.2 Hz, 2H), 4.99 (d, *J* = 10.6 Hz, 2H), 4.12 (ddd, *J* = 15.6, 6.3, 1.4 Hz, 6H), 2.82 – 2.47 (m, 1H), 1.10 (d, *J* = 6.8 Hz, 9H).

^{13}C NMR: **(151 MHz, $CDCl_3$)** δ 158.13, 146.49, 137.22, 127.70, 115.91, 113.99, 71.54, 70.72, 55.31, 55.27, 48.59, 45.36, 42.76, 38.21, 34.50, 21.71, 21.55.

MS (GC-MS) Calculated *m/z* = 272.18, Found *m/z* for [M+H] = 272.20

IR (thin film): 3089, 3032, 2961, 2932, 2870, 2836, 1058, 1730, 1653, 1607, 1577, 1511, 1462, 1420, 1357, 1309, 1249

1-((*E*)-3-(((*E*)-4-benzylpenta-2,4-dien-1-yl)oxy)prop-1-en-1-yl)-4-methoxybenzene (2b)

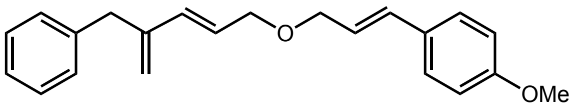

Compound **2b** was synthesized according to general procedure D using 800 mg (x mmol) **s13** and 1.51 g 4-methoxycinnamyl alcohol. The product was obtained in a 22% yield as a tan oil after purification by column chromatography on silica using DCM:HX (1:3).

^{1}H NMR: **(400 MHz, CDCl$_3$)** δ 7.32 (dd, *J* = 17.2, 7.9 Hz, 5H), 7.23 (d, *J* = 7.5 Hz, 4H), 6.88 (d, *J* = 8.3 Hz, 2H), 6.55 (d, *J* = 15.8 Hz, 1H), 6.38 (d, *J* = 15.9 Hz, 1H), 6.17 (dt, *J* = 15.9, 6.2 Hz, 1H), 5.86 (dt, *J* = 15.8, 6.1 Hz, 1H), 5.20 (s, 1H), 4.92 (s, 1H), 4.08 (dd, *J* = 10.1, 6.2 Hz, 4H), 3.82 (s, 3H), 3.60 (s, 2H).

^{13}C NMR: **(151 MHz, CDCl$_3$)** δ 159.15, 144.25, 139.23, 134.26, 132.28, 129.30, 128.80, 128.23, 127.61, 126.34, 126.33, 125.98, 123.50, 118.29, 118.27, 113.83, 70.80, 70.47, 55.20, 55.16, 38.54, 38.53.

MS (GC-MS) Calculated *m/z* = 320.18, Found *m/z* for [M+H] = 320.20

IR (thin film): 3434, 3028, 2932, 2836, 1651, 1607, 1509, 1454, 1357, 1248, 1174

1-((*E*)-3-(((*E*)-4-cyclohexylpenta-2,4-dien-1-yl)oxy)prop-1-en-1-yl)-4-methoxybenzene (2c)

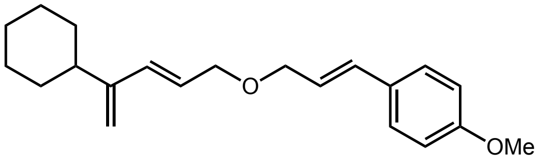

Compound **2b** was synthesized according to general procedure D using xx mg (x mmol) **s13** and xx mg 4-methoxycinnamyl alcohol. The product was obtained as an off white oil after purification by column chromatography on silica using DCM:HX (1:3).

^{1}H NMR: **(600 MHz, $CDCl_3$)** δ 7.33 (d, *J* = 8.7 Hz, 2H), 6.85 (d, *J* = 8.7 Hz, 2H), 6.56 (d, *J* = 15.8 Hz, 1H), 6.32 – 6.09 (m, 2H), 5.86 (dt, *J* = 15.9, 6.3 Hz, 1H), 4.99 (s, 1H), 4.95 (s, 1H), 4.11 (dd, *J* = 27.2, 6.3 Hz, 4H), 3.81 (s, 3H), 2.44 – 2.13 (m, 1H), 1.95 – 1.74 (m, 4H), 1.71 (d, *J* = 13.2 Hz, 1H), 1.44 – 1.24 (m, 2H), 1.24 – 1.08 (m, 3H).
^{13}C NMR: **(151 MHz, $CDCl_3$)** δ 159.25, 151.22, 134.94, 132.27, 129.47, 127.66, 124.40, 123.76, 113.93, 113.03, 77.21, 77.00, 76.79, 70.92, 70.89, 55.27, 39.75, 32.93, 26.89, 26.48.
MS (GC-MS) Calculated *m/z* = 312.21, Found *m/z* for [M+H] = 312.20
IR (thin film): 3023, 2926, 2851, 1731, 1607, 1511, 1449, 1358, 1303, 1249, 1174, 1105, 1035

HPLC Traces

3a:

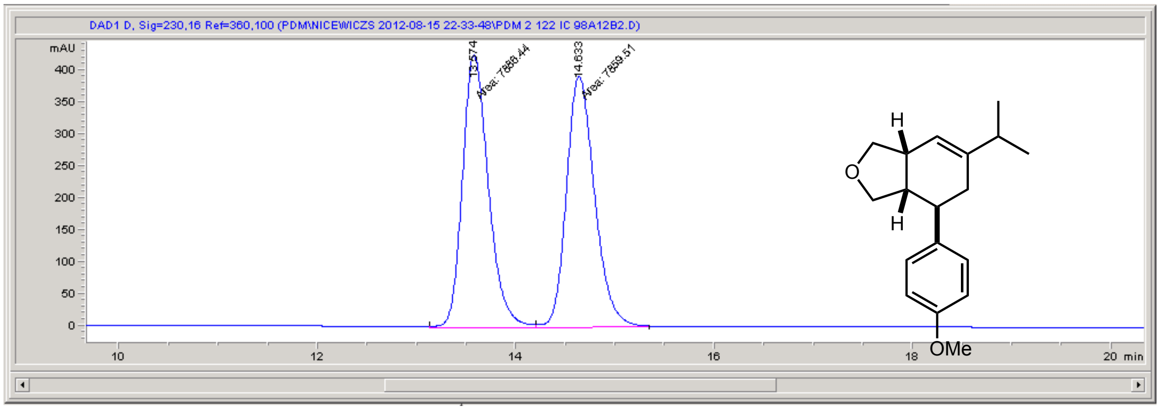

```
Signal 4: DAD1 D, Sig=230,16 Ref=360,100

Peak RetTime Type  Width      Area       Height     Area
  #   [min]        [min]    [mAU*s]      [mAU]       %
----|-------|----|-------|----------|----------|--------|
   1  13.574 MF    0.3065 7886.43848  428.83115  50.0855
   2  14.633 FM    0.3319 7859.51025  394.71118  49.9145

Totals :                  1.57459e4   823.54233
```

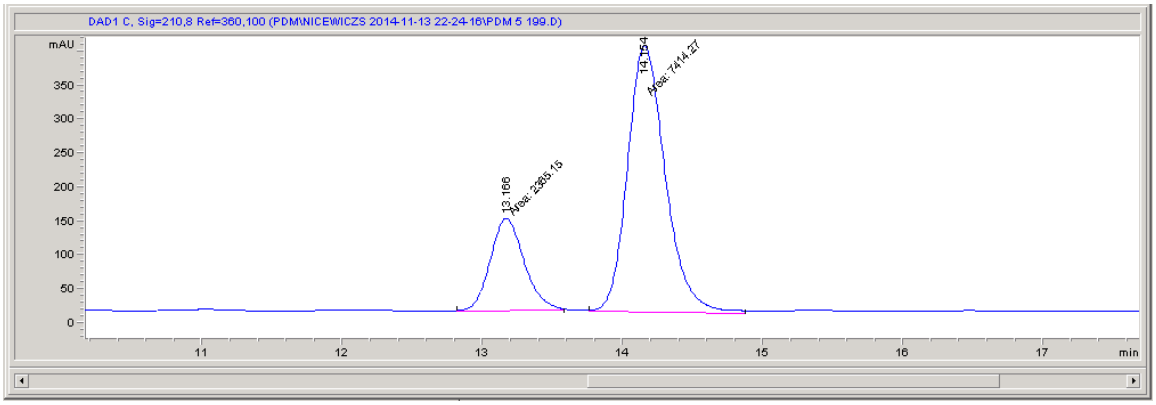

```
Signal 3: DAD1 C, Sig=210,8 Ref=360,100

Peak RetTime Type  Width     Area       Height      Area
  #   [min]        [min]   [mAU*s]      [mAU]        %
----|-------|----|-------|----------|----------|--------|
   1  13.166 MM    0.2867 2365.15332  137.49609  24.1850
   2  14.154 MM    0.3143 7414.26563  393.11993  75.8150

Totals :                  9779.41895  530.61603
```

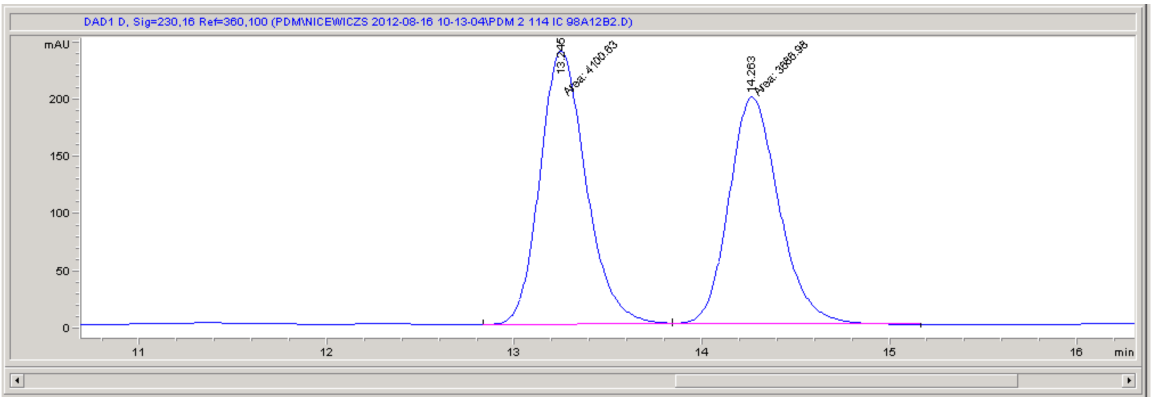

```
Signal 4: DAD1 D, Sig=230,16 Ref=360,100

Peak RetTime Type  Width     Area       Height      Area
  #   [min]        [min]   [mAU*s]      [mAU]        %
----|-------|----|-------|----------|----------|--------|
   1  13.245 MF    0.2860 4100.62793  238.93929  52.6558
   2  14.263 FM    0.3094 3686.97583  198.59125  47.3442

Totals :                  7787.60376  437.53053
```

3b

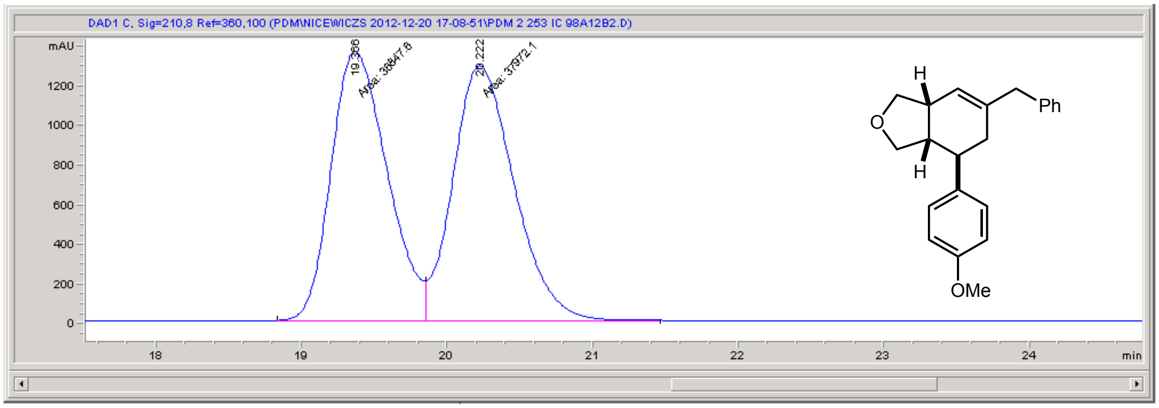

```
Signal 3: DAD1 C, Sig=210,8 Ref=360,100

Peak RetTime Type  Width     Area      Height     Area
  #   [min]        [min]   [mAU*s]     [mAU]       %
----|-------|----|-------|----------|----------|--------|
   1  19.366 MF     0.4507 3.68476e4 1362.73218  49.2486
   2  20.222 FM     0.4910 3.79721e4 1289.03601  50.7514

Totals :                   7.48197e4 2651.76819
```

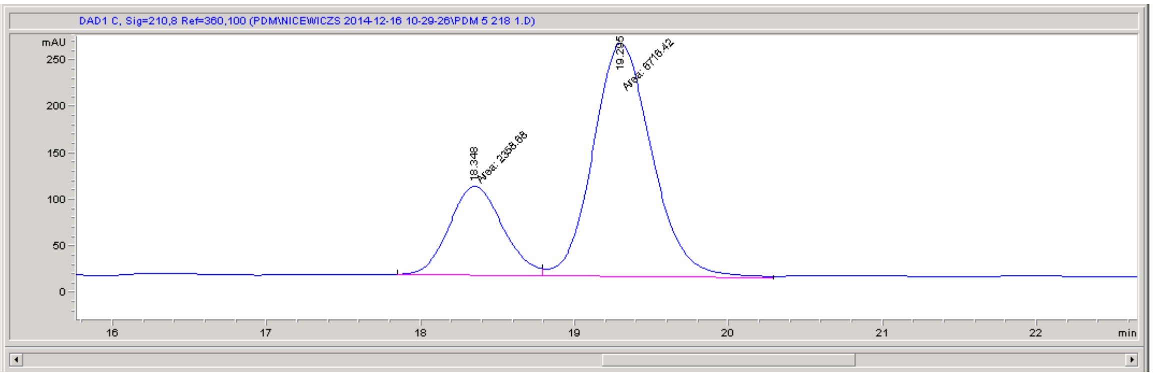

```
Signal 3: DAD1 C, Sig=210,8 Ref=360,100

Peak RetTime Type  Width     Area      Height     Area
  #   [min]        [min]   [mAU*s]     [mAU]       %
----|-------|----|-------|----------|----------|--------|
   1  18.348 MF    0.4075 2358.67578   96.47877  25.9906
   2  19.295 FM    0.4456 6716.42188  251.19687  74.0094

Totals :                  9075.09766  347.67564
```

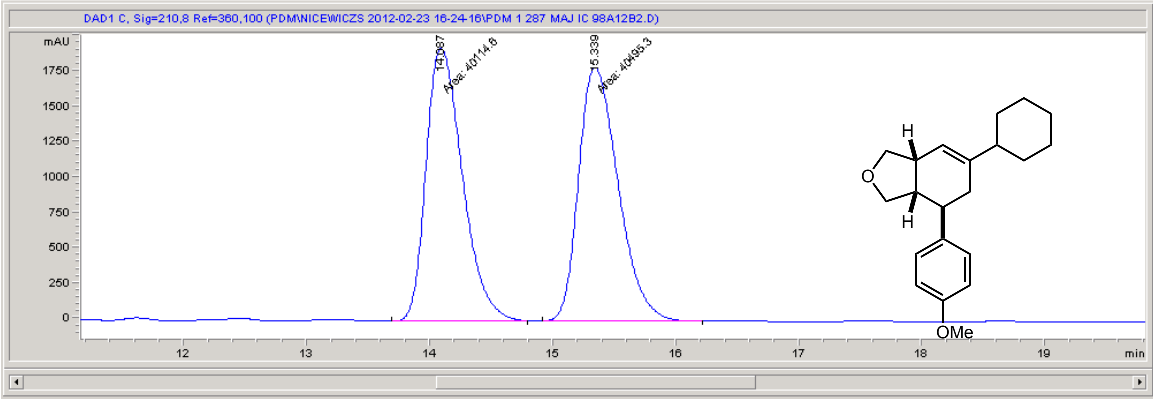

3c

```
Signal 3: DAD1 C, Sig=210,8 Ref=360,100

Peak RetTime Type  Width     Area      Height     Area
  #   [min]        [min]   [mAU*s]     [mAU]        %
----|-------|----|-------|----------|----------|--------|
   1  14.087 MM    0.3457 4.01146e4  1933.92993  49.7638
   2  15.339 MM    0.3752 4.04953e4  1798.80701  50.2362

Totals :                  8.06099e4  3732.73694
```

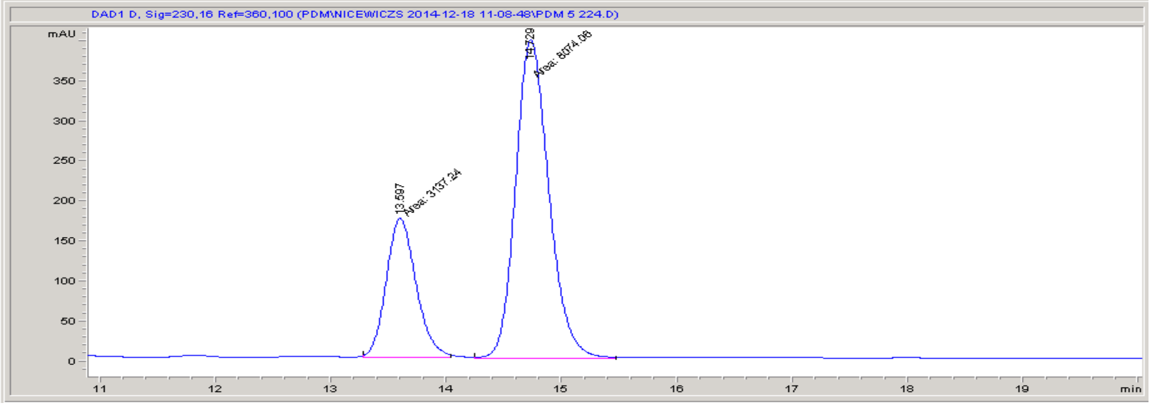

```
Signal 4: DAD1 D, Sig=230,16 Ref=360,100

Peak RetTime Type  Width     Area      Height     Area
  #   [min]        [min]   [mAU*s]     [mAU]        %
----|-------|----|-------|----------|----------|--------|
   1  13.597 MM    0.3004 3137.23608  174.05907  27.0373
   2  14.729 MM    0.3484 8466.14160  404.97379  72.9627

Totals :                  1.16034e4   579.03285
```

4a

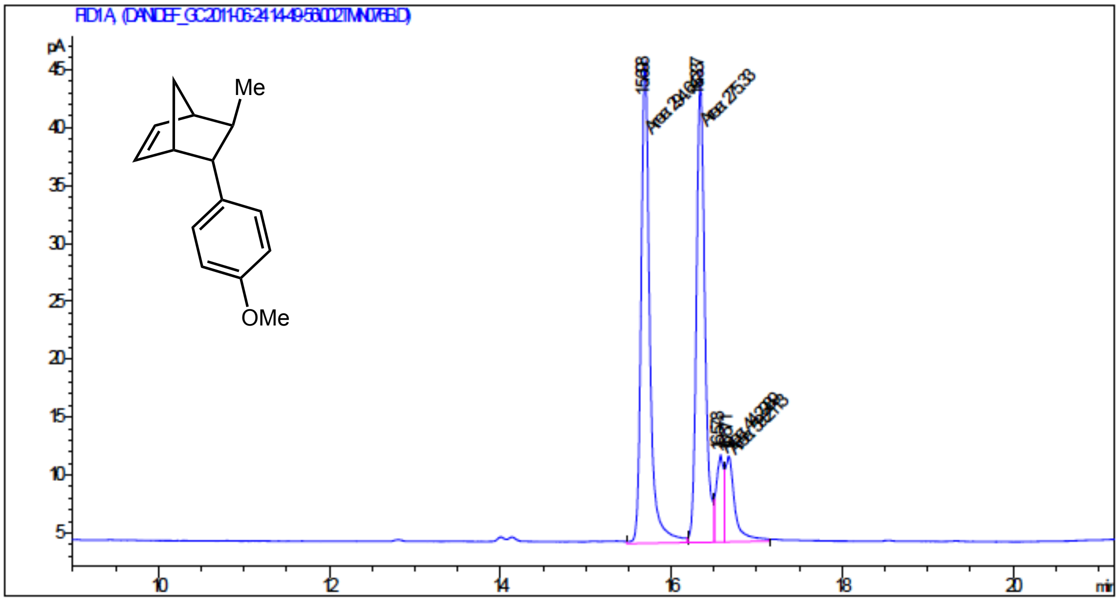
FID1A, (DANDEF_GC2011-06-24 14-49-58\002TMN076B.D)
pA
45
40
35
30
25
20
15
10
5
Me
OMe
15.698
Area: 2946.9
16.337
Area: 2753.3
16.578
10
12
14
16
18
20
min

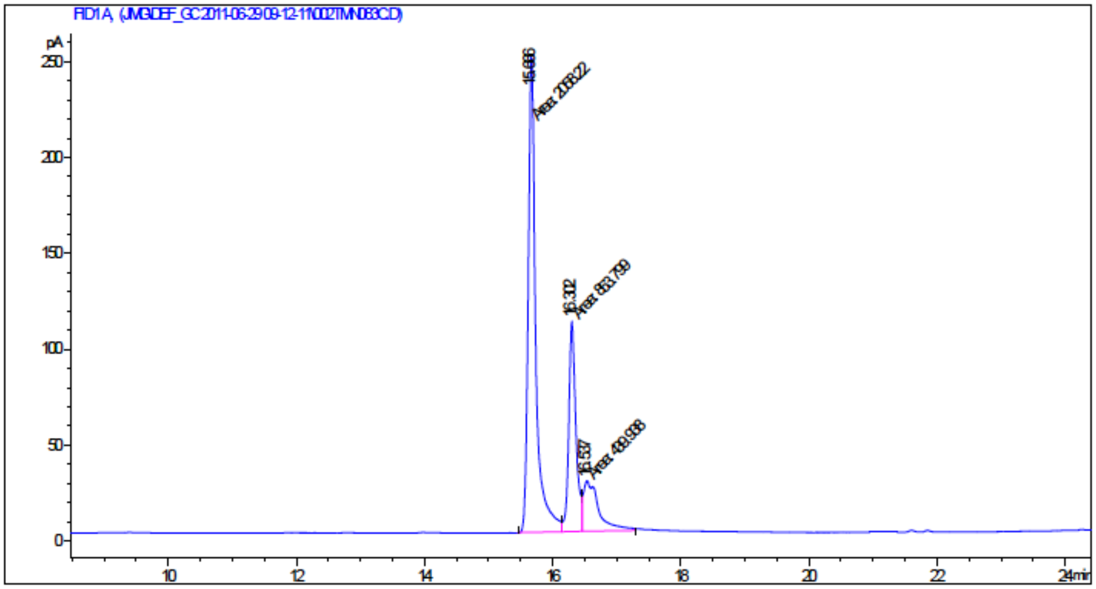
FID1A, (JMGDEF_GC2011-06-29 09-12-11\002TMN083C.D)
pA
250
200
150
100
50
0
15.686
Area: 2068.22
16.302
Area: 853.799
16.537
Area: 499.938
10
12
14
16
18
20
22
24
min

4b

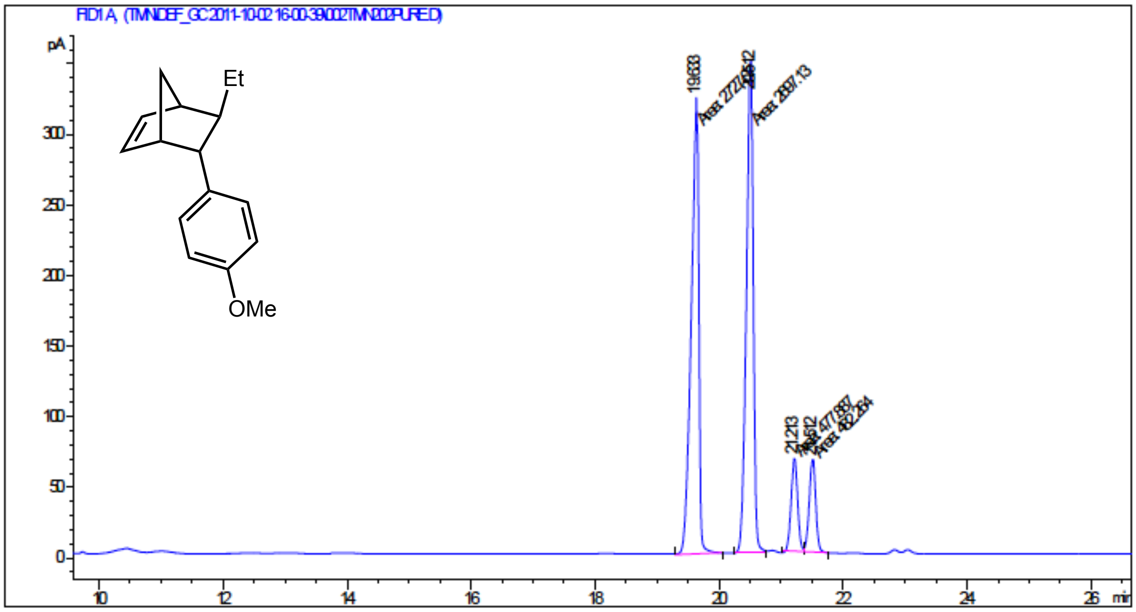
FID1 A, (TMNDEF_GC2011-10-02 16-00-39\002TMN202PURED)
pA
300
250
200
150
100
50
0
10
12
14
16
18
20
22
24
26
min
Et
OMe
19633
Area: 2724
20512
Area: 2897.13
21213
21512
Area: 477.887
Area: 482.264

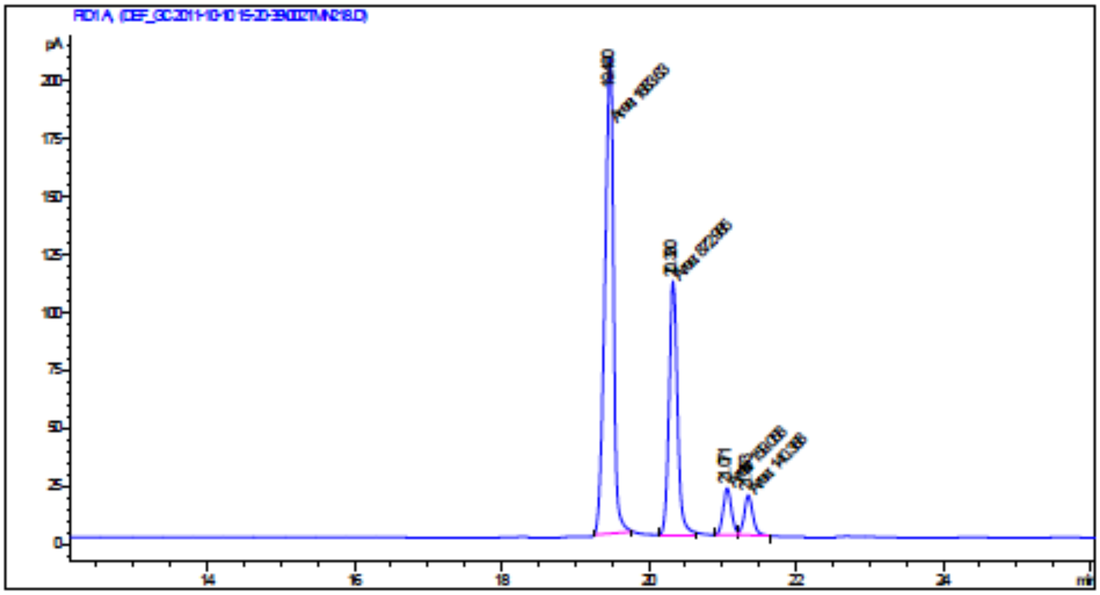
FID1 A, (DEF_GC 2011-10-10 15-20-39\002TMN218.D)
pA
200
175
150
125
100
75
50
25
0
14
16
18
20
22
24
min

4c

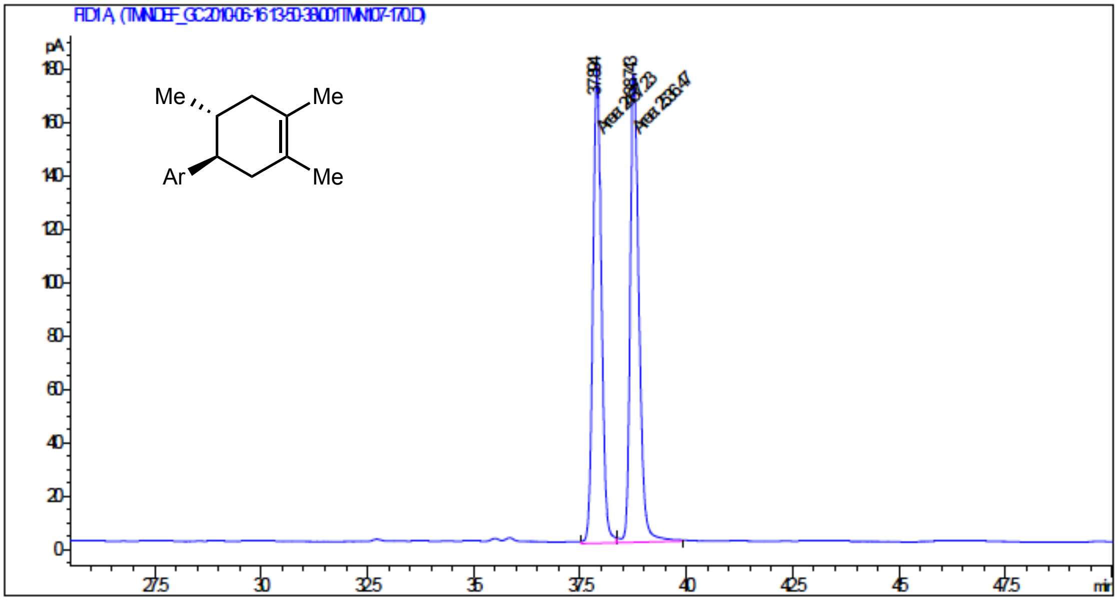
FID1 A, (TMNDEF_GC2010-06-16 13-50-38\001TMN107-170.D)
pA
180
160
140
120
100
80
60
40
20
0
Me
Me
Ar
Me
37.894
Area: 2687.23
38.743
Area: 2536.47
27.5
30
32.5
35
37.5
40
42.5
45
47.5
min

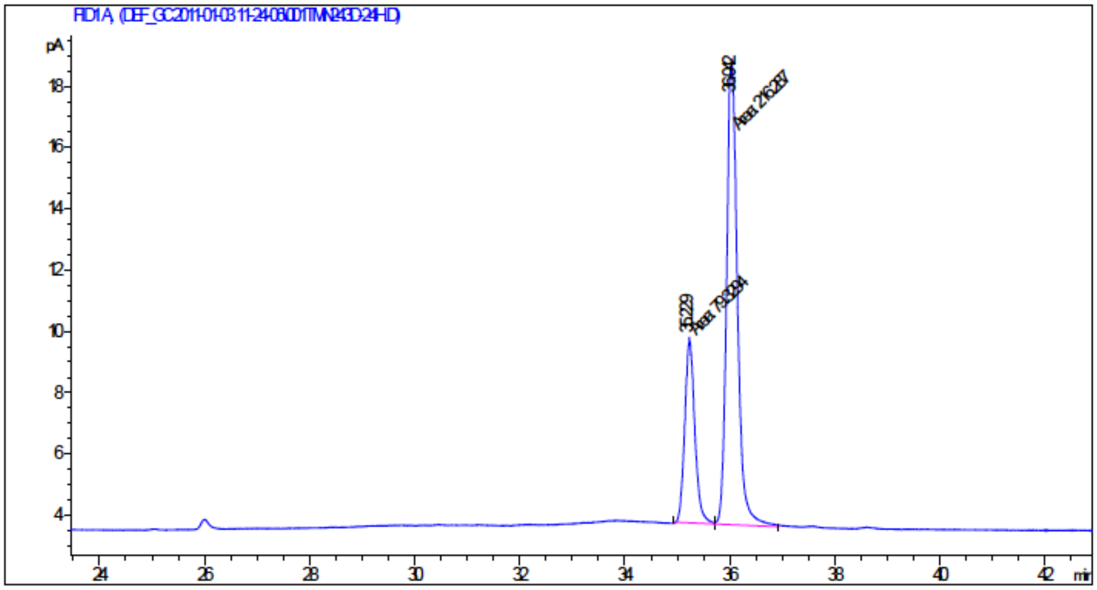
FID1 A, (DEF_GC2011-01-03 11-24-06\001TMN243D-24H.D)
pA
18
16
14
12
10
8
6
4
35.229
Area: 79.3084
36.042
Area: 216.287
24
26
28
30
32
34
36
38
40
42
min

APPENDIX 2: SUPPORTING INFORMATION FOR THE PHOTOREDOX CATALYZED HYDROFUNCTIONALIZATION REACTIONS FOR THE SYNTHESIS OF OXAZOLINES AND THIAZOLINES

General Methods. Infrared (IR) spectra were obtained using a Jasco 260 Plus Fourier transform infrared spectrometer. Proton, carbon, and fluorine magnetic resonance spectra (^{1}H NMR and ^{13}C NMR) were recorded on a Bruker model DRX 400 or 600 (^{1}H NMR at 400 MHz or 600 MHz and ^{13}C NMR at 100 MHz or 150 MHz spectrometer. Chemical shifts for protons are reported in parts per million downfield from tetramethylsilane and are referenced to residual protium in solvent (^{1}H NMR: $CHCl_3$ at 7.26 ppm). Chemical shifts for carbons are reported in parts per million downfield from tetramethylsilane and are referenced to the carbon resonances of the residual solvent peak (^{13}C NMR: $CDCl_3$ at 77.0 ppm). NMR data are represented as follows: chemical shift, multiplicity (s = singlet, d = doublet, dd = doublet of doublet, ddd = doublet of doublet of doublet, dddd = doublet of doublet of doublet of doublet, dtd = doublet of triplet of doublet, t = triplet, q = quartet, qd = quartet of doublet, sept = septuplet, m = multiplet), coupling constants (Hz), and integration. Mass spectra were obtained using either a Micromass Quattro II (triple quad) instrument with nanoelectrospray ionization or an Agilent 6850 series gas chromatograph instrument equipped with a split-mode capillary injection system and Agilent 5973 network mass spec detector (MSD). Thin layer chromatography (TLC) was performed on SiliaPlate 250 μm thick silica gel plates purchased from Silicycle. Visualization was accomplished using fluorescence quenching, $KMnO_4$ stain, or ceric ammonium molybdate (CAM) stain followed by heating. Organic solutions were concentrated under reduced pressure using a Büchi rotary evaporator. Purification of the reaction products was carried out by chromatography using Siliaflash-P60 (40-63 μm) or Siliaflash-T60 (5-20 μm) silica gel purchased from Silicycle. All reactions were carried out under an inert atmosphere of nitrogen in

flame-dried glassware with magnetic stirring unless otherwise noted. Irradiation of photochemical reactions was carried out using a Par38 Royal Blue Aquarium LED lamp (Model # 6851) fabricated with high-power Cree LEDs as purchased from Ecoxotic (www.ecoxotic.com), with standard borosilicate glass vials purchased from Fisher Scientific. Yield refers to isolated yield of analytically pure material unless otherwise noted. NMR yields were determined using hexamethyldisiloxane as an internal standard. Cyclic voltammograms were obtained with a glassy carbon working electrode, Ag/AgCl reference electrode, platinum wire counter electrode, and Pine Instruments Wavenow potentiostat. All measurements were taken in N_2-sparged MeCN with 0.1 M tetrabutylammonium hexafluorophosphate ($TBAPF_6$) as a supporting electrolyte where the analyte concentration was 5-10 mM. The potential was scanned from 1.0 V to a vertex potential of 2.5 V in the forward direction at a sweep rate of 100 mV/s, and the reverse sweep showed no indication of a reversible electrochemical event. The half-wave potential for irreversible oxidation is estimated at $E_{p/2}$ the potential where the current is equal to one-half the peak current of the oxidation event. The values for $E_{p/2}$ are referenced to SCE (Saturated Calomel Electrode) by adding +30 mV to the potential measured against Ag/AgCl (3 M NaCl) .

Materials. Commercially available reagents were purchased from Sigma Aldrich, Acros, Alfa Aesar, or TCI, and used as received unless otherwise noted. Diethyl ether (Et_2O), dichloroethane (DCE), dichloromethane (DCM), tetrahydrofuran (THF), toluene, and dimethylformamide (DMF) were dried by passing through activated alumina columns under nitrogen prior to use. Triethylamine (Et_3N) was distilled from calcium hydride. Other common solvents and chemical reagents were purified by standard published methods if noted.

Preparation of 9-Mesityl-10-methylacridinium tetrafluoroborate

The photocatalyst used in this study, 9-mesityl-10-methylacridinium tetrafluoroborate, was synthesized by the method of Fukuzumi et al[23]. Tetrafluoroboric acid (diethyl ether complex) was substituted for perchloric acid during the hydrolysis. The spectral data matched the values reported in the literature for the perchlorate and hexafluorophosphate salts.

^{1}H NMR (600 MHz, CDCl3) δ 8.60 (d, *J* = 9.0 Hz, 2H), 8.37 (t, *J* = 9.0 Hz, 2H), 7.84 (s, 4H), 7.23 (s, 2H), 4.81 (s, 3H), 2.46 (s, 3H), 1.68 (s, 6H).

Preparation of Substrates

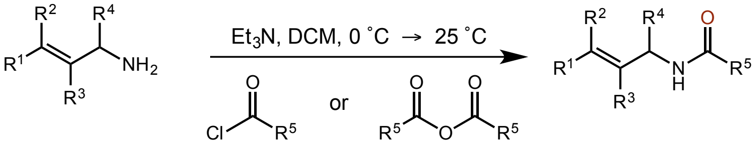

General Procedure A: The allylic amide substrates were synthesized according to a modified literature procedure[1]. The allylic amine (1.0 equiv.) was added to a flame-dried round bottom flask equipped with a stir bar, which was sealed with a septum and purged with nitrogen. Dry dichloromethane [0.2 M] was added and the reaction was cooled to 0 °C. Freshly distilled triethylamine (1.2 equiv.) was added dropwise by syringe, followed by dropwise addition of the appropriate acyl chloride or anhydride (1.5 equiv.). The reaction was allowed to warm to room temperature and stirred overnight. The reaction was then diluted with an equal volume of water and extracted with dichloromethane (3 times). The organic layer was washed with water followed by brine, and dried over Na_2SO_4. After concentration, the crude mixture was purified by either recrystallization or flash chromatography.

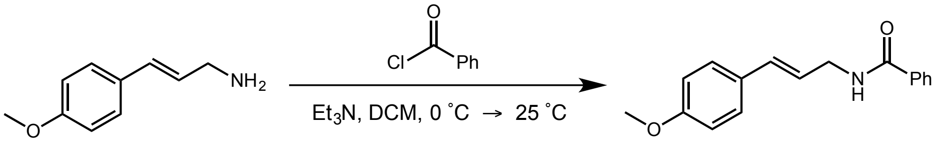

(*E*)-*N*-(3-(4-methoxyphenyl)allyl)benzamide (**3a**): Substrate **3a** was prepared according to General Procedure **A** using 500 mg (*E*)-4-methoxycinnamylamine (3.06 mmol), 0.51 mL triethylamine (3.67 mmol), 0.53 mL benzoyl chloride (4.59 mmol), and 15 mL DCM. Product was purified by recrystallization from ethyl acetate and hexanes to furnish 458 mg pure product as colorless crystals in 56% yield. Spectral data was in agreement with reported literature values[24].

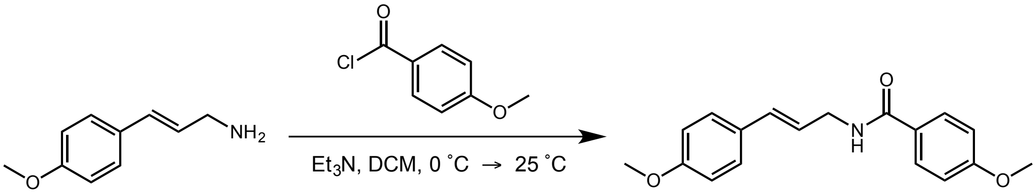

(*E*)-4-methoxy-*N*-(3-(4-methoxyphenyl)allyl)benzamide (3b): Substrate **3b** was prepared according to General Procedure **A** using 500 mg (*E*)-4-methoxycinnamylamine (3.06 mmol), 0.53 mL triethylamine (4.59 mmol), 0.83 mL 4-methoxybenzoyl chloride (6.12 mmol), and 15 mL DCM. Product was purified by flash chromatography on silica gel (50% EtOAc/Hexanes) and recrystallization from ethyl acetate and hexanes to furnish 340 mg pure product as pale yellow crystals in 34% yield.

^{1}H NMR (600 MHz, $CDCl_3$) δ 7.76 (d, *J* = 8.9 Hz, 1H), 7.31 (d, *J* = 8.6 Hz, 1H), 6.93 (d, *J* = 8.8 Hz, 1H), 6.85 (d, *J* = 8.7 Hz, 1H), 6.54 (d, *J* = 15.8 Hz, 0H), 6.20 – 6.12 (m, 1H), 4.21 (ddd, *J* = 6.7, 5.8, 1.5 Hz, 1H), 3.85 (s, 2H), 3.81 (s, 2H).

^{13}C NMR (151 MHz, $CDCl_3$) δ 166.72, 162.16, 159.31, 132.01, 129.26, 128.69, 127.57, 126.74, 123.31, 114.00, 113.75, 55.40, 55.28, 42.17.

MS (ESI) Calculated *m/z* for $[M+H]^+$ = 298.14, Found *m/z* for $[M+H]^+$ = 298.22

IR (thin film): 2906, 2836, 1603, 1548, 1506, 1456, 1297, 1251

CV $E_{p/2}$ = +1.30 V vs. SCE

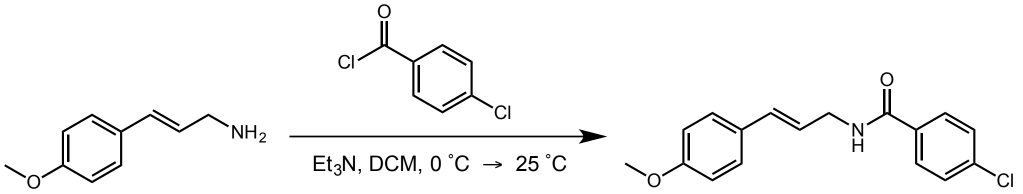

(*E*)-4-chloro-*N*-(3-(4-methoxyphenyl)allyl)benzamide (**3c**): Substrate **3c** was prepared according to General Procedure **A** using 730 mg (*E*)-4-methoxycinnamylamine (4.47 mmol), 0.75 mL triethylamine (5.36 mmol), 0.49 mL 4-chlorobenzoyl chloride (6.70 mmol), and 20 mL DCM. Product was purified by recrystallization from ethyl acetate and hexanes to furnish 603 mg pure product as colorless crystals in a 43% yield.

^{1}H NMR (600 MHz, $CDCl_3$) δ 7.74 (d, *J* = 8.5 Hz, 1H), 7.41 (d, *J* = 8.7 Hz, 1H), 7.31 (d, *J* = 8.7 Hz, 1H), 6.85 (d, *J* = 8.7 Hz, 1H), 6.55 (d, *J* = 15.8 Hz, 1H), 6.14 (dt, *J* = 15.8, 6.6 Hz, 1H), 4.22 (t, *J* = 6.1 Hz, 1H), 3.81 (s, 1H).

^{13}C NMR (151 MHz, $CDCl_3$) δ 166.17, 159.43, 137.77, 132.84, 132.49, 129.10, 128.87, 128.36, 127.62, 122.73, 114.05, 55.31, 42.35.

MS (ESI) Calculated *m/z* for $[M+H]^+$ = 302.19, Found *m/z* for $[M+H]^+$ = 302.22

IR (thin film): 3299, 3079, 3029, 2911, 1785, 1632, 1547, 1508, 1422, 1315, 1248

CV $E_{p/2}$ = +1.40 V vs. SCE

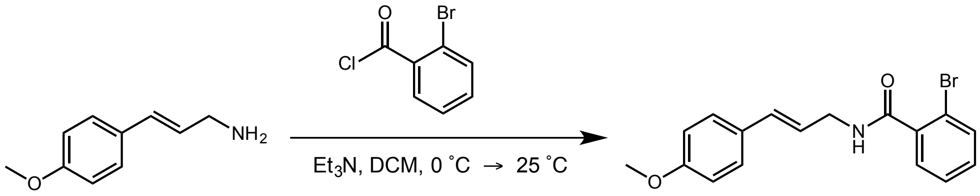

(*E*)-2-bromo-*N*-(3-(4-methoxyphenyl)allyl)benzamide (3d): Substrate **3d** was prepared according to General Procedure **A** using 1.00 g 4-methoxycinnamylamine (6.2 mmol), 1.0 mL triethylamine (7.32 mmol), 2.0 g 2-bromobenzoyl chloride (9.15 mmol) (prepared according to literature procedure), and 30 mL DCM. Product was purified by flash chromatography on silica (25% EtOAc/Hexanes) to furnish 930 mg pure product as colorless crystals in a 43% yield.

^{1}H NMR (600 MHz, $CDCl_3$) δ 7.55 (ddd, *J* = 25.2, 7.8, 1.4 Hz, 3H), 7.39 – 7.22 (m, 6H), 6.85 (d, *J* = 8.7 Hz, 2H), 6.57 (d, *J* = 15.8 Hz, 1H), 6.17 (s, 1H), 6.14 (dt, *J* = 15.8, 6.4 Hz, 1H), 4.21 (td, *J* = 6.0, 1.5 Hz, 3H), 3.80 (s, 4H).

^{13}C NMR (151 MHz, $CDCl_3$) δ 167.37, 159.29, 137.73, 133.31, 132.19, 131.19, 129.51, 129.18, 127.57, 127.49, 122.51, 119.22, 113.96, 55.24, 42.18.

MS (ESI) Calculated *m/z* for $[M+H]^+$ = 346.04, Found *m/z* for $[M+H]^+$ = 346.02

IR (thin film): 3414, 3263, 1645, 1607, 1510, 1465, 1297, 1250, 1175

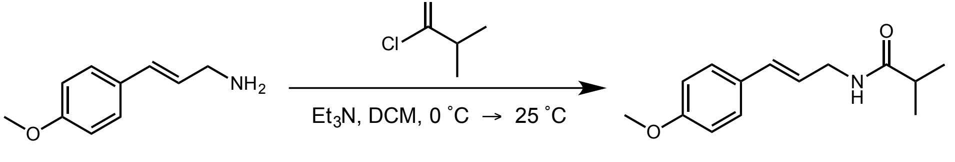

(*E*)-*N*-(3-(4-methoxyphenyl)allyl)isobutyramide (3e): Substrate **3e** was prepared according to General Procedure **A** using 1.00 g (*E*)-4-methoxycinnamylamine (6.2 mmol), 1.0

mL triethylamine (7.32 mmol), 0.96 mL isobutyrl chloride (9.15 mmol), and 30 mL DCM. Product was purified by recrystallization from ethyl acetate and hexanes to furnish 374 mg pure product as colorless crystals in a 26% yield.

^{1}H NMR (600 MHz, $CDCl_3$) δ 7.28 (d, *J* = 8.7 Hz, 2H), 6.84 (d, *J* = 8.7 Hz, 2H), 6.45 (d, *J* = 15.8 Hz, 1H), 6.04 (dt, *J* = 15.8, 6.5 Hz, 1H), 5.62 (s, 1H), 4.00 (ddd, *J* = 6.7, 5.8, 1.5 Hz, 3H), 3.80 (s, 4H), 2.38 (hept, *J* = 6.9 Hz, 1H), 1.18 (d, *J* = 6.9 Hz, 8H).

^{13}C NMR (151 MHz, $CDCl_3$) δ 176.65, 159.25, 131.70, 129.27, 127.50, 123.42, 113.95, 55.25, 41.55, 35.68, 19.64.

MS (ESI) Calculated *m/z* for $[M+H]^+ = 234.24$, Found *m/z* for $[M+H]^+ = 234.10$

IR (thin film): 3292, 2973, 2871, 1644, 1511, 1438, 1245, 1188

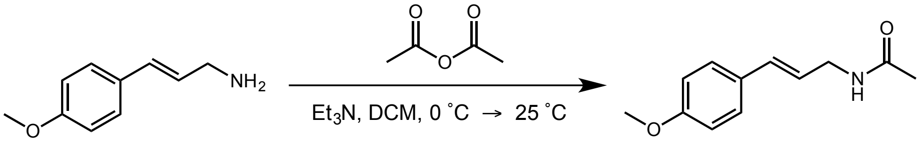

(*E*)-*N*-(3-(4-methoxyphenyl)allyl)acetamide (3f): Substrate **3f** was prepared according to General Procedure **A** using 1.00 g (*E*)-4-methoxycinnamylamine (6.2 mmol), 1.0 mL triethylamine (7.32 mmol), 0.48 mL acetic anhydride (12.32 mmol), and 30 mL DCM. Product was purified by recrystallization from ethyl acetate to furnish 516 mg pure product as colorless crystals in a 41% yield. Spectral data were in agreement with literature values[25].

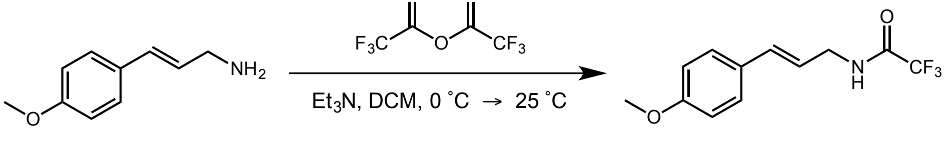

(*E*)-2,2,2-trifluoro-*N*-(3-(4-methoxyphenyl)allyl)acetamide (3g): Substrate **3g** was prepared according to General Procedure **A** using 500 mg (*E*)-4-methoxycinnamylamine (3.06 mmol), 0.51 mL triethylamine (3.67 mmol), 0.65 mL trifluoroacetic anhydride (4.59 mmol), and 15 mL DCM. Product was purified by flash chromatography on silica gel (15% EtOAc/Hexanes) to furnish 587 mg pure product as a white solid in 74% yield.

^{1}H NMR (600 MHz, $CDCl_3$) δ 7.31 (d, *J* = 8.7 Hz, 1H), 6.87 (d, *J* = 8.7 Hz, 1H), 6.70 – 6.47 (m, 1H), 6.38 (s, 1H), 6.03 (dt, *J* = 15.7, 6.7 Hz, 1H), 4.12 (td, *J* = 6.3, 1.4 Hz, 1H), 3.82 (s, 2H).

^{13}C NMR (151 MHz, $CDCl_3$) δ 159.69, 157.08, 156.84, 133.91, 128.53, 127.76, 120.25, 116.76, 114.09, 55.29, 42.07.

MS (ESI) Calculated *m/z* for $[M+H]^+$ = 260.18, Found *m/z* for $[M+H]^+$ = 260.17

IR (thin film): 3287, 3112, 2955, 2837, 1702, 1555, 1513, 1435, 1307, 1258, 1178

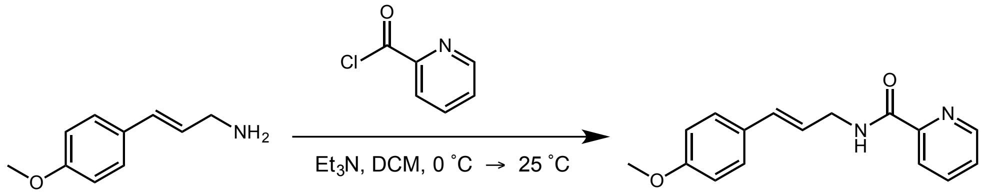

(*E*)-*N*-(3-(4-methoxyphenyl)allyl)picolinamide (3h): Substrate **3h** was prepared according to General Procedure **A** using 1.09 g (*E*)-4-methoxycinnamylamine (6.66 mmol), 1.11 mL triethylamine (7.99 mmol), 1.40 g 2-pyridinecarboxylic acid chloride (9.99 mmol) (prepared according to literature procedure[26] and used without purification). In a slight modification to the procedure, the amine substrate and triethylamine were stirred in 15 mL DCM at 0 °C, and the crude acid chloride was dissolved in an additional 15 mL DCM in a separate round bottom flask and added via cannula. The reaction was noted to immediately turn deep purple and was then allowed to warm to room temperature and was subjected to the same workup procedure. Product was purified by flash chromatography using silica gel (33% EtOAc/Hexanes + 2% triethylamine) giving 337 mg of the desired product as an off white solid in 18% yield.

^{1}H NMR (600 MHz, $CDCl_3$) δ 8.55 (d, *J* = 4.7 Hz, 0H), 8.23 (d, *J* = 7.9 Hz, 1H), 8.18 (s, 1H), 7.86 (td, *J* = 7.7, 1.7 Hz, 1H), 7.43 (ddd, *J* = 7.6, 4.7, 1.2 Hz, 1H), 7.31 (d, *J* = 8.7 Hz, 1H), 6.84 (d, *J* = 8.8 Hz, 1H), 6.56 (d, *J* = 15.8 Hz, 1H), 6.16 (dt, *J* = 15.8, 6.4 Hz, 1H), 4.25 (td, *J* = 6.2, 1.5 Hz, 2H), 3.80 (s, 3H).

^{13}C NMR (151 MHz, $CDCl_3$) δ 164.09, 159.24, 149.91, 148.06, 137.35, 131.79, 129.38, 127.57, 126.16, 123.14, 122.29, 113.95, 55.27, 41.55.

MS (ESI) Calculated *m/z* for $[M+H]^+$ = 269.22, Found *m/z* for $[M+H]^+$ = 269.14

IR (thin film): 3390, 2934, 1666, 1590, 1510, 1464, 1288, 1248, 1175

***N*-cinnamylbenzamide (3j)**: Substrate **3j** was prepared according to published procedure; spectral data were in agreement with literature values[27].

***N*-(3-methylbut-2-en-1-yl)benzamide (3k)**: Substrate **3k** was prepared according to published procedure; spectral data were in agreement with literature values[28].

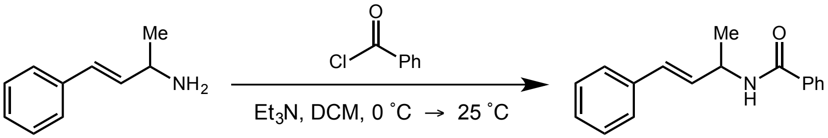

(*E*)-*N*-(4-phenylbut-3-en-2-yl)benzamide (3l): Substrate **3l** was prepared according to General Procedure **A** using 640 mg (*E*)-1-phenylbut-3-en-2-amine (4.3 mmol), 0.73 mL triethylamine (5.2 mmol), 0.75 mL benzoyl chloride (6.45 mmol), and 15 mL DCM. Product was purified by flash chromatography on silica gel (25% EtOAc/Hexanes) furnish 270 mg pure product as a colorless solid in a 25% yield. (*E*)-1-phenylbut-3-en-2-amine was prepared according to published procedure. Spectral data were in agreement with literature values[29].

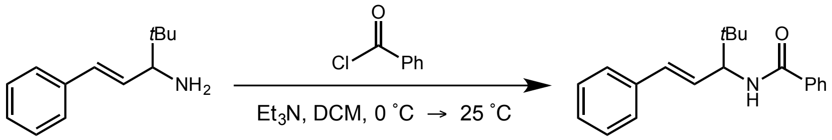

(*E*)-*N*-(4,4-dimethyl-1-phenylpent-1-en-3-yl)benzamide (3m): Substrate **3m** was prepared according to General Procedure **A** using 1.5 g (*E*)-4,4-dimethyl-1-phenylpent-1-en-3-amine (4.59 mmol), 0.77 mL triethylamine (5.63 mmol), 0.80 mL benzoyl chloride (6.88 mmol), and 25 mL DCM. Product was purified by flash chromatography on silica gel (10% EtOAc/Hexanes) to give 430 mg of product as a white solid in 32% yield. (*E*)-4,4-dimethyl-1-phenylpent-1-en-3-amine was prepared according to published procedure. Spectral data were in agreement with literature values[29].

***N*-(2-phenylallyl)benzamide (3n)**: Substrate **3n** was prepared according to published procedure; spectral data were in agreement with literature values[30].

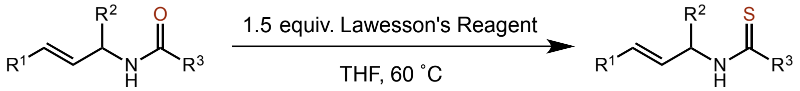

General Procedure B: The allylic thioamide substrates were synthesized according to a published procedure[31]. The allylic amide (1 equiv.) and Lawesson's Reagent (1.5 equiv.) were added to a dried round bottom flask with stir bar added, sealed with a septum, and purged with nitrogen. Dry THF was added via syringe ([0.1 M]) and the reaction heated to 60 °C with stirring for 4 hours. The reaction was cooled to room temperature, and solvent was removed by rotary evaporation. Crude material was then purified using column chromatography (25% ethyl acetate/hexanes) to furnish the desired product.

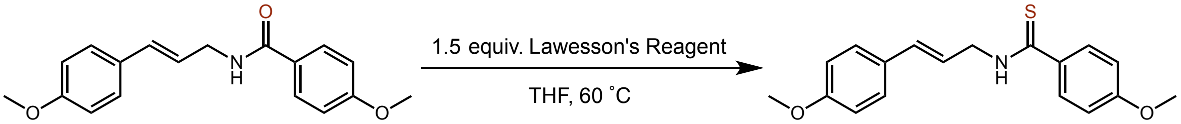

(*E*)-4-methoxy-*N*-(3-(4-methoxyphenyl)allyl)benzothioamide (3o): Substrate **3o** was prepared according to General Procedure **B** using 490 mg **3b** (1.65 mmol), 1.00 g Lawesson's Reagent, and 15 mL THF. The pure product was obtained as a yellow solid in 48% yield after chromatography.

^{1}H NMR (600 MHz, CDCl$_3$) δ 7.79 (d, *J* = 8.9 Hz, 1H), 7.51 (s, 1H), 7.34 (d, *J* = 8.7 Hz, 1H), 6.88 (dd, *J* = 11.4, 8.8 Hz, 2H), 6.64 (d, *J* = 15.9 Hz, 1H), 6.23 (dt, *J* = 15.8, 6.8 Hz, 1H), 4.60 (ddd, *J* = 6.8, 5.3, 1.4 Hz, 2H), 3.84 (s, 2H), 3.82 (s, 2H).

^{13}C NMR (151 MHz, CDCl$_3$) δ 197.83, 162.20, 159.58, 134.11, 133.97, 128.87, 128.49, 127.73, 120.71, 114.06, 113.65, 55.48, 55.30, 49.04.

MS (ESI) Calculated *m/z* for $[M+H]^+$ = 314.11, Found *m/z* for $[M+H]^+$ = 314.17

IR (thin film):3271, 2933, 1835, 1604, 1504, 1379, 1296, 1249, 1174, 1115

CV $E_{p/2}$ = +1.14 V vs. SCE

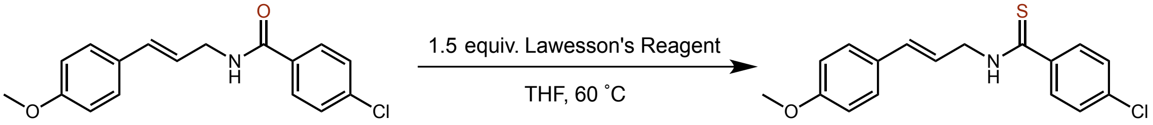

(*E*)-4-chloro-*N*-(3-(4-methoxyphenyl)allyl)benzothioamide (3p): Substrate **3p** was prepared according to General Procedure **B** using 350 mg **3c** (1.11 mmol), 677 mg Lawesson's Reagent, and 15 mL THF. The pure product was obtained as a yellow solid in 35% yield after chromatography.

^{1}H NMR (600 MHz, CDCl$_3$) δ 7.72 (d, *J* = 8.6 Hz, 1H), 7.55 (s, 1H), 7.35 (dd, *J* = 16.0, 8.6 Hz, 2H), 6.87 (d, *J* = 8.7 Hz, 1H), 6.64 (d, *J* = 15.8 Hz, 1H), 6.22 (dt, *J* = 15.8, 6.8 Hz, 1H), 4.57 (ddd, *J* = 6.8, 5.2, 1.3 Hz, 1H), 3.82 (s, 2H).

^{13}C NMR (151 MHz, CDCl$_3$) δ 197.46, 159.67, 139.95, 137.38, 134.54, 128.72, 128.68, 128.00, 127.76, 120.17, 114.09, 55.31, 49.18.

MS (ESI) Calculated *m/z* for $[M+H]^+$ = 318.06, Found *m/z* for $[M+H]^+$ = 318.15

IR (thin film):3433, 1644, 1509, 1403, 1248, 1174, 1091

CV $E_{p/2}$ = +1.23 V vs. SCE

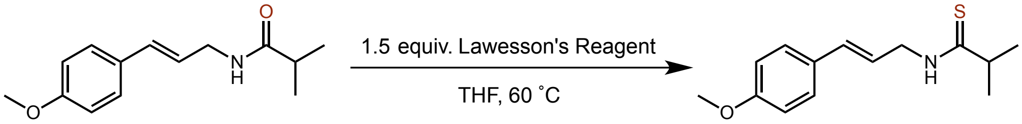

(*E*)-*N*-(3-(4-methoxyphenyl)allyl)-2-methylpropanethioamide (3q): Substrate **3q** was prepared according to General Procedure **B** using 290 mg **3c** (1.24 mmol), 754 mg Lawesson's Reagent, and 12 mL THF. The pure product was obtained as a yellow solid in 60% yield after chromatography.

^{1}H NMR (600 MHz, $CDCl_3$) δ 7.72 (d, *J* = 8.7 Hz, 1H), 7.54 (s, 1H), 7.35 (dd, *J* = 17.4, 8.6 Hz, 2H), 6.87 (d, *J* = 8.7 Hz, 1H), 6.65 (d, *J* = 15.8 Hz, 1H), 6.22 (dt, *J* = 15.8, 6.8 Hz, 1H), 4.58 (ddd, *J* = 6.7, 5.3, 1.4 Hz, 2H), 3.82 (s, 2H).

^{13}C NMR (151 MHz, $CDCl_3$) δ 197.50, 159.70, 139.98, 137.41, 134.58, 128.71, 128.02, 127.78, 120.19, 114.12, 55.33, 49.20.

MS (ESI) Calculated *m/z* for $[M+H]^+$ = 250.12, Found *m/z* for $[M+H]^+$ = 250.14

IR (thin film): 3255, 2966, 2930, 1606, 1511, 1441, 1294, 1250, 1175

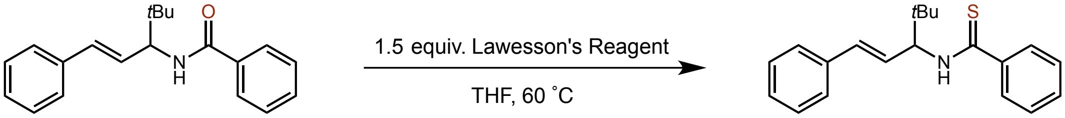

(*E*)-*N*-(4,4-dimethyl-1-phenylpent-1-en-3-yl)benzothioamide (3r): Substrate **3r** was prepared according to General Procedure **B** using 398 mg **3l** (1.36 mmol), 823 mg Lawesson's Reagent, and 14 mL THF. The pure product was obtained as a yellow oil in 61% yield after chromatography.

^{1}H NMR (600 MHz, CDCl$_3$) δ 7.75 (d, *J* = 7.0 Hz, 1H), 7.60 (d, *J* = 9.7 Hz, 1H), 7.48 (t, *J* = 7.4 Hz, 1H), 7.47 – 7.36 (m, 5H), 7.31 (t, *J* = 7.6 Hz, 2H), 7.24 (t, *J* = 7.4 Hz, 1H), 6.67 (d, *J* = 15.8 Hz, 1H), 6.21 (dd, *J* = 15.8, 7.3 Hz, 1H), 5.42 (ddd, *J* = 9.6, 7.3, 1.2 Hz, 1H), 1.11 (s, 9H).

^{13}C NMR (151 MHz, CDCl$_3$) δ 198.80, 142.72, 136.53, 133.43, 130.98, 128.62, 128.55, 127.80, 126.54, 126.49, 124.49, 65.59, 35.67, 26.65.

MS (ESI) Calculated *m/z* for $[M+H]^+$ = 310.26, Found *m/z* for $[M+H]^+$ = 310.18

IR (thin film): 3393, 3058, 2962, 2867, 1508, 1474, 1371, 1317

***N*-allylbenzothioamide (3r)**: Substrate **3r** was prepared according to published procedure; spectral data were in agreement with literature values[31].

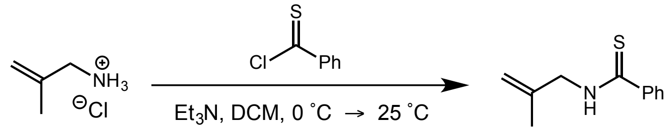

***N*-(2-methylallyl)benzothioamide (3s)**: Substrate **3s** was prepared according to General Procedure **A** using 1.07 g 2-methylprop-2-en-1-aminium chloride (10 mmol), 3.5 mL triethylamine (25 mmol, 2.5 equiv), 1.57 g thiobenzoyl chloride (10 mmol), and 5 mL DCM. Thiobenzoyl chloride was dissolved in an additional 5 mL DCM in a separate flask and added to the reaction via cannula. Product was purified by flash chromatography (25% ethyl acetate/hexanes) to furnish pure product as a yellow oil (56% yield). Thiobenzoyl chloride was prepared according to published procedure[32] and was used without purification.

General Procedure for Alkene Hydrofunctionalization

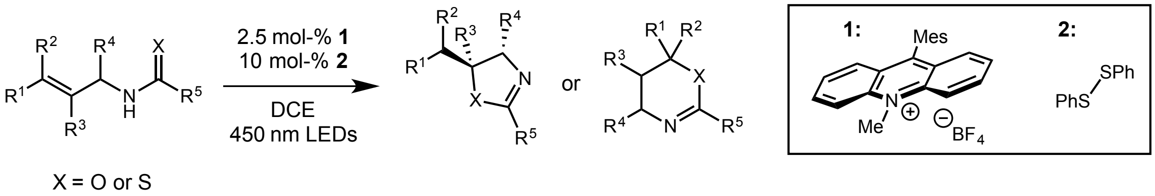

General Procedure C: Substrate (100 mg), 9-mesityl-10-methylacridinium tetrafluoroborate (2.5 mol %), and phenyl disulphide (10 mol %) were added to a flame-dried 2-dram vial equipped with a stir bar. Inside a glove-box, dichloroethane (0.1 [M] final concentration) was added to the vial, which was then sealed by a polypropylene cap equipped with a PTFE/silicone septum and removed from the glove box. The reaction was placed on a magnetic stir plate approximately 3cm from the light source (450 nm), and a hood of tin foil was placed over the entire setup. The reaction was then irradiated for the indicated amount of time. The test reactions appear bright yellow initially and gradually turn deep red over the course of the reaction. Upon completion, the stir bar was removed and the reaction concentrated. The crude mixture was purified by flash chromatography to furnish the final product. A small quantity of DCM is sometimes used to aid in solubilizing the material for flash chromatography.

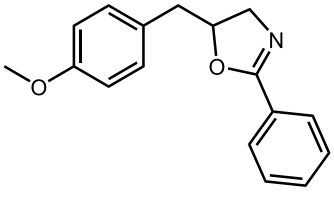

5-(4-methoxybenzyl)-2-phenyl-4,5-dihydrooxazole (4a): The average yield for the title compound was 82% (2 trials), using 100 mg (0.37 mmol) **3a**, 3.7 mg **1** (0.009 mmol), and 8.1 mg **2** (0.037 mmol). Irradiated for 14 hours. Eluent for purification: 25% ethyl acetate/hexanes.

^{1}H NMR (600 MHz, CDCl$_3$) δ 7.94 (dd, *J* = 8.4, 1.4 Hz, 2H), 7.54 – 7.45 (m, 1H), 7.41 (dd, *J* = 8.2, 6.8 Hz, 2H), 7.18 (d, *J* = 8.6 Hz, 2H), 6.87 (d, *J* = 8.6 Hz, 1H), 4.90 (dtd, *J* = 9.5, 7.0, 6.2 Hz, 1H), 4.06 (dd, *J* = 14.6, 9.4 Hz, 1H), 3.80 (s, 3H), 3.79 – 3.61 (m, 1H), 3.05 (dd, *J* = 14.1, 7.0 Hz, 1H), 2.85 (dd, *J* = 14.1, 6.2 Hz, 1H).

^{13}C NMR (151 MHz, CDCl$_3$) δ 163.81, 158.40, 131.21, 130.28, 128.75, 128.28, 128.07, 127.87, 113.96, 80.40, 59.40, 55.20, 40.48.

MS (GC-MS) Calculated *m/z* = 267.13, Found *m/z* = 267.1

IR (thin film): 2954, 1645, 1607, 1509, 1463, 1345, 1301, 1299, 1168

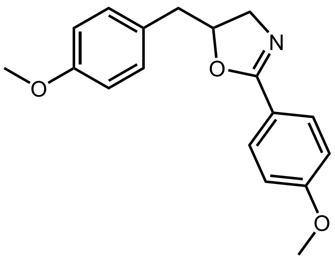

5-(4-methoxybenzyl)-2-(4-methoxyphenyl)-4,5-dihydrooxazole (4b): The average yield for the title compound was 77% (2 trials), using 100 mg (0.336 mmol) **3b**, 3.4 mg **1** (0.0084 mmol), and 7.3 mg **2** (0.0336 mmol). Irradiated for 14 hours. Eluent for purification: 50% ethyl acetate/hexanes.

^{1}H NMR (600 MHz, CDCl$_3$) δ 7.88 (d, *J* = 7.4 Hz, 1H), 7.17 (d, *J* = 7.7 Hz, 1H), 6.91 (d, *J* = 7.3 Hz, 1H), 6.86 (d, *J* = 7.1 Hz, 1H), 4.87 (p, *J* = 6.9 Hz, 1H), 4.03 (dd, *J* = 14.5, 9.1 Hz, 1H), 3.84 (s, 2H), 3.79 (s, 1H), 3.74 (dd, *J* = 14.4, 7.0 Hz, 1H), 3.04 (dd, *J* = 14.1, 7.0 Hz, 1H), 2.83 (dd, *J* = 14.1, 6.2 Hz, 1H).

^{13}C NMR (151 MHz, $CDCl_3$) δ 163.58, 161.94, 158.37, 130.28, 129.77, 128.88, 120.43, 113.94, 113.62, 80.28, 59.37, 55.30, 55.20, 40.50.

MS (GC-MS) Calculated *m/z* for $[M+H]^+ = 297.13$, Found *m/z* for $[M+H]^+ = 297.2$

IR (thin film): 3420, 2935, 2836, 2359, 1646, 1609, 1512, 1461, 1346, 1302, 1252, 1170

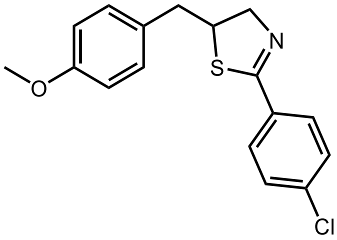

2-(4-chlorophenyl)-5-(4-methoxybenzyl)-4,5-dihydrooxazole (4c): The average yield for the title compound was 78% (2 trials), using 100 mg (0.319 mmol) **3c**, 3.2 mg **1** (0.0080 mmol), and 7.0 mg **2** (0.032 mmol). Irradiated for 14 hours. Eluent for purification: 25% ethyl acetate/hexanes.

^{1}H NMR (600 MHz, $CDCl_3$) δ 7.86 (d, $J = 8.6$ Hz, 1H), 7.38 (d, $J = 8.6$ Hz, 1H), 7.16 (d, $J = 8.6$ Hz, 2H), 6.86 (d, $J = 8.6$ Hz, 1H), 4.90 (dtd, $J = 9.5, 7.0, 6.1$ Hz, 1H), 4.05 (dd, $J = 14.7, 9.4$ Hz, 1H), 3.80 (s, 3H), 3.76 (dd, $J = 14.7, 7.1$ Hz, 1H), 3.03 (dd, $J = 14.1, 6.9$ Hz, 1H), 2.85 (dd, $J = 14.1, 6.2$ Hz, 1H).

^{13}C NMR (151 MHz, $CDCl_3$) δ 163.00, 158.49, 137.43, 130.31, 129.47, 128.64, 128.60, 126.43, 114.03, 80.67, 59.48, 55.26, 40.47.

MS (GC-MS) Calculated *m/z* = 309.09, found = 309.1

IR (thin film): 3362, 3033, 2934, 2870, 2834, 1718, 1650, 1598, 1512, 1490, 1403, 1344, 1248, 1178

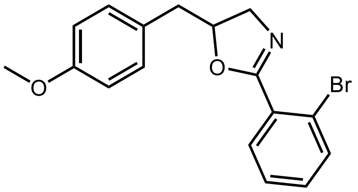

2-(2-bromophenyl)-5-(4-methoxybenzyl)-4,5-dihydrooxazole (4d): The average yield for the title compound was 77% (2 trials), using 100 mg (0.289 mmol) **3d**, 2.9 mg **1** (0.0072 mmol), and 7.1 µL 4-methoxythiophenol (0.058 mmol). Irradiated for 14 hours. Eluent for purification: 25% ethyl acetate/hexanes.

^{1}H NMR (600 MHz, $CDCl_3$) δ 7.69 – 7.61 (m, 2H), 7.33 (td, *J* = 7.6, 1.3 Hz, 1H), 7.30 – 7.25 (m, 1H), 7.19 (d, *J* = 8.6 Hz, 2H), 6.86 (d, *J* = 8.6 Hz, 2H), 4.93 (dq, *J* = 9.6, 6.7 Hz, 1H), 4.10 (dd, *J* = 14.7, 9.6 Hz, 1H), 3.82 (dd, *J* = 14.7, 7.2 Hz, 1H), 3.79 (s, 3H), 3.11 (dd, *J* = 14.1, 6.7 Hz, 1H), 2.88 (dd, *J* = 14.2, 6.4 Hz, 1H).

^{13}C NMR (151 MHz, $CDCl_3$) δ 163.04, 158.39, 133.78, 131.49, 131.25, 130.26, 129.73, 128.54, 127.01, 121.71, 113.95, 80.63, 59.68, 55.17, 40.28.

MS (GC-MS) Calculated *m/z* = 345.04, found *m/z* = 345.1

IR (thin film): 3062, 3032, 3005, 2934, 2834, 1651, 1612, 1590, 1512, 1464, 1431, 1341, 1246, 1178

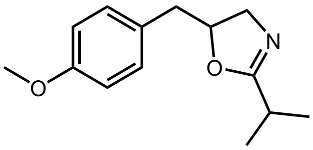

2-isopropyl-5-(4-methoxybenzyl)-4,5-dihydrooxazole (4e): The average yield for the title compound was 79% (2 trials), using 100 mg (0.428 mmol) **3e**, 4.3 mg **1** (0.011 mmol), and 9.3 mg **2** (0.0428 mmol). Irradiated for 14 hours. Eluent for purification: 50% ethyl acetate/hexanes.

^{1}H NMR (600 MHz, $CDCl_3$) δ 7.12 (d, *J* = 8.6 Hz, 2H), 6.84 (d, *J* = 8.6 Hz, 2H), 4.68 (dd, *J* = 9.5, 6.5 Hz, 1H), 3.85 – 3.78 (m, 1H), 3.78 (s, 4H), 3.52 (dd, *J* = 14.0, 6.7 Hz, 1H), 2.90 (dd, *J* = 14.0, 6.8 Hz, 1H), 2.73 (dd, *J* = 14.1, 6.2 Hz, 1H), 2.54 (hept, *J* = 7.0 Hz, 1H), 1.18 (d, *J* = 7.0 Hz, 5H).

^{13}C NMR (151 MHz, $CDCl_3$) δ 171.92, 158.39, 130.32, 128.82, 113.93, 79.85, 58.79, 55.23, 40.47, 28.20, 19.72, 19.61.

MS (GC-MS) Calculated *m/z* = 233.14, found *m/z* = 233.2

IR (thin film): 3378, 2970, 2935, 2875, 2835, 1732, 1662, 1612, 1513, 1466, 1388, 1309, 1247, 1199

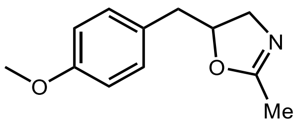

5-(4-methoxybenzyl)-2-methyl-4,5-dihydrooxazole (4f): The average yield for the title compound was 77% (2 trials), using 100 mg (0.487 mmol) **3f**, 4.9 mg **1** (0.0122 mmol), and 10.6 mg **2** (0.049 mmol). Irradiated for 14 hours. Eluent for purification: ethyl acetate.

^{1}H NMR (600 MHz, $CDCl_3$) δ 7.12 (d, *J* = 8.3 Hz, 2H), 6.84 (d, *J* = 8.4 Hz, 2H), 4.70 (dq, *J* = 9.5, 6.7 Hz, 1H), 3.93 – 3.79 (m, 1H), 3.78 (s, 3H), 3.51 (dd, *J* = 14.0, 7.0 Hz, 1H), 2.91 (dd, *J* = 14.1, 6.8 Hz, 1H), 2.76 (dd, *J* = 14.1, 6.2 Hz, 1H), 1.95 (s, 2H).

^{13}C NMR (151 MHz, $CDCl_3$) δ 164.75, 158.38, 130.17, 128.69, 113.92, 80.14, 59.09, 55.19, 40.42, 14.10.

MS (GC-MS) Calculated *m/z* = 205.11, found *m/z* = 205.1

IR (thin film): 3096, 2934, 2835, 1736, 1669, 1582, 1512, 1440, 1393, 1300, 1246, 1178, 1110

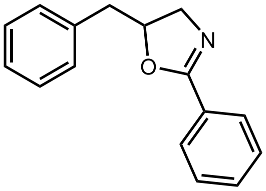

5-(4-methoxybenzyl)-2-phenyl-4,5-dihydrooxazole (4j): The average yield for the title compound was 76% (2 trials), using 100 mg (0.447 mmol) **3j**, 4.3 mg **1** (0.011 mmol), and 9.7 mg **2** (0.044 mmol). Eluent for purification: 25% ethyl acetate/hexanes.

^{1}H NMR (600 MHz, $CDCl_3$) δ 7.98 – 7.92 (m, 1H), 7.51 – 7.47 (m, 1H), 7.42 (dd, *J* = 8.2, 6.8 Hz, 1H), 7.34 (dd, *J* = 8.1, 6.8 Hz, 2H), 7.27 (d, *J* = 13.5 Hz, 2H), 4.95 (dtd, *J* = 9.5, 7.1, 6.1 Hz, 1H), 4.09 (dd, *J* = 14.6, 9.4 Hz, 1H), 3.80 (dd, *J* = 14.6, 7.1 Hz, 1H), 3.13 (dd, *J* = 14.0, 7.1 Hz, 1H), 2.91 (dd, *J* = 14.0, 6.2 Hz, 1H).

^{13}C NMR (151 MHz, $CDCl_3$) δ 163.77, 136.77, 131.21, 129.29, 128.53, 128.27, 128.07, 127.84, 126.69, 80.19, 59.53, 41.42.

MS (GC-MS) Calculated *m/z* = 237.12, found = 237.2

IR (thin film): 3062, 3028, 2940, 2869, 1649, 1579, 1495, 1451, 1345, 1259, 1176

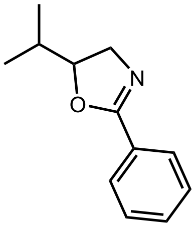

5-isopropyl-2-phenyl-4,5-dihydrooxazole (4k): The average yield for the title compound was 59% (2 trials), using 100 mg (0.57 mmol) **3k**, 5.7 mg **1** (0.014 mmol), and 12.5 mg **2** (0.057 mmol). Eluent for purification: 25% ethyl acetate/hexanes.

^{1}H NMR (600 MHz, CDCl$_3$) δ 7.95 (d, *J* = 6.9 Hz, 1H), 7.47 (t, *J* = 7.3 Hz, 1H), 7.41 (t, *J* = 7.6 Hz, 2H), 4.45 (ddd, *J* = 9.7, 7.8, 6.6 Hz, 1H), 4.05 (dd, *J* = 14.7, 9.7 Hz, 1H), 3.74 (dd, *J* = 14.7, 7.8 Hz, 1H), 1.89 (h, *J* = 6.7 Hz, 1H), 0.99 (dd, *J* = 38.1, 6.8 Hz, 6H).

^{13}C NMR (151 MHz, CDCl$_3$) δ 164.13, 131.13, 128.27, 128.05, 84.86, 57.68, 32.68, 17.71, 17.50.

MS (GC-MS) Calculated *m/z* = 189.12, found = 189.1

IR (thin film): 3330, 3062, 2962, 2875, 1717, 1648, 1579, 1536, 1494, 1450, 1346, 1287, 1259, 1176

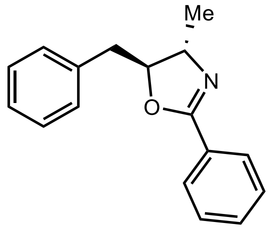

5-benzyl-4-methyl-2-phenyl-4,5-dihydrooxazole (4l): The average yield for the title compound was 64% (2 trials), using 100 mg (0.398 mmol) **3l**, 4.0 mg **1** (0.01 mmol), and 8.7 mg **2** (0.04 mmol). Eluent for purification: 25% ethyl acetate/hexanes.

^{1}H NMR (400 MHz, CDCl$_3$) δ 7.94 (d, *J* = 7.9 Hz, 2H), 7.68 (d, *J* = 7.7 Hz, 2H), 7.52 – 7.14 (m, 16H), 4.42 (q, *J* = 6.7 Hz, 1H), 4.29 (p, *J* = 6.9 Hz, 1H), 4.04 (p, *J* = 6.7 Hz, 1H), 3.13 (dd, *J* = 13.9, 7.2 Hz, 1H), 2.89 (dd, *J* = 13.9, 6.1 Hz, 1H), 2.74 (t, *J* = 7.9 Hz, 2H), 1.90 (q, *J* = 7.4 Hz, 2H), 1.29 (d, *J* = 6.5 Hz, 3H), 1.23 (d, *J* = 6.7 Hz, 3H).

^{13}C NMR (101 MHz, CDCl$_3$) δ 166.81, 162.67, 141.74, 136.78, 134.87, 133.17, 131.33, 131.29, 130.05, 129.35, 128.59, 128.52, 128.37, 128.36, 128.32, 128.22, 127.96, 126.78, 126.73, 125.96, 87.05, 66.81, 45.75, 41.01, 38.63, 32.53, 21.43, 21.12.

MS (GC-MS) Calculated *m/z* = 251.13, found *m/z* = 251.2

IR (thin film): 3062, 3029, 2931, 1644, 1579, 1495, 1450, 1351, 1298, 1269

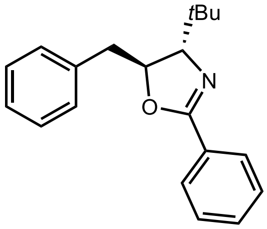

5-benzyl-4-(*tert*-butyl)-2-phenyl-4,5-dihydrooxazole (4m): The average yield for the title compound was 81% (2 trials), using 100 mg (0.341 mmol) **3m**, 3.4 mg **1** (0.0085 mmol), and 7.4 mg **2** (0.0341 mmol). Eluent for purification: 15% ethyl acetate/hexanes.

^{1}H NMR (600 MHz, $CDCl_3$) δ 8.01 – 7.96 (m, 2H), 7.96 – 7.91 (m, 0H), 7.56 – 7.44 (m, 1H), 7.47 – 7.39 (m, 2H), 7.39 – 7.22 (m, 7H), 4.89 (ddd, *J* = 11.3, 8.7, 2.3 Hz, 0H), 4.64 (dt, *J* = 7.6, 5.4 Hz, 1H), 4.01 (d, *J* = 8.7 Hz, 0H), 3.70 (d, *J* = 5.4 Hz, 1H), 3.16 (dd, *J* = 14.0, 2.3 Hz, 0H), 3.10 – 2.97 (m, 1H), 2.82 (dd, *J* = 13.9, 5.4 Hz, 1H), 1.21 (s, 2H), 0.86 (s, 9H).

^{13}C NMR (151 MHz, $CDCl_3$) δ 163.00, 162.17, 139.21, 137.10, 131.14, 129.59, 129.26, 128.51, 128.48, 128.41, 128.33, 128.28, 128.28, 128.26, 128.20, 128.13, 126.70, 126.42, 84.75, 81.26, 80.71, 77.54, 42.72, 37.18, 34.21, 34.10, 28.03, 25.75.

MS (GC-MS) Calculated *m/z* for = 293.16, found *m/z* = 293.1

IR (thin film): 3063, 3028, 2956, 2868, 1650, 1603, 1580, 1495, 1465, 1394, 1340, 1299, 1252, 1176

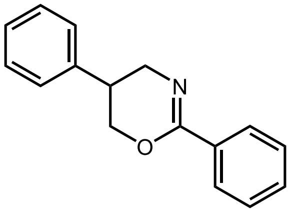

2,5-diphenyl-5,6-dihydro-4*H*-1,3-oxazine (4n): The average yield for the title compound was 53% (2 trials), using 100 mg (0.429 mmol) **3n**, 4.3 mg **1** (0.011 mmol), and 52.7

μL 4-methoxythiophenol (0.429 mmol, 1.0 equiv.). Eluent for purification: 25% ethyl acetate/hexanes.

^{1}**H NMR** (600 MHz, CDCl$_3$) δ 7.95 (dd, *J* = 7.1, 1.3 Hz, 2H), 7.50 – 7.42 (m, 1H), 7.42 – 7.36 (m, 4H), 7.34 – 7.28 (m, 1H), 7.28 – 7.23 (m, 2H), 4.52 (ddd, *J* = 10.5, 4.3, 2.8 Hz, 1H), 4.29 (t, *J* = 10.6 Hz, 1H), 3.89 (ddd, *J* = 16.6, 5.1, 2.8 Hz, 1H), 3.71 (dd, *J* = 16.5, 10.5 Hz, 1H), 3.21 (ddd, *J* = 10.6, 5.9, 4.7 Hz, 1H).

^{13}**C NMR** (151 MHz, CDCl$_3$) δ 155.18, 139.43, 133.61, 130.44, 128.90, 128.07, 127.49, 127.34, 127.03, 69.21, 49.64, 37.94.

MS (GC-MS) Calculated *m/z* = 237.12, found *m/z* = 237.1

IR (thin film):2058, 2942, 2908, 1652, 1491, 1445, 1334, 1264, 1130

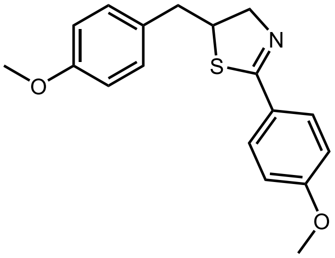

5-(4-methoxybenzyl)-2-(4-methoxyphenyl)-4,5-dihydrothiazole (4o): The average yield for the title compound was 80% (2 trials), using 100 mg (0.32 mmol) **3o**, 3.2 mg **1** (0.0080 mmol), and 7.0 mg **2** (0.032 mmol). Eluent for purification: 25% ethyl acetate/hexanes.

^{1}**H NMR** (600 MHz, CDCl$_3$) δ 7.78 (d, *J* = 8.8 Hz, 2H), 7.14 (d, *J* = 8.6 Hz, 2H), 6.91 (d, *J* = 8.8 Hz, 2H), 6.86 (d, *J* = 8.6 Hz, 2H), 4.34 (dd, *J* = 15.6, 4.2 Hz, 1H), 4.25 (dd, *J* = 15.6, 7.8 Hz, 1H), 4.10 (qd, *J* = 7.7, 4.2 Hz, 1H), 3.85 (s, 3H), 3.80 (s, 3H), 2.88 (d, *J* = 7.7 Hz, 2H).

^{13}**C NMR** (151 MHz, CDCl$_3$) δ 167.03, 161.89, 158.37, 131.04, 130.01, 129.91, 126.24, 113.91, 113.73, 69.09, 55.39, 55.25, 53.07, 41.40.

MS (GC-MS) Calculated *m/z* = 313.11, found *m/z* = 313.1

IR (thin film): 3006, 2967, 2933, 2915, 2840, 1608, 1512, 1444, 1302, 1249, 1180, 1107

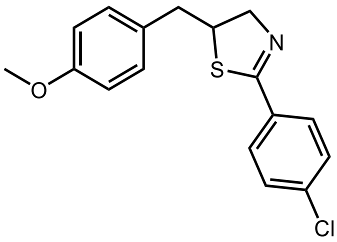

2-(4-chlorophenyl)-5-(4-methoxybenzyl)-4,5-dihydrothiazole (4p): The average yield for the title compound was 60% (2 trials), using 100 mg (0.303 mmol) **3p**, 3.0 mg **1** (0.010 mmol), and 6.6 mg **2** (0.040 mmol). Eluent for purification: 25% ethyl acetate/hexanes.

^{1}H NMR (600 MHz, CDCl$_3$) δ 7.76 (d, *J* = 8.6 Hz, 1H), 7.38 (d, *J* = 8.6 Hz, 1H), 7.14 (d, *J* = 8.6 Hz, 2H), 6.86 (d, *J* = 8.6 Hz, 1H), 4.36 (dd, *J* = 15.9, 4.3 Hz, 1H), 4.28 (dd, *J* = 15.9, 7.9 Hz, 1H), 4.15 (qd, *J* = 7.8, 4.2 Hz, 1H), 3.80 (s, 3H), 2.89 (d, *J* = 7.7 Hz, 2H).

^{13}C NMR (151 MHz, CDCl$_3$) δ 166.65, 158.46, 137.19, 131.93, 130.77, 130.02, 129.53, 128.71, 113.98, 69.28, 55.27, 53.48, 41.40.

MS (GC-MS) Calculated *m/z* = 317.83, found *m/z* = 317.1

IR (thin film): 3031, 2933, 2835, 1608, 1511, 1439, 1399, 1301, 1247, 1176, 1092

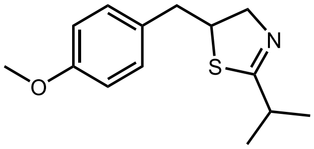

2-isopropyl-5-(4-methoxybenzyl)-4,5-dihydrothiazole (4q): The average yield for the title compound was 62% (2 trials), using 100 mg (0.303 mmol) **3q**, 4.0 mg **1** (0.010 mmol), and 8.7 mg **2** (0.030 mmol). Eluent for purification: 25% ethyl acetate/hexanes.

^{1}H NMR (600 MHz, $CDCl_3$) δ 7.10 (d, *J* = 8.6 Hz, 2H), 6.84 (d, *J* = 8.6 Hz, 2H), 4.10 (dd, *J* = 15.2, 4.3 Hz, 1H), 4.03 (dd, *J* = 15.1, 7.8 Hz, 1H), 3.96 (qd, *J* = 7.6, 4.2 Hz, 1H), 3.79 (s, 3H), 2.85 – 2.73 (m, 3H), 1.21 (dd, *J* = 6.9, 2.1 Hz, 6H).

^{13}C NMR (151 MHz, $CDCl_3$) δ 176.85, 158.32, 130.98, 129.97, 113.83, 68.41, 55.22, 52.59, 41.37, 34.09, 21.11, 20.98.

MS (GC-MS) Calculated *m/z* = 249.12, found *m/z* = 249.1

IR (thin film): 2965, 2933, 1835, 1654, 1613, 1512, 1464, 1440, 1300, 1247, 1178, 1109

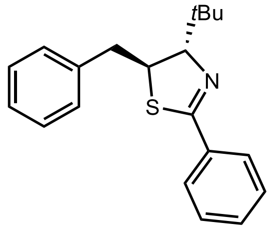

5-benzyl-4-(*tert*-butyl)-2-phenyl-4,5-dihydrothiazole (4r): The average yield for the title compound was 82% (2 trials), using 100 mg (0.32 mmol) **3r**, 3.2 mg **1** (0.0081 mmol), and 6.7 mg **2** (0.032 mmol). Eluent for purification: 10% ethyl acetate/hexanes.

^{1}H NMR (400 MHz, $CDCl_3$) δ 7.85 (d, *J* = 6.7 Hz, 1H), 7.42 (ddd, *J* = 14.5, 7.9, 6.2 Hz, 3H), 7.33 (dd, *J* = 7.9, 6.7 Hz, 2H), 7.26 (d, *J* = 7.2 Hz, 3H), 4.35 (d, *J* = 3.3 Hz, 1H), 4.03 (ddd, *J* = 8.3, 6.8, 3.3 Hz, 1H), 3.08 – 2.85 (m, 2H), 0.95 (s, 9H).

^{13}C NMR (101 MHz, $CDCl_3$) δ 164.80, 138.86, 133.58, 130.90, 129.29, 128.47, 128.37, 126.68, 92.03, 52.98, 45.61, 36.65, 26.40.

MS (GC-MS) Calculated *m/z* = 309.16, found *m/z* = 309.1

IR (thin film): 3058, 2958, 2868, 1580, 1504, 1462, 1390, 1340, 1252, 1227, 1157, 1172

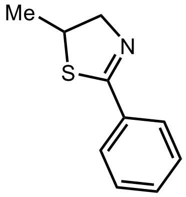

5-methyl-2-phenyl-4,5-dihydrothiazole (4s): The average yield for the title compound was 60% (2 trials), using 100 mg (0.56 mmol) **3s**, 5.6 mg **1** (0.014 mmol), and 13.9 μL **2** (0.11 mmol). Eluent for purification: 15% ethyl acetate/hexanes. Spectral data were in agreement with literature values[31].

^{1}H NMR (400 MHz, $CDCl_3$) δ 7.87 – 7.80 (m, 2H), 7.51 – 7.36 (m, 3H), 4.40 (dd, *J* = 15.7, 7.9 Hz, 1H), 4.20 (dd, *J* = 15.7, 4.4 Hz, 1H), 4.11 – 3.96 (m, 1H), 1.40 (d, *J* = 6.8 Hz, 3H).

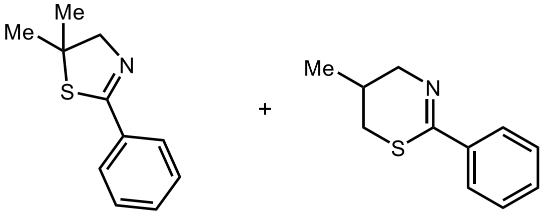

The average yield for the title compound was 75% (2 trials), using 100 mg (0.52 mmol) **3t**, 5.2 mg **1** (0.013 mmol), and 12.8 μL **2** (0.10 mmol). Eluent for purification: 15% ethyl acetate/hexanes. Spectral data were in agreement with literature values[31].

5-methyl-2-phenyl-5,6-dihydro-4*H*-1,3-thiazine (4t): **^{1}H NMR** (400 MHz, CDCl3) δ 7.77 (dt, *J* = 6.7, 1.7 Hz, 1H), 7.57 – 7.32 (m, 2H), 4.26 – 3.91 (m, 1H), 3.41 (dd, *J* = 16.6, 9.5 Hz, 1H), 3.26 – 3.02 (m, 1H), 2.88 (dd, *J* = 12.0, 10.1 Hz, 1H), 1.96 (ddt, *J* = 9.9, 6.5, 3.2 Hz, 0H), 1.11 (d, *J* = 6.6 Hz, 2H).

5,5-dimethyl-2-phenyl-4,5-dihydrothiazole (5t): **^{1}H NMR** (400 MHz, CDCl3) δ 7.80 (dd, *J* = 8.2, 1.5 Hz, 1H), 7.63 – 7.32 (m, 1H), 4.13 (s, 1H), 1.58 (s, 3H).

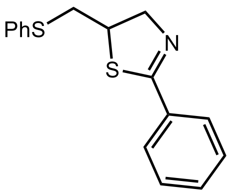

2-phenyl-5-((phenylthio)methyl)-4,5-dihydrothiazole (6s): The yield of the title compound was 11%, using 100 mg **3r** (0.56 mmol) and 12.2 mg **2** (0.056 mmol). Eluent for purification: 10% ethyl acetate/hexanes.

^{1}H NMR (600 MHz, CDCl$_3$) δ 7.83 (d, *J* = 7.0 Hz, 1H), 7.49 – 7.45 (m, 1H), 7.44 – 7.39 (m, 4H), 7.32 (t, *J* = 7.6 Hz, 2H), 7.27 – 7.20 (m, 1H), 4.65 (dd, *J* = 16.2, 3.1 Hz, 1H), 4.31 (dd, *J* = 16.2, 8.0 Hz, 1H), 4.00 (dddd, *J* = 9.2, 8.1, 6.3, 3.0 Hz, 1H), 3.17 (dd, *J* = 13.6, 6.3 Hz, 1H), 3.05 (dd, *J* = 13.6, 8.8 Hz, 1H).

^{13}C NMR (151 MHz, CDCl$_3$) δ 167.20, 134.66, 133.09, 131.23, 130.47, 130.46, 129.14, 128.47, 128.27, 126.89, 77.21, 77.00, 76.79, 68.75, 49.87, 39.92.

MS (GC-MS) Calculated *m/z* = 285.06, found *m/z* = 285.1

IR (thin film): 3366, 3266, 1622, 1449, 1397, 1325, 1279

APPENDIX 3: SUPPORTING INFORMATION FOR THE APPLICATION OF A POLAR-RADICAL CROSSOVER CYCLOADDITION REACTION TOWARDS THE TOTAL SYNTHESIS OF RUBRIFLORDILACTONE B

General Methods. Infrared (IR) spectra were obtained using a Jasco 260 Plus Fourier transform infrared spectrometer. Proton, carbon, and fluorine magnetic resonance spectra (^{1}H NMR and ^{13}C NMR) were recorded on a Bruker model DRX 400 or 600 (^{1}H NMR at 400 MHz or 600 MHz and ^{13}C NMR at 100 MHz or 150 MHz spectrometer. Chemical shifts for protons are reported in parts per million downfield from tetramethylsilane and are referenced to residual protium in solvent (^{1}H NMR: $CHCl_3$ at 7.26 ppm). Chemical shifts for carbons are reported in parts per million downfield from tetramethylsilane and are referenced to the carbon resonances of the residual solvent peak (^{13}C NMR: $CDCl_3$ at 77.0 ppm). NMR data are represented as follows: chemical shift, multiplicity (s = singlet, d = doublet, dd = doublet of doublet, ddd = doublet of doublet of doublet, dddd = doublet of doublet of doublet of doublet, dtd = doublet of triplet of doublet, t = triplet, q = quartet, qd = quartet of doublet, sept = septuplet, m = multiplet), coupling constants (Hz), and integration. Mass spectra were obtained using either a Micromass Quattro II (triple quad) instrument with nanoelectrospray ionization or an Agilent 6850 series gas chromatograph instrument equipped with a split-mode capillary injection system and Agilent 5973 network mass spec detector (MSD). Thin layer chromatography (TLC) was performed on SiliaPlate 250 μm thick silica gel plates purchased from Silicycle. Visualization was accomplished using fluorescence quenching, $KMnO_4$ stain, or ceric ammonium molybdate (CAM) stain followed by heating. Organic solutions were concentrated under reduced pressure using a Büchi rotary evaporator. Purification of the reaction products was carried out by chromatography using Siliaflash-P60 (40-63 μm) or Siliaflash-T60 (5-20 μm) silica gel purchased from Silicycle. All reactions were carried out under an inert atmosphere of nitrogen in

flame-dried glassware with magnetic stirring unless otherwise noted. Irradiation of photochemical reactions was carried out using a Par38 Royal Blue Aquarium LED lamp (Model # 6851) fabricated with high-power Cree LEDs as purchased from Ecoxotic (www.ecoxotic.com), with standard borosilicate glass vials purchased from Fisher Scientific. Yield refers to isolated yield of analytically pure material unless otherwise noted. NMR yields were determined using hexamethyldisiloxane as an internal standard. Cyclic voltammograms were obtained with a glassy carbon working electrode, Ag/AgCl reference electrode, platinum wire counter electrode, and Pine Instruments Wavenow potentiostat. All measurements were taken in N_2-sparged MeCN with 0.1 M tetrabutylammonium hexafluorophosphate ($TBAPF_6$) as a supporting electrolyte where the analyte concentration was 5-10 mM. The potential was scanned from 1.0 V to a vertex potential of 2.5 V in the forward direction at a sweep rate of 100 mV/s, and the reverse sweep showed no indication of a reversible electrochemical event. The half-wave potential for irreversible oxidation is estimated at $E_{p/2}$ the potential where the current is equal to one-half the peak current of the oxidation event. The values for $E_{p/2}$ are referenced to SCE (Saturated Calomel Electrode) by adding +30 mV to the potential measured against Ag/AgCl (3 M NaCl) .

Materials. Commercially available reagents were purchased from Sigma Aldrich, Acros, Alfa Aesar, or TCI, and used as received unless otherwise noted. Diethyl ether (Et_2O), dichloroethane (DCE), dichloromethane (DCM), tetrahydrofuran (THF), toluene, and dimethylformamide (DMF) were dried by passing through activated alumina columns under nitrogen prior to use. Triethylamine (Et_3N) was distilled from calcium hydride. Other common solvents and chemical reagents were purified by standard published methods if noted.

trimethyl((3-methylfuran-2-yl)oxy)silane (TMS-21)

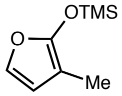

Prepared according to a published literature procedure. Spectral data were in agreement with literature values.[27]

***tert*-butyldimethyl((3-methylfuran-2-yl)oxy)silane (TBS-21)**

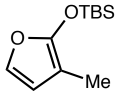

Prepared according to a published literature procedure. Spectral data were in agreement with literature values.[28]

5-(1-hydroxyallyl)-3-methylfuran-2(5*H*)-one (22)

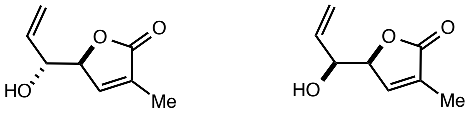

A flame-dried round bottom flask or 2-dram vial was equipped with a stir bar and purged with N_2. Anhydrous DCM was added (to 0.5 M), followed by the Lewis acid (1.2 equiv. for BF_3•OEt, $TiCl_2(Oi\text{-}Pr)_2$, 10 mol % for metal-BOX/metal-PyBOX catalysts) and the flask/vial was cooled to -78 °C. At -78 °C, acrolein (1.2 equiv.) was added and the Lewis acid/acrolein mixture was allowed to stir for 0.5 h. After 0.5 h, the siloxyfuran nucleophile of choice (TBS-**31** or TMS-**31**, 1 equiv.) was added in DCM dropwise. The temperature of the reaction was maintained at -78 °C and stirred for 4-5 h. Upon completion, the reaction was warmed to room temperature, quenched with DI water/sat. aqueous $NaHCO_3$ and diluted with DCM. The organic phase was separated and the aqueous phase extracted three times with DCM. The combined organics were washed with brine, dried with $MgSO_4$, and concentrated to yield the crude product, which was purified by column chromatography on silica gel (50% EtOAc/hexanes) to afford the alkenol product as a mixture of diastereomers. **Note 1**: reactions using *in situ* generated $TiCl_2(O\textit{i}\text{-}Pr)_2$ were prepared as follows: $TiCl_4$ (0.6 equiv.) stirred at room temperature in DCM, $Ti(O\textit{i}\text{-}Pr)_4$ (0.6 equiv.) was then added dropwise. The reaction was stirred for 1.5 h and cooled to -78 °C. Acrolein was then added. **Note 2**: reactions using metal-BOX or metal-PyBOX catalysts were prepared as follows: Metal triflate salt (10 mol %) and ligand (10 mol %) were suspended in anhydrous DCM and stirred for 1 h. Acrolein was then added and the procedure above was followed. **Note 3**: referenced MVAR procedures were carried out according to the published procedure. Analytical data for **23**:

^{1}H NMR for *anti* diastereomer (600 MHz, $CDCl_3$): δ 7.04 (pent, 1H), 5.87 (ddd, *J* = 17.2 Hz, *J* = 10.7 Hz, *J* = 5.3 Hz, 1H), 5.42 (dt, *J* = 17.2 Hz, *J* = 1.4 Hz, 1H), 5.31 (dt, *J* = 10.7 Hz, *J* = 1.4 Hz, 1H), 4.87 (m, 1H), 4.43 (m, 1H), 1.91 (s, 3H); **^{13}C NMR** for *anti* diastereomer (150 MHz, $CDCl_3$) δ 174.0, 144.0, 134.6, 131.8, 118.1, 83.1, 72.1, 10.8

^{1}H NMR for *syn* diastereomer (600 MHz, $CDCl_3$): δ 7.00 (pent, *J* = 1.7 Hz, 1H), 5.84 (ddd, *J* = 17.1 Hz, *J* = 10.5 Hz, *J* = 6.4 Hz, 1H), 5.41 (dt, *J* = 17.2 Hz, *J* = 1.3 Hz, 1H), 5.32 (dt, *J* = 10.5 Hz, *J* = 1.2 Hz, 1H), 4.83 (m, 1H), 4.17 (m, 1H), 1.92 (t, *J* = 1.8 Hz, 3H);

MS (EI/GC-MS): *m/z* calculated for $C_8H_{10}O_3$ $[M]^+$ 154.06, found 154.10.

3-(4-methyl-5-oxo-2,5-dihydrofuran-2-yl)propanal (23)

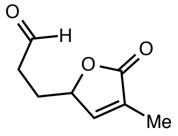

Isolated as the minor product in MVAR procedures producing **23** (or as the major product if a Lewis acid is omitted). Spectral data were in agreement with literature values.[27] Analytical data for **32**:

^{1}H NMR (600 MHz, $CDCl_3$): δ 9.78 (s, 1H), 6.99 (pent, J = 1.7 Hz, 1H), 4.93 (m, 1H), 2.63 (m, 2H), 2.18 (m, 1H), 1.89 (s, 3H), 1.77 (m, 1H).

General procedure for the polar radical crossover cyclization between indene and alkenol 23:

The acridinium catalyst (**31**, 5 mol %), H-atom donor (1 equiv. 2-PMN or 9-CNFl) and the alkenol nucleophile **23** (2 equiv.) were weighed and dispensed into a flame dried 1-dram vial equipped with a stir bar and Teflon-coated septum cap. The vial was moved to an inert atmosphere (glove box, N_2), where solvent was dispensed by syringe (DCM to 0.4 M), followed by indene via microsyringe (1 equiv.). The vial was then sealed and removed from the inert environment. If using thiophenol as an H-atom donor, it was added to the reaction after reagent dispensing (20 mol % PhSH added via microsyringe through the Teflon-coated septum in a fume hood). The vial and cap were sealed with electrical tape and PTFE tape. The reaction was irradiated (2x450 nm blue LED lamps) and stirred for 4 days. Upon completion, the crude reaction was concentrated and products isolated by column chromatography on silica gel (20% EtOAc/hexanes).

5-(1-((2,3-dihydro-1*H*-inden-2-yl)oxy)allyl)-3-methylfuran-2(5*H*)-one (26)

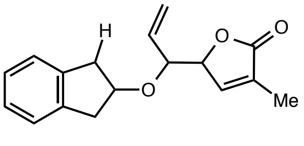

Isolated as a mixture of two inseparable diastereomers (1.2:1 according to crude ^{1}H NMR analysis), along with 9-CNFl and 2-PMN. Uncyclized product **33** could not be separated from 9-CNFl or 2-PMN. Isolated as the major product in polar radical crossover cyclizations with *syn*-**23** or *anti*-**23** with indene and thiol or carbon H-atom donors. Analytical data for **33**:

^{1}H NMR (600 MHz, $CDCl_3$): δ 7.5-7.0 (m, 8H), 7.05 (t, *J* = 1.7 Hz, 1H), 6.93 (t, *J* = 1.7 Hz, 1H), 5.91 (m, 2H), 5.43 (m, 4H), 4.92 (br s, 1H), 4.85 (d, *J* = 3.2 Hz, 1H), 4.82 (m, 2H), 4.25 (t, *J* = 5.9 Hz, 1H), 4.16 (t, *J* = 6.1 Hz, 1H), 3.20 (m, 2H), 3.04 (m, 2H), 2.96 (m, 2H), 2,69 (m, 2H), 1.89 (t, *J* = 1.8 Hz, 3H), 1.87 (t, *J* = 1.8 Hz, 3H); **^{13}C NMR** (150 MHz, $CDCl_3$) δ 174.1, 174.0, 145.8, 145.6, 134.8, 134.6, 130.4, 130.1, 129.3, 128.8, 128.2, 127.2, 126.5, 126.2, 125.4, 125.2, 125.1, 124.33, 124.32, 120.6, 120.0, 111.7, 86.4, 85.8, 82.6, 82.2, 79.2, 79.1, 50.7, 50.0, 42.1, 41.7, 37.9, 37.88, 37.03, 37.00, 36.96, 34.5, 34.2, 28.0, 10.8, 10.75; **MS** (EI/GC-MS): *m/z* calculated for $C_{17}H_{18}O_3$ $[M]^+$ 270.13, found 270.0.

1-(4-methyl-5-oxo-2,5-dihydrofuran-2-yl)allyl 4-chlorobenzoate

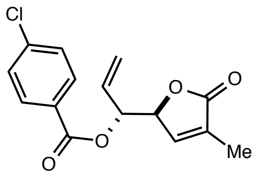

To a flame-dried round bottom flask equipped with a stir bar was added anhydrous DCM (to 0.2 M). The stirring DCM was cooled to 0 °C and 1.5 equiv. Et_3N was added, followed by 1.2 equiv. alkenol-**23** (6.7:1 diastereomeric mixture). Next, 4-chlorobenzoyl chloride (1 equiv.) was added to the stirring solution dropwise. The reaction was warmed to room temperature and stirred overnight. The next morning, the reaction was quenched with 2N HCl and partitioned with DCM/DI water. The organic phase was extracted and aqueous phase washed with DCM three times. The combined organics were washed with brine, dried with $MgSO_4$, and concentrated to give the crude product. The ester was purified by column chromatography on silica gel (20% EtOAc/hexanes). The major diastereomer was enriched through chromatography (10% to 20% EtOAc/hexanes gradient) and recrystallized from EtOAc/hexanes to yield x-ray quality crystals (~20:1 d.r. after major diastereomer enrichment). Analytical data for ester:

^{1}H NMR (600 MHz, $CDCl_3$): δ 7.93 (d, *J* = 8.3 Hz, 2H), 7.41 (d, *J* = 8.5 Hz, 2H), 7.05 (br s, 1H), 5.84 (ddd, *J* = 17.0 Hz, *J* = 10.6 Hz, *J* = 6.3 Hz, 1H), 5.69 (m, 1H), 5.40 (m, 2H), 5.12 (br s, 1H), 1.96 (s, 3H).

3-methyl-5-(3-methyl-3,3a,8,8a-tetrahydro-2*H*-indeno[2,1-*b*]furan-2-yl)furan-2(5*H*)-one

(25)

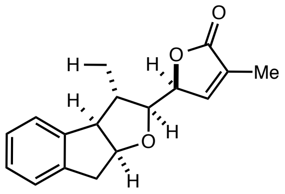

PRCC product produced in 3:1 d.r. (major diastereomer shown above). Produced in PRCC reaction between indene and *syn*-**22** as the minor product, along with uncyclized product (**26**). Analytical data for **25**:

^{1}H NMR major diastereomer (600 MHz, $CDCl_3$): δ 7.19 (m, 3H), 7.11 (m, 1H), 6.28 (pent, *J* = 1.6 Hz, 1H), 4.87 (td, *J* = 5.7 Hz, *J* = 2.0 Hz, 1H), 4.75 (m, 1H), 3.87 (dd, *J* = 6.2 Hz, *J* = 4.9 Hz, 1H), 3.34 (ddd, *J* = 6.0 Hz, *J* = 3.9 Hz, *J* = 1.0 Hz, 1H), 3.09 (d, *J* = 5.4 Hz, 1H), 3.07 (d, *J* = 2.0 Hz, 1H), 2.11 (m, 1H), 1.76 (t, *J* = 1.8 Hz, 3H), 1.27 (d, *J* = 7.0 Hz, 3H); **^{13}C NMR** major diastereomer (150 MHz, $CDCl_3$): δ 173.8, 145.9, 144.0, 141.1, 131.1, 127.3, 126.9, 125.3, 124.4, 86.4, 83.7, 80.5, 58.2, 41.0, 39.1, 19.6, 10.8; **^{1}H NMR** minor diastereomer (600 MHz, $CDCl_3$): δ 7.18 (m, 4H). 6.95 (m, 1H), 4.85 (m, 1H), 4.69 (br s, 1H), 3.81 (m, 1H), 3.48 (m, 1H), 3.20 (dd, *J* = 16.3 Hz, *J* = 5.9 Hz, 1H), 2.90 (dd, *J* = 16.3 Hz, *J* = 3.2 Hz, 1H), 2.76 (m, 1H), 1.93 (t, *J* =

1.8 Hz, 3H), 1.23 (d, 3H). **MS** (EI/GC-MS): *m/z* calculated for $C_{17}H_{18}O_3$ $[M]^+$ 270.13, found 270.2.

(*E*)-3-(trimethylsilyl)acrylaldehyde

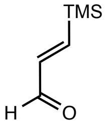

Prepared according to a published literature procedure. Spectral data were in agreement with literature values.[29] Analytical data:

^{1}H NMR (600 MHz, $CDCl_3$): δ 9.48 (d, *J* = 7.6 Hz, 1H), 7.16 (d, *J* = 18.6 Hz, 1H), 6.49 (dd, *J* = 18.6 Hz, *J* = 7.6 Hz, 1H), 0.15 (s, 9H).

5-((*E*-1-hydroxy-3-(trimethylsilyl)allyl)-3-methylfuran-2(5*H*)-one

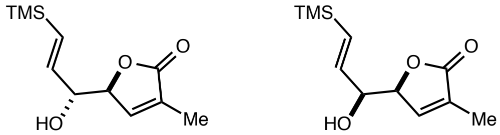

MVAR product produced (as major product) when using vinyl-TMS in place of acrolein. Vinylogous aldol procedure otherwise unaltered and *anti* selective under most conditions tested. Analytical data:

^{1}H NMR for *anti* diastereomer (600 MHz, $CDCl_3$): δ 7.02 (m, 1H), 6.04 (m, 2H), 4.86 (m, 1H), 4.39 (br s, 1H), 1.92 (t, *J* = 1.8 Hz, 3H), 0.07 (s, 9H);

^{1}H NMR for *syn* diastereomer (600 MHz, $CDCl_3$): δ 6.97 (t, *J* = 1.7 Hz, 1H), 6.04 (m, 2H), 8.82 (m, 1H), 4.14 (t, *J* = 5.6 Hz, 1H), 1.91 (t, 3H), 0.06 (s, 9H);

MS (EI/GC-MS): *m/z* calculated for $C_{11}H_{18}O_3Si$ $[M]^+$ 226.10, found 226.2.

Carreira Schiff base catalyst (20)

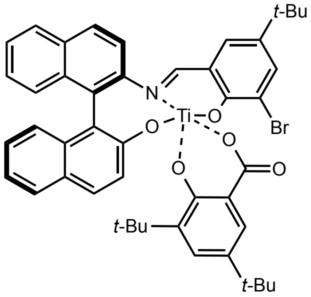

Prepared according to published literature procedure from purchased precursors.[26]

3-methyl-5-(3-((trimethylsilyl)methyl)-3,3a,8,8a-tetrahydro-2*H*-indeno[2,1-*b*]furan-2-yl)furan-2(5*H*)-one (29)

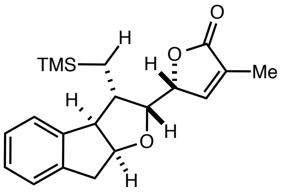

Product produced in trace amounts in PRCC reaction between indene and alkenol with vinyl TMS. Adduct **29** was solated as one diastereomer (shown). Relative stereochemistry of the product was assigned using ^{1}H NMR and NOESY analysis.

^{1}**H NMR** major (600 MHz, CDCl$_3$): δ 7.24 (m, 3H), 7.07 (m, 1H), 5.92 (pent, J = 1.6 Hz, 1H), 4.85 (t, J = 4.6 Hz, 1H), 4.64 (dt, J = 5.7 Hz, J = 1.9 Hz, 1H), 3.97 (dd, J = 5.7 Hz, J = 4.2 Hz, 1H), 3.34 (d, J = 5.0 Hz, 1H), 3.10 (d, J = 16.9 Hz, 1H), 3.05 (dd, J = 16.9 Hz, J = 4.4 Hz, 1H), 2.14 (m, 1H), 1.69 (t, J = 1.8 Hz, 3H), 0.96 (d, J = 10.7 Hz, 1H), 0.94 (d, J = 10.7 Hz, 1H), 0.10 (s, 9H); ^{13}**C NMR** major (150 MHz, CDCl$_3$): δ 173.5, 146.0, 144.2, 141.5, 131.1, 127.2, 126.9, 125.4, 124.7, 88.9, 84.1, 81.0, 58.4, 41.3, 38.9, 29.7, 10.7, -0.9

(S)-5-((S)-1-hydroxy-3-(triisopropylsilyl)prop-2-yn-1-yl)-3-methylfuran-2(5H)-one (30)

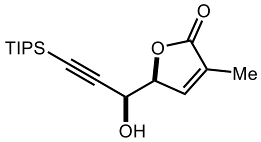

^{1}H NMR major (400 MHz, CDCl$_3$): δ 7.13 (t, *J* = 1.6 Hz 1H), 4.98 (dt, *J* = 2.0 Hz, *J* = 3.6 Hz, 1H), 4.75 (dd, *J* = 3.6 Hz, *J* = 7.6 Hz, 1H), 2.29 (s, 1H), 2.07 (m, 3H), 1.09 (s, 18H)

MS (GC-MS): Calculated *m/z* = 308.18, found *m/*z = 308.2

(S)-5-((S)-1-hydroxyprop-2-yn-1-yl)-3-methylfuran-2(5H)-one (31)

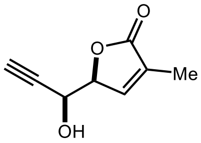

^{1}H NMR major (400 MHz, CDCl$_3$): δ 7.14 (m, 2H), 4.99 (dt, *J* = 1.6 Hz, *J* = 6 Hz, 1H), 4.47 (t, *J* = 4.0 Hz, 1H), 2.61 (d, *J* = 1.6 Hz, 1H), 2.54 (d, *J* = 4.8 Hz, 1H), 2.07 (m, 3H), 1.09 (s, 18H)

MS (GC-MS): Calculated *m/z* = 152.05, found *m/*z = 152.2